The low-temperature thermo-tectonic evolution of the western Tian Shan, Uzbekistan

Gilby Jepson[*1], Stijn Glorie[1], Dmitry Konopelko[2,3], Rustam Mirkamalov[4], Martin Danišík[5], and Alan S. Collins[1]

[1]*Centre for Tectonics, Resources, and Exploration (TRaX, Department of Earth Sciences, The University of Adelaide, 5005, Australia.*

[2]*Saint Petersburg State University, 7/9 University Embankment, SPb 199034, Russia.*

[3]*Novosibirsk State University, 2 Pirogova St., Novosibirsk, 630090, Russia.*

[4]*State Committee of the Republic of Uzbekistan on Geology and Mineral Resources, Tashkent, Uzbekistan.*

[5]*John de Laeter Centre, TIGeR, School of Earth and Planetary Sciences, Curtin University, Perth, 6846, Australia.*

Accepted on: August 24, 2018

Key Points

The Uzbek western Tian Shan underwent three discrete periods of exhumation in the Mesozoic-Cenozoic.

In the Cretaceous, rapid exhumation is focused only in the core of relict suture zones or major faults.

The Cretaceous Uzbek Tian Shan landscape developed as a series of parallel linear mountain belts.

Abstract

The Kyzylkum-Nurata region represents a key area in understanding the tectonic evolution of the western Tian Shan. In this study, we present new thermochronological data (apatite fission track

[*]corresponding author (gilby.jepson@adelaide.edu.au)

and apatite (U-Th-Sm)/He) and associated thermal history models for 45 igneous samples from the Kyzylkum-Nurata Segment of South Tian Shan on the territory of Uzbekistan and Tajikistan. Our data show that the Kyzylkum-Nurata Segment experienced a multi-phase Mesozoic thermal history that differs from previously studied segments of the Tian Shan. A Triassic (~220–200 Ma) cooling signal is widespread throughout the Tian Shan and is interpreted as being associated with exhumation following the closure of the Palaeo-Asian Ocean. Following this period of fast cooling, the Kyzylkum-Nurata Segment experienced a period of slow cooling and erosion in the Early Jurassic (~190–160 Ma). However, in contrast to other parts of the Tian Shan, our study area preserves evidence for rapid cooling during the Late Jurassic–Early Cretaceous (~160–120). Given that this rapid cooling signal was only recorded for samples in association with major structures (e.g., relic suture-shear zones), we interpret this event as a period of fault reactivation related with tectonic processes at the Eurasian margin of the Tethys Ocean. Subsequently, the Late Cretaceous–early Palaeogene (~100–50 Ma) is characterised by slow cooling and erosion. Since the late Palaeogene, the basement of the Tian Shan experienced cooling related to the India-Eurasia collision. The thermal signal of this collision has been extensively recorded in the high-altitude Kyrgyz Tian Shan. Within the low-relief Kyzylkum-Nurata Segment, this Cenozoic overprint is not recorded, allowing for a detailed assessment of the Mesozoic thermal and landscape evolution of the western Tian Shan. Our study demonstrates that the Cretaceous Uzbek Tian Shan was characterised by a series of parallel, linear mountain belts that formed along suture zones during fault reactivation.

1 Introduction

Central Asia hosts one of the world's largest active orogen, the intracontinental mountain range of the Tian Shan. The Tian Shan provides an excellent natural laboratory for investigating the impact of marginal tectonic processes on the continental interior. The Tian Shan is situated to the north of the active Cenozoic continental margin collisional orogenic belts of the Himalaya, Pamir, and Tibet, and south of the Palaeozoic orogens of Kazakhstan and Mongolia (Brookfield 2000, Alexeiev et al. 2009). The ancestral Tian Shan orogen formed during the Palaeozoic due to the accretion of several microcontinents and island arcs to the southern margin of Palaeo-Kazakhstan (Windley et al. 2007, Biske & Seltmann 2010, Xiao et al. 2013, Burtman 2015, Konopelko et al. 2017a). Throughout the Mesozoic and Cenozoic, progressive ocean closure along the southern margin of Eurasia generated regional deformation and the reactivation of existing structures (Bullen et al. 2001, 2003, De Grave et al. 2007, Glorie et al. 2010, 2011, Jepson et al. 2018). As a result, these intracontinental structures in the Tian Shan have been the focus of many geo- and thermochronological studies in order to generate

a model for the formation of the Tian Shan intracontinental orogenic system (e.g. Sobel & Dumitru 1997, Dumitru et al. 2001, Bullen et al. 2001, De Grave et al. 2007)

Previous thermochronological studies of the Tian Shan have identified several major periods of Mesozoic exhumation-related basement cooling, which have been interpreted to be related to exhumation in response to the collision of Cimmerian blocks with the southern Eurasian continental margin (e.g. Sobel et al. 2006b, Glorie et al. 2011, De Grave et al. 2013, Macaulay et al. 2014, Glorie & De Grave 2016). In addition, thermochronometers have been successful in identifying the widespread presence of Cenozoic cooling, which has been interpreted as exhumation due to the ongoing India-Eurasia collision (e.g. Sobel et al. 2006a, De Grave et al. 2012, Bande et al. 2017b, Käßner et al. 2017b, Nachtergaele et al. 2017, Jepson et al. 2018). The majority of previous thermochronological studies have focused on high relief areas within the core of the Tian Shan. However, there has been little work done on the eastern and western extremities of this vast mountain range. In this study we specifically target the westernmost extremity of the Tian Shan in Uzbekistan in order to provide constraints on the thermo-tectonic and landscape evolution of this largely unstudied, low relief segment of the Tian Shan. Filling this gap in the thermochronology allows for a more accurately constrained model on the tectonic evolution of the Tian Shan intracontinental system as a whole. In this study, we present new apatite fission track (AFT) and apatite (U-Th-Sm)/He (AHe) ages from the westernmost extent of the Tian Shan, termed the Kyzylkum-Nurata Segment of the South Tian Shan (Figure 1), specifically targeting the Gissar, Zeravshan, and South Tian Shan (STS) sutures in western Uzbekistan (Figure 3, Burtman 2015, Dolgopolova et al. 2017, Konopelko et al. 2017a).

2 Geological Background

The Uzbek western Tian Shan formed during the Palaeozoic, due to the collision between Precambrian microcontinents and island-arcs in the south with the Palaeozoic Kazakhstan continent to the north, as a response to the progressive closure of the Palaeo–Asian Ocean (Windley et al. 2007, Biske & Seltmann 2010, Xiao et al. 2013, Dolgopolova et al. 2017). The Tian Shan can be subdivided into three terranes: (1) the Northern Tian Shan (NTS), representing the deformed margin of the Palaeo-Kazakhstan microcontinent; (2) the Middle Tian Shan (MTS), comprised of Precambrian microcontinental slivers, such as the Karakum, and superimposed island-arcs, such as the Chatkal-Kurama; and (3) the Southern

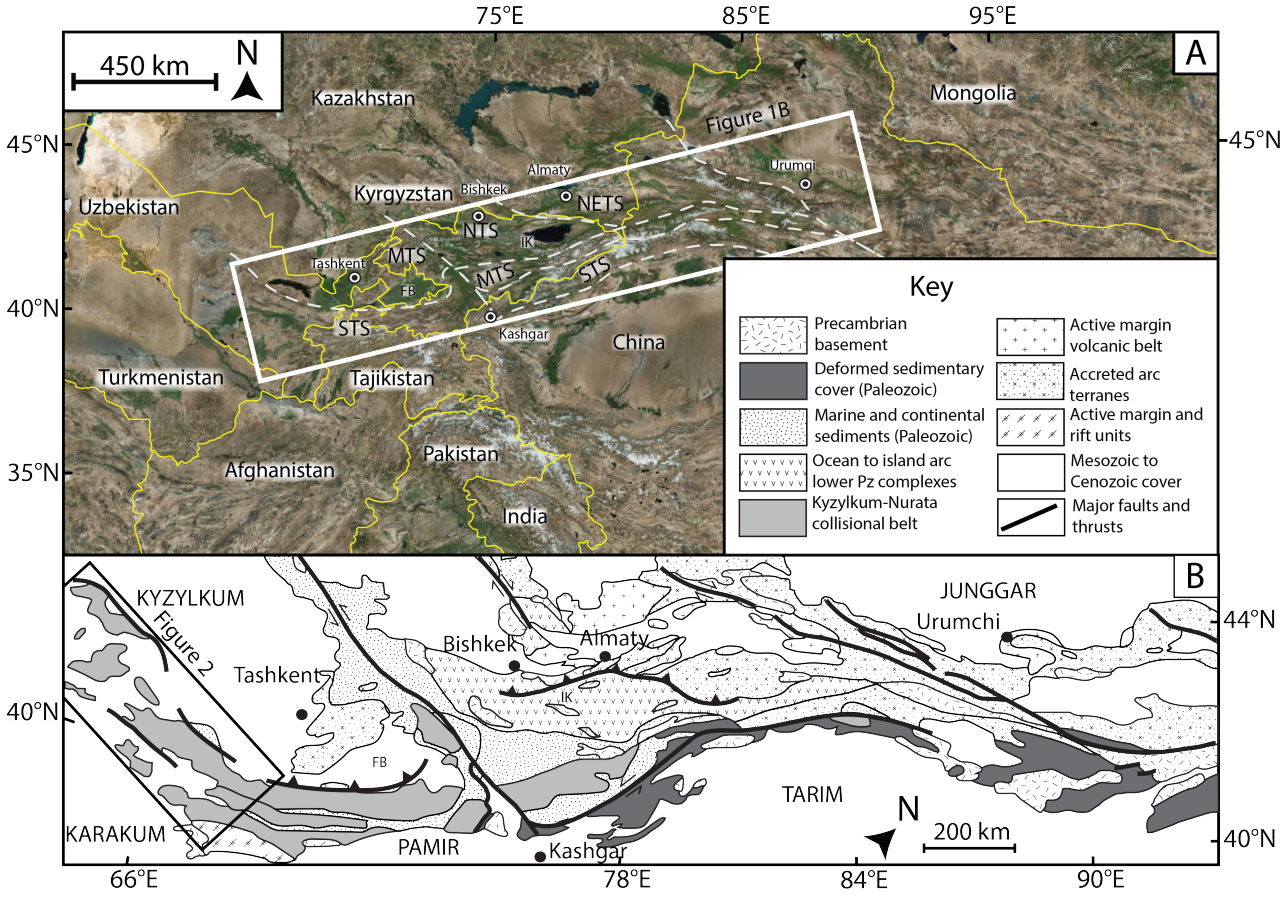

Figure 1: (a) Location map of the Tian Shan split into its main components; NETS is the north-eastern Tian Shan, NTS is the North Tian Shan, MTS is the Middle Tian Shan, and STS is the South Tian Shan (after Glorie et al. 2011). FB is the Fergana Basin, and IK is lake Issyk-Kul. (b) Simplified map of the Palaeozoic Tian Shan outlining study area (after Biske & Seltmann 2010).

Tian Shan (STS), a late Palaeozoic fold-and-thrust belt (Figure 1, Biske & Seltmann 2010, Burtman 2015, Konopelko et al. 2017a).

The STS is traditionally subdivided into four segments from west to east; the Kyzylkum-Nurata Segment, the Gissar Segment, the Alai Segment, and the Kokshaal Segment. Our study area, the Kyzylkum-Nurata Segment (Dolgopolova et al. 2017), is located in the westernmost extent of the South Tian Shan (STS, Figure 1). The Kyzylkum-Nurata Segment formed due to the closure of the Paleo-Asian Ocean in the Late Carboniferous, accreting the Kyzylkum-Alai terranes onto the Middle Tian Shan, generating the South Tian Shan fold belt (Burtman 2015, Konopelko et al. 2017a, Dolgopolova et al. 2017). Prior to the closure of the Paleo-Asian Ocean, the Kyzylkum-Alai terrane developed as the southern passive margin of the Paleo-Asian Ocean since the Neoproterozoic (Konopelko et al. 2015, Kempe et al. 2016, Dolgopolova et al. 2017). The Turkestan ocean closed in the Carboniferous-Permian, accreting the Kyzylkum-Alai terrane to the margin of the Middle Tian Shan which formed the South Tian Shan Suture, this accretion initiated the broadly synchronous closure of the Vashan and Gissar Basins, which had formed due to rifting in the Karakum continent further south (Figure 2). The closure of the Vashan Basin formed the Zeravshan suture (Figure 3, Dolgopolova et al. 2017), while the short-lived Gissar Basin was associated with rift and subduction related mamatism during the Carboniferous, and its closure resulted in the final amalgamation of the Gissar Segment to the South Tian Shan (Figure 2, Burtman 1975, Biske & Seltmann 2010, Seltmann et al. 2011, Konopelko et al. 2017a, 2018). The synchronous closure of the Vashan, Gissar, and Turkestan oceanic basins led to the emplacement of voluminous post-collisional granitoid magmatism (Figure 2, Biske & Seltmann 2010, Seltmann et al. 2011, Käßner et al. 2017a). The Late Palaeozoic ocean closure and collision resulted in the southward thrusting of carbonate platforms, forming a large nappe system (Dolgopolova et al. 2017). This oceanic closure was subsequently followed by a period of post-collisional granitoid magmatism throughout the Kyzylkum-Nurata Segment and the greater South Tian Shan during the early Permian (Konopelko et al. 2011, 2015, Kempe et al. 2016, Konopelko et al. 2017a, Dolgopolova et al. 2017). During the Late Permian–Early Triassic, the western Tian Shan experienced uplift and erosion resulting in a notable absence of Triassic sediments over such an extensive area (Figure 2, McCann 2016b).

During the Mesozoic, the South Tian Shan experienced punctuated episodes of deformation and reactivation (e.g. De Grave et al. 2007, Jolivet et al. 2010, 2013, De Grave et al. 2013). The closure of the Palaeo–Tethys Ocean during the Mesozoic initiated the accretion of Cimmerian continental

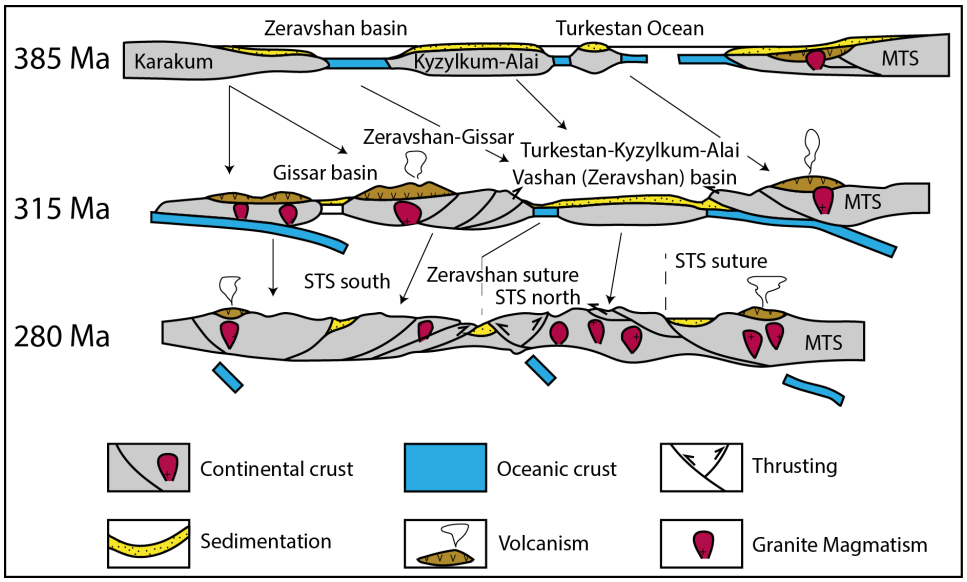

Figure 2: A schematic geodynamic model of the Palaeozoic western Tian Shan, modified after Dolgopolova et al. (2017)

fragments with the southern margin of Laurasia, causing widespread deformation (e.g. De Grave et al. 2007, Jolivet et al. 2010, Glorie et al. 2011, Xiao et al. 2013). Known collectively as the Cimmerian Orogeny, these events include the collisions of the Qiangtang block during the Late Triassic–Early Jurassic, the Lhasa block during the Late Jurassic–Early Cretaceous, and the Kohistan-Ladakh arc during the Late Cretaceous (e.g Yin & Harrison 2000, Angiolini et al. 2013, De Grave et al. 2013, Jolivet et al. 2013, Glorie & De Grave 2016, Käßner et al. 2017a). The series of collisions and other tectonic processes at the Tethyan margin are thought to have caused exhumation induced basement cooling within the Tian Shan and have been recorded using multi-chronometric methods (Glorie et al. 2010, Jolivet et al. 2010, De Grave et al. 2013, Jolivet et al. 2013, Gillespie et al. 2017). More specifically, the Tian Shan has been shown to have experienced two main deformation events in the Mesozoic. A rapid Triassic–Early Jurassic (~230–200 Ma) thermo-tectonic cooling that is recorded regionally throughout the Tian Shan and is thought to be related with the final closure of the Palaeo-Asian Ocean at ~250 Ma (Xiao et al. 2013) and/or the Qiangtang collision at ~180 Ma (e.g. Ratschbacher et al. 2003, Robinson 2015). Followed by a period of rapid cooling in the Cretaceous, recorded by samples taken in the vicinity to relic suture-shear zones that dissect the Tian Shan (Figure 3, e.g. Glorie et al. 2010, De Grave et al. 2013, De Pelsmaeker et al. 2015, Nachtergaele et al. 2017). In contrast, away from the suture-shear zones, the Tian Shan as a whole experienced slow cooling and peneplanation during the Cretaceous period (Jolivet et al. 2010, Macaulay et al. 2014). The extent of this period of Cretaceous fault reactivation is particularly not well understood for the western Tian Shan and is the main target

of this study.

The ongoing closure of the Neo-Tethys Ocean culminated in the collision of the continent of India with the southern margin of Eurasia during the Cenozoic (e.g. Beck et al. 1995, Aitchison et al. 2007, Najman et al. 2010, van Hinsbergen et al. 2011). The India-Eurasia collision caused widespread deformation and rapid exhumation in the Tian Shan (e.g. Sobel et al. 2006a, De Grave et al. 2007, Jolivet et al. 2010, Macaulay et al. 2014, Bande et al. 2017b). In the South Tian Shan, previous studies have identified initiation of exhumation at ~30-20 Ma and accelerating of exhumation since ~15-10 Ma, which correlates with periods of Pamir convergence (e.g. De Grave et al. 2012, De Pelsmaeker et al. 2015, Käßner et al. 2017b, Rutte et al. 2017, Nachtergaele et al. 2017, Jepson et al. 2018).

3 Methodology

In this study, new thermochronological data for 45 granitoid rock samples from the western extent of the South Tian Shan are presented (Figure 3). Two different thermochronological methods were applied; (1) apatite fission track (partial annealing zone ~120–60°C, Green et al. 1986), and (2) apatite (U-Th-Sm)/He dating (partial retention zone ~80–40°C, Zeitler et al. 1987).

3.1 Apatite Fission Track

The apatite fission track method (AFT) is based on the temperature dependent annealing of mineral lattice damage features, known as 'fission tracks', which are created by the spontaneous fission decay of ^{238}U (e.g. Fleischer et al. 1975, Wagner & Van den haute 1992, Gleadow et al. 2015). Fission tracks record the thermal history of a rock sample through the apatite partial annealing zone (APAZ) of ~120–60°C (Green et al. 1986). Apatite grains were picked and mounted in epoxy resin, then polished to expose internal sections, and were subsequently chemically etched in a 5M HNO_3 solution for 20s at 20°C to reveal the natural spontaneous fission tracks (Gleadow et al. 2002). Fission track analysis was performed at The University of Adelaide using an Autoscan system. The concentration of uranium (^{238}U) and chlorine (^{35}Cl) of each apatite grain was measured using Laser Ablation-Inductively Coupled Plasma-Mass Spectrometry. Data reduction was performed in Iolite using the Trace Elements DRS (data reduction scheme, Paton et al. 2011). Instrumental drift correction was carried out using NIST610 as an external standard, and elemental concentrations were calculated using ^{43}Ca as the internal standard (Pearce et al. 1997, Vermeesch 2017). Age calculation was carried out as described

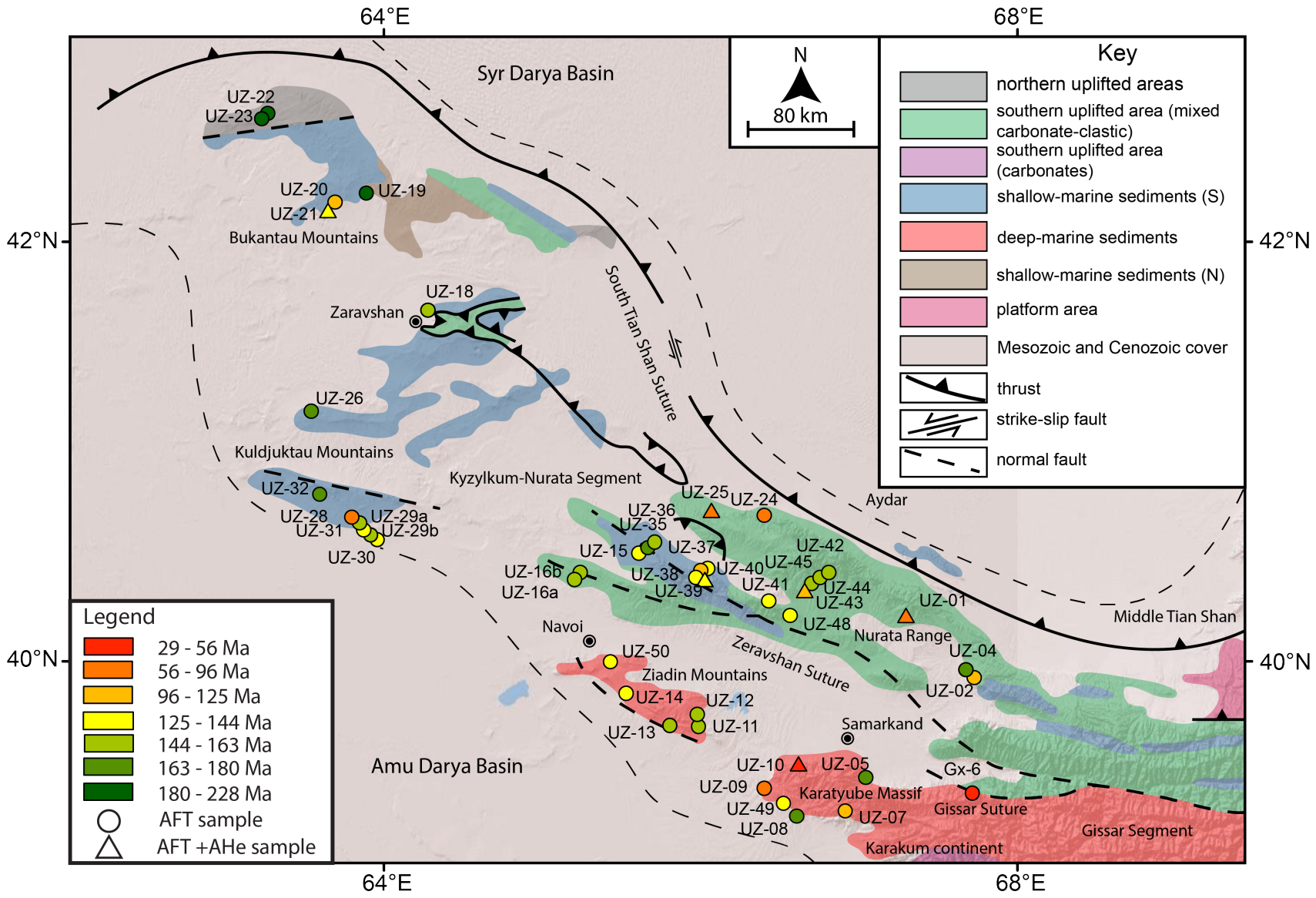

Figure 3: Structural units of the western segment of the Southern Tian Shan outlining the major Palaeozoic and Mesozoic structures (after Brookfield 2000). The map displays the locations and regional subdivisions for the apatite fission track (AFT) and apatite (U-Th-Sm)/He (AHe) data obtained in this study. Sample symbols are colour coded following AFT and AHe central ages.

in Hasebe et al. (2004) and De Grave et al. (2012), using the Durango apatite (McDowell et al. 2005) to perform a zeta calibration (Vermeesch 2017). For a detailed methodology see Glorie et al. (2017) and Gillespie et al. (2017).

3.2 Apatite (U-Th-Sm)/He

The (U-Th-Sm)/He thermochronometer is based on the accumulation and thermal diffusivity of radiogenic ^{4}He. Partial retention of He in apatite occurs between ~80–40°C making it valuable for constraining the most recent basement cooling event (Zeitler et al. 1987, Farley 2002). The apatite (U-Th-Sm)/He analyses for this study were undertaken at the John de Laeter Centre, Curtin University and followed the protocols described in Danišík et al. (2012).

Apatite crystals were hand-picked following the recommendations of Farley (2002), photographed and measured for physical dimensions, before being loaded in Pt microtubes. Helium (^{4}He) was extracted for apatite at ~900°C, under ultra-high vacuum using a diode laser and measured by isotope dilution on a Pfeiffer Prisma QMS-200 mass spectrometer. A "re-extract" was run after each sample to verify complete outgassing of the crystals. Helium gas results were corrected for blank, determined by heating empty microtubes using the same procedure. After the ^{4}He measurements, tubes containing the crystals were retrieved from the laser cell, spiked with ^{235}U and ^{230}Th and dissolved. Sample, blank, and spiked standard solutions were analysed by isotope dilution for ^{238}U and ^{232}Th, and by external calibration for ^{147}Sm on an Agilent 7500 ICP-MS. The total analytical uncertainty (TAU) was calculated as a square root of sum of squares of uncertainty on He and weighted uncertainties on U, Th, Sm and He measurements, and is typically <5% (1σ). The raw (U–Th-Sm)/He ages were corrected for alpha ejection (Ft correction) after Farley et al. (1996), whereby a homogenous distribution of U, Th and Sm was assumed for the crystals. Replicate analyses of internal standard Durango apatite (n = 10) measured over the period of this study, yielded mean (U–Th–Sm)/He ages of 31.9 ± 1.9 Ma (1σ), consistent with the reference Durango (U–Th–Sm)/He age of 31.02 ± 1.01 Ma (McDowell et al. 2005).

3.3 Thermal History Modelling

Thermal history models were produced for samples using their mean track length (MTL), AFT ages, AHe ages, and confined track length distributions. The QTQt software (version 5.6.0) was applied, which uses Bayesian trans-dimensional Markov Chain Monte Carlo statistics to determine models for

the cooling pathway of the sample (Gallagher 2012). An initial unconstrained run is performed to explore the statistical space, followed by adjustments to the search parameters or the addition of geological constraints where necessary. This approach follows the Bayesian philosophy of the software, which seeks to minimize the complexity of the model by statistical means. Many iterations ($>> 10,000$) are run to generate a range of models that create a probability distribution, from which individual models can be selected, including the maximum likelihood and "expected" (weighted mean) paths. The range of the general prior was set as t = AFT central age ± AFT central age, temperature = 70 ± 70°C. Acceptance rates for models were between 0.2 and 0.6 and birthdeath ratio was ~1. Spherical geometry and the radiation damage model of Gautheron et al. (2009) were used for modeling AHe data. The annealing model from Ketcham et al. (2007) was used for fission track data with D_{par} as the kinetic parameter. More details on the modelling approach can be found in Gallagher (2012) and Gillespie et al. (2017).

4 Results

The Kyzylkum-Nurata Segment hosts several relict suture zones, the South Tian Shan Suture, the Zeravshan suture, and the Gissar suture (Figure 3, Burtman 1975, Biske & Seltmann 2010, Seltmann et al. 2011, Dolgopolova et al. 2017). In this study, forty-five granitoid samples were analysed from outcropping rocks along, and away from, the suture zones. The samples yielded a range of ages from Triassic to Palaeogene, from both AFT and AHe methods (Figure 3). For a more thorough description, samples have been subdivided into six geographical clusters of samples based on regional proximity to each other. The groups are named after the ranges or nearby features that they were sourced from: (1) the Bukantau Mountains, (2) the Kuldjuktau Mountains, (3) the Nurata Range, (4) Aydar, (5) the Ziadin Mountains, and (6) the Karatyube Massif (Figure 3). Mean track lengths are referred to their relative length following the outline established in Figure 5, with samples that produce MTLs 12.9-13.5 μm refered to as "long", MTLs of 12.6-12.8 μm are "moderate", and MTLs of 11.4-12.5 μm are refered to as "short". Tables 4.1 and 4.2 summarise the AFT and AHe data. Detailed tables and figures for all single-grain AFT, mean track length (MTL) data, individual thermal history models, and modelling parameters are available in Supplementary files (Supplementary files 1, 2, 3, and 4).

Table 1: Apatite fission track data: n is the number of grains analysed per sample and # of lengths is the number of confined track lengths identified in each sample. Age is the central age calculated for each sample, and P Age is the pooled age of each sample. Samples in italics represent samples with fewer than 40 confined tracks, and a represented as dashed lines in the thermal history modelling.

Sample	Lat	Long	Elev	*n*	Age±1σ	P Age±1σ	#	MTL	±1σ
Bukantau Mountains									
UZ-18	*41.676*	*64.278*	*370*	*5*	*154.0±12.0*	*151.4±13.0*	*8*	*12.8*	*0.9*
UZ-19	42.227	63.889	242	30	220.9±9.0	214.1±17.0	72	13.1	1.0
UZ-20	*42.184*	*63.691*	*256*	*29*	*127.8±6.7*	*111.8±9.6*	*33*	*12.5*	*0.9*
UZ-21	42.181	63.686	250	36	130.4±3.5	126.0±10.0	93	12.8	1.2
UZ-22	*42.599*	*63.264*	*405*	*40*	*209.7±7.9*	*202.3±18.4*	*20*	*12.8*	*1.0*
UZ-23	42.599	63.264	405	40	228.0±9.9	221.1±19.9	50	13.4	1.1
Kuldjuktau Mountains									
UZ-26	41.200	63.540	484	27	178.0±11.0	181.5±16.2	49	11.6	1.2
UZ-28	*40.666*	*63.825*	*310*	*13*	*92.0±12.0*	*98.1±9.0*	*37*	*11.9*	*1.1*
UZ-29a	40.640	63.887	310	37	125.0±3.9	129.4±11.8	53	12.9	1.3
UZ-29b	40.640	63.887	310	38	150.9±4.9	155.1±13.8	80	12.7	0.9
UZ-30	40.642	63.878	312	38	136.6±3.9	138.9±12.5	48	12.3	1.3
UZ-31	*40.665*	*63.846*	*322*	*35*	*153.8±7.6*	*152.3±10.2*	*31*	*12.5*	*1.1*
UZ-32	*40.802*	*63.594*	*409*	*28*	*180.0±9.5*	*178.4±17.8*	*33*	*12.2*	*1.0*
Aydar									
UZ-01	40.214	67.334	1092	33	83.2±6.0	84.7±6.9	46	12.4	1.8
UZ-24	*40.701*	*66.402*	*418*	*39*	*92.0±4.8*	*85.1±7.5*	*35*	*12.5*	*1.2*
UZ-25	40.724	66.099	455	35	92.6±3.8	93.4±8.3	94	12.6	1.1
Nurata Range									
UZ-02	*39.921*	*67.728*	*1012*	*28*	*114.5±9.2*	*133.1±12.6*	*35*	*13.5*	*1.3*
UZ-04	39.959	67.677	820	26	176.1±7.0	162.8±8.8	94	12.5	1.1
UZ-42	40.400	66.765	1019	31	151.7±8.5	148.8±14.1	82	12.6	1.2
UZ-43	*40.357*	*66.686*	*1050*	*34*	*112.1±4.6*	*107.6±6.9*	*37*	*13.1*	*1.1*
UZ-44	40.366	66.684	1095	42	152.0±8.4	136.0±19.5	46	13.0	1.1
UZ-45	*40.390*	*66.725*	*1291*	*43*	*149.0±7.4*	*140.6±13.4*	*22*	*13.0*	*1.2*

UZ-15	*40.530*	*65.628*	*578*	*40*	*139.7±6.9*	*131.4±11.2*	*35*	*13.0*	*1.3*
UZ-16a	40.428	65.239	572	39	152.0±9.6	141.6±12.3	66	12.8	1.1
UZ-16b	*40.428*	*65.239*	*572*	*37*	*163.3±8.0*	*156.3±13.6*	*35*	*12.4*	*1.0*
UZ-35	40.539	65.641	585	36	177.0±12.0	166.7±16.3	89	12.5	1.1
UZ-36	*40.560*	*65.669*	*506*	*38*	*160.0±10.0*	*152.7±13.6*	*38*	*13.0*	*1.3*
UZ-37	40.433	66.025	805	29	143.9±7.3	142.3±13.2	70	12.6	1.4
UZ-38	*40.404*	*65.970*	*1498*	*35*	*138.6±9.2*	*132.6±12.4*	*26*	*12.8*	*1.0*
UZ-39	40.401	66.005	1240	35	115.6±7.8	94.8±7.8	104	12.9	1.2
UZ-40	*40.417*	*66.005*	*1023*	*39*	*109.8±5.2*	*110.2±9.8*	*26*	*13.0*	*1.1*
UZ-41	*40.291*	*66.430*	*1125*	*42*	*131.1±5.4*	*133.8±12.0*	*35*	*12.9*	*1.0*
UZ-48	40.220	66.565	1009	33	134.1±9.6	140.0±9.4	44	12.9	1.1

Ziadin Mountains

UZ-11	39.683	65.988	559	38	156.0±7.7	139.1±12.5	95	13	0.9
UZ-12	39.742	65.978	708	41	154.2±6.3	150.3±12.8	55	13.2	1.1
UZ-13	39.689	65.807	572	29	150.9±6.6	139.1±8.4	44	12.3	1.0
UZ-14	*39.845*	*65.528*	*472*	*32*	*132.8±6.1*	*127.5±10.6*	*16*	*12.9*	*0.9*
UZ-50	39.997	65.431	615	27	141.4±6.6	129.1±11.0	144	13.2	1.0

Karatyube Massif

UZ-05	*39.435*	*67.043*	*923*	*31*	*177.0±11.0*	*167.5±10.4*	*37*	*12.7*	*1.0*
UZ-07	39.271	66.914	1206	41	124.2±3.4	121.6±6.1	71	12.5	1.2
UZ-08	*39.247*	*66.608*	*724*	*37*	*177.0±11.0*	*159.8±11.9*	*33*	*12.1*	*1.1*
UZ-09	*39.382*	*66.401*	*682*	*11*	*96.6±7.8*	*84.5±8.4*	*18*	*12.2*	*1.5*
UZ-10	39.499	66.628	911	29	56.1±4.0	52.8±5.9	93	12	1.5
UZ-49	39.309	66.524	890	36	130.3±4.4	126.4±7.5	66	12.4	1.4
GX-6	39.360	67.717	1752	36	29.5±1.8	30.0±2.4	-	-	-

4.1 Apatite Fission Track

4.1.1 Bukantau Mountains

The Bukantau Mountains is the northern-most extent of the Kyzylkum-Nurata Segment and lies directly on the margin of the Syr-Darya Block, and hosts the Teskuduk ophiolite complex of the South Tien Shan (Figure 3, Brookfield 2000, Dolgopolova et al. 2017). The Bukantau Mountains yielded the oldest AFT ages of all samples of the Kyzylkum-Nurata Segment, with the north-eastern samples UZ-19, UZ-22, and UZ-23 producing AFT central ages of 221 ± 9 Ma, 210 ± 8 Ma, and 228 ± 10 Ma, respectively. The samples of Triassic AFT age corresponded with long to moderate MTLs of 13.1 ± 1.0 μm, 12.8 ± 1.0 μm, 13.4 ± 1.1 μm, respectively. In the south-west of the Bukantau Mountains, samples UZ-18, UZ-20, and UZ-21 yield Jurassic and Cretaceous AFT ages of 154 ± 12 Ma, 124 ± 7 Ma, and 130 ± 4 Ma, and moderate MTLs of 12.8 ± 0.9 μm, 12.5 ± 0.9 μm, and 12.8 ± 1.2 μm, respectively (Figure 3, 5, and Table 1).

4.1.2 Kuldjuktau Mountains

The Kuldjuktau Mountains is the south-western most extent of both the Gissar and Zeravshan sutures, and represents the last set of outcrops of the South Tian Shan North of the Amu Darya Basin (Figure 3, Burtman 2000, McCann 2016a). Samples from the Kuldjuktau Mountains yielded Jurassic and Cretaceous AFT central ages. North of the Kuldjuktau Mountains, in the southern Tamdy mountains, sample UZ-26 yielded a Jurassic AFT central age of 178 ± 11 Ma, with a MTL of 11.6 ± 1.2 μm. The remaining samples formed a transect across several minor faults (Figure 5). Samples UZ-29b, UZ-31, UZ-32 yielded Jurassic AFT central ages of 151 ± 5 Ma, 154 ± 8 Ma, and 180 ± 10 Ma, respectively. The samples of Jurassic AFT age produced moderate to short MTLs of 12.7 ± 0.9 μm, 12.5 ± 1.1 μm, and 12.2 ± 1.0 μm, respectively. Samples UZ-28, UZ-29a, and UZ-30 yielded Cretaceous AFT central ages of 92 ± 12 Ma, 125 ± 4 Ma, and 137 ± 4 Ma, respectively. The Cretaceous-aged samples yielded both long and short MTLs of 11.9 ± 1.1 μm, 12.9 ± 1.3 μm, and 12.3 ± 1.3 μm, respectively Figure 3, 5 and Table 1).

4.1.3 Nurata Range

The Nurata Range is the main segment of the South Tian Shan Suture that crops out within Uzbekistan, which extends to the Turkistan-Alai Suture in Kyrgyzstan (De Grave et al. 2012, Dolgopolova

et al. 2017). The Nurata Range can be further divided into two subsets, the northern Nurata Range and the southern Nurata Range (Figure 3). In this study, four samples were taken along a transect in the core of the northern Nurata Range, and two samples from its extent into the Nurata-Turkestan-Alai region (Figure 1). The northern Nurata Range transect strikes from north-east (UZ-42) to south-west (UZ-43). Samples UZ-42, UZ-45, and UZ-44 yielded Jurassic AFT central ages of 152 ± 9 Ma, 155 ± 7 Ma, 152 ± 8 Ma, receptively. From the same transect, UZ-43 yielded a Cretaceous central age of 112 ± 5 Ma. The transect yielded long to moderate MTLs of 12.6 ± 1.2 μm, 13.0 ± 1.2 μm, and 13.0 ± 1.1 μm, respectively for the Jurassic samples, and 13.1 ± 1.1 μm for the Cretaceous samples. In the Turkestan-Alai segment, sample UZ-04 yielded a Jurassic AFT central age of 176 ± 7 Ma, and sample UZ-02 yielded a Cretaceous AFT central age of 115 ± 9 Ma, with MTLs of 13.5 ± 1.3 μm and 12.5 ± 1.1 μm, respectively (Figure 3, 5 and Table 1).

The southern section of the Nurata Range represents the inferred western extent of the Zeravshan suture, which formed due to the closure of the Vashan basin in the late Palaeozoic (Dolgopolova et al. 2017). Three samples were taken along the north-western extent, two samples were taken from the south-western extent, two samples were taken from the eastern extent, and one vertical profile of four samples were obtained from the core of the southern Nurata Range (Figure 3). Across the north-western extent, sample UZ-36, UZ-35, and UZ-15 produced AFT central ages of 160 ± 10 Ma, 177 ± 12 Ma, and 140 ± 7 Ma, with long to moderate MTLs of 13.0 ± 1.3 μm, 12.5 ± 1.1 μm, and 13.0 ± 1.3 μm, respectively. The two samples, UZ-16a and UZ-16b, from the south-western extent, yielded indistinguishable Jurassic AFT central ages of 152 ± 10 Ma and 163 ± 8 Ma, respectively. Samples UZ-16a and UZ-16b produced MTLs of 12.8 ± 1.1 μm and 12.4 ± 1.0 μm, respectively. The vertical profile in the core of the southern Nurata Range consists of four samples, from ~800m to ~1500m with a ~200m sample interval, with all samples returning Cretaceous AFT central ages and relatively long MTLs. At the base of the profile, sample UZ-37 (840m) yielded an age of 144 ± 7 Ma, sample UZ-40 (1010m) yielded an age of 140 ± 7 Ma, sample UZ-39 (1235m) yielded a major age peak of 116 ± 8 Ma, and sample UZ-38 (1520m) yielded an age of 139 ± 9 Ma. All four samples along the vertical profile returned similar long to moderate MTLs of 12.6 ± 1.4 μm, 13.0 ± 1.1 μm, 12.9 ± 1.2 μm, and 12.8 ± 1.0 μm, respectively. To the east of the southern Nurata Range, both UZ-41 and UZ-48 yielded Cretaceous AFT central ages of 131 ± 5 Ma and 134 ± 10 Ma, respectively, with these samples producing MTLs of 12.9 ± 1.0 μm and 12.9 ± 1.1 μm, respectively (Figure 3, 5 and Table 1).

4.1.4 Aydar

Samples from along the northern margin of the Nurata Range and the southern margin of the Aydar lake yield markedly different AFT ages compared to the rest of the Nurata Range (Figure 3). Three samples were collected from the boundary between the Nurata Range and the Aydar lake, samples UZ-25, UZ-24, and UZ-01. Samples UZ-25 and UZ-24 produced Cretaceous AFT central ages of 92 ± 5 Ma and 93 ± 4 Ma and moderate to short MTLs of 12.5 ± 1.2 μm and 12.6 ± 1.1 μm, respectively. To the east, sample UZ- 01 yielded a Cretaceous AFT central age of 83 ± 6 Ma and a MTL of 12.4 ± 1.8 μm (Figure 3, 5 and Table 1).

4.1.5 Ziadin Mountains

The Ziadin Mountains is the inferred western continuation of the Gissar suture outcropping in Uzbekistan, between the Kuldjuktau Mountains to the north-west and the Karatyube Massif to the south-east (Dolgopolova et al. 2017). Five samples were taken from the Ziadin Mountains along the Gissar suture. The three eastern samples, UZ-11, UZ-12, and UZ-13, all yielded similar Jurassic AFT central ages of 156 ± 8 Ma, 154 ± 6 Ma, and 151 ± 7 Ma, respectively. The samples of Jurassic age produced MTLs of 13.0 ± 0.9 μm, MTL of 13.2 ± 1.1 μm, and 12.3 ± 1.0 μm, respectively. The two western samples UZ-14 and UZ-50 both yielded Cretaceous AFT central ages of 133 ± 6 Ma, and 141 ± 7 Ma and long MTLs of 12.9 ± 0.9 μm and 13.2 ± 1.0 μm, respectively (Figure 3, 5 and Table 1).

4.1.6 Karatyube Massif

The large Karatybe Massif is located on the western termination of the Gissar range mountain range that largely crops out in Tajikistan (Konopelko et al. 2017a). The seven samples from the Karatyube Massif yielded a range of ages over the Mesozoic and Cenozoic, two produced Jurassic AFT central ages, three produced Cretaceous AFT central ages, and two produced Palaeogene AFT central ages. Samples UZ-05 and UZ-08 yielded identical ages of 177 ± 11 Ma, and both samples produced moderate to short MTLs of 12.7 ± 1.0 μm and 12.1 ± 1.1 μm, respectively. Three samples yielded a Cretaceous AFT central age; UZ-07, UZ-09, and UZ-49 yielded ages of 124 ± 3 Ma, 97 ± 8 Ma, and 130 ± 4 Ma, respectively. The Cretaceous ages were associated with short MTLs of 12.5 ± 1.2 μm, 12.2 ± 1.5 μm, and 12.4 ± 1.4 μm, respectively. The two Palaeogene AFT central ages identified in the Karatyube Massif are the youngest basement AFT ages for the entire Kyzylkum-Nurata Segment. Sample UZ-10

yielded an AFT central age of 56 ± 4 Ma, and sample Gx-6 yielded an age of 30 ± 2 Ma. Sample UZ-10 displayed a short MTL of 12.0 ± 1.5 μm. Sample Gx-6, despite being irradiated with ^{252}Cf to increase the number of confined tracks, did not produce enough tracks to produce a reliable MTL and length distribution (Figure 3, 5 and Table 1).

4.2 Apatite (U-Th-Sm)/He

Table 2: Apatite (U-Th-Sm)/He age and chemistry data. ^{232}Th, ^{238}U, and ^{147}Sm concentrations are in ng, He is the concentration of helium measured in ncc, Th/U is the ratio of thorium to uranium. Raw is the age before the *Ft* correction is made. *Ft* is the alpha-ejection correction parameter of Farley et al. (1996). Age is the age after applying the *Ft* correction, eU is the effective uranium concentration, and TAU is the total analytical uncertainty. Samples in italics represent grains that were excluded due to inclusions or poor quality.

Apatite (U-Th-Sm)/He data

Sample	^{232}Th	±(%)	^{238}U	±(%)	^{147}Sm	±(%)	He±(%)	TAU	eU	Th/U	Raw±1σ	F_T	Age±1σ
UZ-01-1	0.041	5.7	0.028	5.8	0.011	0.9	0.198±1.0	4.7	1.46	53.71	43.1±2.0	0.51	84.3±9.3
UZ-01-2	0.056	4.1	0.034	4.2	0.016	1.2	0.355±1.1	3.4	1.63	32.26	60.8±2.1	0.66	91.9±5.6
UZ-01-3	0.058	5.7	0.037	5.9	0.014	0.8	0.294±0.7	4.6	1.54	49.53	47.1±2.2	0.58	81.0±8.9
UZ-01-4	0.133	4.0	0.085	4.2	0.026	0.8	0.733±0.7	3.4	1.56	64.61	51.5±1.7	0.65	79.2±4.8
UZ-01-5	*0.085*	*4.0*	*0.055*	*4.2*	*0.022*	*0.4*	*0.607±0.8*	*3.4*	*1.52*	*55.73*	*65.6±2.2*	*0.64*	*103.2±6.2*
											UZ-01 Age±1σ= 84.1±7.1		
UZ-10-1	0.032	5.7	0.029	5.8	0.009	1.1	0.101±1.6	5.0	1.08	36.94	22.5±1.1	0.59	38.4±4.3
UZ-10-2	0.107	4.0	0.082	4.2	0.021	0.5	0.275±1.2	3.6	1.29	80.38	20.9±0.7	0.58	36.3±3.8
UZ-10-3	0.042	5.7	0.035	5.8	0.009	0.9	0.084±1.8	5.1	1.19	58.31	15.5±0.8	0.65	23.9±1.7
UZ-10-4	0.067	4.0	0.045	4.2	0.013	0.8	0.144±1.7	3.7	1.48	73.24	19.5±0.7	0.65	29.9±1.9
UZ-10-5	0.097	5.7	0.079	5.8	0.019	0.5	0.325±1.0	4.8	1.22	85.18	26.2±1.3	0.70	37.6±2.6
UZ-10-6	0.096	4.0	0.114	4.2	0.026	0.5	0.328±1.0	3.7	0.83	52.71	19.7±0.7	0.75	26.3±1.6
UZ-10-7	0.073	5.7	0.060	5.8	0.015	0.7	0.153±1.2	4.8	1.21	77.92	16.2±0.8	0.59	27.6±3.1
UZ-10-8	0.099	4.0	0.073	4.2	0.020	0.6	0.196±1.0	3.5	1.35	74.97	16.7±0.6	0.64	26.2±1.6
											UZ-10 Age±1σ= 30.8±2.6		
UZ-21-1	0.019	4.1	0.093	4.2	0.020	0.7	1.189±0.7	4.1	0.20	53.52	99.4±4.1	0.75	132.5±8.6
UZ-21-2	0.025	5.7	0.123	5.8	0.034	0.6	1.440±0.7	5.6	0.20	49.13	90.5±5.1	0.73	123.7±9.3

UZ-21-3	*0.069*	*12.8*	*0.720*	*5.8*	*0.062*	*0.6*	*13.131±0.7*	*5.7*	*0.10*	*137.53*	*144.6±8.3*	*0.80*	*180.1±13.7*
UZ-21-4	*0.043*	*14.8*	*0.193*	*4.2*	*0.036*	*0.6*	*4.621±0.8*	*4.1*	*0.22*	*70.10*	*183.6±7.5*	*0.75*	*244.6±15.8*
UZ-21-5	*0.024*	*14.2*	*0.077*	*5.8*	*0.018*	*0.7*	*1.290±0.9*	*5.5*	*0.31*	*48.91*	*126.3±6.9*	*0.71*	*179.1±13.3*
UZ-21-6	*0.007*	*6.7*	*0.052*	*4.2*	*0.012*	*0.6*	*0.892±0.9*	*4.2*	*0.13*	*52.87*	*135.8±5.7*	*0.69*	*195.7±12.8*

UZ-21 Age±1σ= 128.1±8.9

UZ-25-1	0.005	5.8	0.018	5.8	0.005	1.1	0.143±1.4	5.7	0.27	29.54	60.5±3.4	0.61	98.8±7.5
UZ-25-2	0.005	5.8	0.092	5.8	0.011	0.8	0.749±0.9	5.8	0.06	57.68	65.5±3.8	0.71	91.8±7.0
UZ-25-3	0.010	5.8	0.018	5.8	0.008	0.9	0.144±1.3	5.3	0.57	15.28	59.1±3.2	0.68	86.6±6.3
UZ-25-4	0.007	4.4	0.056	4.2	0.007	0.9	0.451±0.8	4.2	0.13	53.11	64±2.7	0.63	101.6±6.6
UZ-25-5	*0.009*	*4.3*	*0.095*	*4.2*	*0.020*	*0.5*	*1.028±0.8*	*4.2*	*0.10*	*35.33*	*85.9±3.6*	*0.75*	*114.8±7.5*
UZ-25-6	*0.015*	*4.1*	*0.099*	*4.2*	*0.022*	*0.6*	*1.089±0.7*	*4.1*	*0.15*	*32.61*	*86.7±3.6*	*0.74*	*117.0±7.6*
UZ-25-7	*0.037*	*5.7*	*0.039*	*5.8*	*0.011*	*0.6*	*0.765±0.8*	*4.9*	*0.96*	*17.76*	*130.2±6.4*	*0.74*	*176.4±12.4*
UZ-25-8	*0.016*	*4.1*	*0.064*	*4.2*	*0.009*	*0.9*	*0.730±0.7*	*4.0*	*0.26*	*50.75*	*88.2±3.5*	*0.66*	*134.5±8.6*

UZ-25 Age±1σ= 94.7±6.9

UZ-39-1	0.015	5.7	0.721	5.8	0.035	0.5	9.921±0.6	5.8	0.02	192.65	111.4±6.5	0.78	142.8±11.0
UZ-39-2	0.013	4.2	0.394	4.2	0.021	0.6	5.436±0.8	4.2	0.03	159.96	111.3±4.7	0.73	151.9±10.0
UZ-39-3	0.021	5.7	0.328	5.8	0.024	0.6	4.640±0.6	5.8	0.06	140.20	113.2±6.5	0.76	148.3±11.3
UZ-39-4	0.027	4.1	0.329	4.2	0.032	0.6	4.169±0.7	4.2	0.08	86.84	101.1±4.2	0.78	129.3±8.4
UZ-39-5	0.020	5.7	0.298	5.8	0.034	0.6	4.200±0.7	5.8	0.06	66.99	112.7±6.5	0.73	154.1±11.8
UZ-39-6	0.028	4.1	0.509	4.2	0.054	0.6	5.899±0.6	4.2	0.05	83.86	93.1±3.9	0.82	114.0±7.4
UZ-39-7	*0.008*	*5.7*	*0.202*	*5.8*	*0.013*	*0.5*	*4.691±0.7*	*5.8*	*0.04*	*115.60*	*185.4±10.7*	*0.71*	*262.9±20.1*

UZ-39 Age±1σ= 140.9±10.0

UZ-43-1	0.062	5.7	0.069	5.8	0.009	0.6	0.988±0.8	5.0	0.89	31.85	96.1±4.8	0.75	128.1±9.0
UZ-43-2	0.059	4.1	0.047	4.2	0.015	0.7	0.582±0.8	3.5	1.23	44.56	77.8±2.7	0.69	112.4±6.8
UZ-43-3	0.171	5.7	0.142	5.8	0.054	0.4	1.928±0.7	4.7	1.19	101.75	86.3±4.1	0.71	122.4±8.4
UZ-43-4	0.041	4.1	0.043	4.2	0.015	0.7	0.477±0.8	3.6	0.97	40.10	74.4±2.7	0.65	113.9±7.0
UZ-43-5	*0.048*	*5.7*	*0.045*	*5.8*	*0.020*	*0.6*	*0.333±1.1*	*4.9*	*1.06*	*33.62*	*48.1±2.4*	*0.67*	*71.6±5.0*
UZ-43-6	*0.202*	*4.0*	*0.137*	*4.2*	*0.046*	*0.5*	*2.406±0.8*	*3.4*	*1.47*	*89.85*	*106.0±3.6*	*0.73*	*144.8±8.7*

UZ-43 Age±1σ= 119.2±7.8

Six samples were selected for AHe analysis (Table 2). Samples that produced young AFT ages and relatively long MTLs were prioritised in order to better constrain the Cretaceous–Cenozoic phase of cooling experienced by the Kyzylkum-Nurata Segment. In the Bukantau Mountains, sample UZ-21 yielded a Cretaceous AHe age of 128 ± 9 Ma, which overlaps with the AFT central age from sample UZ-21 of 130 ± 4 Ma (Table 1 and 2). For the Nurata Range, one sample was selected from the northern area and one sample was selected from the southern area. Sample UZ-43 yielded an AHe age of 119 ± 8 Ma, which is within error with its respective AFT age (AFT central age of 112 ± 5 Ma, Table 1 and 2). In the southern Nurata Range, sample UZ-39 produced an AHe age of 141 ± 10 Ma with significant single-grain age scatter. Compared to the AFT age for this sample (99 Ma central age, 116 Ma oldest age peak), the AHe age is significantly older. This discrepancy may be explained by the anomalously high eU (effective uranium, Table 2). However, the AHe age is in excellent agreement with the other samples in the vertical profile (AFT age range ~140–110 Ma, Table 1 and 4.2, Supplementary File 1). Two samples from the Aydar – Nurata Range margin were selected for AHe analysis; UZ-01 (AFT central age of 83 ± 6 Ma) yielded an AHe age of 84 ± 7 and UZ-25 (AFT central age of 93 ± 4 Ma) yielded an AHe age of 95 ± 7 Ma. Both AHe ages from the Aydar area were thus, in excellent agreement with their respective AFT age (Table 1 and 2). Sample UZ-10 (AFT central age of 56 ± 4 Ma) from the Karatyube Massif yielded an AHe age of 31 ± 3 Ma (Table 1). Although, the ages produced by the AFT and AHe thermochronometers do not overlap, the presence of a young ~30 Ma AHe age combined with the regionally proximal ~30 Ma AFT central age for sample Gx-6, does suggest the presence of a Eocene–Oligocene cooling signal in the south-eastern end of the Kyzylkum-Nurata Segment (Figure 3 and Table 2).

4.3 Thermal History Modelling

Thermal history modelling was conducted for thirty-nine samples. Models that are based on less than 40 confined tracks are thought to be less accurate and are, therefore, drawn as dashed lines in the thermal history modelling figures (Figure 4 and Table 1). All models were constrained to start at temperatures greater than the APAZ (>120°C ± 20°C). For all samples the AFT annealing model Ketcham et al. (2007) was used. In addition, apatite helium data were integrated into relevant thermal models, using the He radiation damage model of Gautheron et al. (2009). Individual models, confined track distributions, and modelling parameters are available in Figure 4 and Supplementary Files 3, and 4 (following Flowers et al. 2015).

The thermal models produced two distinct Mesozoic and Cenozoic thermal histories. The six regions identified in the results can, therefore, be further subdivided into two tectonic groups with discrete thermal evolutions. The first group can be identified by samples that were taken in close proximity to relict suture zones, comprising of the the Nurata Range and the Ziadin Mountains. The second group is identified by samples that were taken from regions that were distal to the main suture zones, the Kuldjuktau Mountains, the Bukantau Mountains, the Aydar area, and the Karatyube Massif (Figure 4).

4.3.1 Tectonic Group One: Near Major Structures

For the Nurata Range, sixteen samples were modelled (five from the northern and eleven from the southern range). Samples UZ-43 and UZ-39 were constrained using additional AHe data (Table 2). The models show rapid cooling in the Late Triassic–Early Jurassic (~210–180 Ma), slower cooling in the Jurassic (~180–150 Ma), faster cooling in the Late Jurassic–Early Cretaceous (~150–120 Ma), and slow cooling in the middle to Late Cretaceous (~120-100 Ma, Figure 4a). Five thermal history models were obtained from the Ziadin Mountains in southern Uzbekistan. No additional constraints were placed on any of the five thermal history models. All five thermal history models identified relatively rapid cooling during the Late Jurassic–Early Cretaceous (~160–130 Ma). The thermal evolution for the regions that comprise Tectonic Group One preserve two pulses of relatively rapid cooling during (1) the Late Triassic–Early Jurassic (~210–180 Ma) and (2) the Late Jurassic–Early Cretaceous (~160–130 Ma, Figure 4).

4.3.2 Tectonic Group Two

Thermal history modelling was performed on seven samples from the Kuldjuktau Mountains. There were no AHe or additional data, all seven models were allowed to run unconstrained. The Kuldjuktau Mountains displays a broad range of thermal histories dominated by slow cooling throughout the Mesozoic from ~220 Ma to ~110 Ma. However, one sample displays a variation from the theme of slow cooling, UZ-29b, which shows rapid cooling at ~170 Ma (Figure 4c).

For the Aydar region, thermal history models were produced for all three samples. Two of the three samples had corresponding AHe data which was used by each respective model (Table 2 and Supplementary File 3 and 4). All three samples produced Late Cretaceous AFT ages, with two samples

modelling relatively fast cooling through the APAZ at ~110–90 Ma. In contrast, sample UZ-01 displays protracted cooling throughout the Late Cretaceous (Figure 4d).

Thermal history modelling was performed on five samples from the Karatyube Massif, with one sample modelled with its respective AHe data. The four thermal history models without AHe constraints all produced slow cooling thermal histories, entering the upper APAZ in the Early Jurassic and cooling to below the APAZ in the mid-Cretaceous. Two samples which produced thermal histories with an extended residence in the APAZ during the Late Jurassic–Early Cretaceous (Figure 4e). The Palaeogene sample, UZ-10, demonstrates a relatively rapid rate of cooling at ~50 Ma. After exiting the APAZ, sample UZ-10 shows a deviation in its thermal history model, constrained by the AHe data obtained for that sample at ~30 Ma, before cooling to surface temperatures at ~15 Ma (Figure 4e and 5, and Supplementary File 3).

Five samples from the Bukantau Mountains were suitable for modelling. Four of the five thermal history models were run without additional AHe constraints, with one sample constrained by Cretaceous AHe data (UZ-21). The thermal history models for the Bukantau Mountains record a dominant rapid Triassic cooling signal (~220–200 Ma) while also displaying a period of rapid cooling in the Late Jurassic (~140 Ma), and a period of relatively slow cooling in the Late Cretaceous (~110 Ma, Figure 4f).

The thermal evolution for the regions that comprise Tectonic Group Two is generally defined by slow cooling throughout the Jurassic and Cretaceous–early Palaeogene, excluding a few samples which demonstrate faster cooling. In addition, the thermal model for one sample (UZ-10), shows evidence for renewed cooling in the late Palaeogene (Figure 4c, 4d, 4e, and 4f).

5 Interpretation and Discussion

The results of this study reveal that the Kyzylkum-Nurata Segment, and the relict suture zones that it hosts, underwent a multi-phase cooling history during the Mesozoic and Cenozoic.

5.1 Mesozoic and Cenozoic Thermal History and Control of the Suture Zones

The Kyzylkum-Nurata Segment is dominated by three relict suture zones, the South Tian Shan Suture in the north, the Zeravshan suture in the centre, and the Gissar suture to the south (Figure 5, Burtman

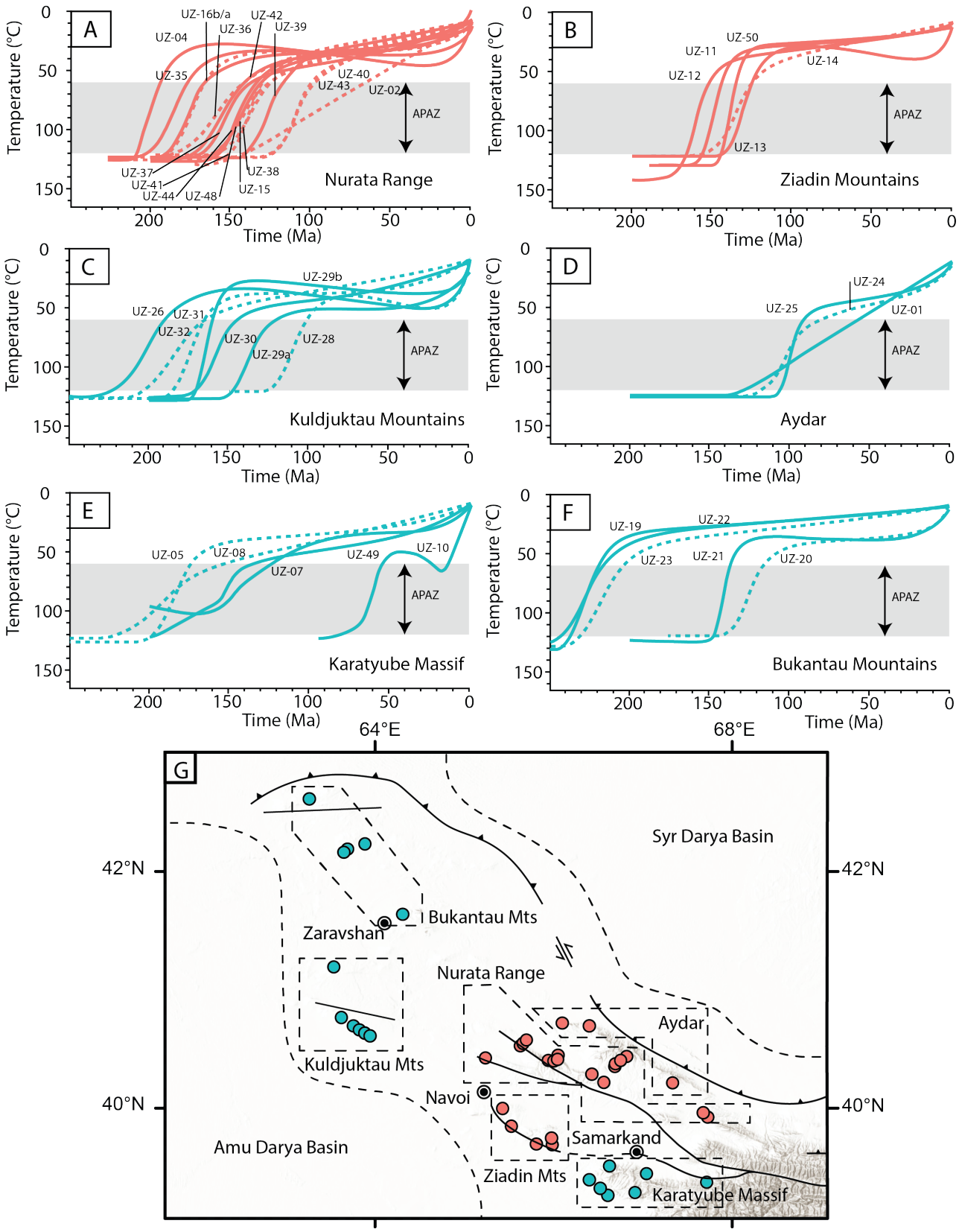

Figure 4: Caption next page

Figure 4: Plots displaying the modelled temperature-time paths for all samples within the Kyzylkum-Nurata Segment that yielded sufficient confined track data for modelling purposes (>40). Modelling was performed using QTQt Gallagher (2012), with the bold and dashed lines representing the expected temperature-time pathway modelled. Apatite (U-Th-Sm)/He data was used to refine the thermal models where appropriate (see thermal model section). The thermal history models are grouped in their corresponding region; with associated sample location inset (g). Bold lines represent thermal history models from samples which contained at least 40 confined tracks, with dashed lines representing thermal history models from samples which contained between 40 and 25 confined tracks. The grey bar represents the apatite partial annealing zone (APAZ) between 120°C and 60°C. For detailed individual thermal history models and modelling parameters see Supplementary File 3 and 4)

1975, Konopelko et al. 2017a). These three sutures are the dominant control on the current topography of the Kyzylkum-Nurata Segment, as most of the ranges and outcropping rocks either lie on, or along strike of, each of the suture zones (Figure 5, Dolgopolova et al. 2017). In order to evaluate the control of these suture zones on the Mesozoic topography, Figure 5 was produced to plot the geospatial location of the confined track MTL for each analysed samples. Longer MTL values correspond to faster cooling (as shown in the thermal history models of Figure 4) and show a close relationship with the samples in close vicinity to the sutures (Figure 5).

The Nurata Range strikes along the Zeravshan suture and is dominated by long MTLs and fast cooling during the Late Jurassic–Early Cretaceous. In contrast, the Kuldjuktau Mountains, which is located to the south of the western extent of the Zeravshan suture, is characterised by mostly slow cooling during the Late Jurassic–Early Cretaceous and exhibits associated short MTLs (Figures 4.4 and 4.5). This pattern suggests that the Nurata Range was exhumed in the Early Cretaceous, controlled by the reactivation of the Zeravshan suture. At the northern slopes of the Nurata Range, in the Aydar region, the thermal history models show a mixture between relatively fast, Late Cretaceous cooling, and slow, protracted cooling (Figure 4d). Here, the AFT ages are younger (Late Cretaceous) and the associated MTLs are shorter on average and show broad distributions (Figures 4.3 and 4.5). This suggests that the AFT ages of the Aydar region may represent mixing ages between two thermal events that are not clearly identified by the thermal history modelling. The Aydar samples are in relatively close vicinity to the South Tian Shan Suture, which has been reactivated in the Cenozoic (e.g. Glorie et al. 2011, Käßner et al. 2017b), and therefore, the AFT ages may have been affected by this reactivation event.

The Bukantau Mountains preserve Early Triassic rapid cooling in the north-east and rapid Early Cretaceous cooling the south-west, suggesting that the Cretaceous fault reactivation seen in the Nurata Range also affected the Bukantau Mountains (Figures 4.3, 4.4, and 4.5). However, given that Early

Triassic AFT cooling ages are preserved in the region, the oldest preserved cooling signal identified in the Kyzylkum-Nurata Segment, the area would have not been extensively affected by the Cretaceous deformation and exhumation.

In the south of the Kyzylkum-Nurata Segment, along the Gissar suture, there is a section displaying fast cooling (Ziadin Mountains), and a section displaying slow cooling (Karatyube Massif, Figure 5). In more detail, samples taken from along a granitoid pluton to the south of the Gissar suture (UZ-08, UZ-09, and UZ-49) display a mixed series of ages from Jurassic to Late Cretaceous along with slow cooling models and relatively short MTLs (Figures 4.3, 4.4, and 4.5). In contrast, samples taken to the north of the Gissar suture, within the Ziadin Mountains, display fast cooling during the Early Cretaceous and associated with long MTLs (Figures 4.4 and 4.5). The differential record of cooling ages on either side of the suture suggests that the suture was reactivated in the Early Cretaceous, leading to the rapidly cooled AFT ages and long MTLs observed in the Ziadin Mountains. Within the suture and particularly in the high relief areas of the Karatyube Massif, Palaeogene AFT and AHe ages, and fast cooling models were obtained, suggesting that the eastern extent of the suture was reactivated during the Cenozoic (Figure 5).

In summary, the Kyzylkum-Nurata Segment records a clear spatial relationship between MTLs and their associated thermal history models, and proximity to a major suture zone. Samples that were taken from ranges and outcrops that lie directly along the suture zones display a different thermal history from samples that were taken from the suture zone peripheries (Figure 4). This implies that the main NW–SE striking suture zones were reactivated during the Early Cretaceous. Therefore, the Early Cretaceous topography was likely characterised by a series of linear NW-SE striking ridges that built on the reactivated fault zones.

5.2 AFT Age-Confined Track Length Plot

In order to further distinguish periods of tectonic reactivation and exhumation (fast cooling) from periods of erosion and peneplanation (slow cooling), the mean track length for each sample was plotted against its respective age (Figure 6). Called a “boomerang plot”, this plot demonstrates the relationship between AFT ages and MTL for a set of samples from a region which has likely experienced a multiple thermo-tectonic events (Green 1986, Gallagher & Brown 1997, Gallagher et al. 1998). In such a plot for the Kyzylkum-Nurata Segment, a characteristic “boomerang” trend can be identified, the descending segment defined by comprise Tectonic Group Two samples with Triassic-Early Jurassic AFT ages and

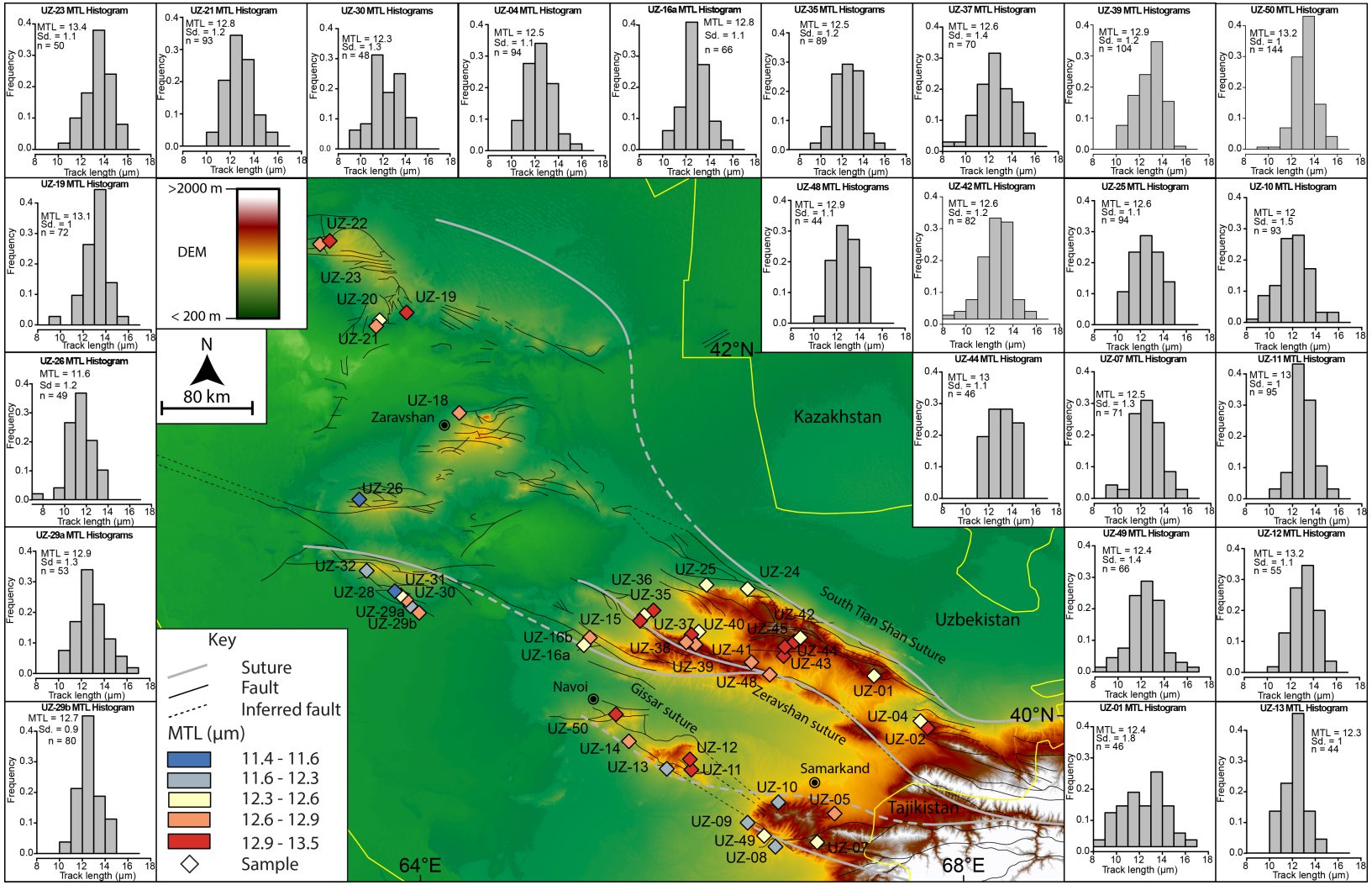

Figure 5: Digital elevation map (DEM) of the Kyzylkum-Nurata Segment outlining both the major faults and major sutures (from Survey 2012, Dolgopolova et al. 2017), as well as confined track histograms for modelled samples. The map displays the mean track length (MTL) in μm obtained for each sample with red representing long MTLs, and blue representing short MTLs. In the histograms, Sd. is the standard deviation in μm, and n is the number of confined tracks measured for that sample.

the ascending segment defined by published data from the proximal, high elevation (>2km) region of the Gissar Range (Käßner et al. 2017b).

In more detail, Tectonic Group Two demonstrates that the Kyzylkum-Nurata Segment experienced a partial 'boomerang' in the Mesozoic, beginning with fast cooling in the Late Triassic–Early Jurassic (~220–180 Ma), followed by a protracted period of thermal stability, defined by short MTLs, from the Early Jurassic to the Late Cretaceous (~200-50 Ma, blue symbols in Figure 6). Within this period of thermal stability, the data is rather scattered by may hint to a gentle increase of MTLs and cooling rate during the Early Cretaceous. The fast-cooling Cenozoic AFT data from the Gissar Range, identified by Käßner et al. (2017b), compliments the Mesozoic data obtained in this study, defining the Cenozoic segment to complete the Mesozoic–Cenozoic MTL boomerang (~50–5 Ma, black symbols in Figure 6).

In contrast to the complete boomerang recorded by Tectonic Group Two and the published data (Käßner et al. 2017b), samples from Tectonic Group One record a distinct period of rapid cooling during the Late Jurassic–Early Cretaceous (~160–130 Ma, red symbols in Figure 6). The samples that comprise Tectonic Group One were sampled either directly or proximal to the major structures of the South Tian Shan and Zeravshan sutures, further highlighting that these suture zones were affected by a secondary phase of exhumation that is only slightly recorded further away from these structures (Figure 5 and 6).

The interpretation of two discrete thermo-tectonic histories for the Kyzylkum-Nurata Segment can also be identified when comparing the sample elevation to its relative AFT age (Figure 7). The age-elevation plot reveals a clear trend of increasing AFT ages with increasing elevation (Figure 7). The oldest samples (Triassic) in the Kyzylkum-Nurata Segment are found at the lowest elevation (~200 m). The relationship between age and elevation for Group One and Two diverge in the Jurassic–Cretaceous. In this time period, samples from Group Two (away from the sutures) show significant scatter and a large variation in AFT age at a given elevation, implying slow cooling and thus, a prolonged residence in the APAZ. In contrast, samples from Group One show a strong linear trend of increasing age with elevation during the Late Jurassic–Early Cretaceous.

Combined, both Tectonic Group One and Two chart the thermal evolution of the Kyzylkum-Nurata Segment (Figure 6). Although classified as Tectonic Group One, the Bukantau Mountains along the Southern Tian Shan Suture displays a similarity to both Tectonic Group One and Two. The Bukantau Mountains hosts low relief and old ages, synonymous with the regions that define Tectonic Group

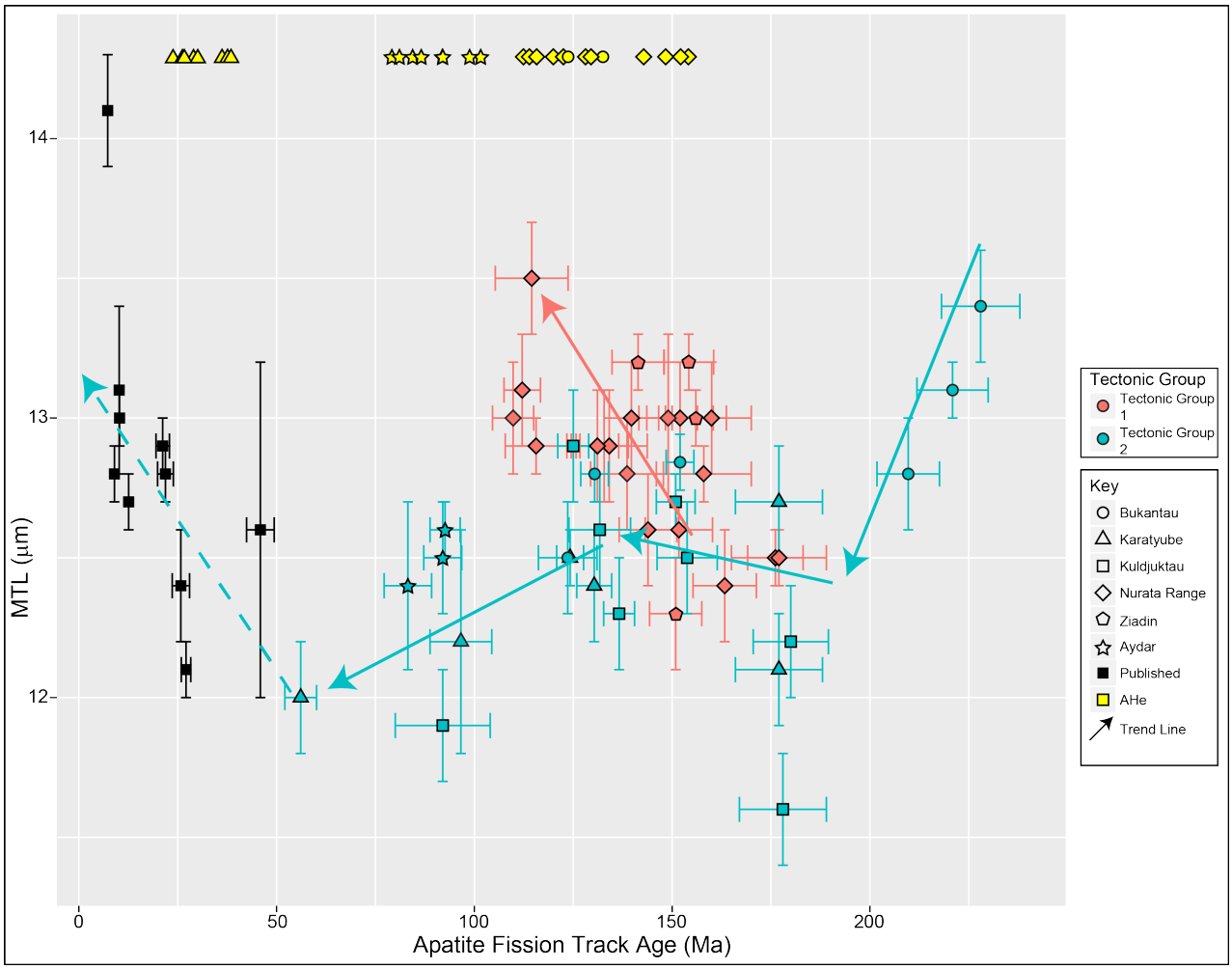

Figure 6: A 'boomerang' plot displaying apatite fission track (AFT) central age, and apatite (U-Th-Sm)/He (AHe) ages against mean track lengths (MTL, Table 1 and 2). Red filled symbols represent samples that correspond to Tectonic Group One and blue filled symbols represent samples that correspond to Tectonic Group Two. Black filled samples are AFT and MTL data obtained from the nearby Gissar Range (Käßner et al. 2017b). The solid arrows outline the thermal pathways defined in this study, and the dashed arrows outline a thermal pathway inferred from this study and the data from Käßner et al. (2017b).

Two. However, it also hosts fast, suture zone cooling that is characteristic of the regions that comprise Tectonic Group One. As this region shows similarities of both groups, it is reasonable to suggest that the Bukantau Mountains hosts the thermo-tectonic relic of the ancestral Tian Shan which the modern Tian Shan is built upon. Away from the main suture zones, in low-relief areas, the Kyzylkum-Nurata Segment records slow cooling and erosion throughout the Mesozoic, since the Late Triassic (~220 Ma). In the main suture zone, a second phase of rapid uplift and fast cooling has been identified in the Early Cretaceous, overprinting the ancestral Tian Shan thermal history of regional slow cooling (Figure 4 and 5, De Grave et al. 2012). Finally, the Karatyube Massif and Aydar regions of the Kyzylkum-Nurata Segment host samples that document the transition between the Jurassic–Cretaceous thermal history, and the rapid Cenozoic deformation identified elsewhere in the South Tian Shan (Figure 6).

5.3 Thermotectonic evolution of the Kyzylkum-Nurata Region

5.3.1 Triassic Exhumation

The Kyzylkum-Nurata Segment, hosts three samples which produced a Triassic AFT central age. All three are located in the north-western region of the Bukantau Mountains on the margin of the Syr Darya Basin (Figure 3). The three samples yielded central ages of ~230-210 Ma, and were associated with relatively long MTLs and thermal history models showing fast cooling (Figure 4). A recent study by Dolgopolova et al. (2017) into the emplacement age and origin of the Kyzylkum-Nurata Segment magmatism, found that all granitoid samples (including a sample from the same region in the Bukantau Mountains) exhibited Permian ages of ~293–273 Ma. The difference in the zircon uranium-lead (ZrUPb) age and the fast cooling, Triassic AFT central ages, suggest that following emplacement, the Kyzylkum-Nurata Segment experienced steady, post-emplacement magmatic cooling. A similar relationship between the Triassic Tian Shan thermochronology and the Syr Darya block has also been found in the Chatkal-Kurama range in the western Tian Shan, with fast cooling Triassic AFT ages identified on the Chatkal-Kurama–Syr Darya margin.

Previous thermchonological studies in the Tian Shan ascribe Triassic–Early Jurassic AFT ages to the closure of the Turkestan Ocean in the Permian and the subsequent collision of the Qiangtang Block with the Eurasian margin (e.g. Xiao et al. 2009, Glorie et al. 2010, De Grave et al. 2011, Macaulay et al. 2014, Glorie & De Grave 2016). During this period, samples from along the north-western margin of the Kyzylkum-Nurata Segment were rapidly cooled to surface temperatures (Figure 4c). Thus, we

interpret the Triassic fast cooling signal in our data to be related with exhumation associated with the closure of the Turkestan Ocean and/or the Qiangtang convergence in the Triassic–Early Jurassic.

5.3.2 Jurassic–Cretaceous Regional Tectonic Stability and Peneplanation

The Jurassic-Cretaceous thermo-tectonic evolution of the Kyzylkum-Nurata Segment is defined by two discrete trends outlined by the "boomerang plot" (Figure 6); one profile demonstrating thermo-tectonic stability, and one profile demonstrating an increased basement cooling via exhumation. The samples that comprise Tectonic Group Two record a regional trend of tectonic stability and pleneplanation.
A series of samples from across the Kyzylkum-Nurata Segment yielded Early to Middle Jurassic AFT central ages (Figure 2). The Early to Middle Jurassic AFT ages were largely associated with low MTLs, and the associated thermal history models showing slow cooling (Figures 4.4 and 4.5). These data are indicative of protracted residence in the APAZ, suggesting a period of steady, slow denudation and tectonic quiescence at that time. A recent study into the lowest part of the Mesozoic cover of the Kyzylkum-Nurata Segment by McCann (2016b) identified the presence of Lower Jurassic alluvial-fan, river valley, lagoonal, and shallow marine sedimentation (distinct absence of Triassic sedimentation). The source of the sedimentation is assessed as derived from the weathering and erosion of the recently uplifted Kyzylkum-Nurata Segment (McCann 2016b). This conclusion fits with the Triassic exhumation identified in this study, indicating that the Triassic exhumation provided the source that underwent subsequent erosion and sedimentary deposition in the Kyzylkum-Nurata Segment during the Jurassic.

During the Jurassic, the greater western Tian Shan experienced periodic marine incursions by the Paratethys Sea into the Amu Darya, Tajik, Fergana, and Tarim basins (Bosboom et al. 2011, 2014, Bande et al. 2017b, De Pelsmaeker et al. 2018). The series of marine incursions by the Paratethys Sea to the western Tian Shan indicates that there was a period of tectonic stability, erosion, and sedimentation experienced by the Kyzylkum-Nurata Segment during the Jurassic (Figure 7).

5.3.3 Localised Late Jurassic to Early Cretaceous Exhumation

In contrast to the regional tectonic stability, defined by samples from Tectonic Group Two, samples taken in vicinity of the faults (Tectonic Group One) record rapid basement cooling and exhumation during the Late Jurassic–Early Cretaceous. During the Late Jurassic–Early Cretaceous, the sutures of the Kyzylkum-Nurata Segment underwent a period of exhumation, deformation, and mountain building.

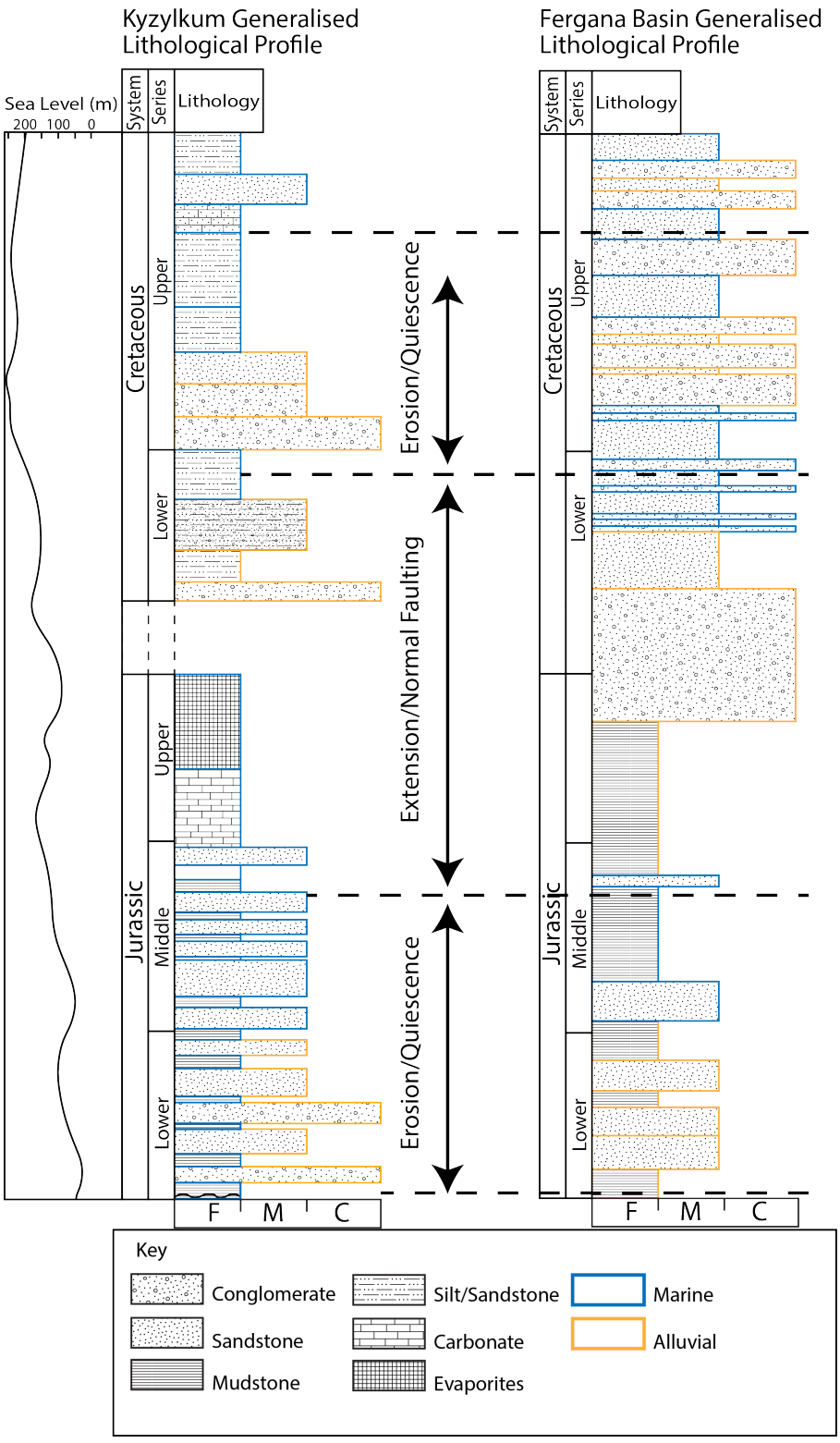

Figure 7: Generalised lithological profiles for both the Kyzylkum (McCann 2016a,b), and the nearby Fergana Basin (De Pelsmaeker et al. 2018), as well as the global eustasy for the Jurassic and Cretaceous (Haq et al. 1987). Compared against the relationship between the apatite fission track (AFT) age and mean track length (MTL) of samples from the Kyzylkum-Nurata Segment in order to identify periods of uplift, erosion, and tectonic stability. Sediment grain size is defined by fine (F), medium (M), or coarse (C).

This period of deformation and reactivation is evidenced by samples with overlapping closure temperatures, long MTLs, and rapid cooling thermal history models (Figure 6). Recent thermochronological studies on the basement of the proximal Gissar Range by Käßner et al. (2017b) and Käßner et al. (2017a) also identified the presence of a Late Jurassic–Early Cretaceous cooling signal, however, this signal was largely obscured due to a prolific Cenozoic thermal overprint (e.g. Bande et al. 2017b, Käßner et al. 2017b,a, Jepson et al. 2018). The basement outcrops in the Kyzylkum-Nurata Segment preserve this Cretaceous cooling event, as the faults and ranges have been sheltered from the major impacts of subsequent Mesozoic–Cenozoic collisions, further evidenced work by De Pelsmaeker et al. (2018) indicating that Talas-Fergana Fault (Figure 1) acted as a barrier to the strain that was being experienced by the Tian Shan east of the Talas-Fergana Fault.

The Mesozoic sedimentary record in the Kyzylkum desert identified by McCann (2016a,b) and simplified in Figure 7, shows a period of marine incursion depositing a carbonate layer, transitioning into a salt dominated layer, before a distinct hiatus and subsequent coarse clastic sedimentation at the start of the Early Cretaceous. The marine sediment transition and unconformity could represent a response to exhumation along the Kyzylkum-Nurata Segment, leading to a lack of sedimentation during the Early Cretaceous. At the same time, in the Fergana Basin, thick packages of coarse alluvial sediments were being deposited, indicating that some of the coarse sediment preserved in the Fergana Basin could have been sourced from the exhumed Kyzylkum-Nurata Segment (Figure 7).

To the east of the Kyzylkum-Nurata Segment, in the Kyrgyz Tian Shan, other geo- and thermochronological studies have identified Late Jurassic–Early Cretaceous exhumation. Nachtergaele et al. (2017) and De Pelsmaeker et al. (2018) found that the areas to the east of the Talas–Fergana fault underwent rapid Early Cretaceous basement cooling, and that the fault acted as a structural divide between the Cretaceous exhumed Tian Shan to the east and the Paratethys Ocean to the west. The Late Jurassic–Early Cretaceous thermochronological signal has previously been interpreted as a relic of the Cimmearan collisions that drove much of the deformation in the Middle Tian Shan (De Grave et al. 2007, Glorie & De Grave 2016, Käßner et al. 2017a, Nachtergaele et al. 2017). Given that the exhumation at the time was solely focused on suture zones within the Kyzylkum-Nurata Segment, it may be more likely that the suture zones were reactivated by an extensional tectonic event. Stockli et al. (2002) demonstrated that extension and associated rapid footwall exhumation can result in (tilted) sections where samples record rapid localised cooling, without the need for voluminous denudation.

Recent geodynamic models by Hall (2012) and Zahirovic et al. (2016) have suggested that the southern Eurasia margin was undergoing slab rollback related extension during the mid-Cretaceous (~155 Ma), which could have been a possible mechanism for footwall exhumation and basement cooling identified in the sampled suture zones. Therefore, we envisage the Cretaceous Tian Shan landscape and deformation style to be comparable to the present-day Basin and Range province in the south-western USA.

5.3.4 Late Cretaceous to Early Palaeogene Tectonic Stability and Denudation

From the mid Cretaceous to the early Palaeogene, the low-temperature thermochronology of the Kyzylkum-Nurata Segment shows a decline in fast cooling and exhumation, and thus, transitioning into a period of slow cooling and erosion, with distinct absence of thermochronology data from ~80–50 Ma (Figure 6). Similarly, in the Gissar Range, Käßner et al. (2017b) also identifies a period of Late Jurassic to Oligocene quiescence from ~150 to 25 Ma.

McCann (2016a) identified the presence of Cretaceous sedimentation from the Albian to the Maastrichian in fluvial and shallow marine environments indicative of a coastal-marine transitional zone. During the Late Cretaceous the Kyzylkum-Nurata Segment experienced coastline change due to major marine incursions, with much of the material for sedimentation coming from the Late Jurassic-Early Cretaceous exhumed regions in the Kyzylkum-Nurata Segment (Figure 7). The sedimentary evidence, in conjunction with the thermochronological data provided in this paper, suggest that the Kyzylkum-Nurata Segment experienced a period of erosion and denudation causing sedimentation during the Late Cretaceous–early Palaeogene (McCann 2016a).

The Late Cretaceous stability is contrasted by samples of the Aydar region, close to the South Tian Shan suture, which display over-lapping AFT and AHe thermochronometers (Figure 5 and 6, Tables 1 and 2). McCann (2016a) found that the northern and southern extents experienced a phase of terrestrial sedimentation during the Upper Cretaceous. The terrestrial sedimentation and over-lapping thermochronometers implies that the margins of the Northern Nurata Range experienced some degree of exhumation during the Late Cretaceous. Although, it is likely that the Cretaceous AFT and AHe ages represent mixing ages between the Early Cretaceous and late Palaeogene thermal events.

5.3.5 Palaeogene Reactivation

During the Palaeogene, the Eurasian continent was redeformed as a result of the collision of India with Eurasia (e.g. Beck et al. 1995, Aitchison et al. 2007, Najman et al. 2010, van Hinsbergen et al. 2011). In the Kyzylkum-Nurata Segment we identify only a minor thermochronological response to this collision in the Karatyube Massif, proximal to the high elevation Gissar Range (Figure 3). In addition, it is possible that the presence of mixing ages in the Aydar region may also be an indicator of Palaeogene thermal activity, as explained above. Given the lack of relief within the Kyzylkum-Nurata Segment, the thermo-tectonic response to the India–Eurasia collision has not been exhumed to the surface yet.

In the South Tian Shan, numerous thermochronological studies report Palaeogene and Neogene ages that correspond with the collision and ongoing indenture of the Indian continent with Eurasia (Sobel et al. 2006a, De Grave et al. 2012, Bande et al. 2017b, Käßner et al. 2017b, Nachtergaele et al. 2017, Jepson et al. 2018). Since only a slight Palaeogene thermochronological signal can be identified in the Kyzylkum-Nurata Segment, it is likely that much of the exhuming strain and deformation produced by the India–Eurasia collision is partitioned away from the western margin of the South Tian Shan and into the core of the Tian Shan.

5.4 Conclusion

In this study we presented low-temperature apatite thermochronological analysis of forty-five samples from the western segment of the Southern Tian Shan, the Kyzylkum-Nurata Segment, in order to track its thermo-tectonic evolution through the Mesozoic–Cenozoic. The Kyzylkum-Nurata Segment experienced a phase of fast basement cooling and exhumation in the Triassic that is interpreted as a response to the closure of the Palaeo-Asian Ocean. During the Jurassic and Cretaceous, the study area experienced regional slow cooling. However, the major suture zones that dissect the Kyzylkum-Nurata Segment record rapid cooling during the Late Jurassic–Early Cretaceous, coincident with increased sedimentation in the Kyzylkum and Fergana Basins. We interpret this event of fault reactivation to be related with footwall exhumation as a response to extensional tectonics in the Tethys Ocean. In the Late Cretaceous, the Kyzylkum-Nurata Segment experienced a second phase of marine incursion, erosion, and slow cooling until the early Palaeogene. Finally, in the Palaeogene, the Kyzylkum-Nurata Segment records minor evidence for cooling and exhumation due to the collision of India with the Eurasian margin.

This study has revealed that the western segment of the South Tian Shan has experienced a different thermo-tectonic evolution when compared to its core, where thermo-tectonic evolution of the South Tian Shan has been overprinted via rapid Cenozoic exhumation. The western segment preserves a detailed archive of the Mesozoic tectonic activity that Eurasia experienced prior to the India–Eurasia collision.

5.5 Acknowledgements

We are grateful to Farid Divaev, Vladimir Chirikin, and Yunus Mamadjanov, who were responsible for logistics and transportation in the field. This study was supported by an Australian Research Council Discovery grant (DP150101730). D. Konopelko was supported by the Ministry of Education and Science of the Russian Federation (project No 14.Y26.31.0018) and by travel grant (mer. 6-2018) from Saint Petersburg State University. Ben Wade and Sarah Gilbert are thanked for assistance with the LA-ICP-MS facility at the University of Adelaide. This paper forms TRaX record 407.

References

Aitchison, J. C., Ali, J. R. & Davis, A. M. (2007), 'When and where did India and Asia collide?', *Journal of Geophysical Research: Solid Earth* **112**(B5).
URL: *https://agupubs.onlinelibrary.wiley.com/doi/abs/10.1029/2006JB004706*

Alexeiev, D. V., Cook, H. E., Buvtyshkin, V. M. & Golub, L. Y. (2009), 'Structural evolution of the Ural–Tian Shan junction: A view from Karatau ridge, South Kazakhstan', *Comptes Rendus Geoscience* **341**(2), 287 – 297. Mécanique de l'orogénie varisque : Une vision moderne de le recherche dans le domaine de l'orogénie.
URL: *http://www.sciencedirect.com/science/article/pii/S163107130800285X*

Angiolini, L., Andrea, Z., Stefano, Z., Alda, N. & Giovanni, V. (2013), 'The Cimmerian geopuzzle: new data from South Pamir', *Terra Nova* **25**(5), 352–360.
URL: *https://onlinelibrary.wiley.com/doi/abs/10.1111/ter.12042*

Bande, A., Sobel, E. R., Mikolaichuk, A. & Torres, A. V. (2017b), 'Talas–Fergana Fault Cenozoic timing of deformation and its relation to Pamir indentation', *Geological Society, London, Special*

Publications **427**(1), 295–311.

URL: *http://sp.lyellcollection.org/content/427/1/295*

Beck, R. A., Burbank, D. W., Sercombe, W. J., Riley, G. W., Barndt, J. K., Berry, J. R., Afzal, J., Khan, A. M., Jurgen, H., Metje, J., Cheema, A., Shafique, N. A., Lawrence, R. D. & Khan, M. A. (1995), 'Stratigraphic evidence for an early collision between northwest India and Asia', *Nature* **373**(6509), 55.

Biske, Y. & Seltmann, R. (2010), 'Paleozoic Tian-Shan as a transitional region between the Rheic and Urals-Turkestan oceans', *Gondwana Research* **17**(2), 602 – 613. The Rheic Ocean: Palaeozoic Evolution from Gondwana and Laurussia to Pangaea.

URL: *http://www.sciencedirect.com/science/article/pii/S1342937X09002160*

Bosboom, R., Dupont-Nivet, G., Grothe, A., Brinkhuis, H., Villa, G., Mandic, O., Stoica, M., Kouwenhoven, T., Huang, W., Yang, W. & Guo, Z. (2014), 'Timing, cause and impact of the late eocene stepwise sea retreat from the tarim basin (west china)', *Palaeogeography, Palaeoclimatology, Palaeoecology* **403**, 101 – 118.

URL: *http://www.sciencedirect.com/science/article/pii/S0031018214001709*

Bosboom, R. E., Dupont-Nivet, G., Houben, A., Brinkhuis, H., Villa, G., Mandic, O., Stoica, M., Zachariasse, W. J., Guo, Z., Li, C. & Krijgsman, W. (2011), 'Late eocene sea retreat from the tarim basin (west china) and concomitant asian paleoenvironmental change', *Palaeogeography, Palaeoclimatology, Palaeoecology* **299**(3), 385 – 398.

URL: *http://www.sciencedirect.com/science/article/pii/S0031018210006954*

Brookfield, M. (2000), 'Geological development and Phanerozoic crustal accretion in the western segment of the southern Tien Shan (Kyrgyzstan, Uzbekistan and Tajikistan)', *Tectonophysics* **328**(1-2), 1–14.

Bullen, M., Burbank, D., Garver, J. & Abdrakhmatov, K. (2001), 'Late Cenozoic tectonic evolution of the northwestern Tien Shan: New age estimates for the initiation of mountain building', *GSA Bulletin* **113**(12), 1544.

URL: *http://dx.doi.org/10.1130/0016-7606(2001)113<1544:LCTEOT>2.0.CO;2*

Bullen, M. E., Burbank, D. W. & Garver, J. I. (2003), 'Building the Northern Tien Shan: Integrated

Thermal, Structural, and Topographic Constraints', *The Journal of Geology* **111**(2), 149–165.
URL: *https://doi.org/10.1086/345840*

Burtman, V. (2000), 'Cenozoic crustal shortening between the Pamir and Tien Shan and a reconstruction of the Pamir–Tien Shan transition zone for the Cretaceous and Palaeogene', *Tectonophysics* **319**(2), 69 – 92.
URL: *http://www.sciencedirect.com/science/article/pii/S0040195100000226*

Burtman, V. S. (1975), 'Structural geology of variscan Tien Shan, USSR', *Am. J. Sci* **275**, 157–186.

Burtman, V. S. (2015), 'Tectonics and geodynamics of the Tian Shan in the Middle and Late Paleozoic', *Geotectonics* **49**(4), 302–319.
URL: *https://doi.org/10.1134/S0016852115040020*

Danišík, M., Štěpančíková, P. & Evans, N. J. (2012), 'Constraining long-term denudation and faulting history in intraplate regions by multisystem thermochronology: An example of the Sudetic Marginal Fault (Bohemian Massif, central Europe)', *Tectonics* **31**(2).
URL: *https://agupubs.onlinelibrary.wiley.com/doi/abs/10.1029/2011TC003012*

De Grave, J., Buslov, M. M. & Van den haute, P. (2007), 'Distant effects of India–Eurasia convergence and Mesozoic intracontinental deformation in Central Asia: Constraints from apatite fission-track thermochronology', *Journal of Asian Earth Sciences* **29**(2), 188 – 204. The 19th Himalaya-Karakoram-Tibet Workshop (HKT19) held at Niseko, Hokkaido, Japan, 10–13 July 2004.
URL: *http://www.sciencedirect.com/science/article/pii/S136791200600071X*

De Grave, J., Glorie, S., Buslov, M. M., Izmer, A., Fournier-Carrie, A., Batalev, V. Y., Vanhaecke, F., Elburg, M. & Van den haute, P. (2011), 'The thermo-tectonic history of the Song-Kul plateau, Kyrgyz Tien Shan: Constraints by apatite and titanite thermochronometry and zircon U/Pb dating', *Gondwana Research* **20**(4), 745 – 763.
URL: *http://www.sciencedirect.com/science/article/pii/S1342937X11001201*

De Grave, J., Glorie, S., Buslov, M. M., Stockli, D. F., McWilliams, M. O., Batalev, V. Y. & Van den haute, P. (2013), 'Thermo-tectonic history of the Issyk-Kul basement (Kyrgyz Northern Tien Shan, Central Asia)', *Gondwana Research* **23**(3), 998 – 1020. Ultrahigh-pressure and high-pressure metamorphic terranes in orogenic belts: reactions, fluids and geological processes.
URL: *http://www.sciencedirect.com/science/article/pii/S1342937X12002377*

De Grave, J., Glorie, S., Ryabinin, A., Zhimulev, F., Buslov, M., Izmer, A., Elburg, M., Vanhaecke, F. & Van den haute, P. (2012), 'Late Palaeozoic and Meso-Cenozoic tectonic evolution of the southern Kyrgyz Tien Shan: Constraints from multi-method thermochronology in the Trans-Alai, Turkestan-Alai segment and the southeastern Ferghana Basin', *Journal of Asian Earth Sciences* **44**, 149 – 168. Asian Climate and Tectonics.
URL: *http://www.sciencedirect.com/science/article/pii/S1367912011001866*

De Pelsmaeker, E., Glorie, S., Buslov, M. M., Zhimulev, F. I., Poujol, M., Korobkin, V. V., Vanhaecke, F., Vetrov, E. V. & De Grave, J. (2015), 'Late-Paleozoic emplacement and Meso-Cenozoic reactivation of the southern Kazakhstan granitoid basement', *Tectonophysics* **662**, 416 – 433. Special issue on Comparative tectonic and dynamic analysis of cratons, orogens, basins, and metallogeny:.
URL: *https://www.sciencedirect.com/science/article/pii/S0040195115003091*

De Pelsmaeker, E., Jolivet, M., Laborde, A., Poujol, M., Robin, C., Zhimulev, F. I., Nachtergaele, S., Glorie, S., Clercq, S. D., Batalev, V. Y. & Grave, J. D. (2018), 'Source-to-sink dynamics in the Kyrgyz Tien Shan from the Jurassic to the Paleogene: Insights from sedimentological and detrital zircon U-Pb analyses', *Gondwana Research* **54**, 180 – 204.
URL: *http://www.sciencedirect.com/science/article/pii/S1342937X17300679*

Dolgopolova, A., Seltmann, R., Konopelko, D., Biske, Y. S., Shatov, V., Armstrong, R., Belousova, E., Pankhurst, R., Koneev, R. & Divaev, F. (2017), 'Geodynamic evolution of the western tien shan, uzbekistan: Insights from u-pb shrimp geochronology and sr-nd-pb-hf isotope mapping of granitoids', *Gondwana Research* **47**, 76 – 109. Continental construction in Central Asia and actualistic comparisons with western Pacific.
URL: *http://www.sciencedirect.com/science/article/pii/S1342937X16304324*

Dumitru, T. A., Zhou, D., Chang, E. Z., Graham, S. A., Hendrix, M. S., Sobel, E. R. & Carroll, A. R. (2001), 'Uplift, exhumation, and deformation in the Chinese Tian Shan', *Memoirs-Geological Society of America* pp. 71–100.

Farley, K. A. (2002), '(U-Th)/He Dating: Techniques, Calibrations, and Applications', *Reviews in Mineralogy and Geochemistry* **47**(1), 819.
URL: *http://dx.doi.org/10.2138/rmg.2002.47.18*

Farley, K., Wolf, R. & Silver, L. (1996), 'The effects of long alpha-stopping distances on (U-Th)/He

ages', *Geochimica et Cosmochimica Acta* **60**(21), 4223 – 4229.
URL: *http://www.sciencedirect.com/science/article/pii/S0016703796001937*

Fleischer, R. L., Price, P. B., Walker, R. M. & W., R. M. (1975), *Nuclear tracks in solids: principles and applications*, Univ of California Press.

Flowers, R. M., Farley, K. A. & Ketcham, R. A. (2015), 'A reporting protocol for thermochronologic modeling illustrated with data from the Grand Canyon', *Earth and Planetary Science Letters* **432**, 425 – 435.
URL: *http://www.sciencedirect.com/science/article/pii/S0012821X15006317*

Gallagher, K. (2012), 'Transdimensional inverse thermal history modeling for quantitative thermochronology', *Journal of Geophysical Research: Solid Earth* **117**(B2).
URL: *https://agupubs.onlinelibrary.wiley.com/doi/abs/10.1029/2011JB008825*

Gallagher, K. & Brown, R. (1997), 'The onshore record of passive margin evolution', *Journal of the Geological Society* **154**(3), 451–457.
URL: *http://jgs.lyellcollection.org/content/154/3/451*

Gallagher, K., Brown, R. & Johnson, C. (1998), 'Fission track analysis and its applications to geological problems', *Annual Review of Earth and Planetary Sciences* **26**(1), 519–572.
URL: *https://doi.org/10.1146/annurev.earth.26.1.519*

Gautheron, C., Tassan-Got, L., Barbarand, J. & Pagel, M. (2009), 'Effect of alpha-damage annealing on apatite (U–Th)/He thermochronology', *Chemical Geology* **266**(3), 157 – 170.
URL: *http://www.sciencedirect.com/science/article/pii/S0009254109002630*

Gillespie, J., Glorie, S., Jepson, G., Zhang, Z. Y., Xiao, W. J., Danišík, M. & Collins, A. S. (2017), 'Differential Exhumation and Crustal Tilting in the Easternmost Tianshan (Xinjiang, China), Revealed by Low-Temperature Thermochronology', *Tectonics* **36**(10), 2142–2158.
URL: *https://agupubs.onlinelibrary.wiley.com/doi/abs/10.1002/2017TC004574*

Gleadow, A., Harrison, M., Kohn, B., Lugo-Zazueta, R. & Phillips, D. (2015), 'The fish canyon tuff: A new look at an old low-temperature thermochronology standard', *Earth and Planetary Science Letters* **424**, 95 – 108.
URL: *http://www.sciencedirect.com/science/article/pii/S0012821X15002927*

Gleadow, A. J., Belton, D. X., Kohn, B. P. & Brown, R. W. (2002), 'Fission Track Dating of Phosphate Minerals and the Thermochronology of Apatite', *Reviews in Mineralogy and Geochemistry* **48**(1), 579.
URL: *+ http://dx.doi.org/10.2138/rmg.2002.48.16*

Glorie, S., Alexandrov, I., Nixon, A., Jepson, G., Gillespie, J. & Jahn, B.-M. (2017), 'Thermal and exhumation history of Sakhalin Island (Russia) constrained by apatite U-Pb and fission track thermochronology', *Journal of Asian Earth Sciences* **143**, 326 – 342.
URL: *http://www.sciencedirect.com/science/article/pii/S1367912017302262*

Glorie, S. & De Grave, J. (2016), 'Exhuming the Meso–Cenozoic Kyrgyz Tianshan and Siberian Altai-Sayan: A review based on low-temperature thermochronology', *Geoscience Frontiers* **7**(2), 155 – 170. Special Issue: Exhuming Asia.
URL: *https://www.sciencedirect.com/science/article/pii/S1674987115000468*

Glorie, S., De Grave, J., Buslov, M., Elburg, M., Stockli, D., Gerdes, A. & Van den haute, P. (2010), 'Multi-method chronometric constraints on the evolution of the Northern Kyrgyz Tien Shan granitoids (Central Asian Orogenic Belt): From emplacement to exhumation', *Journal of Asian Earth Sciences* **38**(3), 131 – 146.
URL: *http://www.sciencedirect.com/science/article/pii/S1367912009002636*

Glorie, S., Grave, J. D., Buslov, M. M., Zhimulev, F. I., Stockli, D. F., Batalev, V. Y., Izmer, A., Van den haute, P., Vanhaecke, F. & Elburg, M. A. (2011), 'Tectonic history of the Kyrgyz South Tien Shan (Atbashi-Inylchek) suture zone: The role of inherited structures during deformation-propagation', *Tectonics* **30**(6).
URL: *https://agupubs.onlinelibrary.wiley.com/doi/abs/10.1029/2011TC002949*

Green, P., Duddy, I., Gleadow, A., Tingate, P. & Laslett, G. (1986), 'Thermal annealing of fission tracks in apatite: 1. A qualitative description', *Chemical Geology: Isotope Geoscience section* **59**, 237 – 253. Calibration of the Phanerozoic Time Scale.
URL: *http://www.sciencedirect.com/science/article/pii/0168962286900746*

Green, P. F. (1986), 'On the thermo-tectonic evolution of Northern England: evidence from fission track analysis', *Geological Magazine* **123**(5), 493–506.

Hall, R. (2012), 'Late Jurassic–Cenozoic reconstructions of the Indonesian region and the Indian

Ocean', *Tectonophysics* **570–571**, 1–41.
URL: *http://www.sciencedirect.com/science/article/pii/S0040195112002533*

Haq, B. U., Hardenbol, J. & Vail, P. R. (1987), 'Chronology of Fluctuating Sea Levels Since the Triassic', *Science* **235**(4793), 1156–1167.
URL: *http://science.sciencemag.org/content/235/4793/1156*

Hasebe, N., Barbarand, J., Jarvis, K., Carter, A. & Hurford, A. J. (2004), 'Apatite fission-track chronometry using laser ablation ICP-MS', *Chemical Geology* **207**(3), 135 – 145.
URL: *http://www.sciencedirect.com/science/article/pii/S0009254104000427*

Jepson, G., Glorie, S., Konopelko, D., Gillespie, J., Danišík, M., Evans, N. J., Mamadjanov, Y. & Collins, A. S. (2018), 'Thermochronological insights into the structural contact between the Tian Shan and Pamirs, Tajikistan', *Terra Nova* **30**(2), 95–104.
URL: *https://onlinelibrary.wiley.com/doi/abs/10.1111/ter.12313*

Jolivet, M., Dominguez, S., Charreau, J., Chen, Y., Li, Y. & Wang, Q. (2010), 'Mesozoic and Cenozoic tectonic history of the central Chinese Tian Shan: Reactivated tectonic structures and active deformation', *Tectonics* **29**(6). TC6019.
URL: *http://dx.doi.org/10.1029/2010TC002712*

Jolivet, M., Heilbronn, G., Robin, C., Barrier, L., Bourquin, S., Guo, Z., Jia, Y., Guerit, L., Yang, W. & Fu, B. (2013), 'Reconstructing the Late Palaeozoic - Mesozoic topographic evolution of the Chinese Tian Shan: available data and remaining uncertainties', *Advances in Geosciences* **37**, 7–18.
URL: *https://hal-insu.archives-ouvertes.fr/insu-00920043*

Kempe, U., Graupner, T., Seltmann, R., de Boorder, H., Dolgopolova, A. & van Emmichoven, M. Z. (2016), 'The Muruntau gold deposit (Uzbekistan) – A unique ancient hydrothermal system in the southern Tien Shan', *Geoscience Frontiers* **7**(3), 495 – 528. Special Issue: Giant Mineral Deposits.
URL: *http://www.sciencedirect.com/science/article/pii/S1674987115001139*

Ketcham, R. A., Carter, A., Donelick, R. A., Barbarand, J. & Hurford, A. J. (2007), 'Improved modeling of fission-track annealing in apatite', *American Mineralogist* **92**(5-6), 799.
URL: *http://dx.doi.org/10.2138/am.2007.2281*

Käßner, A., Ratschbacher, L., Jonckheere, R., Enkelmann, E., Khan, J., Sonntag, B., Gloaguen, R., Gadoev, M. & Oimahmadov, I. (2017b), 'Cenozoic intracontinental deformation and exhumation at the northwestern tip of the India-Asia collision—southwestern Tian Shan, Tajikistan, and Kyrgyzstan', *Tectonics* **35**(9), 2171–2194.
URL: *https://agupubs.onlinelibrary.wiley.com/doi/abs/10.1002/2015TC003897*

Käßner, A., Ratschbacher, L., Pfänder, J. A., Hacker, B. R., Zack, G., Sonntag, B.-L., Khan, J., Stanek, K. P., Gadoev, M. & Oimahmadov, I. (2017a), 'Proterozoic–Mesozoic history of the Central Asian orogenic belt in the Tajik and southwestern Kyrgyz Tian Shan: U-Pb, $^{40}Ar/^{39}Ar$, and fission-track geochronology and geochemistry of granitoids', *GSA Bulletin* **129**(3-4), 281.
URL: *http://dx.doi.org/10.1130/B31466.1*

Konopelko, D., Klemd, R., Mamadjanov, Y., Hegner, E., Knorsch, M., Fidaev, D., Kern, M. & Sergeev, S. (2015), 'Permian age of orogenic thickening and crustal melting in the Garm Block, South Tien Shan, Tajikistan', *Journal of Asian Earth Sciences* **113**, 711 – 727. The Making of Asia.
URL: *http://www.sciencedirect.com/science/article/pii/S1367912015300845*

Konopelko, D. L., Biske, Y. S., Kullerud, K., Seltmann, R. & Divaev, F. (2011), 'The Koshrabad granite massif in Uzbekistan: petrogenesis, metallogeny, and geodynamic setting', *Russian Geology and Geophysics* **52**(12), 1563–1573. Geodynamics, Tectonics, and Metallogeny of Orogenic Belts.
URL: *http://www.sciencedirect.com/science/article/pii/S1068797111002549*

Konopelko, D., Seltmann, R., Mamadjanov, Y., Romer, R., Rojas-Agramonte, Y., Jeffries, T., Fidaev, D. & Niyozov, A. (2017a), 'A geotraverse across two paleo-subduction zones in Tien Shan, Tajikistan', *Gondwana Research* **47**, 110 – 130. Continental construction in Central Asia and actualistic comparisons with western Pacific.
URL: *http://www.sciencedirect.com/science/article/pii/S1342937X16302878*

Konopelko, D., Wilde, S., Seltmann, R., Romer, R. & Biske, Y. S. (2018), 'Early Permian intrusions of the Alai range: Understanding tectonic settings of Hercynian post-collisional magmatism in the South Tien Shan, Kyrgyzstan', *Lithos* **302–303**, 405–420.
URL: *https://doi.org/10.1016/j.lithos.2018.01.024*

Macaulay, E. A., Sobel, E. R., Mikolaichuk, A., Kohn, B. & Stuart, F. M. (2014), 'Cenozoic deformation

and exhumation history of the Central Kyrgyz Tien Shan', *Tectonics* **33**(2), 135–165.
URL: *https://agupubs.onlinelibrary.wiley.com/doi/abs/10.1002/2013TC003376*

McCann, T. (2016a), 'The Cretaceous of the South Kyzylkum and Nuratau Region, Western Tien Shan, Central Uzbekistan', *Geological Society, London, Special Publications* **427**(1), 439–489.
URL: *http://sp.lyellcollection.org/content/427/1/439*

McCann, T. (2016b), 'The Jurassic of the Western Tien Shan: the Central Kyzylkum Region, Uzbekistan', *Geological Society, London, Special Publications* **427**(1), 411–437.
URL: *http://sp.lyellcollection.org/content/427/1/411*

McDowell, F. W., McIntosh, W. C. & Farley, K. A. (2005), 'A precise 40Ar–39Ar reference age for the Durango apatite (U–Th)/He and fission-track dating standard', *Chemical Geology* **214**(3), 249 – 263.
URL: *http://www.sciencedirect.com/science/article/pii/S0009254104004218*

Nachtergaele, S., De Pelsmaeker, E., Glorie, S., Zhimulev, F., Jolivet, M., Danišík, M., Buslov, M. M. & De Grave, J. (2017), 'Meso-Cenozoic tectonic evolution of the Talas-Fergana region of the Kyrgyz Tien Shan revealed by low-temperature basement and detrital thermochronology', *Geoscience Frontiers* .
URL: *http://www.sciencedirect.com/science/article/pii/S1674987117302013*

Najman, Y., Appel, E., Boudagher-Fadel, M., Bown, P., Carter, A., Garzanti, E., Godin, L., Han, J., Liebke, U., Oliver, G., Parrish, R. & Vezzoli, G. (2010), 'Timing of India-Asia collision: Geological, biostratigraphic, and palaeomagnetic constraints', *Journal of Geophysical Research: Solid Earth* **115**(B12). B12416.
URL: *http://dx.doi.org/10.1029/2010JB007673*

Paton, C., Hellstrom, J., Paul, B., Woodhead, J. & Hergt, J. (2011), 'Iolite: Freeware for the visualisation and processing of mass spectrometric data', *Journal of Analytical Atomic Spectrometry* **26**(12), 2508–2518.

Pearce, N. J., Perkins, W. T., Westgate, J. A., Gorton, M. P., Jackson, S. E., Neal, C. R. & Chenery, S. P. (1997), 'A Compilation of New and Published Major and Trace Element Data for NIST SRM 610 and NIST SRM 612 Glass Reference Materials', *Geostandards Newsletter* **21**(1), 115–144.
URL: *https://onlinelibrary.wiley.com/doi/abs/10.1111/j.1751-908X.1997.tb00538.x*

Ratschbacher, L., Hacker, B. R., Calvert, A., Webb, L. E., Grimmer, J. C., McWilliams, M. O., Ireland, T., Dong, S. & Hu, J. (2003), 'Tectonics of the Qinling (Central China): tectonostratigraphy, geochronology, and deformation history', *Tectonophysics* **366**(1), 1 – 53.
URL: *http://www.sciencedirect.com/science/article/pii/S0040195103000532*

Robinson, A. C. (2015), 'Mesozoic tectonics of the Gondwanan terranes of the Pamir plateau', *Journal of Asian Earth Sciences* **102**, 170 – 179. Special Issue on CIMMERIAN TERRANES.
URL: *http://www.sciencedirect.com/science/article/pii/S1367912014004258*

Rutte, D., Ratschbacher, L., Khan, J., Stübner, K., Hacker, B. R., Stearns, M. A., Enkelmann, E., Jonckheere, R., Pfänder, J. A., Sperner, B. & Tichomirowa, M. (2017), 'Building the Pamir-Tibetan Plateau—Crustal stacking, extensional collapse, and lateral extrusion in the Central Pamir: 2. Timing and rates', *Tectonics* **36**(3), 385–419. 2016TC004294.
URL: *http://dx.doi.org/10.1002/2016TC004294*

Seltmann, R., Konopelko, D., Biske, G., Divaev, F. & Sergeev, S. (2011), 'Hercynian post-collisional magmatism in the context of Paleozoic magmatic evolution of the Tien Shan orogenic belt', *Journal of Asian Earth Sciences* **42**(5), 821 – 838. Continental accretion and intra-continental deformation of the Central Asian Orogenic Belt.
URL: *http://www.sciencedirect.com/science/article/pii/S1367912010002646*

Sobel, E. R., Chen, J. & Heermance, R. V. (2006a), 'Late Oligocene–Early Miocene initiation of shortening in the Southwestern Chinese Tian Shan: Implications for Neogene shortening rate variations', *Earth and Planetary Science Letters* **247**(1), 70 – 81.
URL: *http://www.sciencedirect.com/science/article/pii/S0012821X06002834*

Sobel, E. R. & Dumitru, T. A. (1997), 'Thrusting and exhumation around the margins of the western Tarim basin during the India-Asia collision', *Journal of Geophysical Research: Solid Earth* **102**(B3), 5043–5063.
URL: *http://dx.doi.org/10.1029/96JB03267*

Sobel, E. R., Oskin, M., Burbank, D. & Mikolaichuk, A. (2006b), 'Exhumation of basement-cored uplifts: Example of the Kyrgyz Range quantified with apatite fission track thermochronology', *Tectonics* **25**(2). TC2008.
URL: *http://dx.doi.org/10.1029/2005TC001809*

Stockli, D. F., Surpless, B. E., Dumitru, T. A. & Farley, K. A. (2002), 'Thermochronological constraints on the timing and magnitude of Miocene and Pliocene extension in the central Wassuk Range, western Nevada', *Tectonics* **21**(4), 10–1–10–19.
URL: *https://agupubs.onlinelibrary.wiley.com/doi/abs/10.1029/2001TC001295*

Survey, U. G. (2012), 'Geological Map of Uzbekistan', *State Geological Information Centre* .

van Hinsbergen, D. J. J., Steinberger, B., Doubrovine, P. V. & Gassmöller, R. (2011), 'Acceleration and deceleration of India-Asia convergence since the Cretaceous: Roles of mantle plumes and continental collision', *Journal of Geophysical Research: Solid Earth* **116**(B6). B06101.
URL: *http://dx.doi.org/10.1029/2010JB008051*

Vermeesch, P. (2009), 'RadialPlotter: A Java application for fission track, luminescence and other radial plots', *Radiation Measurements* **44**(4), 409–410.

Vermeesch, P. (2017), 'Statistics for LA-ICP-MS based fission track dating', *Chemical Geology* **456**, 19 – 27.
URL: *http://www.sciencedirect.com/science/article/pii/S0009254117301158*

Wagner, G. A. & Van den haute, P. (1992), 'Fission-track dating', *Kluwer Academic Publishers* p. 285.

Windley, B. F., Alexeiev, D., Xiao, W., Kröner, A. & Badarch, G. (2007), 'Tectonic models for accretion of the Central Asian Orogenic Belt', *Journal of the Geological Society* **164**(1), 31.
URL: *http://dx.doi.org/10.1144/0016-76492006-022*

Xiao, W. J., Windley, B. F., Huang, B. C., Han, C. M., Yuan, C., Chen, H. L., Sun, M., Sun, S. & Li, J. L. (2009), 'End-Permian to mid-Triassic termination of the accretionary processes of the southern Altaids: implications for the geodynamic evolution, Phanerozoic continental growth, and metallogeny of Central Asia', *International Journal of Earth Sciences* **98**(6), 1189–1217.
URL: *https://doi.org/10.1007/s00531-008-0407-z*

Xiao, W., Windley, B. F., Allen, M. B. & Han, C. (2013), 'Paleozoic multiple accretionary and collisional tectonics of the Chinese Tianshan orogenic collage', *Gondwana Research* **23**(4), 1316 – 1341.
URL: *http://www.sciencedirect.com/science/article/pii/S1342937X12000469*

Yin, A. & Harrison, T. M. (2000), 'Geologic Evolution of the Himalayan-Tibetan Orogen', *Annual*

Review of Earth and Planetary Sciences **28**(1), 211–280.

URL: *https://doi.org/10.1146/annurev.earth.28.1.211*

Zahirovic, S., Matthews, K. J., Flament, N., Müller, R. D., Hill, K. C., Seton, M. & Gurnis, M. (2016), 'Tectonic evolution and deep mantle structure of the eastern Tethys since the latest Jurassic', *Earth-Science Reviews* **162**, 293–337.

URL: *http://www.sciencedirect.com/science/article/pii/S0012825216302872*

Zeitler, P., Herczeg, A., McDougall, I. & Honda, M. (1987), 'U-Th-He dating of apatite: A potential thermochronometer', *Geochimica et Cosmochimica Acta* **51**(10), 2865 – 2868.

URL: *http://www.sciencedirect.com/science/article/pii/0016703787901645*

6 Supplementary Files

6.1 Supplementary File 1

Apatite fission track data and chemical data: ρ_s is the density of spontaneous tracks within the region of interest and is expressed as 10^5 tracks/cm^2. N_s is the total number of counted spontaneous tracks per sample. ^{238}U is the average concentration in ppm of uranium 238 measured in each grain. ^{35}Cl is the average concentration in ppm of chlorine 35 measured in each grain; concentrations were obtained using laser ablation–inductively coupled plasma–mass spectrometry (LA-ICP-MS). BLOD is below limits of detection, and thus, could not provide a concentration value and was not used in calculating sample concentration averages. Dpar is the length of spontaneous track etch pits in μm. t is the AFT single grain age for each sample in Ma.

Sample	ρ_s	N_s	^{238}U	$\pm1\sigma$	^{35}Cl	$\pm1\sigma$	Dpar	$\pm1\sigma$	t	$\pm1\sigma$
UZ-01-1	13.9	40	26.9	1.5	1820	110	1.7	0.5	107.5	19.6
UZ-01-2	3.3	10	26.1	2.3	10500	5500	2.0	0.1	26.3	8.8
UZ-01-3	3.5	7	21.6	2.4	2270	300	2.2	0.5	33.2	13.3
UZ-01-4	7.6	20	29.0	2.3	11900	4500	2.3	0.9	54.3	13.5
UZ-01-5	11.7	29	23.8	2.4	2400	140	2.5	1.1	102.0	22.8
UZ-01-6	13.4	72	30.3	1.6	29400	8800	2.1	1.0	91.9	13.6
UZ-01-7	13.3	50	31.9	1.8	1840	140	1.9	0.3	86.4	14.6
UZ-01-8	12.0	23	18.9	1.0	2350	140	2.4	0.2	131.5	29.8
UZ-01-9	3.2	10	16.8	1.3	6500	1800	1.9	0.5	39.1	13.0
UZ-01-10	12.2	53	33.0	2.4	2250	150	1.9	0.3	76.6	13.1

UZ-01-11	15.1	25	17.6	1.6	1740	150	2.0	0.6	177.6	41.1
UZ-01-12	13.2	42	17.2	3.2	2310	180	2.1	0.7	159.7	40.3
UZ-01-13	15.5	78	25.8	2.4	2240	150	2.1	0.9	124.8	20.4
UZ-01-14	7.7	21	36.0	2.4	2690	620	1.7	0.3	44.2	10.6
UZ-01-15	10.3	34	32.9	2.1	5600	2100	1.9	0.5	64.9	12.8
UZ-01-16	16.6	66	29.8	1.8	2390	340	1.9	0.4	115.7	17.9
UZ-01-17	5.7	15	23.4	1.4	15400	5100	1.7	0.6	50.4	13.8
UZ-01-18	12.6	37	36.0	2.9	2040	130	1.8	0.3	72.3	14.2
UZ-01-19	4.4	21	11.8	0.7	2360	130	2.1	0.7	77.4	18.3
UZ-01-20	6.0	15	19.3	1.2	2950	220	3.0	2.0	64.0	17.6
UZ-01-21	28.7	54	101.3	7.6	198000	29000	2.0	0.6	58.7	10.1
UZ-01-22	15.1	25	30.3	2.6	1890	160	2.1	0.6	103.5	23.7
UZ-01-23	15.2	19	19.7	1.2	7200	3100	2.6	1.3	159.6	39.6
UZ-01-24	13.7	41	37.6	3.3	5300	2100	1.6	0.3	75.7	14.6
UZ-01-25	12.2	70	25.6	2.4	1750	110	1.6	0.3	98.7	16.6
UZ-01-26	14.8	44	39.9	3.7	11900	5600	1.7	0.3	76.8	14.7
UZ-01-27	9.0	42	30.6	2.4	1560	130	1.8	0.3	61.3	11.5
UZ-01-28	16.5	57	21.3	1.4	1910	200	1.7	0.3	160.2	26.3
UZ-01-29	11.3	25	14.4	1.0	1910	150	1.8	0.4	162.5	36.3
UZ-01-30	16.3	59	36.7	2.7	2940	180	2.1	0.4	92.2	15.3
UZ-01-31	5.9	14	24.6	1.8	11400	4200	2.0	0.7	49.6	14.2
UZ-01-32	13.9	53	38.0	2.8	3250	230	2.1	0.3	75.9	13.0
UZ-01-33	11.4	48	33.4	2.1	2340	190	1.9	0.3	70.5	12.2
UZ-02-1	0.5	1	1.5	0.1	1800	120	3.1	0.7	68.5	68.8
UZ-02-2	23.3	81	38.5	2.1	970	290	2.3	0.8	125.6	18.0
UZ-02-3	0.6	1	1.6	0.1	1740	120	2.9	0.5	71.3	71.7
UZ-02-4	0.6	1	2.2	0.3	2660	680	2.9	0.5	55.4	56.1
UZ-02-5	1.4	4	2.6	0.2	1340	130	2.9	0.5	108.4	55.4
UZ-02-6	1.4	2	3.3	0.2	40100	5600	1.7	0.5	89.2	63.7
UZ-02-7	0.4	1	2.3	0.1	2030	150	4.1	0.7	36.3	36.5
UZ-02-8	2.7	5	2.4	0.2	3030	880	5.8	0.4	234.1	107.5

UZ-02-9	0.9	3	1.7	0.1	1890	120	1.9	0.6	110.7	64.6
UZ-02-10	0.9	4	1.9	0.1	1216	98	2.5	1.1	103.4	52.5
UZ-02-11	1.0	2	2.0	0.1	1550	170	1.9	0.6	100.5	71.7
UZ-02-12	0.9	2	3.7	0.3	16000	11000	1.9	0.6	52.6	37.6
UZ-02-13	1.0	2	2.0	0.1	1810	120	1.9	0.6	107.0	76.3
UZ-02-14	1.0	3	2.1	0.1	1520	130	3.4	0.3	100.3	58.7
UZ-02-15	13.5	65	24.8	1.9	516	93	2.5	0.5	113.1	18.4
UZ-02-16	2.2	4	3.0	0.2	2430	270	2.9	0.2	148.5	75.9
UZ-02-17	19.9	81	33.8	4.2	22000	16000	2.4	0.7	122.2	22.2
UZ-02-18	1.0	4	2.5	0.2	30900	7600	1.9	0.6	87.1	44.4
UZ-02-19	0.9	2	2.4	0.1	1170	140	2.6	0.6	82.2	58.5
UZ-02-20	1.1	5	1.9	0.1	1870	260	3.0	0.1	123.7	56.3
UZ-02-21	2.4	5	2.2	0.1	1390	150	2.2	0.3	231.3	105.9
UZ-02-22	1.1	2	1.9	0.1	2350	180	3.4	0.3	116.4	83.0
UZ-02-23	1.2	3	2.2	0.2	1770	120	3.2	0.2	115.2	67.5
UZ-02-24	3.1	6	2.0	0.1	3230	200	2.9	0.2	329.6	138.3
UZ-02-25	2.1	3	3.7	0.2	18300	7200	3.0	0.8	117.6	68.7
UZ-02-26	18.1	28	17.6	1.3	520	130	2.2	0.3	212.7	45.8
UZ-02-27	0.7	2	2.0	0.2	1910	140	2.4	0.2	77.8	55.6
UZ-02-28	1.5	4	2.4	0.3	9400	4900	3.4	0.3	125.6	65.6
UZ-02-29	3.2	5	2.5	0.1	30000	11000	2.3	0.5	270.7	123.3
UZ-02-30	1.3	3	2.6	0.2	3080	320	2.1	0.5	102.3	60.1
UZ-02-31	1.2	3	2.2	0.1	2730	450	2.1	0.5	110.5	64.5
UZ-02-32	6.6	18	20.1	1.3	540	130	2.8	0.2	68.3	17.4
UZ-04-1	24.8	100	27.2	1.2	3140	290	2.0	0.3	199.4	23.7
UZ-04-2	38.8	105	37.6	1.7	5370	460	2.0	0.3	225.6	26.4
UZ-04-3	26.7	97	46.2	2.1	6030	410	2.0	0.3	126.5	15.3
UZ-04-4	32.3	170	34.6	1.6	5390	430	2.0	0.3	204.1	20.6
UZ-04-5	4.0	16	5.9	0.4	24500	3600	1.7	0.3	149.8	39.2
UZ-04-6	25.1	83	32.8	1.2	6260	460	1.7	0.3	167.8	20.9
UZ-04-7	7.0	24	9.6	0.5	3410	500	1.7	0.2	159.4	34.6

UZ-04-8	27.4	67	35.6	1.4	5520	400	1.9	0.3	168.5	23.0
UZ-04-9	41.2	57	46.0	2.2	8820	580	1.4	0.2	196.2	29.1
UZ-04-10	30.6	81	28.6	1.3	4020	320	1.9	0.3	234.0	30.1
UZ-04-11	15.8	35	35.8	2.3	25600	6600	2.2	0.3	96.5	18.0
UZ-04-12	29.4	70	36.0	1.5	3120	330	1.8	0.3	178.5	24.1
UZ-04-13	44.1	95	51.4	2.1	6140	380	1.8	0.2	187.8	22.5
UZ-04-14	27.7	58	39.7	1.9	6130	500	1.8	0.4	152.6	22.5
UZ-04-15	18.1	34	16.3	1.2	530	250	1.5	0.3	243.3	46.8
UZ-04-16	5.0	18	9.6	0.4	BLOD	BLOD	1.3	0.4	113.0	27.6
UZ-04-17	28.0	76	30.7	1.3	5520	390	1.9	0.2	199.3	26.1
UZ-04-18	28.4	74	30.7	1.4	6040	440	1.8	0.3	202.3	27.0
UZ-04-19	30.5	49	34.0	1.6	6470	490	2.1	0.3	196.1	30.9
UZ-04-20	34.9	100	39.2	2.3	8000	540	2.1	0.3	194.7	24.3
UZ-04-21	27.5	102	36.4	1.6	5770	460	2.0	0.2	165.6	19.5
UZ-04-22	23.8	39	51.2	3.1	5520	920	1.7	0.1	101.7	18.1
UZ-04-23	42.0	79	58.2	3.3	5860	500	1.9	0.3	158.0	21.2
UZ-04-24	29.9	126	38.0	1.6	6520	380	2.1	0.2	172.2	18.8
UZ-04-25	19.9	73	25.4	1.2	3610	360	1.8	0.3	171.7	23.1
UZ-04-26	31.2	143	31.9	2.1	6450	500	2.2	0.3	213.8	24.8
UZ-05-1	10.6	28	10.6	0.6	BLOD	BLOD	1.8	0.1	207.9	41.5
UZ-05-2	17.3	17	19.7	1.0	1510	430	2.1	0.8	183.3	45.9
UZ-05-3	58.3	114	98.2	4.0	900	340	1.8	0.4	124.0	13.5
UZ-05-4	22.7	61	20.9	0.8	620	300	1.9	0.2	226.5	31.4
UZ-05-5	6.9	7	11.7	0.8	19000	4100	1.6	0.0	123.5	47.7
UZ-05-6	27.6	60	33.3	1.6	1070	330	1.7	0.4	173.5	24.8
UZ-05-7	14.5	49	9.3	0.4	780	330	1.2	0.3	326.1	50.0
UZ-05-8	10.9	23	22.7	2.3	2840	790	1.3	0.1	100.5	23.6
UZ-05-9	20.9	21	18.8	1.3	1660	350	1.2	0.3	232.1	53.8
UZ-05-10	9.4	28	6.5	0.3	840	380	1.3	0.2	302.8	60.3
UZ-05-11	31.1	71	37.8	1.8	4700	1200	1.3	0.3	171.8	22.9
UZ-05-12	27.1	60	44.8	1.4	1350	360	1.3	0.4	126.4	17.4

UZ-05-13	14.8	37	14.3	0.9	1160	320	1.3	0.5	216.2	38.9
UZ-05-14	4.2	12	12.0	0.4	710	330	1.0	0.1	73.3	21.5
UZ-05-15	13.6	40	21.9	1.3	BLOD	BLOD	1.1	0.2	130.1	22.5
UZ-05-16	25.2	40	29.7	1.4	BLOD	BLOD	1.2	0.3	177.4	30.0
UZ-05-17	26.4	74	17.9	1.2	BLOD	BLOD	1.2	0.3	308.7	43.0
UZ-05-18	18.6	33	14.4	0.7	970	310	1.5	0.5	270.0	50.0
UZ-05-19	8.9	27	11.3	0.5	860	300	1.2	0.2	165.4	33.2
UZ-05-20	9.6	35	17.3	1.2	870	350	2.2	0.3	116.0	21.6
UZ-05-21	6.4	29	7.6	0.5	BLOD	BLOD	2.2	0.6	176.7	35.1
UZ-05-22	3.6	15	4.5	0.3	BLOD	BLOD	1.2	0.3	169.2	45.1
UZ-05-23	9.5	51	13.1	0.7	1090	400	2.3	0.7	151.7	23.6
UZ-05-24	17.2	23	35.6	3.4	6500	2200	2.7	0.3	100.8	23.4
UZ-05-25	19.1	48	18.7	1.4	990	350	2.1	0.7	213.6	35.6
UZ-05-26	12.4	49	13.3	0.7	BLOD	BLOD	1.5	0.2	194.0	30.5
UZ-05-27	6.1	28	10.5	0.6	BLOD	BLOD	1.6	0.3	122.0	24.4
UZ-05-28	19.6	48	21.4	1.8	BLOD	BLOD	1.6	0.3	191.1	32.7
UZ-05-29	14.7	41	12.8	0.8	27400	2300	1.1	0.2	238.9	41.2
UZ-05-30	11.3	21	14.7	0.6	BLOD	BLOD	1.8	0.6	161.4	36.4
UZ-05-31	17.4	32	16.1	1.2	830	240	1.6	0.2	226.0	44.2
UZ-07-1	20.6	74	40.7	1.3	BLOD	BLOD	1.2	0.3	105.6	13.3
UZ-07-2	23.8	63	32.4	1.1	480	310	1.2	0.3	153.3	20.8
UZ-07-3	13.7	50	33.8	1.3	BLOD	BLOD	1.1	0.2	84.5	12.8
UZ-07-4	18.2	73	29.5	1.5	BLOD	BLOD	0.9	0.2	129.2	17.2
UZ-07-5	19.7	68	44.4	1.5	BLOD	BLOD	0.9	0.2	92.8	12.2
UZ-07-6	19.3	94	30.2	1.4	BLOD	BLOD	1.1	0.2	133.7	15.9
UZ-07-7	27.7	61	43.7	1.8	600	280	1.2	0.2	132.3	18.5
UZ-07-8	14.6	56	32.0	1.6	850	290	1.1	0.2	95.4	14.1
UZ-07-9	15.1	63	25.5	1.2	BLOD	BLOD	1.4	0.3	123.6	17.3
UZ-07-10	2.4	12	2.5	0.2	9190	760	1.5	0.2	199.7	60.3
UZ-07-11	27.6	114	38.3	1.7	550	320	1.7	0.3	150.6	16.6
UZ-07-12	20.0	83	33.0	1.8	2260	470	1.1	0.3	126.6	16.2

UZ-07-13	40.5	169	61.6	2.2	4800	1600	1.4	0.3	137.5	12.7
UZ-07-14	11.2	53	19.2	0.8	BLOD	BLOD	0.8	0.2	121.8	18.1
UZ-07-15	26.7	91	42.8	2.1	BLOD	BLOD	1.5	0.2	130.4	15.9
UZ-07-16	14.8	53	17.7	0.7	830	280	1.2	0.2	174.2	25.8
UZ-07-17	19.1	93	32.6	1.4	BLOD	BLOD	1.3	0.3	122.6	14.5
UZ-07-18	23.8	81	39.5	1.5	BLOD	BLOD	1.1	0.3	125.7	15.5
UZ-07-19	24.3	100	37.8	1.4	520	240	1.0	0.3	134.5	15.2
UZ-07-20	19.9	78	31.6	1.0	690	270	1.0	0.2	131.6	16.2
UZ-07-21	13.4	57	32.4	1.4	BLOD	BLOD	0.9	0.2	86.1	12.4
UZ-07-22	15.7	78	21.5	0.7	BLOD	BLOD	1.2	0.3	152.9	19.0
UZ-07-23	3.9	19	4.5	0.2	1710	340	1.2	0.2	183.5	43.4
UZ-07-24	24.5	126	40.7	1.6	640	300	1.1	0.3	125.7	13.1
UZ-07-25	19.6	80	24.5	1.1	640	270	1.0	0.3	166.9	21.1
UZ-07-26	26.6	107	46.5	2.6	BLOD	BLOD	1.0	0.2	119.7	14.1
UZ-07-27	24.7	93	50.1	3.3	BLOD	BLOD	1.2	0.2	102.9	13.2
UZ-07-28	22.4	81	38.2	1.7	BLOD	BLOD	1.0	0.3	122.3	15.3
UZ-07-29	21.5	100	39.7	1.6	BLOD	BLOD	1.3	0.4	113.4	12.9
UZ-07-30	13.4	63	28.2	1.5	BLOD	BLOD	1.3	0.3	99.3	14.1
UZ-07-31	15.5	74	22.9	0.9	BLOD	BLOD	1.4	0.3	141.4	18.2
UZ-07-32	24.1	91	43.6	1.7	520	250	1.2	0.3	115.5	13.6
UZ-07-33	25.1	106	44.0	2.2	BLOD	BLOD	1.1	0.2	119.2	13.8
UZ-07-34	19.5	86	40.9	1.7	BLOD	BLOD	1.2	0.3	99.8	12.1
UZ-07-35	25.3	78	49.4	2.7	540	320	1.2	0.2	107.1	14.0
UZ-07-36	22.5	113	30.4	2.0	BLOD	BLOD	1.5	0.3	154.9	18.7
UZ-07-37	20.5	44	38.2	2.0	1630	330	1.3	0.3	112.4	18.4
UZ-07-38	23.2	74	49.5	2.2	BLOD	BLOD	1.1	0.6	98.0	12.7
UZ-07-39	21.7	97	22.9	3.4	275000	39000	1.1	0.3	198.1	36.4
UZ-07-40	19.9	94	38.1	2.0	BLOD	BLOD	1.2	0.2	109.2	13.3
UZ-07-41	21.1	62	32.3	1.2	BLOD	BLOD	1.2	0.2	136.6	18.8
UZ-08-1	6.5	20	7.8	0.3	720	270	0.8	0.3	174.7	40.2
UZ-08-2	5.1	15	4.5	0.3	670	340	0.9	0.1	235.0	63.7

UZ-08-3	9.2	8	10.4	0.6	2360	770	0.8	0.2	185.8	66.9
UZ-08-4	22.1	37	46.0	2.2	1060	310	1.6	0.5	100.5	17.6
UZ-08-5	45.8	49	79.3	4.9	1680	380	1.5	0.4	120.7	19.3
UZ-08-6	4.2	7	4.0	0.3	970	270	1.6	0.6	218.0	84.2
UZ-08-7	8.7	10	15.2	1.0	128000	18000	1.2	0.5	119.6	38.8
UZ-08-8	3.5	18	2.9	0.1	610	350	1.8	0.6	255.1	62.1
UZ-08-9	5.4	4	9.6	0.6	2530	560	1.6	0.5	117.7	59.5
UZ-08-10	4.8	10	4.0	0.4	1110	340	1.7	0.3	254.2	84.0
UZ-08-11	6.8	15	5.0	0.4	3300	1400	1.6	0.3	283.2	76.6
UZ-08-12	7.6	17	6.8	0.5	41400	7500	1.6	0.1	233.7	60.0
UZ-08-13	3.5	14	3.3	0.2	610	270	1.2	0.2	223.7	61.8
UZ-08-14	7.9	19	12.1	0.9	83000	14000	1.2	0.4	135.7	33.2
UZ-08-15	4.7	12	8.6	0.7	75000	15000	0.7	0.2	114.9	34.6
UZ-08-16	2.8	14	3.9	0.3	720	250	1.4	0.3	150.7	41.9
UZ-08-17	8.6	20	7.1	0.4	940	310	1.3	0.3	252.0	59.2
UZ-08-18	3.0	6	5.9	0.3	4300	1700	1.4	0.3	105.7	43.6
UZ-08-19	6.1	8	5.6	0.3	660	250	1.2	0.2	229.0	82.1
UZ-08-20	3.0	10	3.5	0.2	600	240	1.5	0.2	182.6	59.0
UZ-08-21	9.6	10	6.1	0.4	920	280	1.5	0.2	331.9	108.4
UZ-08-22	12.9	32	12.3	0.8	BLOD	BLOD	1.5	0.2	219.3	42.1
UZ-08-23	15.5	15	14.4	2.2	2390	630	1.4	0.4	225.6	68.2
UZ-08-24	4.0	7	3.8	0.2	490	250	1.2	0.1	222.7	85.2
UZ-08-25	7.9	11	7.4	0.5	620	260	1.3	0.3	222.3	69.0
UZ-08-26	2.8	15	4.6	0.3	660	280	1.7	0.5	126.6	33.7
UZ-08-27	5.8	12	5.3	0.3	6100	1200	1.8	0.1	228.1	67.3
UZ-08-28	2.2	3	11.0	0.9	1630	330	1.5	0.3	41.3	24.2
UZ-08-29	5.1	20	5.8	0.3	BLOD	BLOD	1.7	0.5	182.3	42.1
UZ-08-30	6.1	21	5.3	0.2	BLOD	BLOD	1.8	0.1	241.9	54.5
UZ-08-31	7.9	16	8.8	0.5	23000	5300	1.8	0.3	188.5	48.6
UZ-08-32	8.1	29	8.7	0.4	BLOD	BLOD	1.4	0.3	194.4	37.6
UZ-08-33	5.0	8	13.3	0.8	700	280	1.9	0.2	77.7	28.0

UZ-08-34	2.7	4	4.0	0.3	490	250	1.4	0.4	137.4	69.5
UZ-08-35	11.3	14	7.8	0.5	590	270	1.3	0.3	301.1	83.8
UZ-08-36	5.7	11	13.9	0.7	BLOD	BLOD	1.4	0.2	85.3	26.3
UZ-08-37	6.0	6	12.5	1.1	950	340	1.3	0.3	100.9	42.3
UZ-09-1	53.2	37	74.4	3.3	930	240	2.2	0.5	149.4	26.0
UZ-09-2	31.2	39	77.8	4.1	BLOD	BLOD	1.8	0.6	83.7	14.5
UZ-09-3	16.5	33	24.6	1.1	740	260	2.0	0.3	139.8	25.7
UZ-09-4	17.4	28	56.9	3.5	14100	8700	1.5	0.3	63.8	12.9
UZ-09-5	30.5	40	66.8	2.4	890	290	2.7	0.7	95.6	15.9
UZ-09-6	47.4	37	120.8	8.8	33600	7700	2.0	0.6	82.0	15.1
UZ-09-7	52.3	75	141.4	5.3	810	280	1.3	0.4	77.4	9.8
UZ-09-8	40.6	49	161.0	10.0	BLOD	BLOD	1.5	0.3	52.6	8.4
UZ-09-9	50.3	30	114.4	7.7	770	390	2.6	0.5	91.9	18.2
UZ-09-10	33.4	29	97.7	6.1	66000	19000	2.0	0.2	71.4	14.2
UZ-09-11	42.3	48	79.4	5.7	760	290	1.8	0.6	111.3	18.4
UZ-09-12	5.3	32	8.1	0.4	670	290	1.6	0.4	136.6	25.6
UZ-10-1	3.8	13	21.1	1.4	BLOD	BLOD	1.0	0.2	37.4	10.7
UZ-10-2	3.3	11	19.1	1.2	690	330	1.1	0.3	35.7	11.1
UZ-10-3	11.2	30	26.8	1.8	560	320	1.2	0.2	87.5	17.3
UZ-10-4	3.2	7	12.0	0.9	4540	720	1.0	0.3	55.8	21.6
UZ-10-5	3.3	13	9.4	0.4	760	270	0.9	0.2	74.4	21.1
UZ-10-6	5.1	13	9.6	0.4	BLOD	BLOD	1.6	0.5	109.8	31.1
UZ-10-7	4.7	15	20.9	1.3	630	320	1.2	0.3	47.0	12.6
UZ-10-8	3.5	9	13.8	0.8	BLOD	BLOD	1.5	0.5	53.3	18.1
UZ-10-9	2.0	7	9.7	0.4	BLOD	BLOD	0.8	0.1	43.4	16.6
UZ-10-10	2.8	9	10.3	0.5	BLOD	BLOD	1.1	0.2	57.4	19.5
UZ-10-11	4.4	14	20.6	1.4	1160	330	1.4	0.4	44.9	12.5
UZ-10-12	3.8	12	8.2	0.4	640	260	1.3	0.3	96.8	28.6
UZ-10-13	4.1	17	9.9	0.6	BLOD	BLOD	0.9	0.3	86.2	21.8
UZ-10-14	6.7	11	18.1	1.6	750	290	0.8	0.2	77.7	24.6
UZ-10-15	4.2	8	18.0	1.8	1140	400	1.3	0.2	48.8	18.0

UZ-10-16	1.0	2	5.1	0.3	740	300	0.2	0.2	40.8	28.9
UZ-10-17	4.7	18	17.9	2.4	BLOD	BLOD	1.3	0.3	54.7	15.0
UZ-10-18	1.6	8	8.6	0.5	BLOD	BLOD	1.3	0.4	38.1	13.7
UZ-10-19	1.6	3	37.0	4.6	89000	43000	1.3	0.4	8.8	5.2
UZ-10-20	4.6	19	13.8	0.8	BLOD	BLOD	1.7	0.5	69.3	16.7
UZ-10-21	3.5	18	11.2	0.7	560	270	1.2	0.3	65.3	16.1
UZ-10-22	1.3	4	10.2	0.5	950	330	1.1	0.4	27.5	13.8
UZ-10-23	2.2	6	7.4	0.4	BLOD	BLOD	1.0	0.2	61.9	25.6
UZ-10-24	5.1	27	17.1	0.8	560	250	1.4	0.4	62.5	12.6
UZ-10-25	3.7	13	11.3	0.8	BLOD	BLOD	1.2	0.1	67.8	19.5
UZ-10-26	1.4	5	10.2	0.6	460	250	1.3	0.1	28.6	12.9
UZ-10-27	1.7	6	11.9	0.6	BLOD	BLOD	1.2	0.3	29.3	12.1
UZ-10-28	5.1	18	15.3	1.2	770	330	1.3	0.2	69.4	17.4
UZ-10-29	2.9	9	19.6	1.6	650	300	1.4	0.1	31.2	10.8
UZ-11-1	10.2	24	11.1	0.6	BLOD	BLOD	1.2	0.2	192.6	41.5
UZ-11-2	14.8	30	14.3	0.6	550	300	1.0	0.2	216.6	41.5
UZ-11-3	8.5	26	12.9	0.7	750	340	1.3	0.2	136.9	28.4
UZ-11-4	22.4	24	47.9	9.1	BLOD	BLOD	1.0	0.2	97.7	27.5
UZ-11-5	13.4	44	12.1	0.5	BLOD	BLOD	1.1	0.2	231.7	37.1
UZ-11-6	19.1	32	15.3	0.9	14300	4400	1.6	0.2	261.2	49.7
UZ-11-7	7.9	34	11.7	0.6	660	310	0.9	0.2	141.7	25.8
UZ-11-8	19.1	33	32.3	1.4	BLOD	BLOD	1.2	0.2	123.8	22.7
UZ-11-9	4.6	21	5.3	0.4	BLOD	BLOD	1.1	0.2	183.7	42.8
UZ-11-10	28.2	50	50.2	1.7	810	320	1.1	0.2	117.3	17.6
UZ-11-11	11.7	14	13.6	0.5	BLOD	BLOD	1.3	0.1	179.6	49.0
UZ-11-12	7.6	14	9.5	0.5	BLOD	BLOD	1.2	0.1	167.4	45.9
UZ-11-13	10.8	18	14.2	0.6	BLOD	BLOD	0.9	0.2	159.1	38.6
UZ-11-14	7.1	8	22.4	2.7	930	320	1.1	0.3	65.9	24.7
UZ-11-15	24.7	43	25.3	1.8	BLOD	BLOD	1.0	0.2	204.2	35.2
UZ-11-16	8.3	18	16.8	1.6	BLOD	BLOD	1.1	0.2	103.3	26.6
UZ-11-17	66.2	105	161.3	5.4	730	310	1.2	0.2	85.7	9.4

UZ-11-18	13.3	55	13.4	1.0	BLOD	BLOD	1.2	0.2	206.1	32.5
UZ-11-19	54.2	90	92.9	2.7	1300	430	1.2	0.2	121.9	14.1
UZ-11-20	5.1	16	4.0	0.2	720	360	1.2	0.3	266.5	68.5
UZ-11-21	14.9	33	14.0	0.7	BLOD	BLOD	0.9	0.1	221.2	40.8
UZ-11-22	33.1	62	52.2	2.0	BLOD	BLOD	1.1	0.2	132.6	18.3
UZ-11-23	61.4	61	95.6	3.5	610	320	1.3	0.2	134.3	18.6
UZ-11-24	44.2	54	63.4	3.7	BLOD	BLOD	1.1	0.2	145.6	22.2
UZ-11-25	26.0	56	42.0	1.1	850	370	1.1	0.2	129.6	18.3
UZ-11-26	14.0	36	13.3	0.6	BLOD	BLOD	1.1	0.2	220.0	38.9
UZ-11-27	31.1	56	42.2	2.1	BLOD	BLOD	1.1	0.2	153.9	22.7
UZ-11-28	37.3	50	51.7	2.1	BLOD	BLOD	1.2	0.2	150.9	22.9
UZ-11-29	6.6	16	13.4	0.8	700	360	1.2	0.2	103.4	26.9
UZ-11-30	25.8	60	37.5	1.8	BLOD	BLOD	1.1	0.2	143.6	20.5
UZ-11-31	10.1	25	12.1	0.6	BLOD	BLOD	1.2	0.3	173.0	36.3
UZ-11-32	11.9	43	22.1	1.5	BLOD	BLOD	1.0	0.2	112.9	19.3
UZ-11-33	15.9	38	13.4	0.5	580	300	1.1	0.2	248.4	42.5
UZ-11-34	11.5	31	13.4	0.6	BLOD	BLOD	1.0	0.3	179.6	34.0
UZ-11-35	2.3	5	65.9	5.5	BLOD	BLOD	1.0	0.3	7.3	3.3
UZ-11-36	20.2	63	47.9	3.5	3700	1600	1.1	0.2	88.3	13.3
UZ-11-37	9.4	17	11.1	0.5	850	380	1.1	0.1	176.4	44.0
UZ-11-38	10.7	51	13.1	0.5	670	340	1.3	0.3	171.4	25.8
UZ-11-39	12.7	18	18.6	0.8	BLOD	BLOD	1.0	0.2	142.9	34.6
UZ-11-40	16.0	21	14.7	0.7	BLOD	BLOD	1.2	0.2	227.6	51.4
UZ-12-1	14.7	47	15.9	0.8	410	180	1.3	0.3	197.7	31.2
UZ-12-2	13.9	24	29.2	1.4	930	240	1.7	0.2	101.6	21.6
UZ-12-3	11.8	35	15.6	0.8	BLOD	BLOD	1.6	0.1	161.8	29.1
UZ-12-4	13.9	23	14.7	0.6	BLOD	BLOD	1.5	0.2	201.2	43.4
UZ-12-5	23.4	68	30.8	1.8	BLOD	BLOD	1.5	0.3	162.7	22.7
UZ-12-6	23.0	53	22.6	1.1	490	240	1.4	0.3	217.3	32.7
UZ-12-7	9.6	19	15.6	0.7	BLOD	BLOD	1.3	0.2	131.7	31.2
UZ-12-8	15.4	22	18.7	0.6	400	210	1.5	0.2	175.8	38.4

UZ-12-9	8.9	26	14.8	0.7	BLOD	BLOD	1.4	0.1	128.5	26.5
UZ-12-10	35.2	69	50.1	2.9	BLOD	BLOD	1.5	0.3	150.0	20.8
UZ-12-11	26.8	61	51.1	2.3	BLOD	BLOD	1.4	0.2	112.0	15.8
UZ-12-12	15.0	32	17.2	0.8	BLOD	BLOD	1.4	0.3	187.1	34.8
UZ-12-13	20.2	34	41.8	3.0	BLOD	BLOD	1.7	0.2	103.5	19.6
UZ-12-14	13.0	31	12.4	0.6	BLOD	BLOD	1.6	0.2	223.6	42.2
UZ-12-15	13.4	28	16.0	0.8	490	160	1.6	0.3	179.1	35.5
UZ-12-16	6.8	21	9.7	0.6	BLOD	BLOD	1.4	0.4	150.6	34.7
UZ-12-17	28.9	61	32.5	2.5	390	260	1.5	0.3	190.0	29.3
UZ-12-18	29.7	39	47.6	2.0	620	250	1.4	0.3	133.3	22.6
UZ-12-19	8.9	16	16.8	0.8	530	180	1.6	0.2	113.1	29.0
UZ-12-20	8.8	17	11.1	0.6	BLOD	BLOD	1.6	0.2	169.2	42.4
UZ-12-21	8.0	23	30.9	2.4	1050	210	1.4	0.3	55.0	12.4
UZ-12-22	8.0	19	14.9	0.7	BLOD	BLOD	1.6	0.2	114.3	27.1
UZ-12-23	23.5	64	21.0	1.0	BLOD	BLOD	1.2	0.3	239.0	33.0
UZ-12-24	13.6	53	16.5	0.7	BLOD	BLOD	1.6	0.5	176.2	26.2
UZ-12-25	10.4	23	16.0	0.6	BLOD	BLOD	1.5	0.3	138.4	29.8
UZ-12-26	19.4	53	35.7	1.8	BLOD	BLOD	1.7	0.3	116.0	17.5
UZ-12-27	8.8	16	22.7	0.8	BLOD	BLOD	1.2	0.3	83.4	21.3
UZ-12-28	27.3	65	31.6	3.6	BLOD	BLOD	1.7	0.3	184.9	31.9
UZ-12-29	12.0	44	17.4	1.0	540	240	1.3	0.4	147.9	24.4
UZ-12-30	14.7	43	15.1	0.8	BLOD	BLOD	1.3	0.3	207.0	34.1
UZ-12-31	7.8	21	15.8	1.2	680	250	1.5	0.3	106.0	24.8
UZ-12-32	13.6	29	19.1	1.0	BLOD	BLOD	1.3	0.2	152.7	30.0
UZ-12-33	11.5	41	24.5	1.5	450	210	1.6	0.2	100.5	17.3
UZ-12-34	17.0	55	16.4	0.8	450	310	1.5	0.2	221.8	32.8
UZ-12-35	7.5	21	13.3	0.6	4140	400	1.5	0.2	119.4	27.0
UZ-12-36	27.6	66	39.2	1.8	BLOD	BLOD	1.5	0.4	150.4	20.5
UZ-12-37	16.3	50	18.5	1.3	1750	400	1.3	0.3	187.9	30.5
UZ-12-38	9.6	32	14.4	0.6	930	230	1.4	0.5	142.0	26.3
UZ-12-39	24.3	61	14.7	0.5	BLOD	BLOD	1.3	0.3	353.6	48.5

UZ-12-40	12.8	63	19.2	0.9	BLOD	BLOD	1.4	0.3	141.7	19.7
UZ-12-41	10.8	30	13.1	0.5	BLOD	BLOD	1.5	0.3	177.2	33.7
UZ-12-42	15.7	49	15.9	0.8	BLOD	BLOD	1.4	0.3	211.6	32.8
UZ-12-43	7.9	23	17.5	1.0	BLOD	BLOD	1.6	0.4	96.6	21.2
UZ-13-1	13.6	32	38.6	2.0	BLOD	BLOD	1.1	0.2	75.2	14.1
UZ-13-2	12.4	36	36.7	1.6	BLOD	BLOD	1.0	0.3	72.1	12.7
UZ-13-3	18.6	55	26.0	1.3	640	310	1.0	0.2	153.2	22.8
UZ-13-4	6.7	22	5.6	0.3	BLOD	BLOD	1.2	0.2	256.4	57.1
UZ-13-5	0.7	1	0.6	0.0	BLOD	BLOD	1.5	0.5	279.2	280.2
UZ-13-6	22.0	67	21.8	0.7	BLOD	BLOD	1.1	0.2	215.8	28.3
UZ-13-7	41.2	78	134.0	11.0	BLOD	BLOD	1.1	0.3	65.7	9.5
UZ-13-8	13.2	44	19.6	1.0	BLOD	BLOD	1.1	0.2	144.1	23.5
UZ-13-9	11.1	11	27.2	1.1	600	370	1.2	0.2	87.4	26.8
UZ-13-10	15.5	23	32.9	1.3	BLOD	BLOD	1.1	0.2	100.9	21.7
UZ-13-11	12.7	24	154.0	14.0	BLOD	BLOD	0.9	0.2	17.6	4.0
UZ-13-12	24.6	64	35.0	1.8	BLOD	BLOD	1.2	0.3	150.0	21.0
UZ-13-13	9.6	9	32.6	1.4	580	280	1.2	0.2	63.0	21.3
UZ-13-14	15.8	55	36.0	1.8	BLOD	BLOD	1.1	0.3	94.0	14.0
UZ-13-15	15.3	25	30.8	1.2	BLOD	BLOD	1.5	0.6	105.9	21.9
UZ-13-16	27.0	58	40.3	1.6	960	320	1.2	0.2	143.4	20.4
UZ-13-17	3.4	6	3.2	0.2	BLOD	BLOD	1.0	0.2	227.1	93.8
UZ-13-18	31.5	64	34.3	1.4	2850	370	1.2	0.4	196.3	26.8
UZ-13-19	18.8	22	23.0	1.4	BLOD	BLOD	1.0	0.3	174.8	39.3
UZ-13-20	14.9	48	22.8	1.1	BLOD	BLOD	0.9	0.3	139.3	21.8
UZ-13-21	9.5	42	12.0	0.8	BLOD	BLOD	0.9	0.2	168.6	28.9
UZ-13-22	5.7	9	15.2	1.4	BLOD	BLOD	1.0	0.3	80.8	28.1
UZ-13-23	17.9	30	34.4	2.8	790	320	1.2	0.3	111.4	22.6
UZ-13-24	24.6	49	32.7	1.9	BLOD	BLOD	1.3	0.3	160.5	25.5
UZ-13-25	26.4	44	22.5	1.6	890	420	1.1	0.3	251.2	42.9
UZ-13-26	30.6	48	30.8	2.2	BLOD	BLOD	1.3	0.4	212.5	35.1
UZ-13-27	18.9	55	29.4	1.4	BLOD	BLOD	1.1	0.3	137.3	20.3

UZ-13-28	11.0	26	12.5	0.6	BLOD	BLOD	1.3	0.2	188.2	38.5
UZ-13-29	11.2	19	16.5	0.7	BLOD	BLOD	1.0	0.3	145.9	34.4
UZ-13-30	23.5	53	28.9	1.2	BLOD	BLOD	1.2	0.2	173.7	25.8
UZ-13-31	18.1	36	26.8	1.1	BLOD	BLOD	1.1	0.3	144.7	25.4
UZ-13-32	7.5	13	14.3	0.8	BLOD	BLOD	1.3	0.2	111.5	31.8
UZ-13-33	18.7	21	33.5	1.7	1130	320	0.9	0.2	119.1	27.1
UZ-13-34	11.1	9	20.5	1.1	BLOD	BLOD	1.7	0.2	115.3	39.2
UZ-13-35	15.5	47	30.3	3.2	BLOD	BLOD	1.2	0.2	109.2	20.1
UZ-13-36	27.2	29	50.7	2.2	BLOD	BLOD	1.0	0.3	114.8	22.3
UZ-13-37	17.3	38	28.9	1.3	BLOD	BLOD	1.3	0.2	128.3	22.1
UZ-13-38	29.8	41	52.5	3.2	BLOD	BLOD	1.1	0.2	121.4	20.9
UZ-13-39	13.5	40	36.8	1.4	BLOD	BLOD	1.1	0.2	78.7	13.1
UZ-13-40	10.1	30	12.6	0.6	BLOD	BLOD	1.2	0.2	172.1	33.0
UZ-14-1	16.2	86	23.9	1.0	BLOD	BLOD	1.1	0.2	125.2	15.2
UZ-14-2	9.3	30	11.3	0.5	BLOD	BLOD	1.0	0.2	153.3	29.4
UZ-14-3	4.8	38	4.9	0.3	BLOD	BLOD	1.1	0.2	179.6	31.4
UZ-14-4	8.3	35	9.9	1.5	BLOD	BLOD	0.9	0.2	155.2	35.7
UZ-14-5	5.2	28	9.3	0.5	BLOD	BLOD	1.2	0.3	104.3	20.7
UZ-14-6	13.4	53	21.3	1.1	BLOD	BLOD	1.1	0.5	116.5	17.7
UZ-14-7	11.6	67	17.1	0.8	BLOD	BLOD	0.9	0.2	125.9	17.1
UZ-14-8	16.5	77	14.6	0.6	BLOD	BLOD	0.9	0.2	209.3	26.4
UZ-14-9	26.2	111	42.7	1.5	BLOD	BLOD	1.0	0.2	113.6	12.3
UZ-14-10	3.1	11	6.8	0.3	BLOD	BLOD	0.8	0.2	85.4	26.2
UZ-14-11	9.3	32	12.3	0.6	BLOD	BLOD	1.0	0.2	140.2	26.2
UZ-14-12	13.1	51	25.8	1.3	BLOD	BLOD	1.1	0.1	93.7	14.4
UZ-14-13	13.4	62	21.7	1.2	BLOD	BLOD	1.0	0.3	114.4	16.4
UZ-14-14	5.2	35	11.6	0.5	BLOD	BLOD	1.4	0.2	82.1	14.7
UZ-14-15	10.9	48	16.1	0.7	BLOD	BLOD	1.1	0.2	125.1	19.4
UZ-14-16	14.5	43	20.0	1.1	1230	400	1.0	0.2	134.0	22.3
UZ-14-17	11.5	48	27.0	1.2	1520	630	1.0	0.2	78.6	12.2
UZ-14-18	17.4	55	24.2	0.9	1650	620	1.0	0.4	133.0	19.3

UZ-14-19	11.3	32	11.7	0.5	10700	820	1.0	0.2	177.6	33.0
UZ-14-20	7.6	28	10.6	0.8	9400	1400	1.1	0.2	131.3	27.0
UZ-14-21	11.2	42	10.9	0.6	960	450	1.0	0.2	188.9	32.0
UZ-14-22	4.5	20	7.2	0.5	1020	570	0.8	0.1	116.1	27.6
UZ-14-23	8.9	37	8.5	0.4	BLOD	BLOD	1.5	0.3	194.2	33.7
UZ-14-24	8.4	50	11.2	0.5	BLOD	BLOD	0.8	0.2	139.0	21.2
UZ-14-25	9.8	40	9.3	0.5	3900	1100	1.1	0.2	195.3	33.3
UZ-14-26	14.7	56	22.1	1.3	BLOD	BLOD	1.0	0.3	123.2	18.6
UZ-14-27	17.7	84	17.3	0.9	BLOD	BLOD	0.9	0.2	189.9	23.9
UZ-14-28	12.8	65	17.9	1.0	BLOD	BLOD	1.4	0.4	132.3	18.5
UZ-14-29	15.0	60	26.2	1.0	BLOD	BLOD	1.1	0.1	105.9	14.8
UZ-14-30	16.2	63	16.4	0.7	BLOD	BLOD	0.9	0.2	181.9	25.3
UZ-14-31	10.0	45	16.1	0.8	BLOD	BLOD	1.0	0.3	115.6	18.7
UZ-14-32	8.5	28	15.4	0.8	BLOD	BLOD	1.0	0.2	101.9	20.3
UZ-15-1	4.0	37	5.6	0.3	BLOD	BLOD	1.5	0.4	131.0	23.0
UZ-15-2	15.9	62	28.4	1.9	BLOD	BLOD	1.6	0.7	103.8	15.4
UZ-15-3	7.5	43	6.5	0.4	BLOD	BLOD	1.5	0.4	212.8	35.4
UZ-15-4	11.1	34	14.5	0.7	BLOD	BLOD	3.3	0.0	141.6	25.8
UZ-15-5	10.4	37	8.6	0.5	BLOD	BLOD	1.6	0.4	223.5	39.9
UZ-15-6	6.2	24	8.9	0.5	BLOD	BLOD	1.2	0.4	127.9	27.4
UZ-15-7	3.7	10	7.1	0.3	BLOD	BLOD	1.8	0.2	97.6	31.3
UZ-15-8	15.5	49	17.7	0.9	BLOD	BLOD	1.7	0.2	162.3	25.3
UZ-15-9	18.3	66	35.3	1.9	BLOD	BLOD	1.7	0.4	95.9	13.4
UZ-15-10	16.4	50	26.1	1.1	BLOD	BLOD	1.2	0.6	116.4	17.7
UZ-15-11	10.5	26	15.2	0.6	BLOD	BLOD	1.0	0.4	127.8	26.1
UZ-15-12	5.1	13	7.1	0.4	BLOD	BLOD	1.1	0.2	134.3	38.4
UZ-15-13	8.3	32	7.7	0.5	BLOD	BLOD	1.6	0.6	200.5	38.4
UZ-15-14	17.2	53	23.8	1.4	BLOD	BLOD	1.7	0.4	134.0	20.7
UZ-15-15	4.8	41	7.4	0.4	BLOD	BLOD	1.4	0.2	121.6	20.5
UZ-15-16	8.9	39	7.3	0.6	BLOD	BLOD	1.4	0.5	224.9	40.7
UZ-15-17	9.3	55	5.5	0.3	BLOD	BLOD	1.6	0.4	313.5	46.9

UZ-15-18	6.8	32	9.1	0.5	BLOD	BLOD	1.6	0.3	137.3	25.9
UZ-15-19	4.8	18	8.8	0.5	BLOD	BLOD	1.6	0.3	102.2	25.0
UZ-15-20	3.9	17	6.1	0.5	BLOD	BLOD	1.9	0.4	118.2	30.3
UZ-15-21	8.7	36	13.1	0.8	BLOD	BLOD	1.5	0.1	122.2	22.1
UZ-15-22	3.9	23	7.5	0.5	2600	1100	1.2	0.2	96.1	21.2
UZ-15-23	17.1	48	32.6	1.6	BLOD	BLOD	0.9	0.4	97.2	15.3
UZ-15-24	9.4	46	7.7	0.4	16500	2700	1.3	0.2	224.1	35.6
UZ-15-25	6.0	32	10.3	0.5	BLOD	BLOD	1.2	0.7	108.6	20.3
UZ-15-26	4.8	20	5.9	0.3	BLOD	BLOD	1.6	0.3	151.4	35.1
UZ-15-27	4.4	13	4.3	0.3	BLOD	BLOD	1.6	0.2	191.2	55.1
UZ-15-28	6.0	28	8.6	0.4	690	390	1.5	0.2	129.9	25.8
UZ-15-29	10.3	24	13.5	0.7	BLOD	BLOD	1.4	0.1	141.5	30.3
UZ-15-30	16.1	36	16.0	0.7	BLOD	BLOD	2.1	0.7	186.4	32.9
UZ-15-31	6.9	35	7.2	0.3	BLOD	BLOD	1.4	0.4	179.1	31.8
UZ-15-32	15.6	62	29.3	1.4	BLOD	BLOD	1.7	0.2	98.2	13.8
UZ-15-33	5.4	24	6.5	0.4	BLOD	BLOD	NA	0.0	154.2	33.2
UZ-15-34	9.7	52	9.8	0.5	BLOD	BLOD	1.6	0.2	183.0	27.9
UZ-15-35	5.2	23	8.2	0.5	BLOD	BLOD	0.8	0.0	116.6	25.5
UZ-15-36	5.6	21	7.6	0.4	BLOD	BLOD	1.5	0.1	135.6	31.0
UZ-15-37	12.5	52	24.3	1.1	BLOD	BLOD	1.4	0.1	95.5	14.4
UZ-15-38	12.3	35	14.9	0.8	BLOD	BLOD	1.6	0.4	152.5	27.7
UZ-15-39	3.6	11	6.3	0.4	BLOD	BLOD	NA	0.0	105.4	32.6
UZ-15-40	7.9	35	13.8	0.6	BLOD	BLOD	1.6	0.2	105.2	18.8
UZ-16a-1	20.5	54	17.8	0.9	650	220	1.4	0.3	246.8	37.1
UZ-16a-2	34.8	47	43.6	1.9	BLOD	BLOD	1.2	0.2	170.4	26.7
UZ-16a-3	32.3	37	127.0	7.8	BLOD	BLOD	0.9	0.3	54.3	9.7
UZ-16a-4	6.7	9	6.5	0.3	BLOD	BLOD	0.9	0.2	219.1	74.4
UZ-16a-5	44.5	76	120.6	6.1	BLOD	BLOD	1.1	0.4	78.8	10.3
UZ-16a-6	36.5	83	27.8	1.2	BLOD	BLOD	1.3	0.2	280.5	34.7
UZ-16a-7	45.4	53	60.2	2.7	BLOD	BLOD	1.4	0.4	161.1	24.0
UZ-16a-8	10.1	25	24.5	3.1	21400	4600	0.9	0.2	87.7	21.0

UZ-16a-9	16.1	44	23.2	1.1	BLOD	BLOD	1.2	0.2	148.5	24.1
UZ-16a-10	32.4	70	44.5	2.5	BLOD	BLOD	1.1	0.4	155.5	21.3
UZ-16a-11	18.6	40	33.8	2.0	BLOD	BLOD	1.5	0.4	117.8	20.4
UZ-16a-12	38.6	72	64.6	4.3	BLOD	BLOD	1.7	0.3	127.6	17.9
UZ-16a-13	28.4	37	47.3	1.7	BLOD	BLOD	1.1	0.2	128.2	22.1
UZ-16a-14	30.2	72	37.0	1.7	BLOD	BLOD	1.3	0.3	174.4	23.0
UZ-16a-15	46.6	47	33.1	1.8	BLOD	BLOD	1.4	0.3	301.0	48.2
UZ-16a-16	17.3	24	21.6	1.6	3040	350	2.6	0.1	171.6	37.8
UZ-16a-17	25.3	13	59.2	5.6	660	280	1.5	0.4	91.5	27.0
UZ-16a-18	19.2	16	58.1	2.8	BLOD	BLOD	1.1	0.2	70.6	18.2
UZ-16a-19	32.6	63	45.7	2.6	BLOD	BLOD	1.2	0.3	152.3	21.8
UZ-16a-20	22.7	49	32.0	1.2	BLOD	BLOD	1.6	0.1	151.6	23.1
UZ-16a-21	39.5	47	59.9	3.2	BLOD	BLOD	1.4	0.5	140.8	22.5
UZ-16a-22	15.9	45	17.3	1.0	1380	220	1.5	0.2	196.4	32.2
UZ-16a-23	10.1	26	15.3	0.8	6400	2500	0.8	0.0	141.5	29.2
UZ-16a-24	39.6	50	46.6	4.2	BLOD	BLOD	1.1	0.2	181.8	31.2
UZ-16a-25	39.4	96	22.4	1.2	BLOD	BLOD	1.2	0.3	375.9	45.6
UZ-16a-26	40.4	124	40.6	2.1	600	220	1.2	0.2	212.5	23.4
UZ-16a-27	5.8	15	4.9	0.2	BLOD	BLOD	0.7	0.2	252.0	66.9
UZ-16a-28	28.2	63	56.0	2.5	620	250	1.1	0.4	107.7	15.0
UZ-16a-29	11.0	21	18.4	1.0	BLOD	BLOD	1.2	0.3	127.9	29.1
UZ-16a-30	13.6	54	3.5	0.4	1580	500	1.4	0.3	828.4	150.1
UZ-16a-31	13.1	22	36.3	1.8	BLOD	BLOD	1.3	0.3	76.9	17.1
UZ-16a-32	44.4	98	57.7	2.9	BLOD	BLOD	1.1	0.3	164.4	19.5
UZ-16a-33	14.8	32	23.8	1.1	BLOD	BLOD	1.0	0.2	132.5	24.7
UZ-16a-34	26.4	58	49.7	3.3	3300	1400	1.2	0.2	113.5	17.2
UZ-16a-35	4.4	16	5.1	0.2	BLOD	BLOD	1.6	0.7	185.2	47.4
UZ-16a-36	5.5	23	5.8	0.3	1320	410	1.4	0.3	203.0	43.9
UZ-16a-37	17.9	45	20.2	1.1	2430	450	1.7	0.3	189.9	31.0
UZ-16a-38	46.5	69	72.4	5.5	BLOD	BLOD	1.4	0.4	137.4	20.2
UZ-16a-39	25.4	67	33.6	2.1	BLOD	BLOD	1.3	0.4	161.5	23.0

UZ-16a-40	9.3	44	17.8	0.9	BLOD	BLOD	0.8	0.2	111.6	18.2
UZ-16a-41	40.2	59	40.4	2.3	BLOD	BLOD	1.4	0.4	212.9	31.3
UZ-18-1	32.9	67	41.2	2.1	1050	250	1.4	0.5	170.5	23.4
UZ-18-2	10.6	21	14.1	0.8	1590	340	1.1	0.2	161.6	36.8
UZ-18-3	12.8	22	25.1	1.2	BLOD	BLOD	1.0	0.2	109.0	24.2
UZ-18-4	9.5	19	14.5	0.5	BLOD	BLOD	1.2	0.3	139.7	32.8
UZ-18-5	38.9	76	51.9	2.6	17800	3900	1.2	0.3	160.1	20.9
UZ-19-1	15.5	20	21.9	0.9	1610	300	1.8	0.7	151.2	34.9
UZ-19-2	35.6	92	53.3	2.6	3210	440	1.7	0.2	142.7	17.3
UZ-19-3	55.2	69	56.8	4.9	3860	510	1.9	0.4	207.6	31.7
UZ-19-4	36.4	87	29.5	1.6	4170	530	1.7	0.4	264.0	33.2
UZ-19-5	21.0	61	26.8	1.1	3420	430	1.7	0.2	167.6	23.4
UZ-19-6	37.3	65	36.5	2.1	4070	440	1.7	0.3	218.2	30.9
UZ-19-7	51.1	85	62.1	2.1	3390	400	1.7	0.3	175.8	21.0
UZ-19-8	37.9	77	31.8	1.4	2940	320	1.2	0.2	254.9	32.6
UZ-19-9	35.7	123	44.7	1.8	3160	360	1.9	0.4	170.5	18.0
UZ-19-10	36.2	75	33.1	1.1	2330	450	1.6	0.3	233.6	29.4
UZ-19-11	43.0	121	43.4	2.5	19900	1100	1.9	0.6	211.6	24.1
UZ-19-12	63.2	64	50.8	2.4	2760	390	1.3	0.4	265.9	36.9
UZ-19-13	32.4	44	41.6	2.0	3160	430	1.8	0.9	166.4	27.1
UZ-19-14	48.4	118	41.0	1.8	2710	420	1.7	0.4	252.4	27.4
UZ-19-15	51.6	65	53.4	2.2	2350	390	1.6	1.3	206.7	28.1
UZ-19-16	31.2	37	20.3	2.5	2490	520	2.2	1.0	328.9	68.7
UZ-19-17	8.1	16	5.2	0.3	860	340	1.6	0.4	333.5	86.1
UZ-19-18	30.3	39	34.9	1.9	4310	550	1.6	0.4	185.7	32.2
UZ-19-19	46.1	41	36.5	1.8	2450	350	1.6	0.2	270.1	45.4
UZ-19-20	72.1	57	35.6	1.5	2260	400	1.4	0.3	433.2	62.3
UZ-19-21	48.8	61	51.6	2.1	2470	340	1.6	0.2	202.1	28.2
UZ-19-22	32.7	58	30.2	1.2	2980	300	1.7	0.6	231.3	32.9
UZ-19-23	23.5	43	21.9	1.3	1850	340	1.6	0.5	229.2	38.5
UZ-19-24	48.4	90	41.3	1.7	2650	310	1.7	0.4	250.4	29.8

UZ-19-25	58.8	83	77.6	3.0	2370	230	1.9	0.4	161.9	19.8
UZ-19-26	44.0	84	41.9	2.6	2310	350	1.7	0.3	224.4	29.4
UZ-19-27	22.9	61	28.1	1.5	1910	350	1.6	0.3	174.3	25.0
UZ-19-28	45.9	52	33.7	1.6	2260	310	1.7	0.3	290.9	44.0
UZ-19-29	55.2	84	37.5	1.9	1790	310	1.6	0.4	314.8	39.6
UZ-19-30	46.0	70	35.6	1.1	2490	250	1.6	0.7	276.0	35.6
UZ-19-31	36.9	50	26.4	0.9	2280	280	1.4	0.5	298.1	44.7
UZ-20-1	11.7	23	22.9	1.2	BLOD	BLOD	1.8	0.3	94.7	20.7
UZ-20-2	22.0	74	26.9	1.4	BLOD	BLOD	1.8	0.4	150.9	20.1
UZ-20-3	11.8	58	13.6	0.6	1120	330	2.3	0.8	160.9	23.0
UZ-20-4	16.8	79	31.0	1.5	BLOD	BLOD	1.6	0.4	100.5	12.9
UZ-20-5	8.4	14	14.5	0.7	BLOD	BLOD	1.5	0.4	107.3	29.5
UZ-20-6	14.8	67	17.2	0.7	BLOD	BLOD	2.1	0.6	159.6	21.3
UZ-20-7	13.3	25	11.2	0.7	BLOD	BLOD	2.2	0.3	219.8	46.5
UZ-20-8	38.5	76	82.7	4.5	BLOD	BLOD	1.9	0.5	86.2	11.4
UZ-20-9	17.6	46	28.9	2.4	BLOD	BLOD	1.6	0.5	112.9	19.6
UZ-20-10	26.3	74	38.7	2.1	BLOD	BLOD	1.8	0.7	125.5	16.8
UZ-20-11	15.9	69	14.2	0.8	BLOD	BLOD	1.9	0.3	207.8	28.9
UZ-20-12	24.0	76	26.9	1.6	BLOD	BLOD	2.0	0.4	165.0	22.2
UZ-20-13	9.0	25	19.3	1.1	BLOD	BLOD	1.4	0.7	86.3	18.2
UZ-20-14	15.2	52	26.7	1.5	BLOD	BLOD	1.8	0.4	105.3	16.3
UZ-20-15	23.6	99	31.0	2.1	BLOD	BLOD	2.1	0.5	141.1	17.9
UZ-20-16	10.4	26	17.0	1.1	BLOD	BLOD	2.2	0.2	113.3	23.8
UZ-20-17	10.6	37	10.9	0.6	BLOD	BLOD	2.8	0.3	179.1	31.6
UZ-20-18	10.1	36	24.0	1.1	BLOD	BLOD	2.8	0.3	77.6	13.7
UZ-20-19	18.2	57	24.1	1.4	BLOD	BLOD	2.5	0.6	139.4	20.8
UZ-20-20	11.2	41	13.6	0.7	BLOD	BLOD	2.3	0.8	152.4	25.7
UZ-20-21	26.6	75	47.7	2.6	1170	460	2.4	0.7	103.2	13.7
UZ-20-22	11.8	29	11.1	0.7	BLOD	BLOD	2.0	0.5	195.8	39.1
UZ-20-23	9.8	50	16.6	0.8	BLOD	BLOD	1.2	0.2	109.6	17.0
UZ-20-24	25.7	84	55.7	2.6	1020	430	0.9	0.2	85.5	10.6

UZ-20-25	34.6	120	52.6	3.1	930	460	1.4	0.6	121.7	14.0
UZ-20-26	10.2	38	17.6	0.9	BLOD	BLOD	1.3	0.6	107.0	18.7
UZ-20-27	18.3	44	26.3	1.6	BLOD	BLOD	1.9	0.3	128.6	21.5
UZ-20-28	17.3	57	15.5	1.0	BLOD	BLOD	1.4	0.5	206.9	31.3
UZ-20-29	27.0	50	44.9	2.5	BLOD	BLOD	1.6	0.3	111.2	17.4
UZ-21-1	23.7	113	28.5	1.1	BLOD	BLOD	2.1	0.4	154.0	16.7
UZ-21-2	22.7	64	34.6	1.6	BLOD	BLOD	1.6	0.6	121.1	16.8
UZ-21-3	44.8	183	76.6	3.9	BLOD	BLOD	2.0	0.4	108.3	10.6
UZ-21-4	21.0	97	31.8	1.6	BLOD	BLOD	1.8	0.3	122.0	14.6
UZ-21-5	25.1	102	35.3	1.4	BLOD	BLOD	1.6	0.4	131.6	14.9
UZ-21-6	30.7	85	37.1	1.4	BLOD	BLOD	1.8	0.8	152.8	18.5
UZ-21-7	29.5	161	35.5	1.2	BLOD	BLOD	2.0	0.4	153.9	14.4
UZ-21-8	16.8	70	25.8	1.5	1920	730	2.1	0.4	120.6	16.7
UZ-21-9	20.2	44	33.2	1.6	BLOD	BLOD	1.3	0.5	112.4	18.3
UZ-21-10	23.8	68	34.0	1.4	BLOD	BLOD	1.9	0.7	129.6	17.3
UZ-21-11	25.9	85	46.2	1.6	BLOD	BLOD	1.5	0.5	103.5	12.4
UZ-21-12	22.6	97	30.4	1.3	BLOD	BLOD	1.7	0.7	137.8	16.1
UZ-21-13	23.4	102	23.3	1.2	BLOD	BLOD	2.0	0.8	185.5	21.9
UZ-21-14	31.6	118	52.9	2.5	BLOD	BLOD	2.1	0.6	110.5	12.2
UZ-21-15	26.4	98	33.7	1.4	700	460	2.3	0.5	145.0	16.8
UZ-21-16	25.4	100	37.2	2.3	BLOD	BLOD	2.1	0.7	126.4	15.6
UZ-21-17	24.4	162	35.7	1.3	BLOD	BLOD	2.1	1.2	126.3	11.9
UZ-21-18	26.6	121	30.0	1.8	3400	1000	1.8	0.4	164.1	18.9
UZ-21-19	30.4	100	51.8	2.3	870	400	2.0	0.6	108.5	12.6
UZ-21-20	45.7	120	84.8	2.8	BLOD	BLOD	1.5	0.5	99.8	10.4
UZ-21-21	24.3	110	38.5	1.8	BLOD	BLOD	2.0	1.0	116.9	13.2
UZ-21-22	42.9	105	71.9	4.8	BLOD	BLOD	1.8	0.7	110.3	13.7
UZ-21-23	30.2	73	34.7	1.7	BLOD	BLOD	1.7	0.4	160.7	21.3
UZ-21-24	25.7	119	36.4	1.6	720	370	1.7	0.3	130.6	14.2
UZ-21-25	29.2	168	54.3	2.7	BLOD	BLOD	2.0	0.5	99.6	9.9
UZ-21-26	25.1	103	31.2	1.5	BLOD	BLOD	1.8	0.9	148.7	17.3

UZ-21-27	30.1	110	34.3	1.5	BLOD	BLOD	1.1	0.3	162.5	18.1
UZ-21-28	21.1	75	25.4	0.9	BLOD	BLOD	1.4	0.5	153.2	19.3
UZ-21-29	24.6	68	34.6	1.6	BLOD	BLOD	1.2	0.4	131.6	17.8
UZ-21-30	23.9	71	32.7	1.4	BLOD	BLOD	1.2	0.5	135.0	17.8
UZ-21-31	21.8	61	33.9	1.5	BLOD	BLOD	1.9	0.3	119.0	16.7
UZ-21-32	24.1	89	31.9	1.7	BLOD	BLOD	1.6	0.7	139.8	17.4
UZ-21-33	20.4	100	31.2	1.5	690	370	2.2	0.5	120.9	14.2
UZ-21-34	25.2	95	32.6	1.6	BLOD	BLOD	2.1	0.5	143.0	17.2
UZ-21-35	26.3	86	42.6	1.9	BLOD	BLOD	2.1	0.6	114.2	14.0
UZ-21-36	30.5	92	36.6	2.5	BLOD	BLOD	2.1	0.3	154.1	20.1
UZ-22-1	5.1	33	3.6	0.2	780	380	1.5	0.3	265.3	50.0
UZ-22-2	7.2	22	8.5	0.5	BLOD	BLOD	0.6	0.0	157.1	35.4
UZ-22-3	8.3	39	6.2	0.3	740	290	1.5	0.3	250.2	43.3
UZ-22-4	4.6	18	6.5	0.4	990	420	2.2	0.2	130.5	32.1
UZ-22-5	5.7	24	6.8	0.3	1010	390	1.8	0.3	156.2	33.0
UZ-22-6	3.6	16	3.9	0.2	1030	370	1.6	0.3	168.7	43.9
UZ-22-7	3.7	13	4.3	0.2	BLOD	BLOD	2.3	0.5	159.7	45.3
UZ-22-8	6.2	24	5.4	0.4	1370	480	2.5	0.3	212.1	46.4
UZ-22-9	6.3	27	7.3	0.6	1090	450	2.0	0.1	160.5	34.0
UZ-22-10	5.2	19	3.9	0.3	1080	490	1.9	0.5	242.2	58.9
UZ-22-11	7.8	27	5.2	0.3	BLOD	BLOD	1.6	0.3	279.5	57.8
UZ-22-12	5.7	32	5.3	0.3	2150	520	2.1	0.2	201.2	38.5
UZ-22-13	4.5	13	4.8	0.3	BLOD	BLOD	1.3	0.4	176.7	50.6
UZ-22-14	7.2	34	6.4	0.3	BLOD	BLOD	1.7	0.3	206.8	37.6
UZ-22-15	5.1	17	5.2	0.3	990	440	1.6	0.2	182.8	46.0
UZ-22-16	7.6	25	6.2	0.3	890	420	2.3	0.7	229.3	48.0
UZ-22-17	5.0	22	4.0	0.3	BLOD	BLOD	1.0	0.2	232.0	52.5
UZ-22-18	3.8	22	3.9	0.2	1770	490	2.2	0.8	178.7	40.0
UZ-22-19	6.8	40	5.7	0.4	1290	500	2.0	0.5	219.6	38.7
UZ-22-20	6.0	36	4.4	0.3	BLOD	BLOD	1.9	0.3	249.1	44.8
UZ-22-21	8.6	34	6.2	0.3	BLOD	BLOD	1.8	0.2	256.1	47.0

UZ-22-22	11.3	35	10.1	0.7	1130	600	2.5	0.3	208.5	38.7
UZ-22-23	6.6	25	4.6	0.3	1780	500	2.1	0.3	267.0	56.3
UZ-22-24	5.3	27	5.2	0.4	990	400	2.0	0.4	188.2	39.4
UZ-22-25	5.3	28	4.8	0.2	1140	410	1.4	0.5	203.0	39.9
UZ-22-26	4.3	21	5.3	0.2	BLOD	BLOD	1.5	0.3	148.4	33.4
UZ-22-27	6.0	39	7.1	0.5	BLOD	BLOD	1.5	0.2	157.5	28.0
UZ-22-28	3.2	29	3.5	0.2	1710	370	1.5	0.4	169.2	33.5
UZ-22-29	6.9	29	6.1	0.3	BLOD	BLOD	2.1	0.9	211.6	41.1
UZ-22-30	7.8	23	4.3	0.2	BLOD	BLOD	1.8	0.2	338.1	73.9
UZ-22-31	9.6	31	6.9	0.3	1100	370	1.8	0.2	257.6	48.8
UZ-22-32	11.7	46	9.8	0.6	1110	450	1.5	0.4	220.2	36.0
UZ-22-33	7.5	47	6.9	0.3	1110	410	1.5	1.0	200.3	31.6
UZ-22-34	9.6	43	5.3	0.3	BLOD	BLOD	1.4	0.9	337.1	57.0
UZ-22-35	3.5	25	5.0	0.4	1290	500	1.7	0.1	131.0	28.2
UZ-22-36	8.3	27	4.4	0.3	BLOD	BLOD	1.5	0.4	349.0	71.3
UZ-22-37	6.5	21	6.2	0.4	BLOD	BLOD	1.9	0.4	194.4	44.6
UZ-22-38	3.2	18	3.4	0.3	106000	18000	2.4	0.3	174.7	44.5
UZ-22-39	4.2	20	4.6	0.2	860	430	1.9	0.3	171.1	39.7
UZ-22-40	4.4	27	3.6	0.3	1170	370	1.1	0.3	225.5	47.1
UZ-23-1	5.3	37	4.2	0.2	2510	440	1.9	0.3	233.0	40.9
UZ-23-2	7.3	25	7.4	0.4	2220	460	2.0	0.3	183.2	38.3
UZ-23-3	3.5	21	4.1	0.2	1820	500	1.7	0.3	157.9	36.2
UZ-23-4	7.4	49	4.7	0.3	2540	450	1.9	0.4	288.2	45.4
UZ-23-5	7.7	33	5.6	0.4	1750	450	1.9	1.1	254.3	48.3
UZ-23-6	9.1	38	6.4	0.3	1680	460	1.7	0.2	264.7	46.1
UZ-23-7	5.2	34	3.7	0.2	2200	460	1.6	0.3	263.7	49.4
UZ-23-8	6.9	38	5.1	0.3	3070	560	1.7	0.4	254.1	45.1
UZ-23-9	8.1	28	6.5	0.4	1370	460	1.8	0.4	229.6	46.0
UZ-23-10	8.4	40	4.4	0.2	2280	480	1.8	0.2	351.8	60.3
UZ-23-11	3.4	16	4.0	0.3	2830	690	1.9	0.3	157.8	41.2
UZ-23-12	5.5	20	4.9	0.3	1850	420	1.8	0.2	211.2	49.4

UZ-23-13	5.1	21	3.9	0.2	1730	460	1.9	0.3	242.5	55.6
UZ-23-14	7.5	29	5.9	0.3	1750	470	2.1	0.5	237.5	46.5
UZ-23-15	7.3	30	4.4	0.3	2240	430	2.2	0.3	305.5	59.9
UZ-23-16	6.0	35	3.7	0.2	1920	510	2.0	0.4	299.0	54.7
UZ-23-17	5.3	21	4.8	0.4	2020	460	1.7	0.3	205.1	48.1
UZ-23-18	4.4	20	4.0	0.2	2060	400	2.2	0.2	207.7	48.5
UZ-23-19	5.8	30	4.6	0.3	2590	450	2.4	0.7	233.6	45.4
UZ-23-20	5.2	17	5.4	0.3	2250	490	2.3	0.3	180.2	45.3
UZ-23-21	3.5	29	4.4	0.3	2060	380	1.5	0.2	143.9	28.7
UZ-23-22	7.3	44	3.8	0.2	2380	530	2.0	0.4	354.0	58.1
UZ-23-23	6.5	33	4.4	0.2	1870	440	2.1	0.2	276.1	51.1
UZ-23-24	3.3	19	4.7	0.5	2060	480	2.3	0.2	128.6	33.2
UZ-23-25	3.0	17	5.1	0.3	2340	440	2.6	0.2	109.7	27.8
UZ-23-26	3.6	21	4.0	0.2	2120	430	2.4	0.3	167.4	37.8
UZ-23-27	11.0	66	10.2	0.6	2330	430	1.9	0.5	200.0	28.0
UZ-23-28	11.1	42	5.3	0.3	2420	430	1.8	0.6	388.2	66.3
UZ-23-29	4.3	18	3.5	0.2	2010	410	2.2	0.3	226.4	55.6
UZ-23-30	5.3	28	3.4	0.2	2150	500	2.1	0.2	292.4	58.3
UZ-23-31	6.6	43	4.8	0.3	2280	450	1.9	0.3	253.8	42.2
UZ-23-32	2.7	18	3.1	0.2	2020	560	2.1	0.3	163.4	40.0
UZ-23-33	5.1	33	6.0	0.4	2360	500	1.8	0.3	160.0	30.2
UZ-23-34	4.0	25	3.5	0.2	2370	430	1.2	0.3	213.3	45.3
UZ-23-35	4.1	25	4.0	0.2	2210	400	2.0	0.3	188.8	39.4
UZ-23-36	7.7	23	6.3	0.3	2280	470	1.6	0.3	227.5	49.5
UZ-23-37	6.2	31	6.3	0.4	2090	500	1.3	0.2	183.1	35.6
UZ-23-38	9.3	40	9.0	0.4	2260	500	1.6	0.2	190.5	32.1
UZ-23-39	5.7	33	4.1	0.3	1820	470	1.8	0.2	254.9	48.2
UZ-23-40	7.0	38	3.8	0.2	1930	490	1.3	0.4	338.2	59.9
UZ-24-1	2.5	11	11.4	0.5	BLOD	BLOD	1.3	0.2	47.5	14.6
UZ-24-2	8.2	35	12.3	0.5	BLOD	BLOD	1.4	0.2	142.8	25.5
UZ-24-3	9.0	12	17.5	1.1	BLOD	BLOD	1.3	0.1	110.3	32.9

UZ-24-4	7.4	26	13.3	0.6	3900	1700	1.0	0.2	118.9	24.3
UZ-24-5	11.2	20	20.0	1.0	BLOD	BLOD	1.7	0.2	119.9	27.8
UZ-24-6	10.4	23	24.6	1.5	780	360	1.6	0.6	90.5	19.9
UZ-24-7	5.8	22	14.7	0.7	BLOD	BLOD	2.0	0.3	84.3	18.6
UZ-24-8	8.2	11	23.1	1.0	BLOD	BLOD	1.9	0.4	75.8	23.3
UZ-24-9	10.4	36	14.7	0.8	BLOD	BLOD	1.9	0.3	150.4	26.8
UZ-24-10	12.4	34	44.2	1.9	BLOD	BLOD	2.3	0.3	59.8	10.8
UZ-24-11	9.9	19	19.4	0.8	BLOD	BLOD	2.5	0.2	108.9	25.7
UZ-24-12	20.6	74	60.6	2.2	610	290	2.3	0.4	72.7	9.3
UZ-24-13	2.7	5	7.9	0.4	BLOD	BLOD	2.1	0.2	73.1	33.0
UZ-24-14	7.3	15	22.7	1.2	BLOD	BLOD	2.4	0.3	68.6	18.3
UZ-24-15	5.1	12	9.6	0.4	BLOD	BLOD	1.9	0.4	113.8	33.4
UZ-24-16	7.0	8	11.5	0.5	BLOD	BLOD	2.1	0.3	129.7	46.5
UZ-24-17	6.9	14	18.3	0.9	BLOD	BLOD	2.2	0.2	81.1	22.2
UZ-24-18	4.7	6	13.6	0.5	BLOD	BLOD	1.5	0.2	74.1	30.5
UZ-24-19	8.2	37	14.4	0.7	BLOD	BLOD	2.4	0.4	120.8	21.3
UZ-24-20	11.5	15	41.4	3.6	BLOD	BLOD	2.0	0.6	59.2	16.3
UZ-24-21	16.2	51	43.8	7.7	BLOD	BLOD	2.0	0.4	79.0	18.0
UZ-24-22	9.7	32	21.0	1.2	BLOD	BLOD	2.3	0.2	98.6	18.7
UZ-24-23	11.8	23	27.2	1.4	BLOD	BLOD	2.4	0.4	92.4	20.2
UZ-24-24	10.2	46	24.9	1.0	BLOD	BLOD	2.8	0.3	87.3	13.7
UZ-24-25	15.0	60	33.4	1.6	BLOD	BLOD	2.3	0.4	95.9	13.7
UZ-24-26	9.9	52	28.7	1.6	BLOD	BLOD	2.3	0.4	73.7	11.4
UZ-24-27	10.5	36	16.4	0.6	BLOD	BLOD	2.4	0.6	137.1	24.0
UZ-24-28	3.4	12	8.4	0.5	630	280	2.2	0.2	86.2	25.6
UZ-24-29	7.1	15	16.2	0.6	BLOD	BLOD	1.9	0.2	94.1	24.8
UZ-24-30	3.7	8	9.7	0.5	BLOD	BLOD	1.9	0.7	81.9	29.5
UZ-24-31	8.9	56	30.1	2.0	630	330	1.3	0.2	63.0	9.7
UZ-24-32	12.7	38	26.7	1.3	BLOD	BLOD	1.4	0.2	101.8	17.7
UZ-24-33	4.7	15	5.4	0.3	BLOD	BLOD	1.1	0.2	186.6	49.6
UZ-24-34	25.4	113	82.6	4.5	BLOD	BLOD	1.4	0.4	65.8	7.6

UZ-24-35	3.0	8	5.5	0.3	BLOD	BLOD	1.3	0.2	118.4	42.5
UZ-25-1	9.7	12	21.5	1.0	BLOD	BLOD	0.9	0.1	93.6	27.6
UZ-25-2	10.7	27	23.9	1.3	BLOD	BLOD	1.2	0.5	92.4	18.9
UZ-25-3	6.6	24	5.9	0.3	BLOD	BLOD	1.0	0.2	231.1	49.1
UZ-25-4	13.6	29	21.4	0.8	490	210	0.9	0.2	131.1	25.4
UZ-25-5	8.0	21	18.8	1.5	BLOD	BLOD	0.8	0.1	88.1	20.8
UZ-25-6	4.2	9	18.4	0.8	BLOD	BLOD	0.6	0.1	46.8	15.9
UZ-25-7	12.1	28	24.0	1.0	BLOD	BLOD	0.9	0.1	104.5	20.7
UZ-25-8	9.7	32	15.6	0.8	420	190	1.3	0.5	128.3	24.3
UZ-25-9	16.2	47	32.7	1.5	BLOD	BLOD	1.4	0.4	102.4	16.2
UZ-25-10	7.9	24	15.3	0.8	620	380	0.8	0.2	107.3	23.0
UZ-25-11	3.2	5	9.2	0.5	810	190	1.6	0.2	73.4	33.2
UZ-25-12	7.7	21	21.3	1.2	510	220	1.4	0.2	75.2	17.2
UZ-25-13	2.9	8	4.3	0.2	BLOD	BLOD	1.0	0.2	138.3	49.7
UZ-25-14	9.6	25	23.4	1.0	BLOD	BLOD	0.9	0.2	84.4	17.6
UZ-25-15	2.9	7	11.3	0.5	BLOD	BLOD	0.9	0.1	53.5	20.5
UZ-25-16	16.0	58	34.0	1.6	BLOD	BLOD	1.0	0.3	97.5	14.2
UZ-25-17	12.0	55	26.7	1.1	BLOD	BLOD	1.1	0.3	93.2	13.7
UZ-25-18	15.7	50	35.2	1.7	BLOD	BLOD	1.3	0.2	92.4	14.3
UZ-25-19	12.2	48	25.9	0.9	BLOD	BLOD	1.0	0.3	97.5	15.0
UZ-25-20	13.4	39	29.6	1.1	BLOD	BLOD	1.0	0.1	93.7	15.9
UZ-25-21	26.1	107	50.6	2.1	BLOD	BLOD	1.1	0.2	106.6	12.1
UZ-25-22	17.7	69	39.7	1.9	BLOD	BLOD	0.9	0.2	91.9	12.5
UZ-25-23	28.0	68	47.2	1.6	570	210	1.0	0.2	122.8	16.3
UZ-25-24	12.0	57	31.3	1.2	BLOD	BLOD	1.0	0.2	78.9	11.4
UZ-25-25	15.1	47	36.7	1.8	BLOD	BLOD	0.9	0.2	84.9	13.5
UZ-25-26	9.9	40	17.0	0.8	BLOD	BLOD	1.1	0.2	120.5	20.5
UZ-25-27	14.4	77	25.3	1.1	BLOD	BLOD	0.9	0.2	117.9	15.2
UZ-25-28	9.2	44	37.0	3.2	BLOD	BLOD	1.0	0.2	51.5	9.2
UZ-25-29	8.8	36	18.9	0.9	390	200	0.8	0.2	96.2	17.2
UZ-25-30	4.1	17	13.0	1.0	BLOD	BLOD	0.7	0.2	65.8	16.9

UZ-25-31	12.3	40	14.7	1.0	BLOD	BLOD	1.1	0.6	172.7	30.6
UZ-25-32	13.9	74	37.0	1.5	BLOD	BLOD	0.8	0.1	77.8	10.1
UZ-25-33	17.2	40	58.4	3.0	BLOD	BLOD	1.1	0.2	60.7	10.4
UZ-25-34	8.5	23	26.4	1.9	BLOD	BLOD	1.5	0.3	66.3	14.9
UZ-25-35	8.6	29	16.6	0.7	BLOD	BLOD	0.8	0.1	107.9	21.0
UZ-25-36	24.0	100	75.3	4.7	310	180	1.0	0.4	65.8	8.2
UZ-25-37	18.3	61	29.1	1.3	BLOD	BLOD	1.2	0.3	130.3	18.5
UZ-25-38	30.2	103	63.2	3.1	BLOD	BLOD	1.3	0.3	98.9	11.6
UZ-25-39	10.2	32	29.9	1.6	530	190	0.9	0.2	70.6	13.4
UZ-25-40	8.5	24	22.9	1.0	460	210	0.9	0.2	76.2	16.2
UZ-26-1	41.0	16.61	13.7	0.7	BLOD	BLOD	1.2	0.3	238.7	39.3
UZ-26-2	61.0	11.44	14.0	1.0	BLOD	BLOD	1.4	0.4	162.2	23.6
UZ-26-3	37.0	12.13	9.1	0.5	BLOD	BLOD	1.3	0.3	261.6	45.7
UZ-26-4	82.0	50	13.4	1.1	BLOD	BLOD	1.4	0.3	257.1	50.8
UZ-26-5	49.0	18.23	13.4	0.9	BLOD	BLOD	1.3	0.4	283.9	40.3
UZ-26-6	50.0	15.35	37.0	4.4	BLOD	BLOD	1.3	0.4	98.0	18.2
UZ-26-7	169.0	50.34	15.1	2.1	BLOD	BLOD	1.3	0.4	200.5	39.8
UZ-26-8	34.0	8.661	44.8	4.0	BLOD	BLOD	1.3	0.5	221.3	26.1
UZ-26-9	98.0	28.7	12.2	1.0	BLOD	BLOD	1.4	0.3	140.7	26.7
UZ-26-10	75.0	13.06	15.4	1.2	63900	7400	1.3	0.3	164.2	26.3
UZ-26-11	22.0	8.116	15.0	0.9	22600	3600	1.2	0.2	172.1	22.3
UZ-26-12	51.0	17.75	10.4	0.9	10700	1900	1.1	0.2	154.5	35.3
UZ-26-13	37.0	9.623	21.7	2.8	10800	1700	1.5	0.6	161.9	30.8
UZ-26-14	40.0	24.53	15.0	1.2	6980	580	1.1	0.3	127.3	23.3
UZ-26-15	45.0	19.04	17.8	2.0	6510	990	1.2	0.4	270.5	52.5
UZ-26-16	69.0	22.46	28.5	2.8	3840	610	1.2	0.4	132.5	23.7
UZ-26-17	16.0	8.692	19.6	2.4	1550	320	1.5	0.5	225.6	38.7
UZ-26-18	40.0	8.935	13.3	1.0	2070	310	1.1	0.3	129.8	33.8
UZ-26-19	12.0	7.158	17.5	1.4	1380	230	1.0	0.3	101.5	18.0
UZ-26-20	39.0	14.85	9.9	0.6	1200	250	1.2	0.4	142.8	42.1
UZ-26-21	49.0	26.52	19.3	1.5	940	150	1.3	0.5	152.4	27.1

UZ-26-22	22.0	9.731	17.5	1.3	660	230	0.5	0.2	296.6	47.8
UZ-26-23	29.0	19.1	12.8	0.7	820	170	1.2	0.2	150.7	33.1
UZ-26-24	83.0	33.63	28.0	2.0	550	180	1.5	0.3	135.3	26.9
UZ-26-25	28.0	26.11	42.6	2.6	BLOD	BLOD	1.1	0.3	156.3	19.6
UZ-26-26	59.0	14.08	16.2	1.1	960	130	1.5	0.4	171.9	25.2
UZ-26-27	55.0	29.31	14.3	0.9	700	160	1.2	0.3	284.2	49.1
UZ-28-1	138.0	34.15	72.0	8.0	BLOD	BLOD	1.1	0.3	71.6	10.0
UZ-28-2	83.0	21.68	34.1	1.5	BLOD	BLOD	1.2	0.2	126.1	14.9
UZ-28-3	32.0	14.67	61.8	4.8	BLOD	BLOD	1.3	0.4	47.4	9.1
UZ-28-4	12.0	1.999	8.1	0.5	BLOD	BLOD	1.2	0.1	73.5	21.7
UZ-28-5	38.0	9.19	15.5	1.4	BLOD	BLOD	1.1	0.3	117.7	21.9
UZ-28-6	34.0	11.52	17.4	1.3	BLOD	BLOD	1.2	0.2	131.3	24.6
UZ-28-7	14.0	4.844	19.8	3.0	10700	1900	1.2	0.2	48.8	15.0
UZ-28-8	37.0	10.44	28.9	1.8	10800	1700	1.2	0.4	72.0	12.7
UZ-28-9	54.0	16.61	28.3	2.1	6980	580	1.2	0.2	116.5	18.1
UZ-28-10	65.0	17.41	37.1	2.8	3840	610	1.4	0.3	93.4	13.6
UZ-28-11	85.0	17.96	22.3	2.0	1550	320	1.2	0.2	159.4	22.4
UZ-28-12	92.0	14.4	15.5	0.9	940	150	1.3	0.2	183.2	22.1
UZ-28-13	14.0	3.821	12.5	0.9	820	170	1.1	0.3	39.0	10.8
UZ-29a-1	18.2	61	17.2	0.7	630	210	3.4	1.1	218.4	30.8
UZ-29a-2	22.3	27	45.3	2.6	670	240	3.5	1.0	101.8	20.9
UZ-29a-3	23.7	69	47.7	3.2	540	220	3.2	1.8	102.8	14.8
UZ-29a-4	16.4	28	20.1	1.6	690	220	3.7	1.5	168.7	35.3
UZ-29a-5	1.6	4	3.4	0.2	540	190	0.6	0.1	99.2	50.1
UZ-29a-6	33.2	60	42.8	1.9	590	200	3.2	3.1	160.4	22.9
UZ-29a-7	21.8	37	46.8	2.6	BLOD	BLOD	3.9	0.5	96.3	17.2
UZ-29a-8	13.0	28	24.2	1.3	BLOD	BLOD	4.3	1.4	111.1	22.3
UZ-29a-9	20.8	50	41.2	1.9	490	260	3.8	0.9	104.6	16.1
UZ-29a-10	29.2	72	43.1	2.1	450	250	3.1	1.2	140.2	18.8
UZ-29a-11	9.2	28	17.1	0.8	BLOD	BLOD	1.6	0.2	111.6	22.2
UZ-29a-12	23.6	45	37.0	1.9	1420	290	5.2	1.7	131.8	21.5

UZ-29a-13	3.0	9	7.0	0.4	BLOD	BLOD	1.5	0.2	90.2	30.7
UZ-29a-14	26.0	80	48.6	2.5	1220	280	3.7	0.4	110.6	14.4
UZ-29a-15	19.5	52	44.8	2.9	BLOD	BLOD	4.2	1.8	90.1	14.3
UZ-29a-16	22.7	54	50.1	4.0	10800	2000	2.2	0.4	93.7	15.3
UZ-29a-17	36.2	125	67.2	3.9	1340	280	3.2	1.1	111.3	12.7
UZ-29a-18	30.4	141	21.2	1.0	BLOD	BLOD	3.2	0.5	296.0	31.1
UZ-29a-19	13.2	24	23.0	1.7	820	310	3.0	0.4	119.0	26.3
UZ-29a-20	21.4	77	42.4	2.2	BLOD	BLOD	2.7	1.4	104.3	13.7
UZ-29a-21	29.0	72	48.6	2.9	BLOD	BLOD	2.0	0.7	123.4	17.1
UZ-29a-22	22.3	44	42.5	2.3	1470	500	3.2	1.8	108.6	18.0
UZ-29a-23	22.4	88	40.6	2.1	880	320	4.4	1.5	113.8	14.3
UZ-29a-24	23.2	56	40.1	1.6	BLOD	BLOD	5.6	1.2	119.5	17.4
UZ-29a-25	24.3	78	37.7	1.8	BLOD	BLOD	3.7	1.9	133.3	17.3
UZ-29a-26	20.0	38	40.7	3.4	BLOD	BLOD	3.9	0.6	101.5	19.0
UZ-29a-27	23.7	93	38.2	2.0	660	310	4.3	1.3	128.2	15.8
UZ-29a-28	21.4	41	40.7	2.4	BLOD	BLOD	2.2	0.5	108.6	18.7
UZ-29a-29	23.9	95	36.9	1.6	950	320	3.9	0.8	133.6	15.9
UZ-29a-30	23.5	46	38.5	2.1	BLOD	BLOD	3.1	0.9	126.1	20.5
UZ-29a-31	31.2	71	34.6	1.7	BLOD	BLOD	1.1	0.2	186.3	25.1
UZ-29a-32	26.7	70	39.8	2.0	1270	430	1.8	0.6	138.5	18.9
UZ-29a-33	25.4	83	44.7	2.0	BLOD	BLOD	2.8	0.5	117.7	14.8
UZ-29a-34	21.6	41	36.3	1.7	1130	460	3.2	1.0	123.0	20.7
UZ-29a-35	20.8	97	32.2	1.5	1120	400	3.8	1.0	133.7	15.9
UZ-29a-36	26.1	81	44.9	2.6	BLOD	BLOD	3.6	0.8	120.3	15.9
UZ-29a-37	27.1	62	34.2	1.9	3630	900	3.8	0.7	163.8	23.7
UZ-29b-1	5.1	18	4.7	0.2	750	330	1.3	0.3	224.2	54.8
UZ-29b-2	28.1	43	40.2	2.3	6800	1800	1.2	0.2	144.5	24.3
UZ-29b-3	32.5	165	37.6	1.7	1430	340	1.8	0.5	178.8	17.7
UZ-29b-4	20.9	35	37.7	1.5	BLOD	BLOD	2.0	0.6	114.6	20.5
UZ-29b-5	32.5	52	39.9	1.8	690	310	2.1	0.2	168.4	25.5
UZ-29b-6	27.9	99	60.9	3.2	BLOD	BLOD	1.8	0.4	94.8	11.4

UZ-29b-7	26.7	62	40.8	2.3	BLOD	BLOD	1.9	0.4	135.4	19.6
UZ-29b-8	32.4	106	39.6	2.1	BLOD	BLOD	1.6	0.3	169.2	20.0
UZ-29b-9	27.0	72	38.0	2.1	1470	340	2.1	0.7	147.1	20.1
UZ-29b-10	28.0	46	38.4	2.0	1210	330	2.3	0.2	150.8	24.4
UZ-29b-11	23.3	63	38.1	1.5	BLOD	BLOD	1.7	0.4	126.7	17.5
UZ-29b-12	22.3	59	36.7	1.5	BLOD	BLOD	1.9	0.5	125.6	17.9
UZ-29b-13	32.8	99	50.0	2.4	810	340	1.5	0.4	135.8	16.1
UZ-29b-14	27.0	60	38.3	1.9	1240	280	1.2	0.3	145.5	21.0
UZ-29b-15	38.6	91	40.7	1.7	930	270	1.4	0.2	196.1	23.6
UZ-29b-16	23.2	38	35.3	1.5	BLOD	BLOD	1.4	0.4	135.7	23.4
UZ-29b-17	40.1	133	33.0	1.8	940	310	1.3	0.3	251.0	27.7
UZ-29b-18	18.9	39	30.2	1.5	BLOD	BLOD	1.5	0.4	129.6	22.4
UZ-29b-19	26.8	78	41.0	2.6	1270	320	1.5	0.2	135.1	18.4
UZ-29b-20	26.8	78	38.2	2.1	BLOD	BLOD	1.6	0.4	145.3	19.2
UZ-29b-21	34.3	110	38.6	2.5	BLOD	BLOD	1.4	0.5	183.6	22.5
UZ-29b-22	39.8	99	48.2	2.2	1100	410	2.1	0.8	170.6	20.1
UZ-29b-23	36.1	123	50.1	3.3	BLOD	BLOD	1.6	0.4	149.0	17.7
UZ-29b-24	25.0	64	29.6	1.4	BLOD	BLOD	2.2	0.2	174.8	24.5
UZ-29b-25	28.9	57	40.5	2.3	4320	920	1.6	0.3	147.6	22.1
UZ-29b-26	30.6	45	37.7	1.7	BLOD	BLOD	2.4	0.6	167.8	27.0
UZ-29b-27	32.9	92	46.4	3.0	990	330	2.7	0.5	146.8	19.0
UZ-29b-28	27.6	70	43.7	2.7	1120	270	2.7	0.3	130.6	18.4
UZ-29b-29	30.2	89	43.3	1.9	BLOD	BLOD	2.3	0.4	144.0	17.6
UZ-29b-30	34.5	86	39.7	2.6	1070	350	2.2	0.4	179.7	23.9
UZ-29b-31	24.5	88	22.6	1.3	BLOD	BLOD	2.2	0.5	224.1	28.7
UZ-29b-32	29.3	68	48.6	2.2	BLOD	BLOD	1.8	0.4	124.4	16.9
UZ-29b-33	28.5	87	34.4	1.5	1680	330	2.1	0.4	171.5	21.1
UZ-29b-34	28.2	82	38.3	1.8	BLOD	BLOD	1.9	0.4	152.0	19.3
UZ-29b-35	28.6	87	44.1	2.1	1200	280	2.2	0.5	134.2	16.7
UZ-29b-36	32.9	138	38.8	1.7	1760	320	2.1	0.7	175.5	18.3
UZ-29b-37	23.1	78	38.9	2.4	BLOD	BLOD	1.3	0.3	122.9	16.6

UZ-29b-38	28.7	63	39.4	1.9	BLOD	BLOD	1.3	0.4	150.7	21.3
UZ-29b-39	19.3	41	40.4	2.2	BLOD	BLOD	1.6	0.6	98.9	16.9
UZ-30-1	24.3	68	36.8	1.7	BLOD	BLOD	2.0	0.4	136.7	18.6
UZ-30-2	18.5	40	36.3	3.0	1020	520	1.7	0.4	105.3	19.3
UZ-30-3	28.2	53	41.2	2.4	BLOD	BLOD	1.8	0.3	141.6	21.9
UZ-30-4	25.2	78	35.9	1.8	540	230	1.9	0.5	144.9	18.9
UZ-30-5	19.4	21	37.9	2.0	BLOD	BLOD	1.2	0.4	105.6	24.1
UZ-30-6	24.7	56	50.9	2.8	BLOD	BLOD	1.5	0.5	100.3	15.1
UZ-30-7	32.7	60	46.0	2.2	BLOD	BLOD	1.5	0.2	146.8	21.1
UZ-30-8	24.4	76	36.7	1.6	BLOD	BLOD	1.5	0.3	137.2	17.8
UZ-30-9	7.4	22	10.0	0.5	BLOD	BLOD	1.2	0.2	153.1	34.2
UZ-30-10	28.3	60	38.1	1.7	BLOD	BLOD	1.6	0.3	153.5	21.9
UZ-30-11	24.0	70	37.3	2.4	BLOD	BLOD	1.5	0.3	133.0	18.9
UZ-30-12	28.5	62	39.8	2.1	650	270	1.5	0.2	148.2	21.3
UZ-30-13	30.2	110	38.1	1.7	BLOD	BLOD	1.5	0.3	164.1	18.6
UZ-30-14	20.7	40	33.8	1.8	600	260	1.7	0.3	126.6	21.8
UZ-30-15	32.2	78	46.4	2.0	BLOD	BLOD	1.4	0.4	143.3	18.4
UZ-30-16	21.9	45	20.9	1.1	BLOD	BLOD	1.4	0.2	216.6	35.4
UZ-30-17	29.8	94	40.6	1.7	BLOD	BLOD	1.8	0.3	151.8	18.0
UZ-30-18	28.1	70	24.1	1.1	BLOD	BLOD	2.0	0.4	240.6	32.4
UZ-30-19	4.1	8	7.6	0.5	BLOD	BLOD	1.5	0.5	110.8	40.2
UZ-30-20	20.2	48	33.2	1.8	660	300	1.5	0.5	126.0	20.1
UZ-30-21	32.0	87	34.5	2.0	18500	4200	1.7	0.4	191.8	24.7
UZ-30-22	32.0	99	33.5	1.6	BLOD	BLOD	1.6	0.3	197.2	23.4
UZ-30-23	27.3	70	55.9	3.4	BLOD	BLOD	1.6	0.3	100.8	14.1
UZ-30-24	23.2	71	37.1	1.9	BLOD	BLOD	2.1	0.6	129.5	17.6
UZ-30-25	28.6	62	41.3	3.6	3400	1100	1.9	0.4	143.1	22.8
UZ-30-26	2.6	18	3.9	0.2	1460	410	1.4	0.6	141.1	34.7
UZ-30-27	26.0	98	40.1	2.7	1340	650	1.5	0.4	134.0	17.2
UZ-30-28	25.4	116	37.1	1.6	BLOD	BLOD	1.4	0.5	141.4	15.6
UZ-30-29	14.9	39	35.5	1.7	BLOD	BLOD	1.2	0.2	87.0	15.0

UZ-30-30	20.5	92	34.5	1.4	1040	390	1.6	0.5	122.7	14.6
UZ-30-31	32.7	110	59.8	2.6	BLOD	BLOD	1.5	0.3	113.0	12.7
UZ-30-32	23.3	67	40.4	2.0	BLOD	BLOD	1.5	0.6	119.0	16.4
UZ-30-33	29.1	81	44.3	1.7	1080	490	2.0	0.4	135.7	16.9
UZ-30-34	28.3	57	54.1	3.1	870	460	2.5	0.4	108.2	16.2
UZ-30-35	28.9	50	37.2	2.6	BLOD	BLOD	1.9	0.3	160.6	26.2
UZ-30-36	31.4	73	44.2	3.1	4400	1400	1.7	0.5	146.9	20.9
UZ-30-37	25.3	56	34.7	1.5	1070	560	1.5	0.3	150.9	22.1
UZ-30-38	30.4	46	40.2	1.7	BLOD	BLOD	1.6	0.3	156.1	24.8
UZ-30-39	19.9	37	36.3	2.0	BLOD	BLOD	1.5	0.3	113.1	20.2
UZ-30-40	28.9	85	37.7	1.9	BLOD	BLOD	1.3	0.3	158.3	20.0
UZ-31-1	12.0	31	9.3	0.6	BLOD	BLOD	1.3	0.2	267.7	51.9
UZ-31-2	23.3	25	41.5	1.8	1050	320	1.5	0.4	116.2	24.3
UZ-31-3	12.8	18	21.5	1.0	710	300	1.4	0.2	123.4	30.1
UZ-31-4	16.3	56	21.1	1.0	640	300	1.3	0.2	160.0	23.6
UZ-31-5	11.7	28	7.5	0.5	BLOD	BLOD	1.1	0.2	323.3	65.5
UZ-31-6	2.8	6	4.4	0.2	BLOD	BLOD	1.1	0.2	129.6	53.6
UZ-31-7	17.3	29	29.0	1.7	600	340	1.3	0.2	123.5	24.6
UZ-31-8	15.4	27	21.1	1.0	590	310	1.6	0.4	151.3	30.6
UZ-31-9	12.3	36	15.6	1.1	4100	1700	1.3	0.3	163.3	30.3
UZ-31-10	2.5	3	4.4	0.2	730	320	1.3	0.2	118.8	69.0
UZ-31-11	6.0	17	8.0	0.4	500	260	1.5	0.2	156.3	39.3
UZ-31-12	19.9	53	32.3	6.0	1140	540	1.3	0.3	127.4	29.9
UZ-31-13	22.0	43	37.7	2.3	1190	430	1.6	0.3	120.4	20.4
UZ-31-14	9.5	11	18.3	1.0	630	240	1.4	0.3	107.4	33.2
UZ-31-15	21.1	47	30.0	1.1	BLOD	BLOD	1.2	0.3	145.1	22.6
UZ-31-16	14.0	42	14.0	0.6	900	240	1.1	0.3	206.3	34.0
UZ-31-17	11.7	32	8.8	0.6	BLOD	BLOD	1.0	0.2	275.4	53.0
UZ-31-18	21.1	96	17.9	0.9	2660	350	1.8	0.2	244.2	29.7
UZ-31-19	4.0	14	4.4	0.3	630	310	1.0	0.2	189.4	52.7
UZ-31-20	23.2	60	22.2	1.3	600	280	1.4	0.2	216.2	31.9

UZ-31-21	17.8	35	24.2	1.4	BLOD	BLOD	1.0	0.3	152.4	28.0
UZ-31-22	6.8	8	12.7	0.9	770	230	1.2	0.2	111.8	40.5
UZ-31-23	21.4	71	20.7	1.3	BLOD	BLOD	1.2	0.3	213.3	30.0
UZ-31-24	31.1	102	68.8	2.8	BLOD	BLOD	1.4	0.3	93.4	10.7
UZ-31-25	10.6	50	17.2	0.7	BLOD	BLOD	1.0	0.2	126.9	19.5
UZ-31-26	12.4	44	12.9	0.7	590	230	1.2	0.3	198.4	32.7
UZ-31-27	30.2	80	31.0	2.5	1650	980	1.0	0.3	201.1	28.9
UZ-31-28	3.4	6	4.8	0.3	450	220	1.6	0.2	148.6	61.8
UZ-31-29	9.6	20	9.3	0.5	740	270	1.0	0.2	211.7	49.6
UZ-31-30	6.3	28	8.2	0.5	BLOD	BLOD	1.2	0.3	159.1	32.1
UZ-31-31	7.1	11	13.1	0.9	BLOD	BLOD	1.0	0.3	111.4	34.8
UZ-31-32	1.8	9	4.1	0.3	BLOD	BLOD	1.5	0.2	91.4	31.2
UZ-31-33	9.6	36	11.0	0.6	BLOD	BLOD	0.9	0.2	179.9	32.4
UZ-31-34	12.4	44	10.8	0.7	BLOD	BLOD	1.2	0.2	235.5	39.8
UZ-31-35	11.8	15	20.8	1.4	BLOD	BLOD	1.1	0.2	116.8	31.5
UZ-31-36	17.5	42	22.2	2.1	BLOD	BLOD	1.3	0.3	162.7	30.2
UZ-31-37	12.3	28	18.0	0.8	BLOD	BLOD	1.2	0.2	140.8	28.0
UZ-31-38	8.7	10	5.8	0.4	300	140	1.7	0.2	306.3	99.5
UZ-31-39	11.9	45	22.4	1.2	460	220	1.4	0.2	109.7	18.0
UZ-32-1	6.8	17	5.9	0.3	BLOD	BLOD	1.1	0.5	237.9	59.9
UZ-32-2	7.5	12	9.2	0.7	1110	280	2.1	0.2	170.1	51.3
UZ-32-3	8.5	10	11.0	0.7	BLOD	BLOD	1.9	0.8	159.5	52.0
UZ-32-4	14.9	12	17.8	1.0	BLOD	BLOD	1.4	0.8	172.7	51.3
UZ-32-5	12.0	16	12.0	0.6	BLOD	BLOD	2.3	0.4	207.8	53.7
UZ-32-6	7.6	22	9.0	0.4	BLOD	BLOD	1.1	0.3	174.5	38.7
UZ-32-7	10.2	10	12.9	1.0	BLOD	BLOD	1.8	0.2	163.4	53.6
UZ-32-8	9.4	19	9.6	0.5	BLOD	BLOD	1.7	0.3	201.2	48.2
UZ-32-9	7.5	20	12.3	0.7	BLOD	BLOD	2.4	0.1	125.6	29.4
UZ-32-10	6.4	13	11.5	0.7	BLOD	BLOD	2.1	0.1	115.4	33.0
UZ-32-11	3.9	5	9.2	0.4	BLOD	BLOD	2.2	0.3	88.2	39.8
UZ-32-12	18.8	35	15.1	0.9	BLOD	BLOD	1.5	0.4	258.3	47.5

UZ-32-13	11.2	20	14.4	0.6	BLOD	BLOD	2.0	0.6	161.6	37.4
UZ-32-14	18.6	15	16.5	0.9	680	240	1.8	0.1	232.7	62.1
UZ-32-15	14.9	51	16.5	0.8	BLOD	BLOD	1.7	0.3	187.4	28.8
UZ-32-16	8.8	35	6.8	0.4	2480	350	1.6	0.3	269.1	50.0
UZ-32-17	20.3	38	25.2	1.3	BLOD	BLOD	2.0	0.3	166.1	29.1
UZ-32-18	14.8	30	13.9	0.6	2250	340	2.7	0.3	219.7	42.1
UZ-32-19	29.2	42	19.5	1.0	BLOD	BLOD	1.9	0.3	310.0	52.0
UZ-32-20	11.5	13	15.9	0.9	BLOD	BLOD	1.6	0.4	148.7	42.5
UZ-32-21	7.7	11	10.0	0.6	21200	4900	1.4	0.6	160.9	49.9
UZ-32-22	13.1	16	23.6	2.9	BLOD	BLOD	1.6	0.5	115.1	32.4
UZ-32-23	9.0	19	22.0	1.3	BLOD	BLOD	1.9	0.5	84.4	20.3
UZ-32-24	17.0	48	28.1	1.4	BLOD	BLOD	1.5	0.4	124.7	19.7
UZ-32-25	7.6	11	8.0	0.5	BLOD	BLOD	1.6	0.9	198.1	61.4
UZ-32-26	9.1	12	14.7	1.0	BLOD	BLOD	1.3	0.0	127.4	38.2
UZ-32-27	6.5	11	10.5	0.5	BLOD	BLOD	1.6	0.3	128.8	39.6
UZ-32-28	9.5	13	9.3	0.5	BLOD	BLOD	2.0	0.2	212.7	60.9
UZ-32-29	8.5	18	6.8	0.3	BLOD	BLOD	2.2	0.1	255.9	62.5
UZ-32-30	9.8	10	7.5	0.4	BLOD	BLOD	1.0	0.2	268.9	87.0
UZ-32-31	10.7	11	14.0	0.7	BLOD	BLOD	1.4	0.3	158.2	48.9
UZ-35-1	17.1	42	12.9	0.8	BLOD	BLOD	1.1	0.3	300.0	51.9
UZ-35-2	12.2	18	9.9	0.9	BLOD	BLOD	1.4	0.3	278.6	71.8
UZ-35-3	16.2	35	16.4	0.6	BLOD	BLOD	1.4	0.5	223.3	40.2
UZ-35-4	6.0	16	7.0	0.4	660	280	1.5	0.6	193.2	50.7
UZ-35-5	8.8	9	9.3	0.6	BLOD	BLOD	1.3	0.2	214.7	73.7
UZ-35-6	6.7	16	10.2	0.5	500	310	1.2	0.3	150.5	39.2
UZ-35-7	5.8	16	6.1	0.3	610	220	1.1	0.1	216.3	56.4
UZ-35-8	11.5	32	10.4	0.5	780	270	1.1	0.2	251.3	47.8
UZ-35-9	5.1	5	3.7	0.3	1100	320	1.2	0.0	315.4	143.5
UZ-35-10	3.6	7	8.6	0.5	700	350	0.9	0.3	94.1	36.3
UZ-35-11	9.2	20	9.3	0.6	BLOD	BLOD	1.1	0.2	223.1	53.1
UZ-35-12	13.6	24	24.3	1.1	BLOD	BLOD	1.0	0.2	126.5	27.2

UZ-35-13	10.7	20	10.2	0.5	790	320	0.6	0.1	239.1	56.0
UZ-35-14	5.7	17	9.6	0.5	BLOD	BLOD	0.8	0.2	136.1	34.4
UZ-35-15	6.5	14	11.4	0.6	BLOD	BLOD	0.9	0.2	128.5	35.6
UZ-35-16	5.0	12	7.1	0.5	BLOD	BLOD	1.2	0.7	160.7	48.2
UZ-35-17	8.2	27	8.4	0.5	BLOD	BLOD	1.2	0.5	223.4	46.2
UZ-35-18	13.1	42	21.9	0.9	BLOD	BLOD	1.0	0.2	135.0	22.5
UZ-35-19	2.7	9	6.3	0.5	BLOD	BLOD	0.9	0.3	97.0	33.6
UZ-35-20	10.5	43	27.0	1.5	890	450	1.0	0.2	88.3	15.0
UZ-35-21	9.4	29	14.3	0.7	BLOD	BLOD	1.2	0.2	149.9	29.8
UZ-35-22	7.6	33	8.9	0.5	BLOD	BLOD	1.0	0.2	191.7	36.4
UZ-35-23	7.4	16	7.1	0.4	1760	600	1.0	0.2	235.7	61.2
UZ-35-24	5.1	8	6.6	0.4	BLOD	BLOD	1.3	0.2	176.9	64.1
UZ-35-25	18.0	49	22.5	1.1	BLOD	BLOD	1.3	0.3	181.5	28.8
UZ-35-26	9.2	26	8.9	0.4	BLOD	BLOD	1.3	0.3	235.5	49.0
UZ-35-27	8.4	38	15.5	1.0	BLOD	BLOD	1.2	0.1	123.2	22.3
UZ-35-28	5.8	17	10.6	0.4	BLOD	BLOD	1.1	0.3	123.4	30.9
UZ-35-29	14.2	38	9.3	0.5	8130	860	1.0	0.3	343.8	60.7
UZ-35-30	15.8	24	15.2	1.3	BLOD	BLOD	1.0	0.3	235.6	53.4
UZ-35-31	12.9	39	8.6	0.4	BLOD	BLOD	1.1	0.2	337.3	59.0
UZ-35-32	8.5	23	18.1	0.9	BLOD	BLOD	1.8	0.4	107.2	23.5
UZ-35-33	16.2	46	16.8	1.1	BLOD	BLOD	1.2	0.2	218.3	36.8
UZ-35-34	11.5	31	25.7	1.5	BLOD	BLOD	1.3	0.1	101.3	19.8
UZ-35-35	8.0	22	13.0	0.6	BLOD	BLOD	1.3	0.2	138.5	31.0
UZ-35-36	5.3	13	11.8	0.6	BLOD	BLOD	1.3	0.3	100.7	28.8
UZ-36-1	6.2	22	5.9	0.3	BLOD	BLOD	1.2	0.2	230.9	51.3
UZ-36-2	4.5	18	5.1	0.3	BLOD	BLOD	1.1	0.2	198.0	48.3
UZ-36-3	3.6	17	4.7	0.3	660	320	1.2	0.3	168.0	43.0
UZ-36-4	5.4	18	11.4	0.8	98000	15000	1.5	0.1	104.2	25.8
UZ-36-5	4.7	23	6.9	0.4	810	310	1.0	0.2	151.2	33.2
UZ-36-6	3.3	14	4.5	0.2	850	410	1.2	0.2	159.4	43.6
UZ-36-7	5.0	23	5.2	0.3	BLOD	BLOD	1.0	0.2	213.8	46.5

UZ-36-8	4.4	15	6.6	0.4	BLOD	BLOD	0.7	0.2	146.3	39.0
UZ-36-9	4.4	16	12.5	1.0	BLOD	BLOD	1.2	0.2	78.4	20.8
UZ-36-10	6.3	19	15.6	0.8	BLOD	BLOD	1.2	0.2	89.1	21.2
UZ-36-11	14.7	51	15.6	0.8	BLOD	BLOD	1.5	0.6	208.1	32.0
UZ-36-12	7.7	35	7.6	0.3	BLOD	BLOD	1.4	0.2	223.9	39.7
UZ-36-13	4.3	19	8.5	0.3	BLOD	BLOD	1.2	0.3	113.0	26.7
UZ-36-14	7.5	21	4.4	0.2	BLOD	BLOD	1.3	0.4	375.2	85.6
UZ-36-15	7.7	28	15.5	1.2	BLOD	BLOD	1.3	0.2	109.2	22.7
UZ-36-16	7.0	26	5.7	0.4	670	280	1.2	0.2	272.5	58.0
UZ-36-17	12.6	44	28.4	1.5	BLOD	BLOD	1.5	0.2	97.8	16.1
UZ-36-18	4.3	18	6.0	0.3	BLOD	BLOD	1.4	0.3	157.6	38.2
UZ-36-19	12.2	39	10.4	0.6	BLOD	BLOD	1.4	0.3	257.8	44.8
UZ-36-20	19.0	80	34.7	1.5	BLOD	BLOD	1.3	0.1	120.9	15.2
UZ-36-21	11.9	45	26.5	1.2	BLOD	BLOD	1.2	0.3	99.5	16.0
UZ-36-22	10.2	32	22.7	1.2	BLOD	BLOD	1.5	0.7	99.2	18.7
UZ-36-23	15.1	44	32.8	1.5	590	240	1.3	0.4	101.9	16.5
UZ-36-24	5.4	23	5.0	0.2	3470	800	1.2	0.2	242.6	52.8
UZ-36-25	4.2	26	6.7	0.4	1690	610	1.2	0.3	138.3	28.7
UZ-36-26	5.0	18	5.0	0.3	590	170	1.2	0.4	220.8	54.1
UZ-36-27	3.8	19	6.1	0.3	420	190	1.1	0.3	136.9	32.3
UZ-36-28	3.2	11	7.9	0.6	8300	1700	1.5	0.3	88.4	27.6
UZ-36-29	8.0	30	9.3	0.7	BLOD	BLOD	1.1	0.3	190.7	38.0
UZ-36-30	5.8	25	6.1	0.4	400	190	1.2	0.3	209.1	44.2
UZ-36-31	6.4	25	7.3	0.4	BLOD	BLOD	1.1	0.2	191.7	40.2
UZ-36-32	4.0	19	5.7	0.3	390	180	1.2	0.3	155.4	36.9
UZ-36-33	11.2	62	7.2	0.4	BLOD	BLOD	1.2	0.2	341.9	48.6
UZ-36-34	1.2	7	3.2	0.2	410	170	1.5	0.3	80.4	30.9
UZ-36-35	5.5	25	6.1	0.4	350	210	1.3	0.2	198.7	42.0
UZ-36-36	3.1	12	5.0	0.3	370	170	1.2	0.2	139.0	41.3
UZ-36-37	5.1	14	7.1	0.4	460	190	1.1	0.2	158.8	43.7

UZ-36-38	6.5	16	6.1	0.3	BLOD	BLOD	1.1	0.2	235.0	60.6
UZ-37-1	28.0	74	47.6	2.2	2680	640	1.2	0.2	130.1	17.0
UZ-37-2	16.2	34	27.5	1.1	880	270	1.2	0.2	130.5	23.5
UZ-37-3	21.7	43	29.4	1.4	930	230	1.3	0.3	163.2	26.8
UZ-37-4	28.4	42	58.0	7.3	3000	1600	1.3	0.3	108.1	21.9
UZ-37-5	26.5	43	29.6	1.3	1430	260	1.3	0.3	197.9	32.3
UZ-37-6	15.8	60	24.7	1.5	1280	240	1.2	0.2	141.7	20.9
UZ-37-7	14.1	46	24.7	1.5	1080	300	1.3	0.2	126.6	20.8
UZ-37-8	23.4	81	32.2	1.8	850	330	1.3	0.2	160.8	20.9
UZ-37-9	14.1	25	21.3	0.8	BLOD	BLOD	1.1	0.2	146.2	30.3
UZ-37-10	27.0	71	59.4	2.5	1200	450	1.4	0.2	100.3	13.2
UZ-37-11	20.7	57	36.0	1.6	620	330	1.6	0.4	127.4	18.5
UZ-37-12	25.0	40	44.1	1.5	1070	330	1.3	0.3	125.2	20.8
UZ-37-13	20.8	29	17.7	0.8	1320	290	1.3	0.3	258.6	50.4
UZ-37-14	37.9	57	52.0	3.3	810	300	1.4	0.3	161.3	24.5
UZ-37-15	33.2	28	48.5	2.3	1170	250	1.5	0.3	151.5	30.1
UZ-37-16	43.2	53	80.2	4.9	38000	15000	1.3	0.4	119.2	18.5
UZ-37-17	19.9	33	23.4	1.3	730	240	1.3	0.3	188.3	35.2
UZ-37-18	11.5	16	23.8	1.5	1150	290	1.4	0.2	106.6	27.8
UZ-37-19	17.1	27	62.5	3.4	780	310	1.2	0.2	60.6	12.3
UZ-37-20	16.2	48	14.5	1.0	1060	240	1.1	0.2	247.7	40.4
UZ-37-21	24.3	46	22.9	1.0	1070	260	1.5	0.2	235.1	37.2
UZ-37-22	26.2	59	42.9	6.3	14000	10000	1.2	0.3	135.2	27.0
UZ-37-23	6.3	20	10.6	0.6	1830	260	1.2	0.2	131.9	30.8
UZ-37-24	33.2	57	88.6	4.1	1300	310	1.2	0.2	82.8	12.0
UZ-37-25	19.9	13	30.2	1.2	850	300	1.2	0.4	145.8	41.2
UZ-37-26	13.9	20	20.4	1.2	1170	350	1.4	0.2	150.7	35.3
UZ-37-27	28.4	40	53.6	2.5	1260	350	1.3	0.4	117.2	19.8
UZ-37-28	15.5	30	30.9	1.5	1580	270	1.5	0.6	111.1	21.4
UZ-37-29	16.8	25	34.3	1.7	1240	310	1.3	0.2	108.3	22.7
UZ-37-30	26.3	22	41.6	2.4	1120	260	1.3	0.2	139.6	31.3

UZ-37-31	22.5	31	80.0	41.0	1040000	290000	1.2	0.3	62.0	33.8
UZ-37-32	20.5	38	36.6	2.7	22300	3700	1.3	0.2	123.8	22.6
UZ-38-1	4.6	27	6.0	0.3	BLOD	BLOD	1.0	0.2	172.0	35.0
UZ-38-2	3.8	12	10.8	0.5	BLOD	BLOD	1.3	0.5	78.3	23.1
UZ-38-3	4.7	13	6.0	0.2	BLOD	BLOD	1.0	0.1	172.4	48.7
UZ-38-4	9.1	46	11.0	0.8	BLOD	BLOD	1.2	0.2	181.7	30.4
UZ-38-5	7.5	17	14.0	0.9	BLOD	BLOD	1.3	0.1	118.3	29.9
UZ-38-6	1.2	8	2.8	0.2	BLOD	BLOD	1.1	0.3	96.6	34.8
UZ-38-7	8.4	34	13.7	0.7	BLOD	BLOD	1.3	0.3	135.6	24.7
UZ-38-8	6.9	24	15.0	0.7	BLOD	BLOD	0.9	0.2	102.1	21.7
UZ-38-9	12.1	27	24.6	1.0	BLOD	BLOD	1.0	0.2	108.4	21.7
UZ-38-10	12.6	61	18.8	1.6	BLOD	BLOD	1.3	0.4	147.8	23.4
UZ-38-11	9.9	21	8.2	0.5	BLOD	BLOD	1.8	0.4	266.2	61.2
UZ-38-12	6.5	15	4.7	0.3	BLOD	BLOD	0.8	0.1	305.3	81.5
UZ-38-13	38.0	45	98.6	4.8	1180	430	1.0	0.2	85.1	13.7
UZ-38-14	4.8	9	8.1	0.6	BLOD	BLOD	1.3	0.3	129.6	44.5
UZ-38-15	8.3	32	11.6	0.4	BLOD	BLOD	0.9	0.2	158.0	29.1
UZ-38-16	1.0	2	1.8	0.2	BLOD	BLOD	1.6	0.1	126.3	90.1
UZ-38-17	5.2	8	12.7	0.9	BLOD	BLOD	0.8	0.2	90.3	32.8
UZ-38-18	1.5	5	2.8	0.2	BLOD	BLOD	1.8	1.8	122.2	55.5
UZ-38-19	1.9	5	4.7	0.3	BLOD	BLOD	1.0	0.3	88.8	40.3
UZ-38-20	23.2	54	43.8	2.1	BLOD	BLOD	1.1	0.2	117.0	17.5
UZ-38-21	2.7	8	3.0	0.2	BLOD	BLOD	1.2	0.4	200.8	72.5
UZ-38-22	2.2	3	6.8	0.3	BLOD	BLOD	0.8	0.2	71.2	41.3
UZ-38-23	6.8	25	11.6	0.6	BLOD	BLOD	1.0	0.2	129.9	27.3
UZ-38-24	17.1	40	16.8	0.8	BLOD	BLOD	1.3	0.2	225.1	38.1
UZ-38-25	2.3	3	13.5	0.8	BLOD	BLOD	1.2	0.3	37.7	21.9
UZ-38-26	2.5	3	2.7	0.2	1310	430	0.7	0.3	207.2	120.6
UZ-38-27	28.0	74	51.6	3.0	1010	370	1.2	0.3	119.8	16.2
UZ-38-28	2.7	8	4.1	0.3	690	350	1.2	0.4	141.9	51.3
UZ-38-29	7.7	19	16.6	0.8	BLOD	BLOD	1.0	0.2	102.7	24.4

UZ-38-30	1.7	4	3.2	0.2	BLOD	BLOD	0.9	0.0	119.0	60.3
UZ-38-31	12.7	14	19.4	0.9	BLOD	BLOD	0.7	0.1	144.2	39.5
UZ-38-32	6.5	15	4.8	0.3	BLOD	BLOD	0.8	0.4	300.9	80.9
UZ-38-33	4.7	9	6.0	0.3	BLOD	BLOD	0.9	0.1	170.8	58.0
UZ-38-34	2.5	10	2.0	0.2	BLOD	BLOD	1.0	0.2	270.8	91.6
UZ-38-35	13.4	32	33.1	2.1	BLOD	BLOD	0.9	0.3	89.4	17.1
UZ-39-1	26.4	75	40.6	2.5	BLOD	BLOD	1.3	0.2	143.8	19.6
UZ-39-2	2.3	11	5.1	0.3	BLOD	BLOD	1.2	0.6	99.8	30.8
UZ-39-3	37.2	117	94.4	5.1	BLOD	BLOD	1.5	0.3	87.2	9.9
UZ-39-4	18.9	76	44.4	2.3	BLOD	BLOD	1.5	0.3	94.2	12.4
UZ-39-5	20.9	75	34.4	1.4	BLOD	BLOD	1.5	0.2	134.2	17.2
UZ-39-6	34.1	126	53.0	2.9	1030	380	1.6	0.5	142.2	15.8
UZ-39-7	41.5	143	79.3	3.3	BLOD	BLOD	1.6	0.3	115.8	11.7
UZ-39-8	47.4	109	141.6	4.9	BLOD	BLOD	1.5	0.2	74.0	8.1
UZ-39-9	11.0	48	22.9	1.1	BLOD	BLOD	1.4	0.2	106.0	16.6
UZ-39-10	17.3	43	36.3	1.7	BLOD	BLOD	1.4	0.4	105.4	17.3
UZ-39-11	37.6	89	72.7	2.3	BLOD	BLOD	1.5	0.4	114.4	13.4
UZ-39-12	18.8	50	101.4	3.5	830	350	1.5	0.2	40.9	6.2
UZ-39-13	23.2	75	99.0	6.9	19500	6600	1.8	0.2	51.8	7.3
UZ-39-14	15.4	66	34.2	1.9	BLOD	BLOD	1.6	0.2	99.7	14.0
UZ-39-15	34.3	99	87.7	3.1	BLOD	BLOD	1.7	0.3	86.5	9.8
UZ-39-16	14.7	75	27.1	1.7	BLOD	BLOD	1.6	0.2	120.0	16.4
UZ-39-17	26.2	91	51.2	2.7	BLOD	BLOD	1.1	0.2	113.3	14.0
UZ-39-18	31.5	102	31.9	1.8	BLOD	BLOD	1.4	0.3	218.0	26.2
UZ-39-19	17.0	89	39.6	2.0	660	390	1.8	0.2	95.0	11.7
UZ-39-20	11.2	28	35.3	1.8	BLOD	BLOD	1.4	0.3	69.9	13.9
UZ-39-21	23.8	81	56.2	4.4	BLOD	BLOD	1.1	0.2	93.4	13.2
UZ-39-22	2.8	10	72.5	3.3	BLOD	BLOD	1.0	0.3	8.6	2.8
UZ-39-23	7.3	36	65.7	2.4	760	290	1.2	0.2	24.4	4.3
UZ-39-24	5.3	33	12.9	0.6	BLOD	BLOD	1.1	0.2	90.7	16.8
UZ-39-25	34.5	134	152.8	7.2	800	330	1.4	0.3	50.0	5.3

UZ-39-26	24.1	142	91.8	4.3	BLOD	BLOD	1.3	0.2	58.1	6.0
UZ-39-27	34.4	121	53.1	3.6	660	340	1.3	0.3	143.1	17.1
UZ-39-28	27.8	136	34.3	1.6	BLOD	BLOD	1.6	0.6	178.9	18.8
UZ-39-29	12.2	61	126.1	8.0	BLOD	BLOD	1.5	0.3	21.3	3.2
UZ-39-30	14.9	49	32.9	1.5	BLOD	BLOD	1.4	0.3	100.1	15.5
UZ-39-31	6.5	36	16.0	0.7	BLOD	BLOD	1.1	0.3	90.2	15.9
UZ-39-32	48.4	261	158.7	7.4	BLOD	BLOD	1.5	0.4	67.4	5.8
UZ-39-33	20.8	74	44.7	2.0	850	350	1.6	0.5	102.8	13.4
UZ-39-34	17.3	66	35.0	1.4	980	350	1.3	0.2	109.5	14.8
UZ-39-35	42.3	174	85.3	3.8	BLOD	BLOD	1.5	0.3	109.7	10.5
UZ-39-36	31.0	182	62.0	2.6	BLOD	BLOD	1.3	0.4	110.5	10.3
UZ-39-37	15.7	78	25.6	1.2	BLOD	BLOD	1.3	0.2	135.5	17.4
UZ-39-38	27.1	113	57.0	2.6	BLOD	BLOD	1.4	0.2	105.2	11.7
UZ-40-1	12.2	45	39.3	2.0	BLOD	BLOD	1.3	0.3	68.6	11.1
UZ-40-2	14.3	15	13.9	1.1	1230	360	1.4	0.9	227.0	61.9
UZ-40-3	12.4	36	24.0	1.8	BLOD	BLOD	1.2	0.2	114.0	21.3
UZ-40-4	7.4	8	9.4	0.5	4700	1100	1.3	0.2	172.8	62.3
UZ-40-5	8.0	14	9.6	0.5	BLOD	BLOD	1.2	0.1	182.8	50.3
UZ-40-6	4.2	6	8.8	0.5	BLOD	BLOD	1.3	0.2	105.1	43.4
UZ-40-7	9.5	15	28.9	1.3	730	310	1.2	0.5	72.7	19.3
UZ-40-8	14.0	27	28.6	1.7	BLOD	BLOD	1.5	0.3	107.8	22.1
UZ-40-9	8.2	26	10.2	0.4	810	300	1.2	0.2	177.1	36.2
UZ-40-10	7.2	25	10.8	0.6	BLOD	BLOD	1.4	0.3	148.1	31.1
UZ-40-11	12.6	27	24.9	1.1	800	240	1.5	0.6	111.8	22.5
UZ-40-12	8.7	21	20.2	1.2	BLOD	BLOD	1.5	0.9	95.5	21.9
UZ-40-13	5.5	14	14.5	0.7	670	210	1.3	0.2	83.1	22.8
UZ-40-14	7.6	21	14.5	0.7	BLOD	BLOD	1.2	0.2	116.6	26.5
UZ-40-15	12.1	24	26.7	1.4	510	200	1.3	0.3	100.0	21.4
UZ-40-16	15.3	57	29.9	1.7	BLOD	BLOD	1.5	0.4	113.4	16.9
UZ-40-17	2.8	9	2.9	0.2	BLOD	BLOD	1.3	0.2	216.2	73.7
UZ-40-18	8.3	22	12.3	0.7	BLOD	BLOD	1.6	0.3	148.3	33.1

UZ-40-19	13.3	39	34.0	2.3	420	230	1.1	0.1	86.2	15.3
UZ-40-20	11.4	37	24.0	1.2	450	230	1.4	0.5	105.0	18.5
UZ-40-21	12.0	33	23.0	1.2	430	220	1.3	0.4	115.2	21.4
UZ-40-22	7.0	27	10.6	0.8	BLOD	BLOD	1.4	0.2	147.3	31.1
UZ-40-23	10.6	41	25.9	1.2	430	220	1.4	0.3	90.4	15.1
UZ-40-24	8.2	24	21.3	1.2	BLOD	BLOD	1.4	0.2	84.6	18.2
UZ-40-25	3.6	23	15.1	0.7	810	210	1.2	0.3	52.0	11.3
UZ-40-26	10.7	28	20.8	0.9	540	230	1.4	0.2	113.8	22.5
UZ-40-27	6.0	11	12.1	1.0	BLOD	BLOD	1.1	0.1	110.3	34.7
UZ-40-28	4.1	26	6.8	0.3	BLOD	BLOD	1.4	1.0	135.4	27.9
UZ-40-29	6.8	26	14.6	0.8	430	190	1.0	0.3	102.7	21.2
UZ-40-30	12.0	26	23.0	1.1	BLOD	BLOD	1.1	0.2	115.4	23.7
UZ-40-31	10.1	28	19.2	1.0	400	180	1.3	0.2	116.3	23.2
UZ-40-32	7.4	32	14.6	0.7	360	170	1.1	0.3	112.7	21.1
UZ-40-33	4.3	8	7.1	0.4	BLOD	BLOD	1.3	0.2	132.2	47.5
UZ-40-34	7.7	22	21.6	1.0	BLOD	BLOD	1.0	0.1	78.6	17.4
UZ-40-35	20.2	40	61.6	2.1	BLOD	BLOD	1.2	0.2	72.6	12.1
UZ-40-36	8.6	36	12.0	0.5	BLOD	BLOD	1.0	0.2	158.8	28.1
UZ-40-37	3.7	6	11.0	0.7	BLOD	BLOD	1.2	0.1	74.6	30.9
UZ-40-38	7.5	12	14.1	0.9	BLOD	BLOD	NA	0.0	118.1	35.3
UZ-40-39	7.2	20	15.4	0.6	BLOD	BLOD	1.3	0.2	103.7	23.9
UZ-41-1	17.1	68	22.0	1.4	1150	290	1.6	0.3	171.5	24.4
UZ-41-2	13.9	43	32.8	2.2	1050	270	2.0	0.6	93.8	16.0
UZ-41-3	15.9	59	29.1	1.4	1300	350	1.3	0.2	120.4	17.3
UZ-41-4	21.6	42	29.6	1.6	750	250	1.5	0.3	161.6	27.1
UZ-41-5	19.3	46	33.8	1.7	1340	250	1.6	0.4	125.9	20.2
UZ-41-6	24.9	51	44.4	1.9	1060	240	1.5	0.3	124.1	18.8
UZ-41-7	18.8	74	34.0	1.6	1110	220	1.7	0.3	122.1	16.0
UZ-41-8	10.8	14	23.9	1.2	1440	270	1.5	0.3	99.6	27.4
UZ-41-9	9.5	11	20.9	0.9	1060	250	1.8	0.1	100.2	30.7
UZ-41-10	18.6	50	17.1	1.0	970	270	1.5	0.3	240.6	38.0

UZ-41-11	11.4	45	18.0	1.2	940	270	1.6	0.5	139.9	23.5
UZ-41-12	15.5	31	33.4	2.2	1070	250	1.3	0.3	102.5	20.0
UZ-41-13	12.9	35	25.2	1.3	1270	250	1.6	0.2	113.2	20.5
UZ-41-14	9.6	15	22.1	1.0	1080	190	1.6	0.3	96.1	25.4
UZ-41-15	17.5	26	33.7	1.5	1060	230	1.4	0.3	114.6	23.5
UZ-41-16	18.1	26	47.4	3.4	13700	3200	1.4	0.2	84.5	17.9
UZ-41-17	12.8	21	27.2	1.2	740	210	1.5	0.4	103.7	23.4
UZ-41-18	23.6	63	29.3	1.8	1070	270	1.3	0.2	177.7	25.8
UZ-41-19	10.2	30	16.9	0.9	1320	300	1.4	0.3	133.5	25.9
UZ-41-20	20.6	41	35.5	1.8	1390	250	1.6	0.6	128.4	21.6
UZ-41-21	21.9	34	30.5	1.1	1350	220	1.6	0.2	158.9	28.5
UZ-41-22	11.7	31	30.5	3.1	3600	1300	1.6	0.5	84.9	17.8
UZ-41-23	17.9	40	31.4	1.6	1050	270	1.5	0.3	126.0	21.5
UZ-41-24	14.9	39	11.4	0.5	1630	280	1.7	0.5	289.8	49.2
UZ-41-25	20.2	44	35.5	1.4	1740	250	1.6	0.3	125.9	20.2
UZ-41-26	16.7	23	32.6	1.3	1130	250	1.6	0.4	113.3	24.4
UZ-41-27	15.7	22	27.1	1.4	1190	230	1.6	0.3	127.7	28.4
UZ-41-28	21.1	44	53.2	2.9	800	260	1.7	0.2	87.9	14.5
UZ-41-29	13.9	33	19.9	1.7	1410	310	1.4	0.3	154.1	30.5
UZ-41-30	11.0	25	14.7	0.6	1030	240	1.6	0.3	165.6	34.5
UZ-41-31	18.9	58	33.5	1.6	1000	210	1.3	0.3	124.9	18.1
UZ-41-32	11.4	26	24.6	1.2	890	250	1.2	0.3	102.2	21.0
UZ-41-33	15.1	48	23.3	1.2	1260	220	1.9	0.3	143.5	22.7
UZ-41-34	16.4	41	15.7	0.9	1010	210	1.6	0.5	230.5	39.2
UZ-41-35	27.4	45	29.6	1.1	1370	230	1.4	0.3	204.3	32.4
UZ-41-36	17.8	41	26.1	1.1	800	220	1.4	0.2	150.8	25.1
UZ-41-37	9.1	21	9.3	0.8	1380	250	0.8	0.2	215.3	50.8
UZ-41-38	14.7	42	19.7	1.1	1130	210	1.5	0.3	164.6	27.7
UZ-41-39	15.3	21	38.2	1.9	930	230	1.6	0.3	88.6	20.1
UZ-41-40	16.7	39	33.4	1.8	1020	190	1.5	0.2	110.3	19.1
UZ-41-41	17.4	31	36.0	1.4	690	210	1.4	0.2	107.0	20.1

UZ-41-42	17.9	41	26.0	1.7	41600	9300	1.4	0.3	151.9	26.4
UZ-41-43	9.6	24	19.9	4.0	20000	15000	1.3	0.3	107.1	31.0
UZ-42-1	4.6	11	5.3	0.3	BLOD	BLOD	0.5	0.2	191.7	59.0
UZ-42-2	1.9	2	8.4	0.5	BLOD	BLOD	1.1	0.4	51.0	36.3
UZ-42-3	6.8	8	6.5	0.4	640	190	1.3	0.3	229.5	82.9
UZ-42-4	6.1	14	7.1	0.5	BLOD	BLOD	1.2	0.1	190.4	53.1
UZ-42-5	4.0	4	7.5	0.5	BLOD	BLOD	1.5	0.2	119.2	60.3
UZ-42-6	4.4	16	11.2	0.6	BLOD	BLOD	0.9	0.2	87.7	22.7
UZ-42-7	3.9	7	14.4	0.8	BLOD	BLOD	1.0	0.1	60.5	23.2
UZ-42-8	8.1	33	26.6	1.3	BLOD	BLOD	1.0	0.2	67.5	12.5
UZ-42-9	10.5	33	21.1	0.9	BLOD	BLOD	1.2	0.2	109.8	20.1
UZ-42-10	4.4	11	9.8	0.6	BLOD	BLOD	1.0	0.1	99.2	30.7
UZ-42-11	3.5	16	5.7	0.4	BLOD	BLOD	1.0	0.1	135.2	35.2
UZ-42-12	8.1	16	6.7	0.3	1430	530	1.1	0.2	269.5	69.5
UZ-42-13	2.6	5	3.5	0.2	BLOD	BLOD	1.0	0.1	163.2	73.6
UZ-42-14	5.7	26	10.0	0.4	BLOD	BLOD	1.3	0.4	127.3	26.0
UZ-42-15	5.8	19	9.3	0.5	BLOD	BLOD	0.7	0.2	137.3	32.6
UZ-42-16	2.4	9	4.7	0.3	BLOD	BLOD	0.6	0.1	114.3	38.9
UZ-42-17	6.6	16	8.6	0.4	BLOD	BLOD	1.1	0.2	169.7	43.8
UZ-42-18	4.5	14	9.4	0.4	BLOD	BLOD	1.1	0.2	107.0	29.2
UZ-42-19	6.7	31	11.4	0.7	BLOD	BLOD	1.1	0.2	130.2	25.2
UZ-42-20	9.3	21	9.7	0.7	BLOD	BLOD	1.2	0.2	212.3	49.8
UZ-42-21	8.4	19	18.6	1.4	BLOD	BLOD	1.5	0.2	99.5	24.3
UZ-42-22	14.6	34	19.3	0.8	BLOD	BLOD	1.1	0.5	167.1	30.2
UZ-42-23	5.5	23	10.5	0.6	BLOD	BLOD	1.0	0.3	115.8	25.4
UZ-42-24	3.1	5	5.4	0.3	BLOD	BLOD	1.0	0.6	128.5	58.1
UZ-42-25	7.2	14	8.3	0.5	BLOD	BLOD	1.3	0.2	192.0	53.0
UZ-42-26	3.5	10	4.4	0.3	BLOD	BLOD	1.2	0.2	178.2	57.8
UZ-42-27	11.0	26	18.5	1.0	BLOD	BLOD	0.8	0.2	131.0	27.1
UZ-42-28	5.7	17	7.3	0.3	BLOD	BLOD	1.0	0.3	172.5	43.1
UZ-42-29	6.2	8	8.9	0.5	BLOD	BLOD	1.0	0.5	152.1	54.7

UZ-42-30	7.4	13	9.0	0.6	BLOD	BLOD	1.2	0.1	182.6	52.4
UZ-42-31	14.1	37	21.6	1.0	BLOD	BLOD	0.9	0.3	144.1	25.2
UZ-42-32	4.3	9	5.4	0.3	400	210	1.4	0.2	175.9	60.0
UZ-42-33	7.2	15	5.8	0.3	BLOD	BLOD	1.3	0.3	276.7	73.4
UZ-42-34	7.7	9	10.3	0.5	BLOD	BLOD	0.8	0.1	165.4	56.1
UZ-42-35	3.1	5	10.9	0.5	BLOD	BLOD	1.2	0.3	62.3	28.1
UZ-42-36	5.9	7	6.0	0.3	BLOD	BLOD	1.4	0.3	218.2	83.8
UZ-43-1	4.6	21	9.9	0.5	BLOD	BLOD	0.6	0.1	85.9	19.6
UZ-43-2	10.5	35	16.6	0.8	BLOD	BLOD	1.0	0.3	116.2	20.9
UZ-43-3	8.5	24	21.2	1.1	BLOD	BLOD	0.7	0.1	74.2	15.9
UZ-43-4	3.5	17	3.5	0.3	BLOD	BLOD	1.6	0.2	185.7	47.6
UZ-43-5	23.4	45	25.2	1.7	18600	5400	1.3	0.4	171.8	28.9
UZ-43-6	10.2	31	14.5	0.6	BLOD	BLOD	0.7	0.1	130.2	24.6
UZ-43-7	18.9	55	51.6	2.9	BLOD	BLOD	1.1	0.3	67.9	10.2
UZ-43-8	8.5	33	15.1	1.0	970	390	1.1	0.3	104.7	19.9
UZ-43-9	27.1	58	58.6	2.7	BLOD	BLOD	1.2	0.3	85.7	12.4
UZ-43-10	7.5	15	13.8	0.7	BLOD	BLOD	0.8	0.2	100.8	26.8
UZ-43-11	7.4	32	13.0	0.7	BLOD	BLOD	1.1	0.2	104.7	19.7
UZ-43-12	3.1	11	3.3	0.2	BLOD	BLOD	1.0	0.2	172.9	53.6
UZ-43-13	14.6	28	25.0	2.0	720	400	1.1	0.2	107.7	22.5
UZ-43-14	8.9	48	22.1	1.1	BLOD	BLOD	1.0	0.2	74.5	11.7
UZ-43-15	14.6	48	19.6	1.1	BLOD	BLOD	0.8	0.2	137.5	21.9
UZ-43-16	6.8	19	10.8	0.8	34200	6700	1.4	0.3	116.8	28.5
UZ-43-17	3.0	13	7.6	0.5	BLOD	BLOD	0.8	0.2	74.2	21.2
UZ-43-18	9.8	20	14.1	1.6	BLOD	BLOD	1.0	0.3	128.3	32.5
UZ-43-19	3.3	7	9.0	0.5	BLOD	BLOD	1.5	0.9	67.3	25.9
UZ-43-20	8.0	27	14.1	0.7	BLOD	BLOD	1.2	0.2	104.6	21.1
UZ-43-21	5.9	17	8.5	0.5	BLOD	BLOD	1.1	0.1	127.2	32.1
UZ-43-22	5.3	23	13.2	0.7	BLOD	BLOD	1.3	0.2	74.8	16.3
UZ-43-23	7.5	17	10.5	0.7	BLOD	BLOD	0.8	0.2	132.2	33.5
UZ-43-24	13.7	32	21.6	1.0	BLOD	BLOD	1.0	0.2	116.9	21.8

UZ-43-25	3.9	11	8.7	0.5	BLOD	BLOD	1.5	0.2	82.8	25.6
UZ-43-26	6.5	22	10.2	0.5	BLOD	BLOD	1.1	0.1	116.7	25.9
UZ-43-27	8.1	45	12.8	0.7	BLOD	BLOD	1.5	0.4	117.6	19.3
UZ-43-28	7.7	46	14.0	0.7	BLOD	BLOD	1.4	0.2	101.0	16.2
UZ-43-29	6.7	27	14.9	0.8	1090	500	0.9	0.2	82.8	16.8
UZ-43-30	20.0	80	30.1	1.3	BLOD	BLOD	1.3	0.2	122.7	15.4
UZ-43-31	5.6	13	8.2	0.4	6900	1600	1.2	0.2	125.3	35.7
UZ-43-32	4.8	17	14.3	0.9	BLOD	BLOD	1.1	0.2	61.8	15.6
UZ-43-33	3.5	16	4.8	0.5	BLOD	BLOD	1.1	0.2	135.5	36.5
UZ-43-34	6.2	30	10.9	0.6	BLOD	BLOD	1.4	0.3	105.9	20.6
UZ-43-35	7.8	29	10.9	0.8	BLOD	BLOD	1.4	0.1	132.8	27.0
UZ-43-36	30.7	60	47.7	2.5	BLOD	BLOD	1.4	0.2	119.2	17.2
UZ-43-37	14.2	37	15.7	0.8	BLOD	BLOD	1.3	0.2	166.6	29.4
UZ-44-1	14.9	40	24.4	1.1	BLOD	BLOD	0.9	0.2	138.5	23.8
UZ-44-2	25.1	42	50.4	2.0	770	340	1.2	0.2	112.8	18.8
UZ-44-3	1.5	6	1.4	0.2	2900	1200	1.5	0.3	246.8	107.8
UZ-44-4	8.3	18	16.7	0.7	BLOD	BLOD	1.1	0.3	112.4	27.5
UZ-44-5	13.1	33	18.1	0.8	BLOD	BLOD	0.9	0.2	163.1	30.3
UZ-44-6	27.1	34	28.0	1.8	BLOD	BLOD	1.3	0.3	219.5	41.6
UZ-44-7	12.6	31	12.0	0.6	BLOD	BLOD	1.0	0.2	238.9	46.2
UZ-44-8	9.8	40	36.6	1.9	BLOD	BLOD	1.3	0.7	60.5	10.5
UZ-44-9	5.2	21	10.3	0.6	BLOD	BLOD	1.3	0.2	113.1	26.1
UZ-44-10	18.8	65	18.3	1.3	BLOD	BLOD	1.4	0.3	232.6	35.1
UZ-44-11	66.3	113	137.5	6.5	BLOD	BLOD	1.2	0.3	109.3	12.7
UZ-44-12	3.7	10	7.6	0.5	1010	800	1.2	0.1	109.6	35.9
UZ-44-13	17.4	37	46.9	1.9	BLOD	BLOD	1.1	0.2	84.0	14.8
UZ-44-14	14.9	55	10.9	0.8	BLOD	BLOD	1.2	0.2	307.6	49.5
UZ-44-15	9.9	38	12.6	0.6	BLOD	BLOD	1.3	0.2	176.7	30.9
UZ-44-16	9.6	38	15.0	0.7	BLOD	BLOD	1.1	0.1	145.0	25.6
UZ-44-17	12.0	50	17.6	0.9	BLOD	BLOD	1.0	0.3	154.9	24.4
UZ-44-18	37.4	92	74.9	3.0	BLOD	BLOD	1.3	0.3	113.2	13.8

UZ-44-19	15.3	30	21.1	1.3	BLOD	BLOD	1.1	0.5	164.5	32.7
UZ-44-20	18.7	55	23.2	1.1	BLOD	BLOD	1.2	0.2	182.9	27.6
UZ-44-21	12.6	53	11.7	0.6	BLOD	BLOD	1.1	0.2	242.5	37.4
UZ-44-22	14.6	45	26.0	1.1	BLOD	BLOD	1.0	0.3	127.3	20.7
UZ-44-23	63.4	147	122.9	5.1	BLOD	BLOD	1.3	0.3	116.8	12.2
UZ-44-24	10.1	29	14.8	0.8	BLOD	BLOD	1.0	0.2	154.1	30.8
UZ-44-25	15.3	64	23.7	1.6	BLOD	BLOD	1.4	0.4	146.3	22.0
UZ-44-26	18.7	60	45.6	2.0	9000	750	1.1	0.3	93.0	13.5
UZ-44-27	17.9	66	23.6	1.3	BLOD	BLOD	1.2	0.3	172.2	24.7
UZ-44-28	7.4	24	33.0	70.0	2400000	2100000	0.8	0.2	50.7	108.1
UZ-44-29	19.6	40	24.7	1.2	BLOD	BLOD	1.2	0.2	180.2	31.1
UZ-44-30	45.1	73	93.0	3.6	BLOD	BLOD	1.3	0.2	110.0	14.6
UZ-44-31	15.8	43	21.6	1.3	620	340	1.4	0.2	166.0	28.4
UZ-44-32	9.9	32	16.4	1.1	BLOD	BLOD	1.4	0.2	136.8	26.7
UZ-44-33	9.3	35	9.3	0.5	BLOD	BLOD	1.5	0.2	226.4	41.7
UZ-44-34	8.7	25	12.9	0.6	800	270	1.3	0.2	154.0	32.5
UZ-44-35	8.4	23	20.9	0.9	600	290	1.6	0.2	91.3	20.0
UZ-44-36	10.2	55	16.8	0.8	BLOD	BLOD	1.3	0.3	137.4	20.8
UZ-44-37	10.9	35	9.4	0.7	720	320	1.1	0.2	262.7	49.9
UZ-44-38	17.2	42	15.1	0.9	BLOD	BLOD	1.3	0.3	257.7	44.6
UZ-44-39	13.3	58	17.4	0.8	BLOD	BLOD	1.2	0.1	173.5	25.7
UZ-44-40	10.5	30	9.9	0.6	BLOD	BLOD	1.1	0.2	239.2	47.4
UZ-44-41	7.9	25	13.0	0.8	BLOD	BLOD	1.2	0.3	137.5	29.7
UZ-44-42	5.5	22	8.4	0.5	BLOD	BLOD	0.9	0.2	149.5	33.8
UZ-45-1	9.8	28	14.8	0.8	BLOD	BLOD	0.9	0.2	150.1	30.3
UZ-45-2	22.6	29	27.3	1.9	BLOD	BLOD	1.1	0.3	187.3	38.3
UZ-45-3	6.1	11	10.3	0.7	BLOD	BLOD	1.0	0.2	133.5	41.7
UZ-45-4	3.2	12	6.2	0.3	BLOD	BLOD	0.9	0.1	116.4	34.6
UZ-45-5	11.2	22	21.4	0.8	BLOD	BLOD	1.4	0.2	119.2	26.4
UZ-45-6	10.4	35	13.4	0.7	BLOD	BLOD	1.0	0.2	174.8	32.0
UZ-45-7	3.8	9	9.5	0.8	BLOD	BLOD	1.1	0.1	90.2	31.2

UZ-45-8	18.3	64	20.2	1.2	BLOD	BLOD	1.1	0.3	205.2	30.1
UZ-45-9	5.5	16	9.4	0.6	BLOD	BLOD	0.7	0.3	131.7	34.4
UZ-45-10	5.7	14	8.1	0.4	BLOD	BLOD	0.9	0.3	159.9	44.2
UZ-45-11	10.1	40	12.1	0.6	BLOD	BLOD	1.1	0.2	188.3	32.7
UZ-45-12	3.7	11	8.9	0.5	BLOD	BLOD	0.6	0.2	94.3	29.2
UZ-45-13	7.6	28	6.3	0.4	BLOD	BLOD	1.2	0.3	275.5	56.2
UZ-45-14	4.5	11	12.9	0.8	BLOD	BLOD	0.5	0.1	79.4	24.7
UZ-45-15	5.0	22	9.3	0.4	BLOD	BLOD	1.1	0.1	122.0	27.3
UZ-45-16	16.1	44	31.1	1.4	BLOD	BLOD	1.1	0.2	117.0	19.3
UZ-45-17	9.3	46	16.5	0.8	BLOD	BLOD	1.0	0.3	128.1	21.0
UZ-45-18	8.7	34	9.6	0.6	BLOD	BLOD	1.0	0.2	204.7	38.9
UZ-45-19	8.0	29	12.1	0.8	BLOD	BLOD	0.9	0.1	149.8	30.3
UZ-45-20	10.9	24	15.9	0.9	BLOD	BLOD	1.1	0.5	155.5	33.7
UZ-45-21	7.0	29	9.4	0.6	BLOD	BLOD	1.0	0.3	169.1	34.0
UZ-45-22	5.2	22	5.6	0.3	BLOD	BLOD	1.3	0.1	209.1	46.8
UZ-45-23	4.1	14	5.3	0.3	BLOD	BLOD	1.0	0.1	174.8	48.3
UZ-45-24	10.9	33	10.3	0.6	BLOD	BLOD	1.1	0.2	239.8	45.7
UZ-45-25	8.7	28	10.2	0.5	BLOD	BLOD	1.3	0.3	193.7	38.9
UZ-45-26	4.0	16	7.7	0.4	BLOD	BLOD	1.1	0.3	116.5	30.3
UZ-45-27	6.4	22	7.7	0.4	BLOD	BLOD	0.8	0.2	190.1	42.6
UZ-45-28	3.7	21	8.4	0.4	BLOD	BLOD	1.6	0.3	100.0	22.8
UZ-45-29	8.1	31	12.2	0.6	BLOD	BLOD	1.1	0.3	151.7	29.3
UZ-45-30	10.1	35	15.4	0.8	BLOD	BLOD	1.0	0.2	148.1	27.2
UZ-45-31	9.4	20	9.0	0.7	BLOD	BLOD	1.0	0.3	237.6	57.8
UZ-45-32	6.9	29	9.7	0.5	BLOD	BLOD	1.6	0.2	162.1	32.4
UZ-45-33	4.0	18	7.0	0.4	BLOD	BLOD	1.0	0.1	128.1	31.8
UZ-45-34	6.7	22	9.0	0.5	BLOD	BLOD	0.7	0.2	166.9	37.7
UZ-45-35	10.6	34	14.4	0.8	BLOD	BLOD	1.0	0.2	167.7	31.2
UZ-45-36	2.8	13	5.3	0.3	BLOD	BLOD	1.1	0.1	117.1	33.5
UZ-45-37	16.6	70	54.8	2.5	BLOD	BLOD	1.3	0.2	68.4	9.4
UZ-45-38	6.9	17	8.5	0.4	BLOD	BLOD	1.5	0.2	183.9	46.3

UZ-45-39	8.8	36	9.6	0.6	BLOD	BLOD	0.6	0.1	207.5	38.1
UZ-45-40	2.4	8	4.9	0.3	BLOD	BLOD	0.9	0.1	112.2	40.5
UZ-45-41	3.8	15	7.6	0.4	BLOD	BLOD	1.1	0.2	113.2	30.3
UZ-45-42	9.8	28	14.8	0.8	BLOD	BLOD	0.9	0.2	150.1	30.3
UZ-48-1	2.9	5	4.3	0.3	19800	3200	1.8	0.5	113.9	51.8
UZ-48-2	6.4	11	5.6	0.4	20900	5200	1.6	0.5	197.9	61.6
UZ-48-3	5.6	11	4.3	0.3	17400	4600	2.1	0.2	226.8	70.3
UZ-48-4	4.0	7	6.0	0.5	4700	1700	1.1	0.4	115.0	44.6
UZ-48-5	16.3	47	11.6	0.4	BLOD	BLOD	1.7	0.3	241.5	37.5
UZ-48-6	4.2	6	6.2	0.5	38400	8900	3.1	0.6	116.6	48.8
UZ-48-7	0.7	1	4.4	0.4	3700	2200	2.3	0.5	25.6	25.7
UZ-48-8	4.0	7	4.9	0.2	1460	400	3.3	1.1	138.0	52.8
UZ-48-9	3.2	6	7.2	0.4	3410	550	1.4	0.4	76.1	31.5
UZ-48-10	5.3	7	6.9	0.4	1230	220	1.2	0.3	130.6	50.2
UZ-48-11	3.2	4	6.5	0.3	1200	210	1.3	0.3	83.3	41.9
UZ-48-12	26.5	49	36.6	1.5	550	190	2.0	0.5	124.8	19.2
UZ-48-13	7.1	14	7.5	0.4	BLOD	BLOD	1.3	0.8	163.8	45.1
UZ-48-14	6.3	10	6.3	0.3	1000	220	2.7	1.1	172.3	55.5
UZ-48-15	1.0	2	6.0	0.3	2540	400	1.5	0.5	28.9	20.5
UZ-48-16	4.0	18	7.1	0.3	1330	240	1.4	0.1	96.4	23.5
UZ-48-17	2.4	5	6.0	0.3	1010	200	1.3	0.3	69.1	31.2
UZ-48-18	3.0	4	5.9	0.3	1270	230	1.5	0.3	88.0	44.3
UZ-48-19	3.1	6	6.4	0.3	1130	240	1.2	0.1	82.8	34.2
UZ-48-20	2.5	3	5.3	0.3	1190	240	1.3	0.2	80.9	47.0
UZ-48-21	35.4	89	48.8	2.2	BLOD	BLOD	1.5	0.6	124.9	15.3
UZ-48-22	30.1	62	31.7	1.3	3940	390	1.6	0.5	163.5	22.8
UZ-48-23	4.4	9	5.9	0.4	18700	4800	1.4	0.3	127.1	43.5
UZ-48-24	3.7	13	6.7	0.3	1300	260	1.2	0.3	93.8	26.6
UZ-48-25	2.8	7	3.8	0.2	1660	510	1.1	0.1	126.7	48.8
UZ-48-26	7.6	32	5.7	0.2	2110	300	1.5	0.2	229.3	42.6
UZ-48-27	5.8	16	4.6	0.3	1360	310	1.4	0.3	216.5	56.5

UZ-48-28	3.8	10	5.5	0.3	1410	320	1.5	0.1	117.6	38.0
UZ-48-29	1.9	3	5.1	0.3	1570	320	1.5	0.3	63.9	37.2
UZ-48-30	2.9	7	6.3	0.4	1320	360	1.6	0.1	80.0	30.8
UZ-48-31	2.2	4	3.1	0.2	1440	260	1.1	0.1	118.9	60.0
UZ-48-32	1.5	3	3.7	0.3	6100	2300	1.1	0.2	68.5	39.9
UZ-48-33	1.7	5	3.4	0.2	2000	430	1.0	0.1	85.6	38.8
UZ-48-34	5.1	12	3.9	0.2	2060	610	1.4	0.1	220.9	65.4
UZ-49-1	47.0	130	80.3	3.5	BLOD	BLOD	1.4	0.2	128.2	13.9
UZ-49-2	16.7	22	32.1	1.5	BLOD	BLOD	1.2	0.2	113.8	25.4
UZ-49-3	22.4	49	48.7	2.9	BLOD	BLOD	0.9	0.4	100.5	16.3
UZ-49-4	37.5	91	60.3	2.8	BLOD	BLOD	1.4	0.3	136.0	16.8
UZ-49-5	18.6	35	36.6	2.3	1350	460	1.1	0.3	111.3	20.7
UZ-49-6	51.6	125	80.3	4.7	5600	2300	1.5	0.5	140.7	16.4
UZ-49-7	41.9	152	81.4	3.6	BLOD	BLOD	1.4	0.5	112.7	11.7
UZ-49-8	13.0	33	25.4	1.1	BLOD	BLOD	1.1	0.3	111.6	20.7
UZ-49-9	38.8	137	88.8	7.2	BLOD	BLOD	1.6	0.5	95.6	12.1
UZ-49-10	39.3	110	63.1	4.8	BLOD	BLOD	1.5	0.3	136.3	17.8
UZ-49-11	23.6	72	53.2	2.5	BLOD	BLOD	1.2	0.4	97.3	13.1
UZ-49-12	43.8	158	74.5	3.8	700	320	1.5	0.4	128.6	13.6
UZ-49-13	22.8	56	21.0	1.1	BLOD	BLOD	1.4	0.5	237.1	35.8
UZ-49-14	16.6	26	33.2	1.4	1030	440	1.2	0.2	109.7	22.6
UZ-49-15	39.0	118	65.5	3.1	BLOD	BLOD	1.2	0.4	130.2	14.8
UZ-49-16	12.2	35	20.9	1.4	BLOD	BLOD	1.2	0.4	127.5	23.9
UZ-49-17	46.1	114	69.3	7.1	7900	1900	1.2	0.3	145.4	21.3
UZ-49-18	29.7	121	47.8	1.4	BLOD	BLOD	1.3	0.3	136.0	14.5
UZ-49-19	47.9	119	78.7	4.5	710	280	1.3	0.3	133.1	15.7
UZ-49-20	23.2	83	32.5	1.5	BLOD	BLOD	1.3	0.3	156.2	20.0
UZ-49-21	30.0	76	46.8	3.3	BLOD	BLOD	1.3	0.3	140.1	20.0
UZ-49-22	36.3	117	91.1	6.1	BLOD	BLOD	1.3	0.4	87.3	10.8
UZ-49-23	44.6	177	52.8	2.7	BLOD	BLOD	1.4	0.4	184.9	18.9
UZ-49-24	27.8	91	30.5	1.6	BLOD	BLOD	1.2	0.2	199.4	25.1

UZ-49-25	30.4	121	56.6	3.9	BLOD	BLOD	1.4	0.4	117.5	14.5
UZ-49-26	18.0	30	31.0	1.7	BLOD	BLOD	1.3	0.2	127.2	25.0
UZ-49-27	21.4	56	42.2	2.1	BLOD	BLOD	1.3	0.4	110.9	16.6
UZ-49-28	50.5	151	71.5	5.8	700	330	1.3	0.3	154.5	19.2
UZ-49-29	25.1	48	37.7	1.8	BLOD	BLOD	1.3	0.2	145.8	23.2
UZ-49-30	31.9	71	56.3	3.1	BLOD	BLOD	1.6	0.5	124.1	17.2
UZ-49-31	39.6	87	83.5	3.5	BLOD	BLOD	1.5	0.5	103.9	12.9
UZ-49-32	23.6	67	34.4	1.5	1470	510	1.6	0.3	150.0	20.7
UZ-49-33	38.3	97	63.4	2.3	660	320	1.3	0.2	132.1	15.5
UZ-49-34	20.9	69	29.7	1.2	BLOD	BLOD	1.3	0.4	154.0	20.8
UZ-49-35	58.0	112	107.1	5.7	BLOD	BLOD	1.3	0.3	118.5	14.0
UZ-49-36	36.5	70	66.2	4.5	BLOD	BLOD	1.3	0.2	120.8	17.5
UZ-50-1	26.2	125	45.8	2.0	930	290	1.6	0.5	125.1	13.7
UZ-50-2	46.6	145	69.9	3.0	2790	370	1.8	0.5	145.9	15.2
UZ-50-3	40.1	207	62.3	2.5	1010	260	1.5	0.3	140.7	13.1
UZ-50-4	31.8	99	39.2	1.4	1890	350	1.6	0.4	177.4	20.7
UZ-50-5	20.0	69	451.0	26.0	2540	690	1.7	0.3	9.7	1.4
UZ-50-6	12.8	37	12.7	1.1	700	430	1.1	0.3	220.6	42.3
UZ-50-7	26.3	119	32.5	1.5	1290	360	1.6	0.4	177.2	20.0
UZ-50-8	24.8	62	35.3	1.6	2300	360	1.7	0.5	153.9	22.0
UZ-50-9	22.9	90	27.3	1.7	1120	360	1.5	0.3	183.3	24.0
UZ-50-10	33.2	63	56.4	2.3	1040	390	1.6	0.4	128.9	18.1
UZ-50-11	37.2	172	70.8	5.7	1600	400	1.6	0.3	115.0	13.8
UZ-50-12	40.2	109	53.1	3.9	2600	420	1.6	0.4	165.7	21.4
UZ-50-13	34.1	64	76.9	2.9	1620	350	1.9	0.6	97.1	13.5
UZ-50-14	24.1	105	55.8	3.1	1170	420	1.4	0.2	94.5	11.5
UZ-50-15	25.3	124	38.5	1.3	1100	270	1.7	0.3	143.7	15.3
UZ-50-16	66.9	191	136.7	5.5	1030	300	1.7	0.5	107.1	10.2
UZ-50-17	39.1	102	52.2	3.0	2750	460	1.6	0.3	164.1	20.3
UZ-50-18	52.6	141	62.9	3.1	2700	470	1.6	0.4	183.1	19.8
UZ-50-19	35.5	144	75.7	3.1	760	270	1.8	0.5	102.6	10.7

UZ-50-20	29.5	72	37.9	1.6	2230	320	1.4	0.2	170.5	22.8
UZ-50-21	25.5	55	118.0	11.0	2990	580	1.6	0.4	47.3	8.1
UZ-50-22	36.0	73	58.1	3.6	2210	460	1.5	0.2	135.7	19.1
UZ-50-23	35.2	73	73.4	2.9	1260	520	1.8	0.5	104.8	13.8
UZ-50-24	52.8	164	73.6	3.0	2240	400	1.6	0.4	156.9	15.6
UZ-50-25	45.4	108	110.1	4.1	1610	420	1.7	0.4	90.2	10.2
UZ-50-26	45.3	101	88.9	5.1	1060	310	1.5	0.4	111.6	13.8
UZ-50-27	28.1	97	34.0	1.8	670	330	1.6	0.3	181.0	22.4
UZ-50-28	57.7	166	72.2	3.7	720	290	1.6	0.4	174.9	18.2
UZ-50-29	32.7	110	36.0	1.9	2110	420	1.9	0.7	198.8	23.6

6.2 Supplementary File 2

1 Single grain apatite fission track data for samples taken from the Kyzylkum-Nurata segment plotted using Vermeesch (2009). Single grain ages are coloured according to their respective uranium 238 (U) measurements.

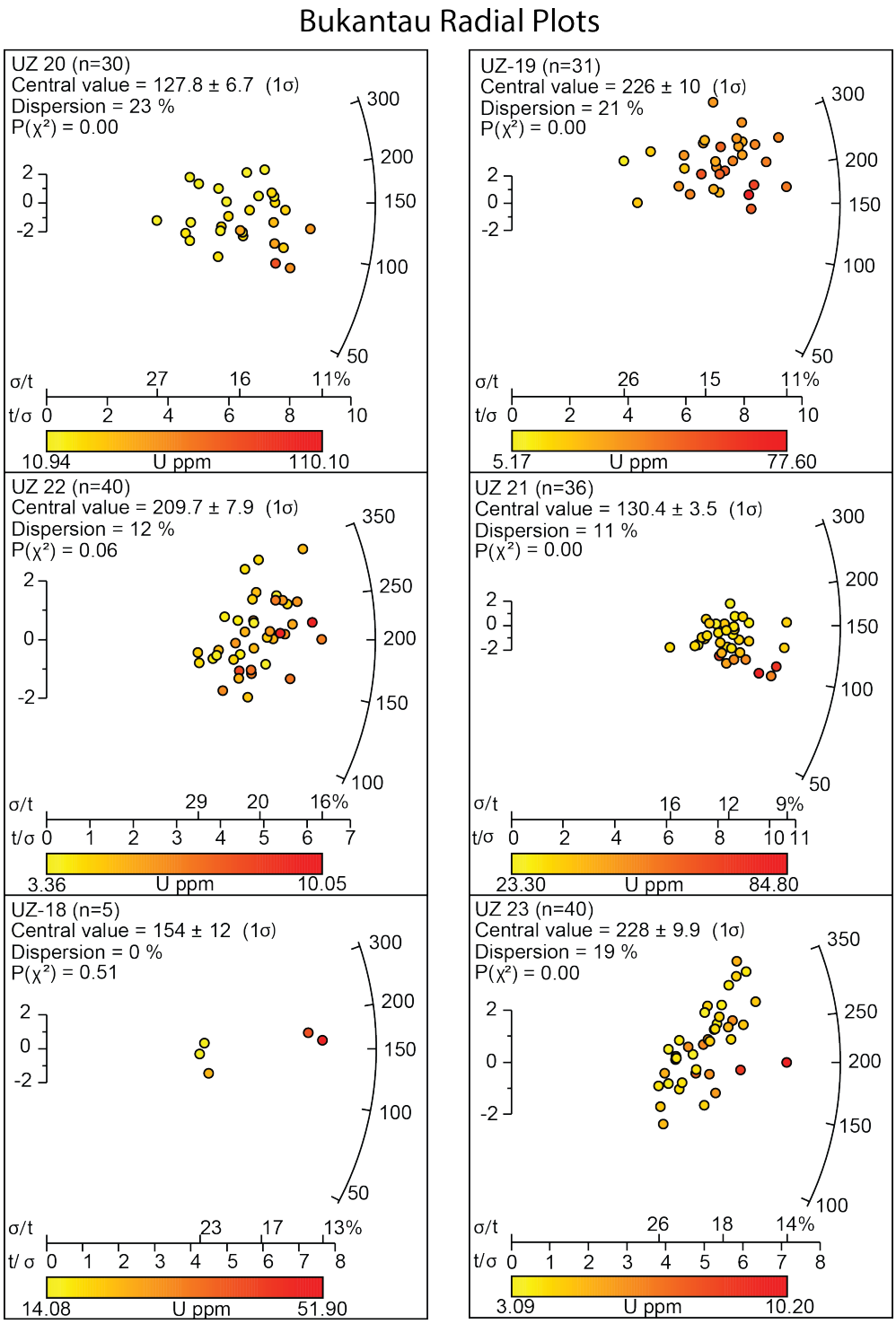

Kuldjuktau Radial Plots_1

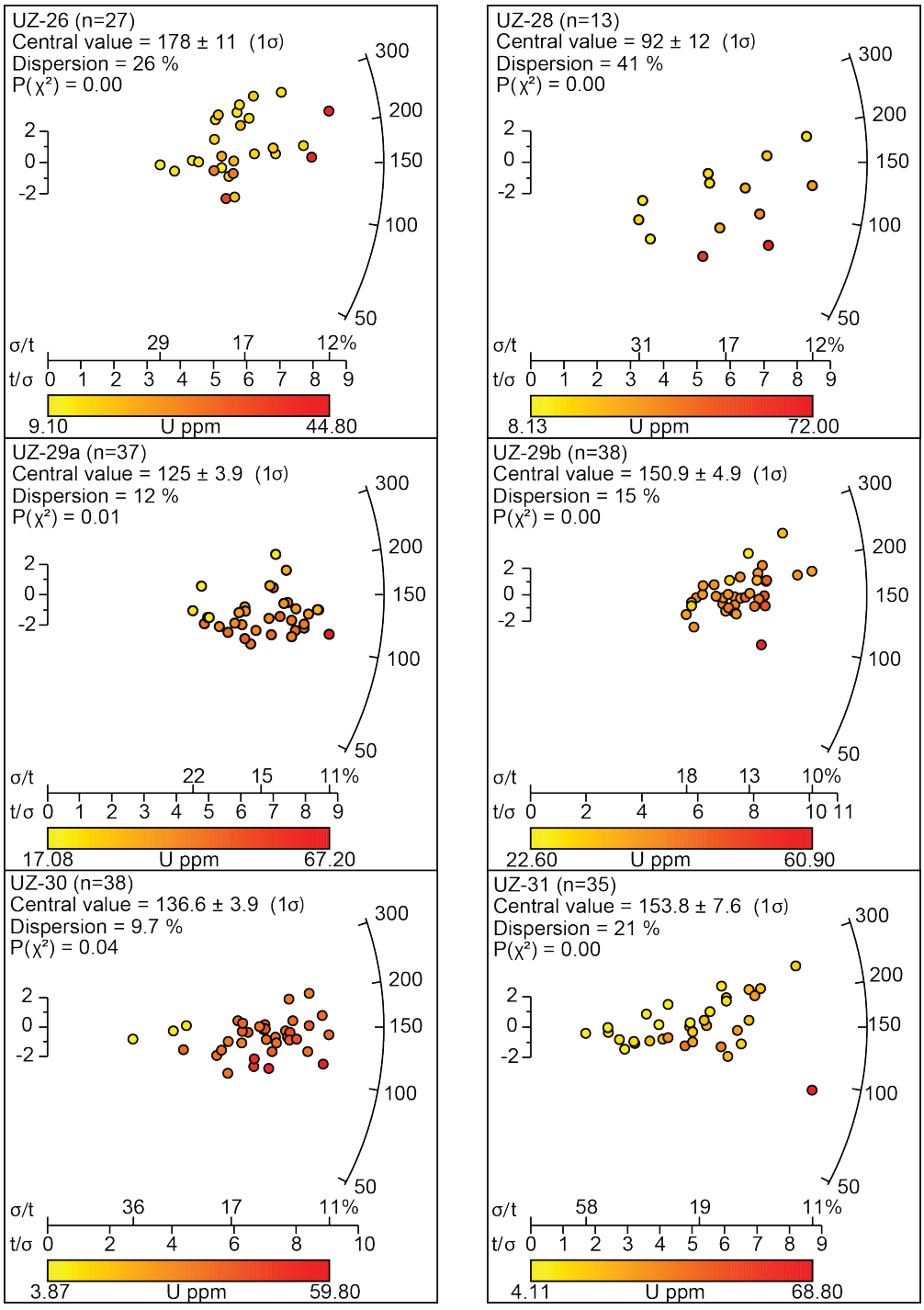

Kuldjuktau Radial Plot_2

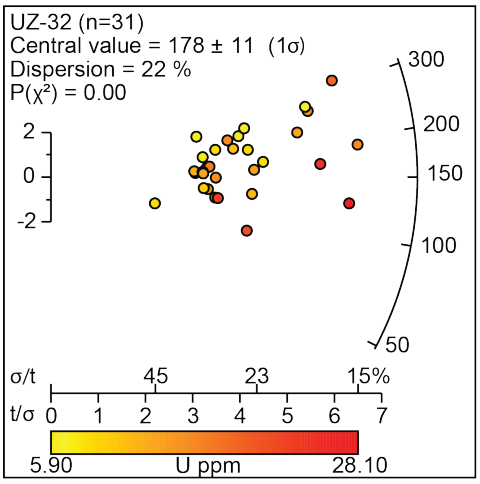

Northern Nurata Radial Plots_1

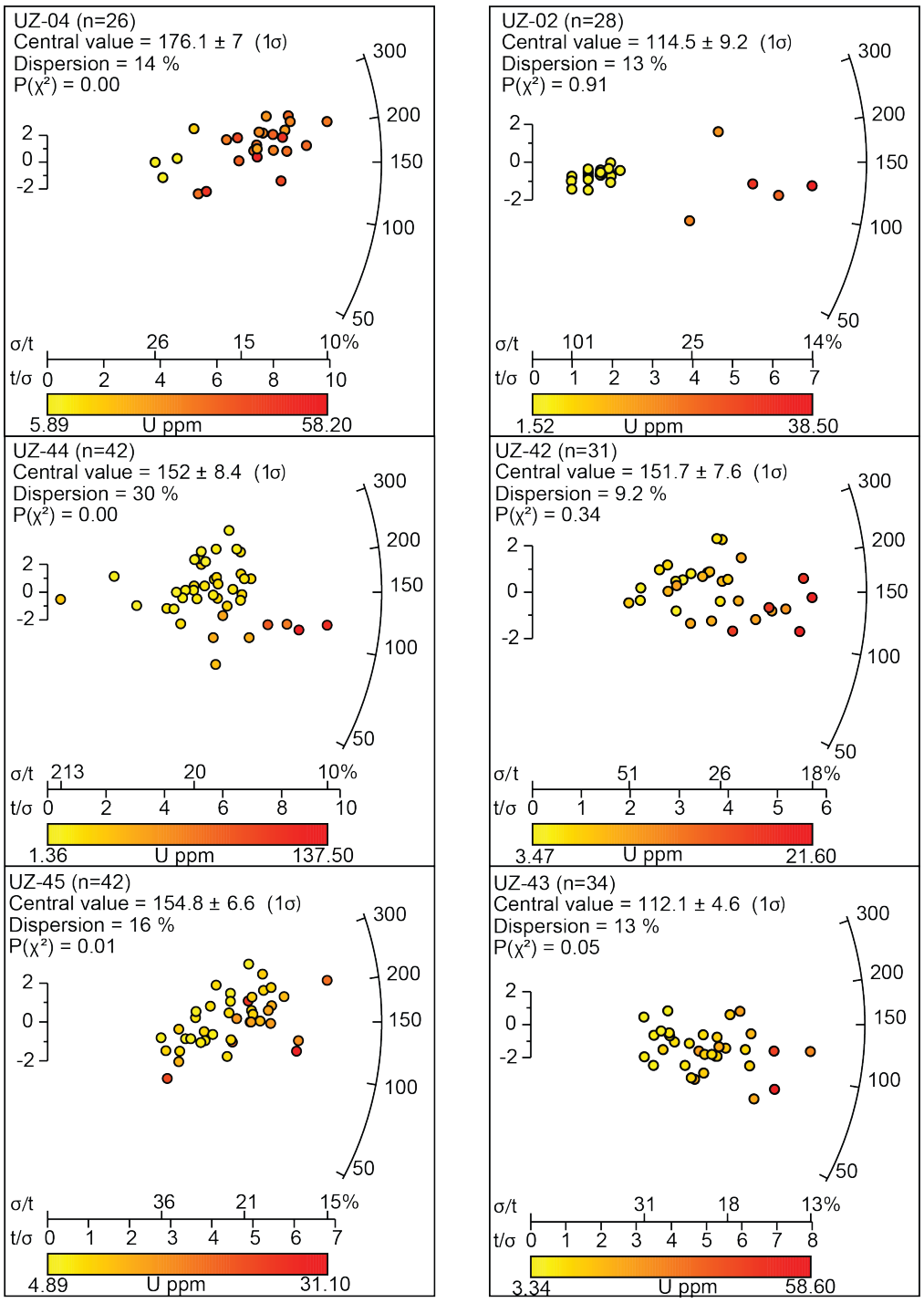

South Nurata Range

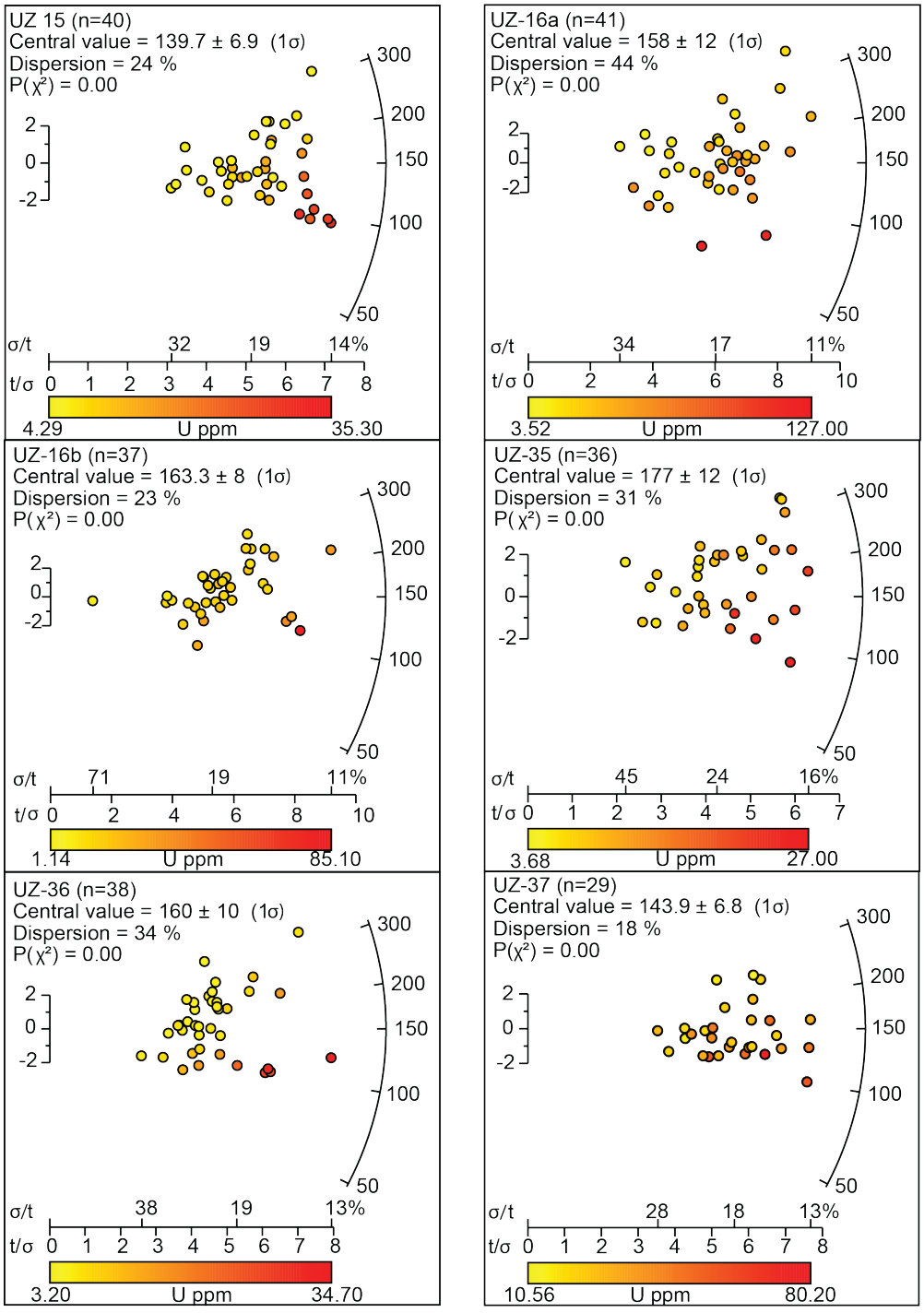

South Nurata Range_2

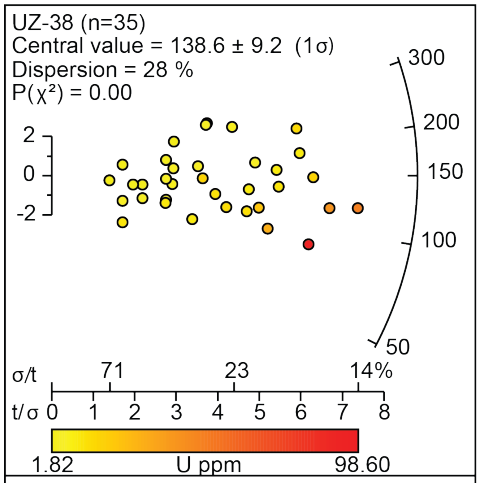

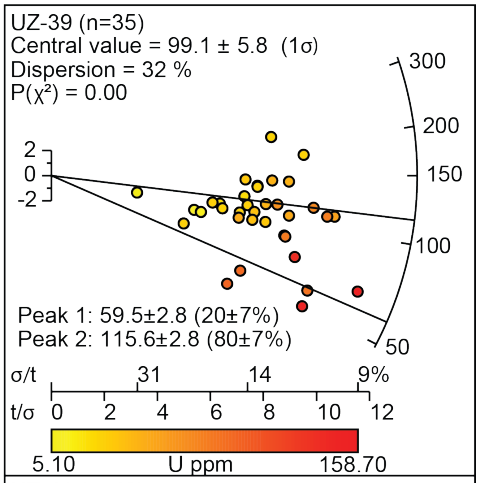

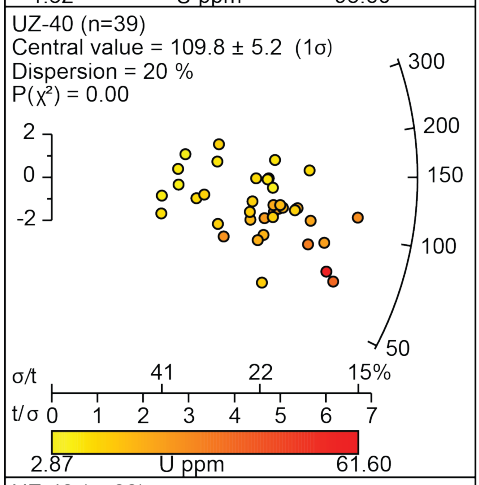

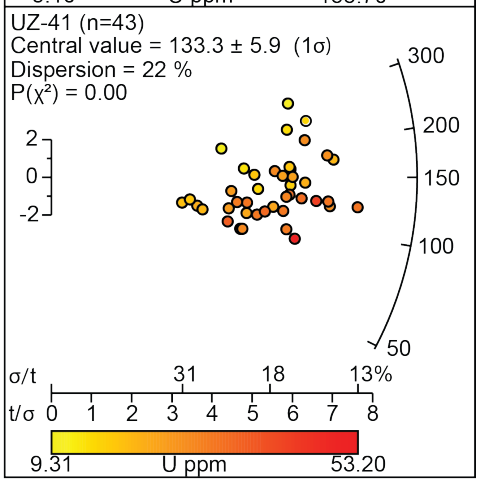

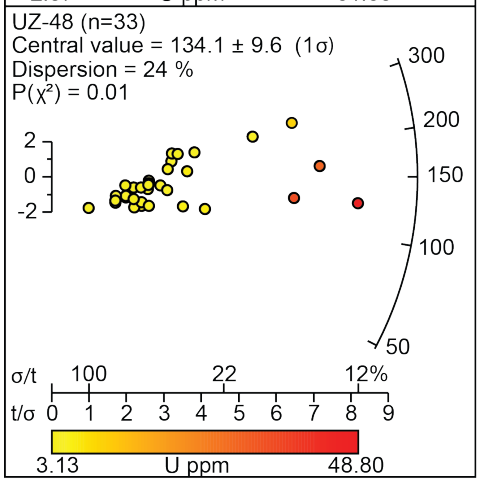

Karatyube Massif Radial Plots_1

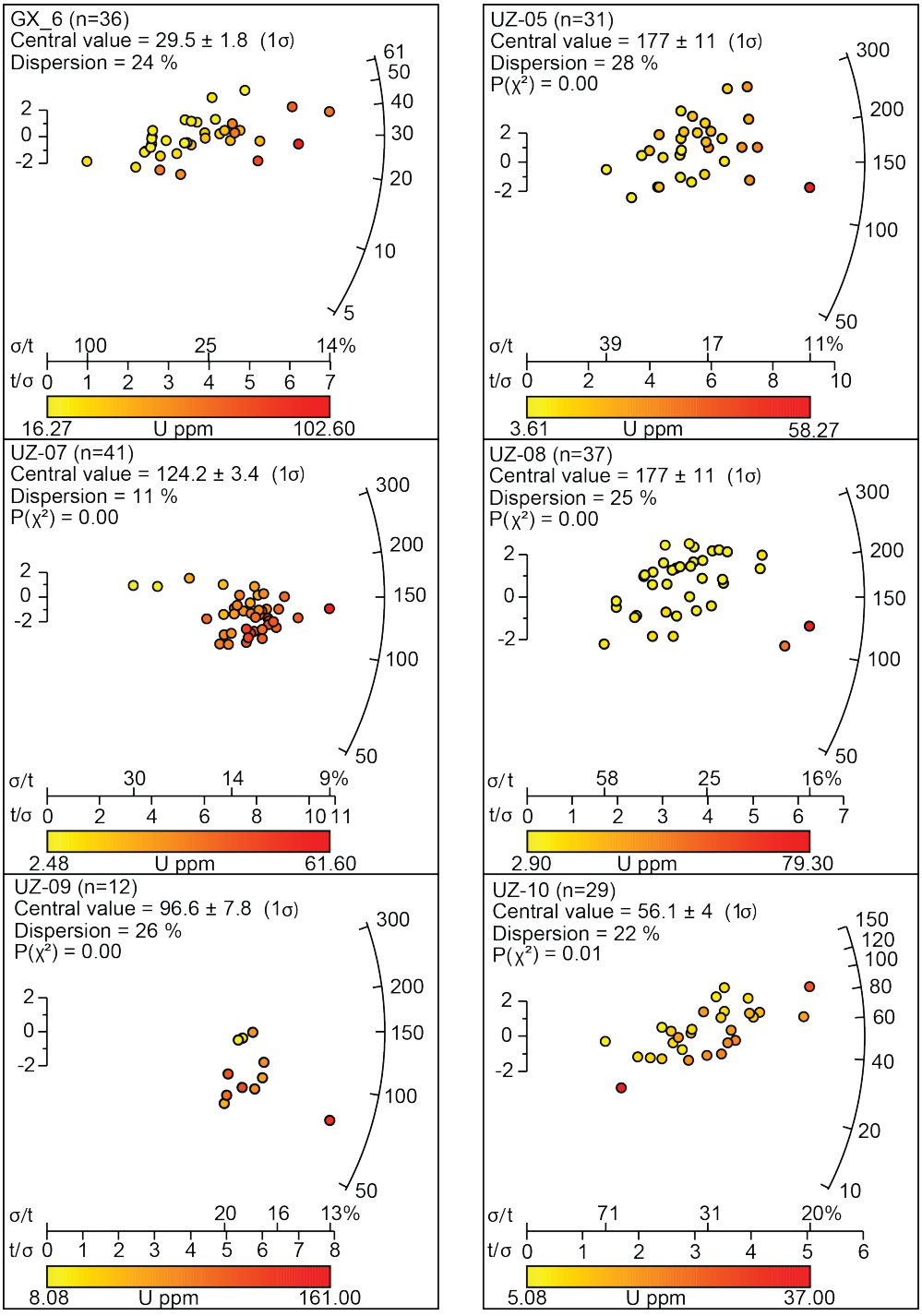

Karatyube Massif Radial Plots_2

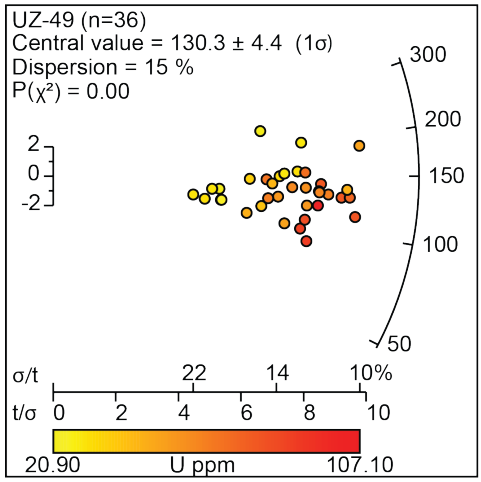

Ziadin Mountains Radial Plots

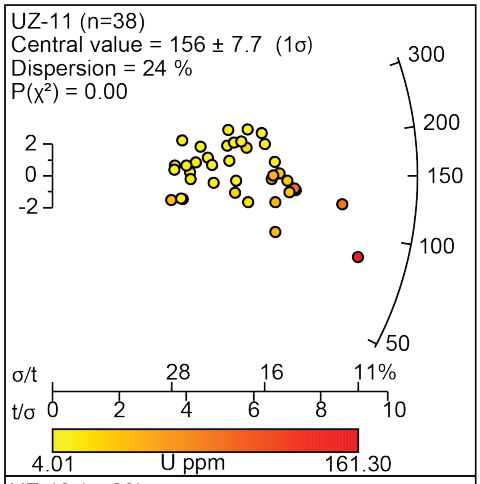

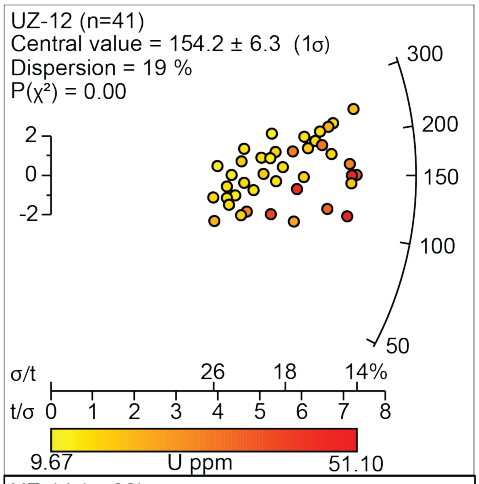

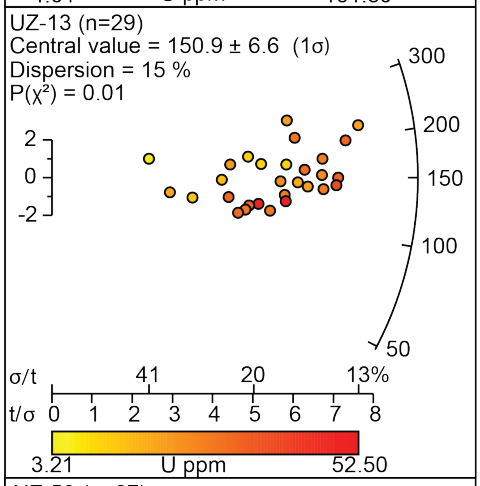

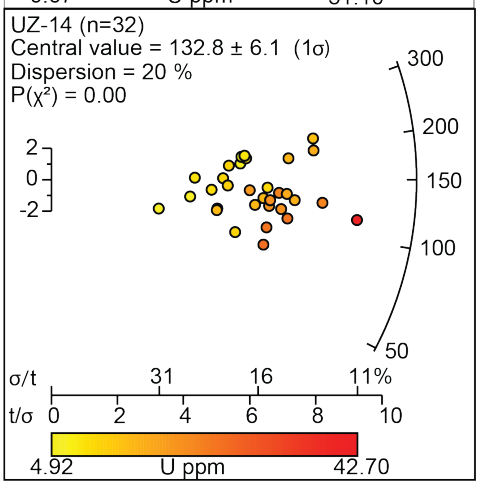

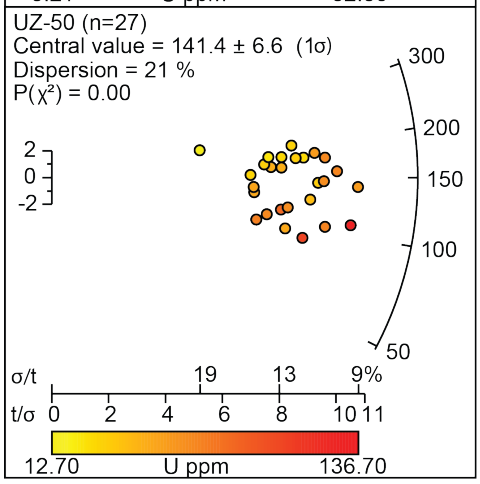

Aydar Radial Plots

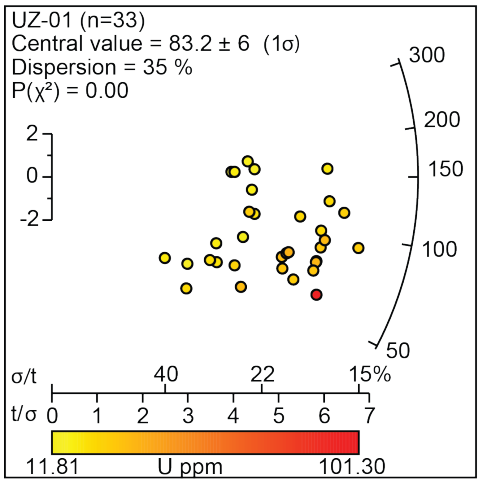

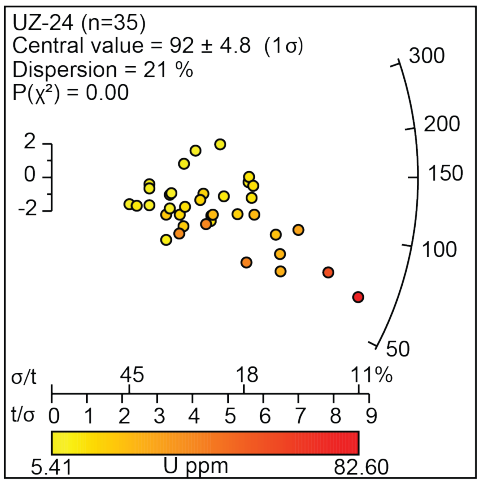

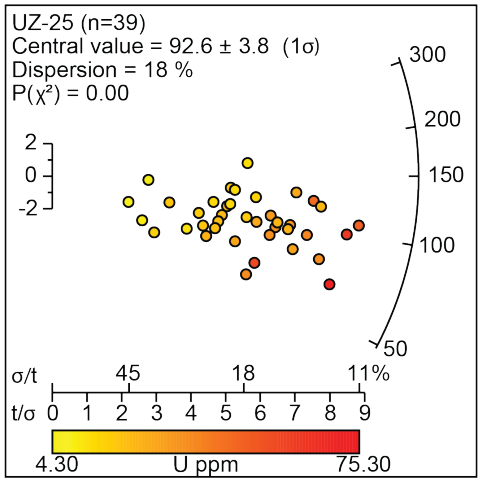

6.3 Supplementary File 3

1 Individual time-temperature plots for each sample modelled using Gallagher (2012). For modelling parameters see Supplementary File 5

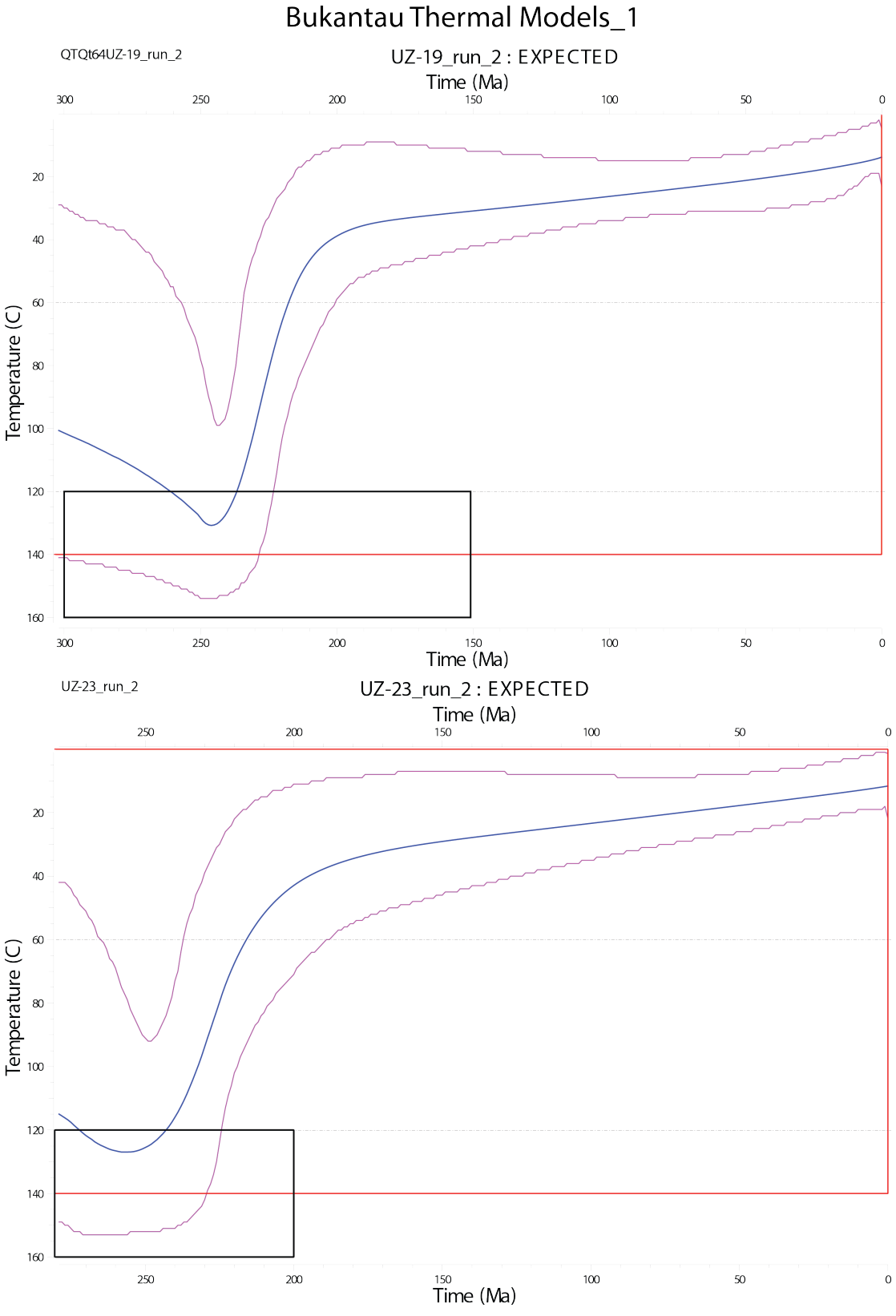

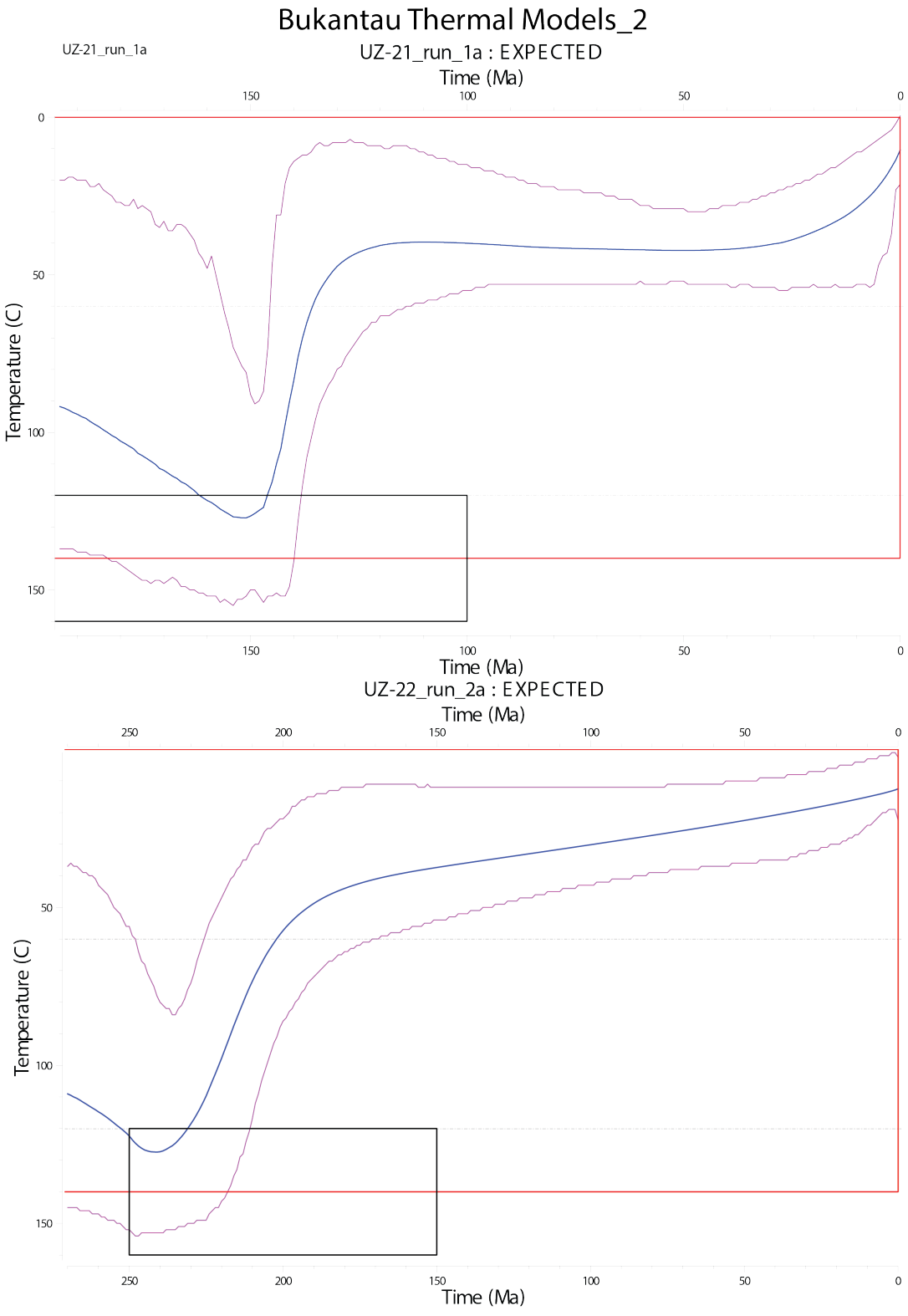
Bukantau Thermal Models_2
UZ-21_run_1a
UZ-21_run_1a : EXPECTED
Time (Ma)
150
100
50
0
Temperature (C)
0
50
100
150
Time (Ma)
UZ-22_run_2a : EXPECTED
Time (Ma)
250
200
150
100
50
0
Temperature (C)
50
100
150
Time (Ma)

3

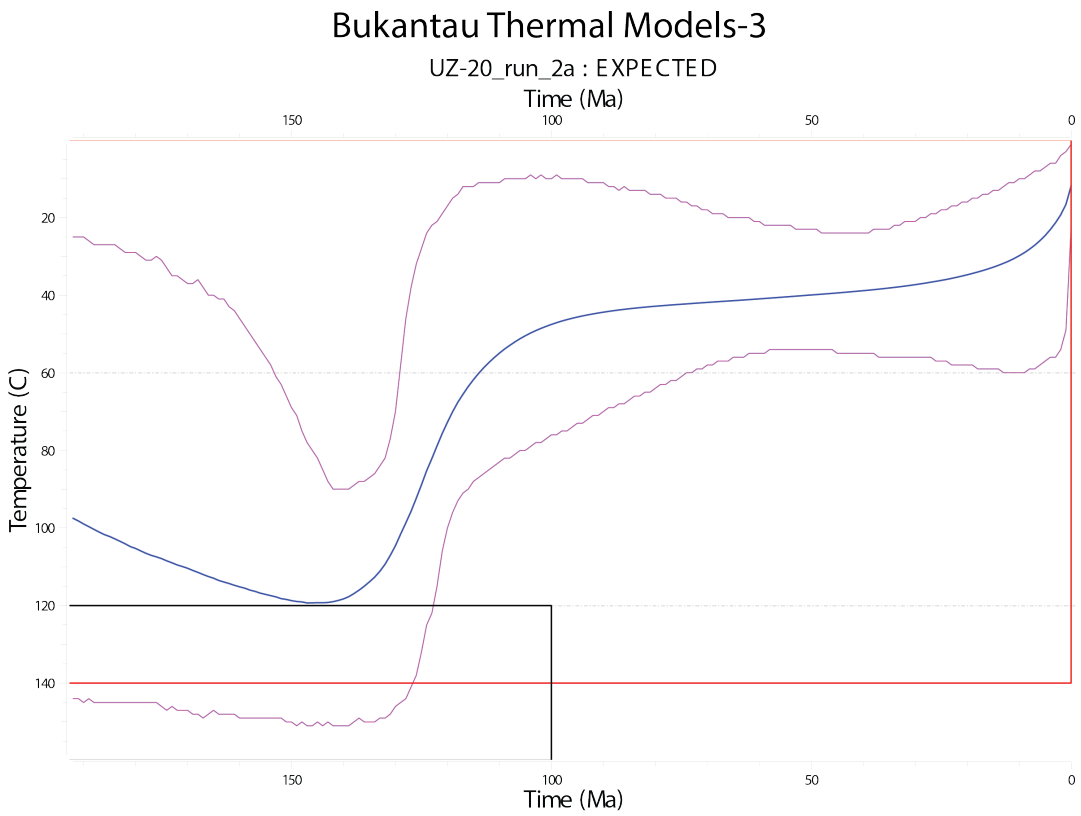
Bukantau Thermal Models-3
UZ-20_run_2a : EXPECTED
Time (Ma)
150
100
50
0
20
40
60
80
100
120
140
Temperature (C)
150
100
50
0
Time (Ma)

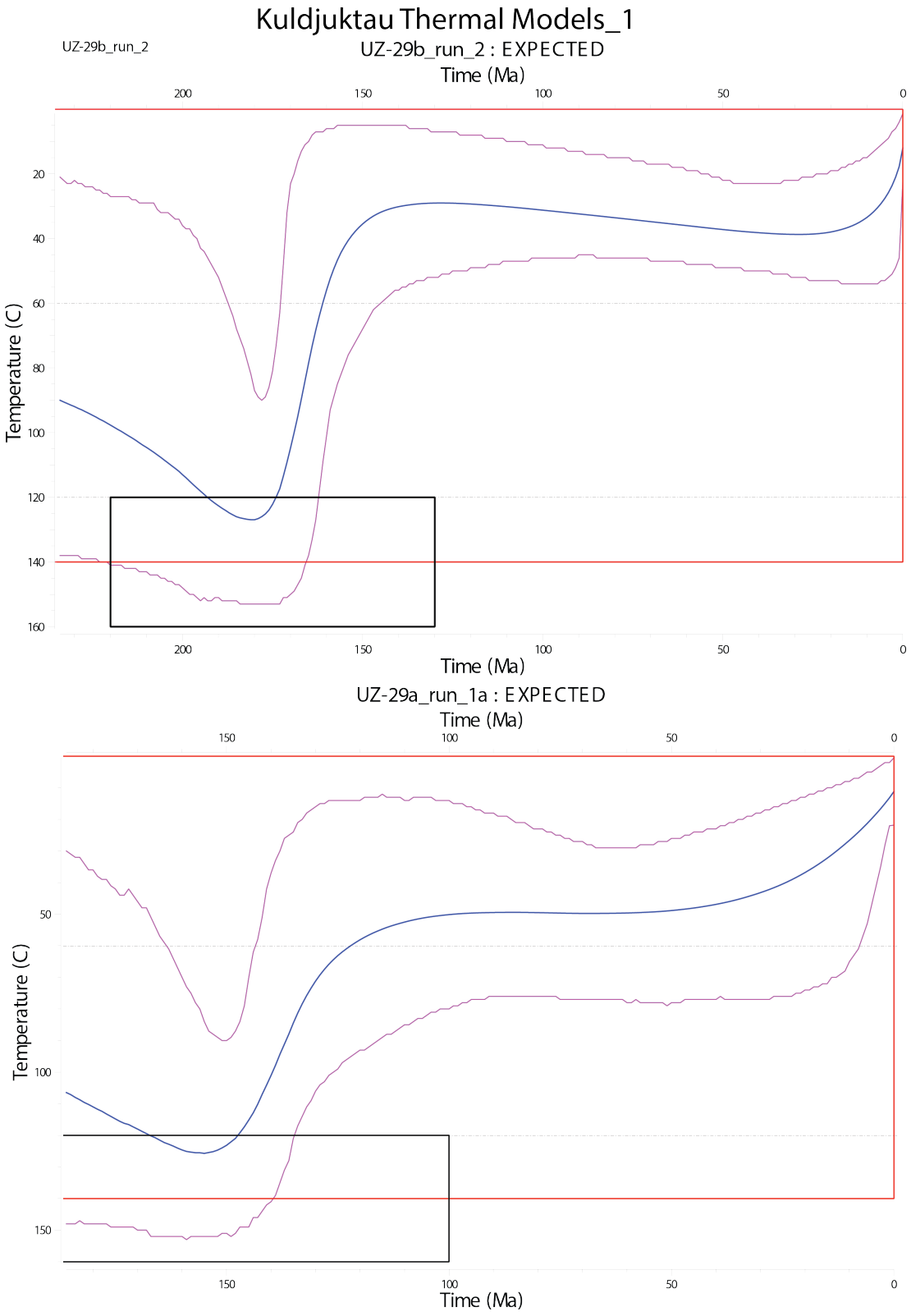
Kuldjuktau Thermal Models_1
UZ-29b_run_2
UZ-29b_run_2 : EXPECTED
Time (Ma)
200
150
100
50
0
20
40
60
80
100
120
140
160
Temperature (C)
Time (Ma)
UZ-29a_run_1a : EXPECTED
Time (Ma)
150
100
50
0
50
100
150
Temperature (C)
Time (Ma)

Kuldjuktau Thermal Models_2

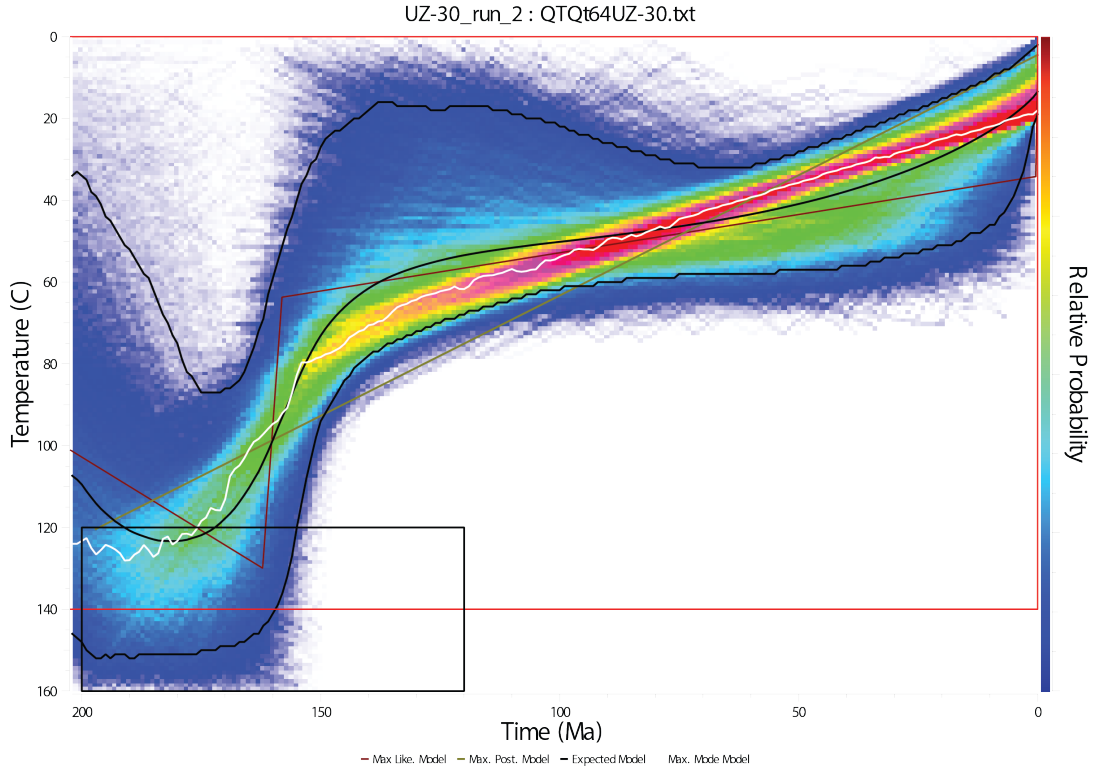

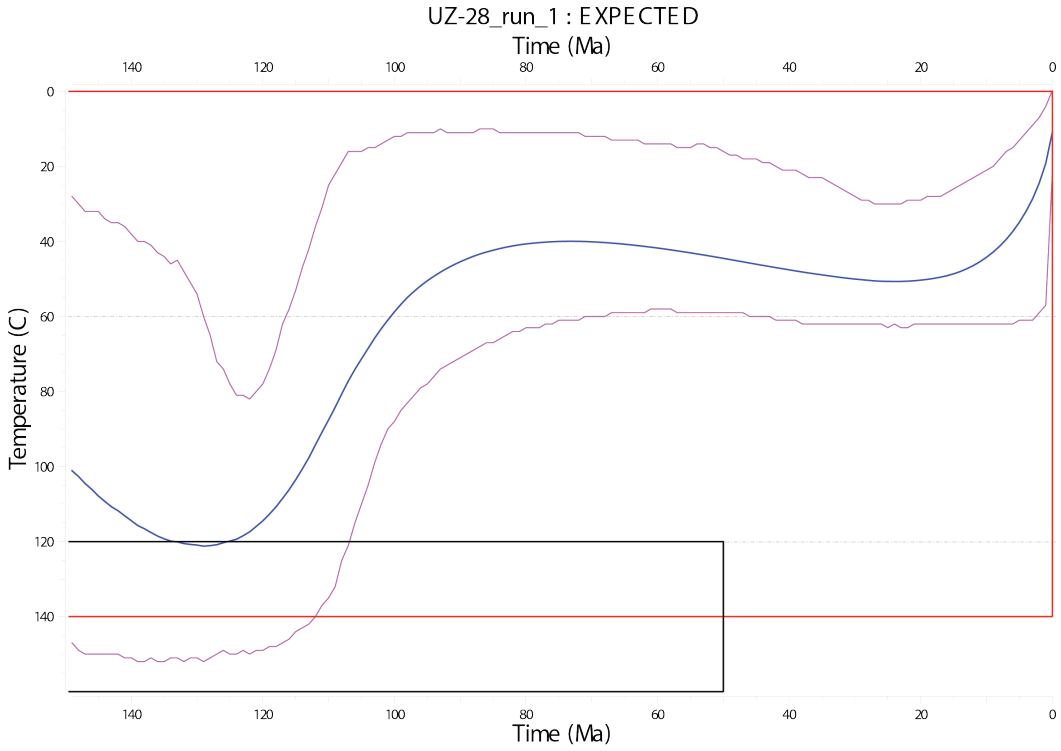

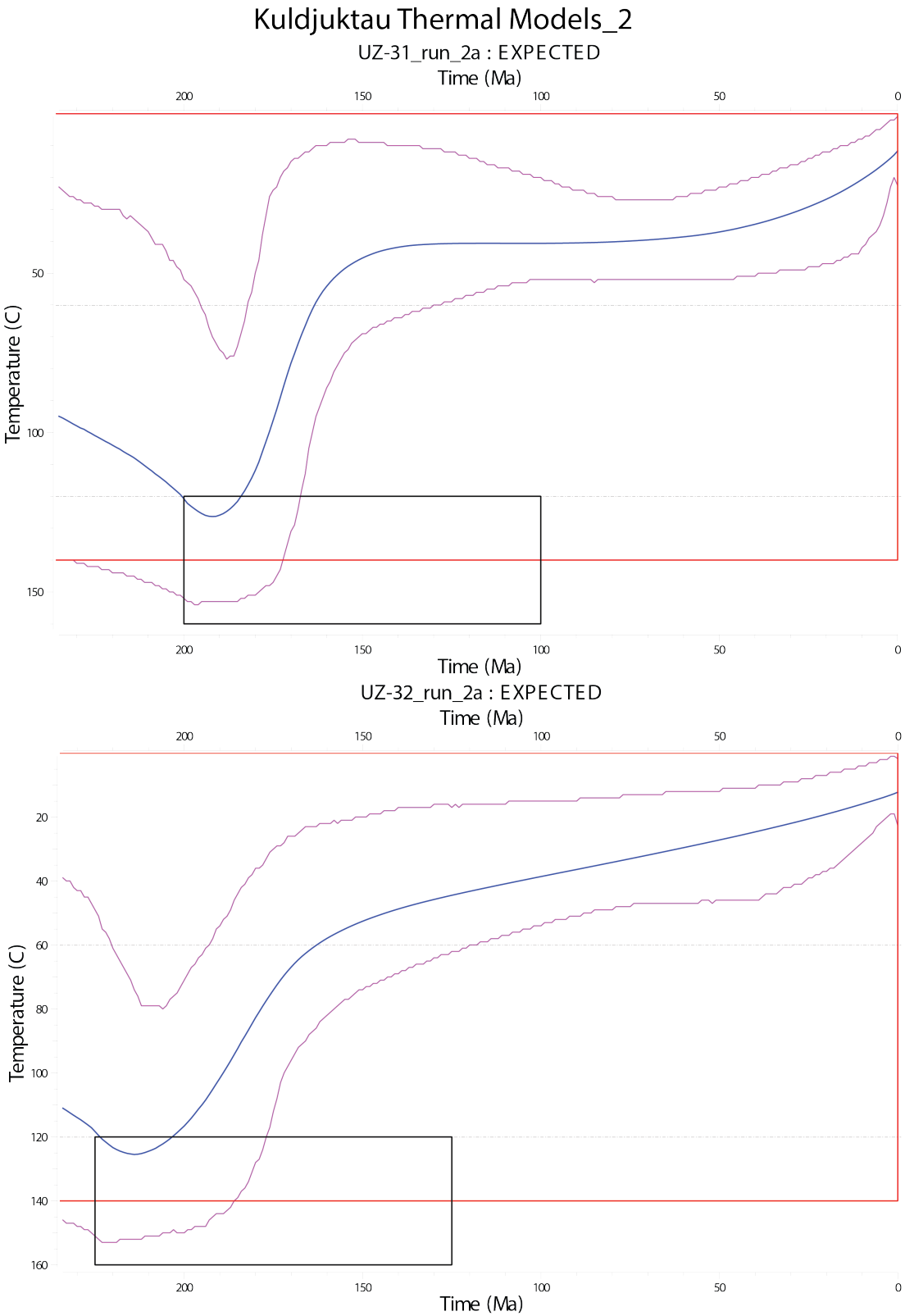
Kuldjuktau Thermal Models_2
UZ-31_run_2a : EXPECTED
Time (Ma)
200
150
100
50
0
Temperature (C)
50
100
150
Time (Ma)
UZ-32_run_2a : EXPECTED
Time (Ma)
200
150
100
50
0
Temperature (C)
20
40
60
80
100
120
140
160
Time (Ma)

Nurata Range Thermal Models_1

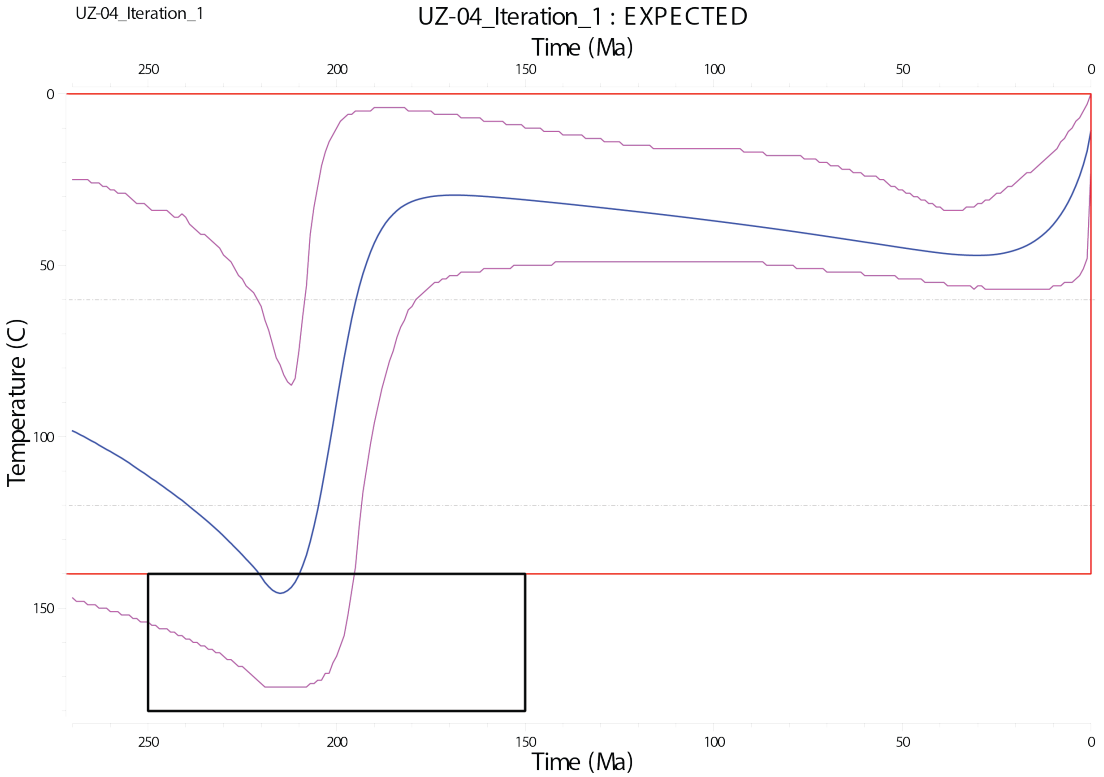

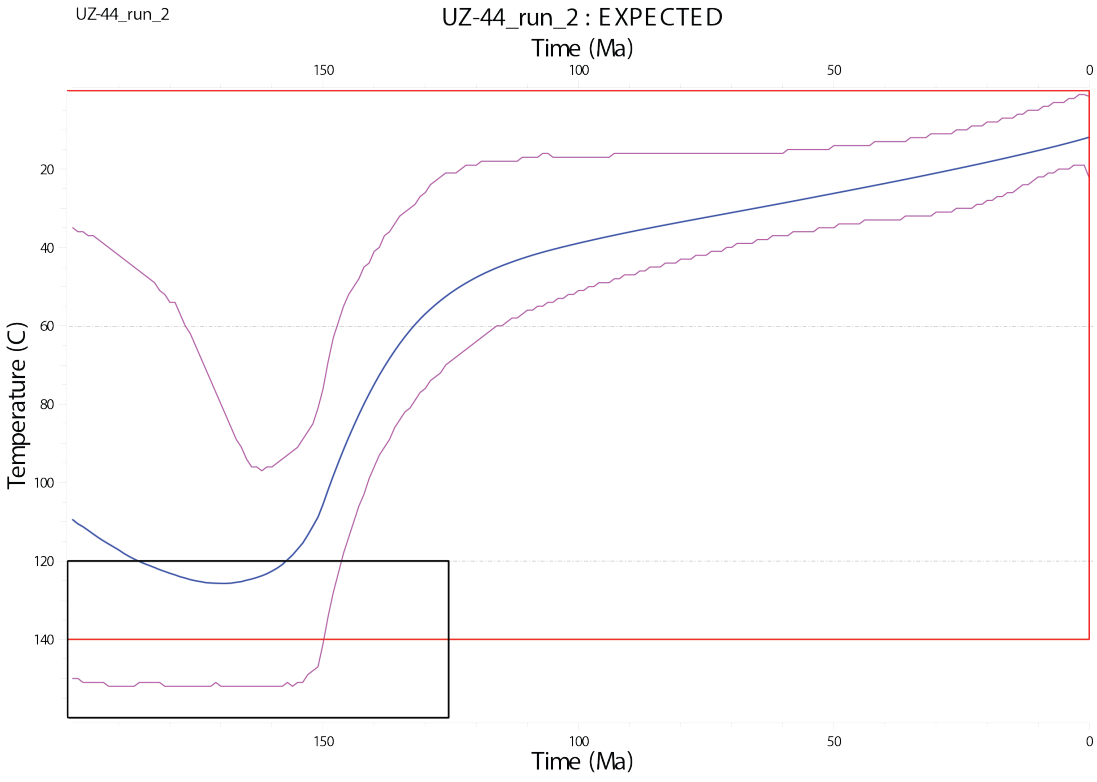

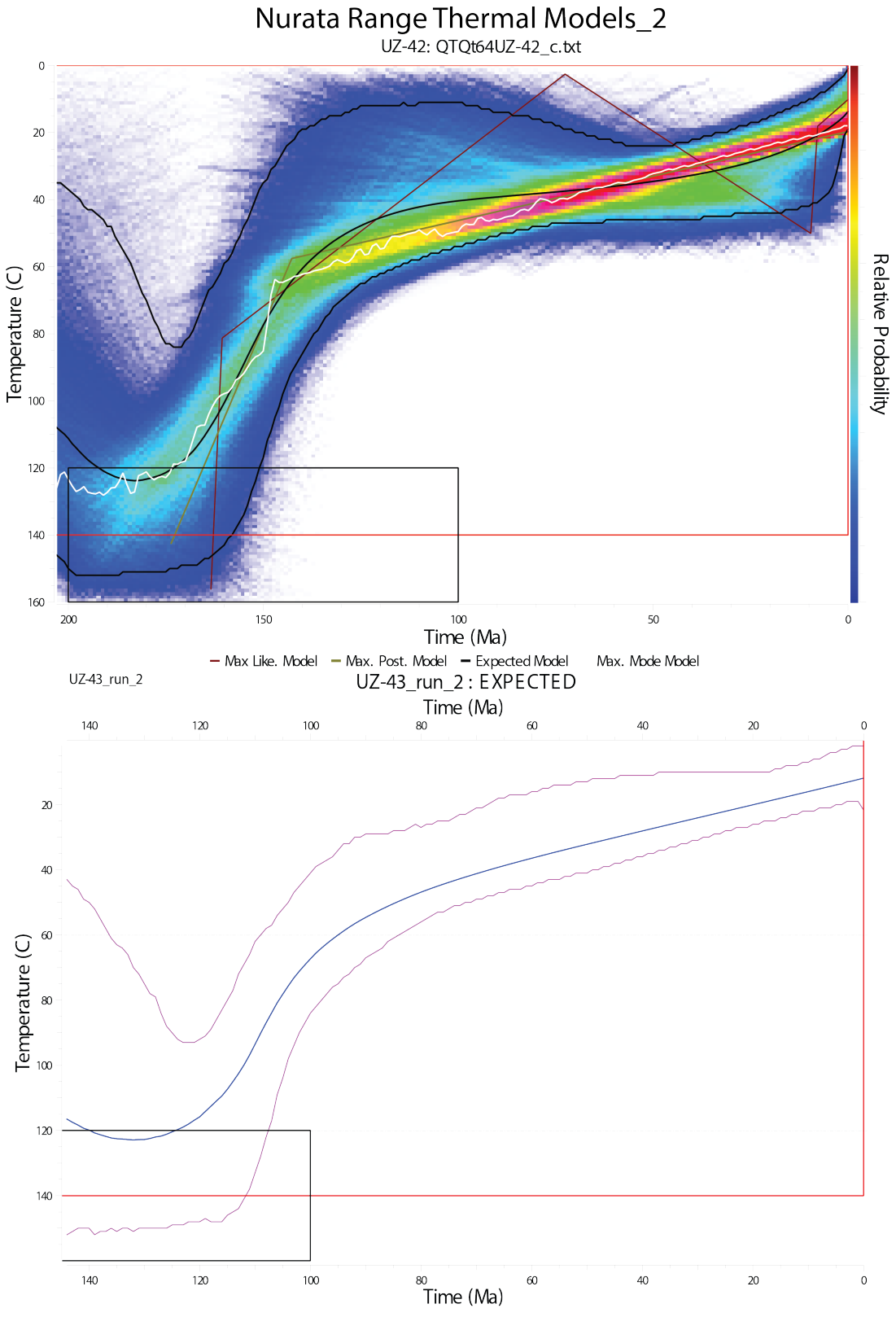
Nurata Range Thermal Models_2
UZ-42: QTQt64UZ-42_c.txt
Temperature (C)
Time (Ma)
Relative Probability
Max Like. Model
Max. Post. Model
Expected Model
Max. Mode Model
UZ-43_run_2
UZ-43_run_2 : EXPECTED
Time (Ma)
Temperature (C)
Time (Ma)

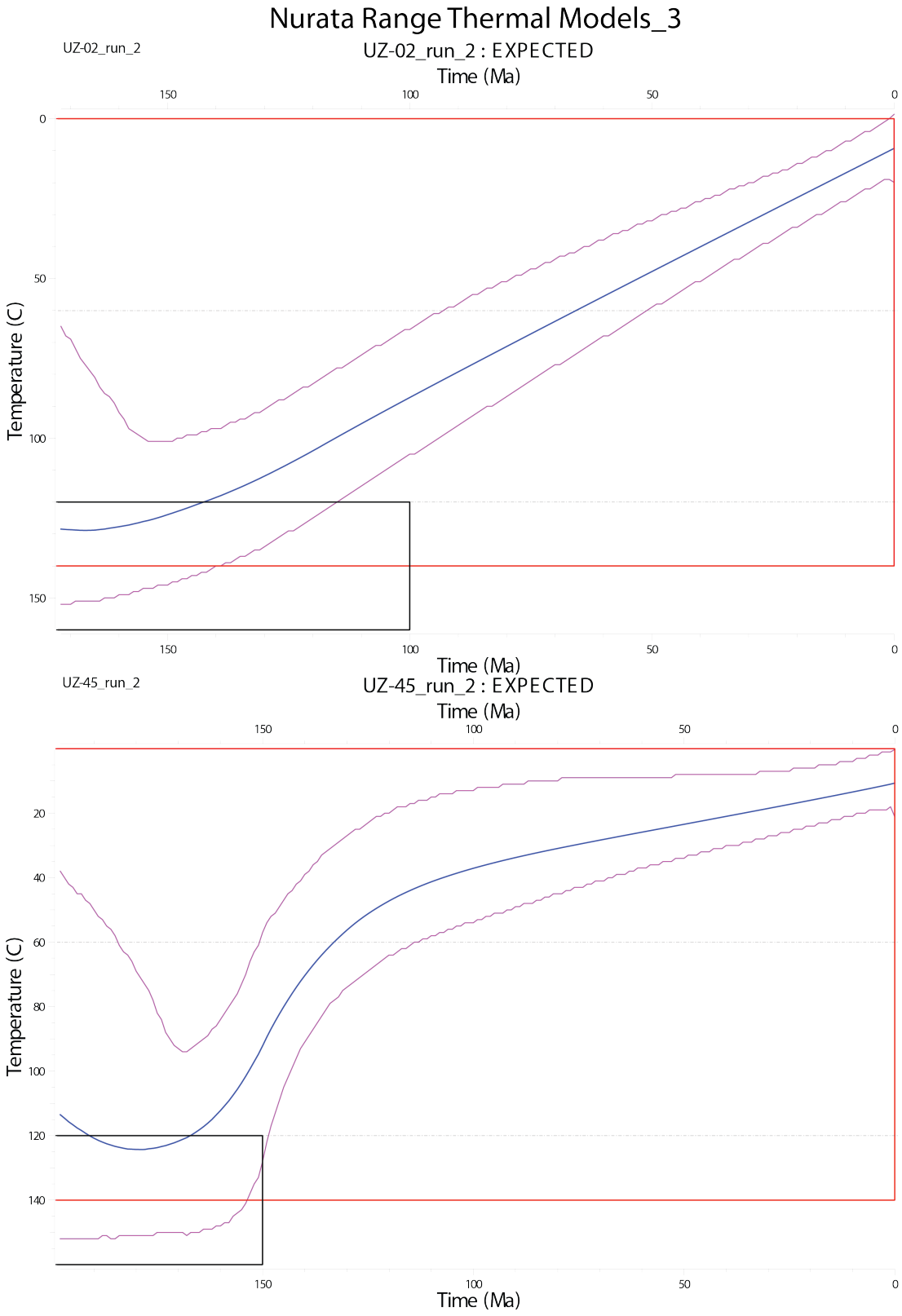
Nurata Range Thermal Models_3
UZ-02_run_2
UZ-02_run_2 : EXPECTED
Time (Ma)
150
100
50
0
Temperature (C)
0
50
100
150
Time (Ma)
UZ-45_run_2
UZ-45_run_2 : EXPECTED
Time (Ma)
20
40
60
80
100
120
140

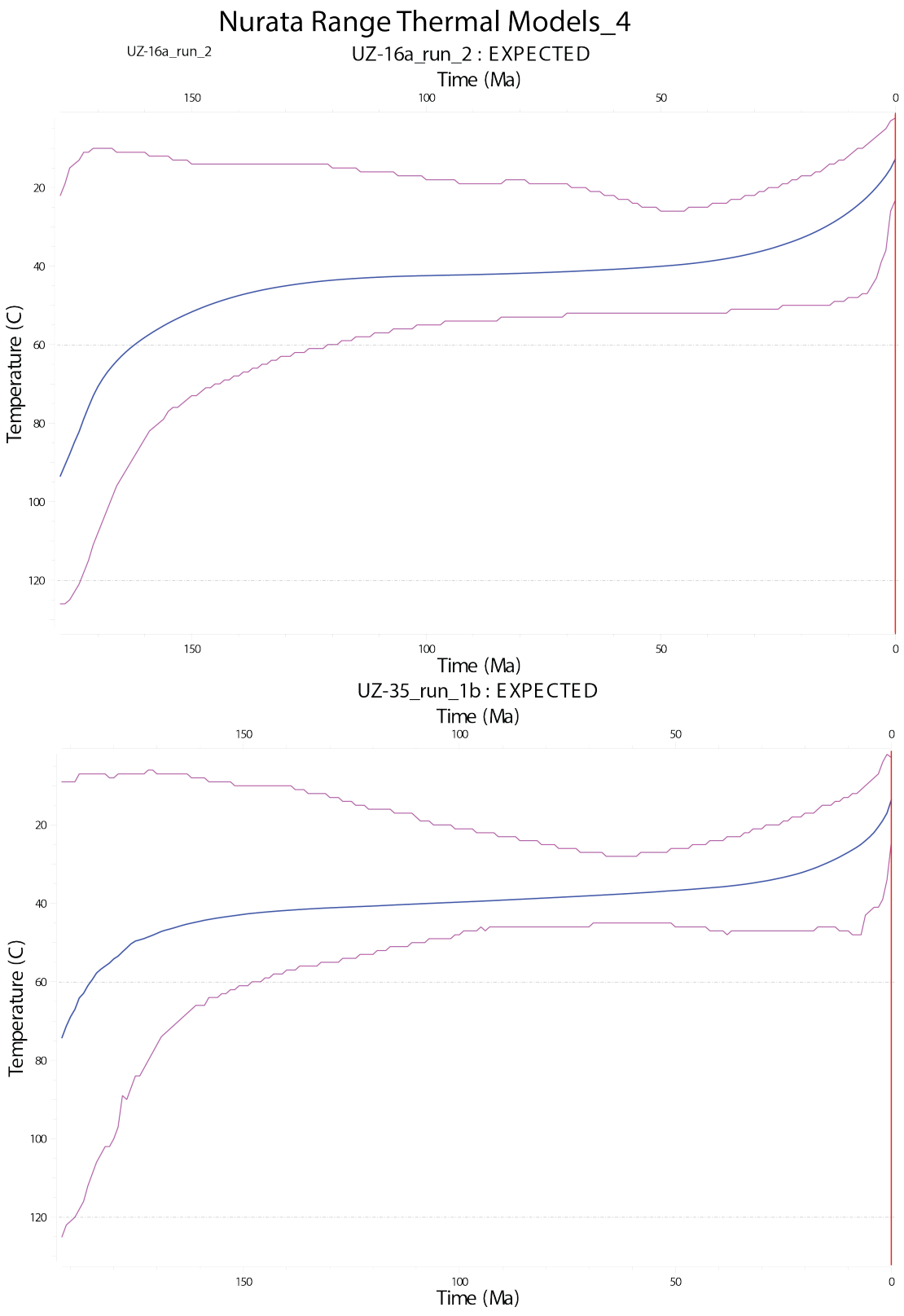
Nurata Range Thermal Models_4
UZ-16a_run_2
UZ-16a_run_2 : EXPECTED
Time (Ma)
150
100
50
0
20
40
60
80
100
120
Temperature (C)
Time (Ma)
UZ-35_run_1b : EXPECTED
Time (Ma)
150
100
50
0
20
40
60
80
100
120
Temperature (C)
Time (Ma)

Nurata Range Thermal Models_5

UZ-48_run_2

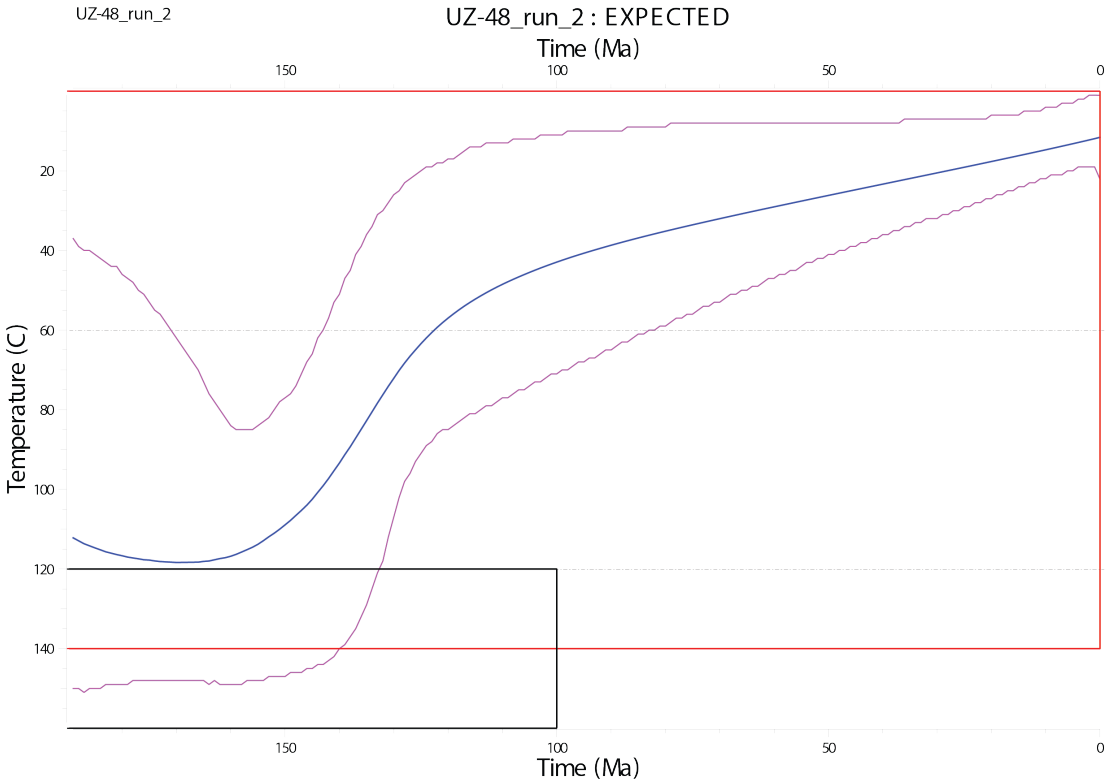

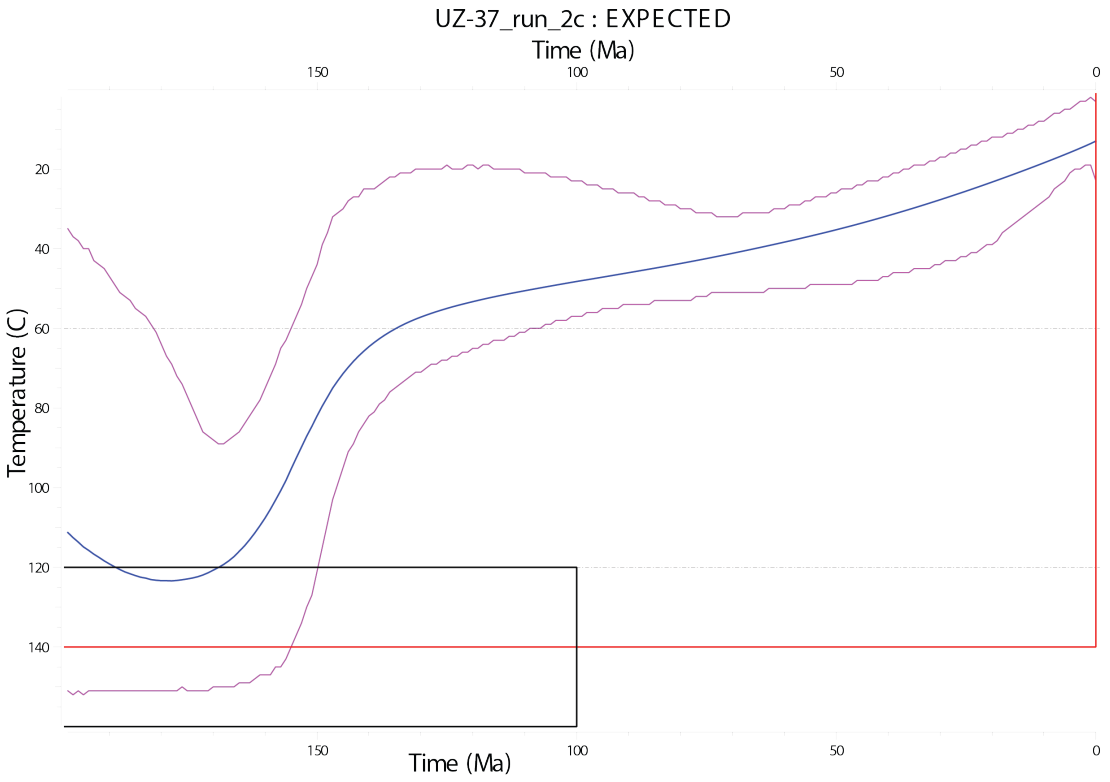

Nurata Range Thermal Models_6

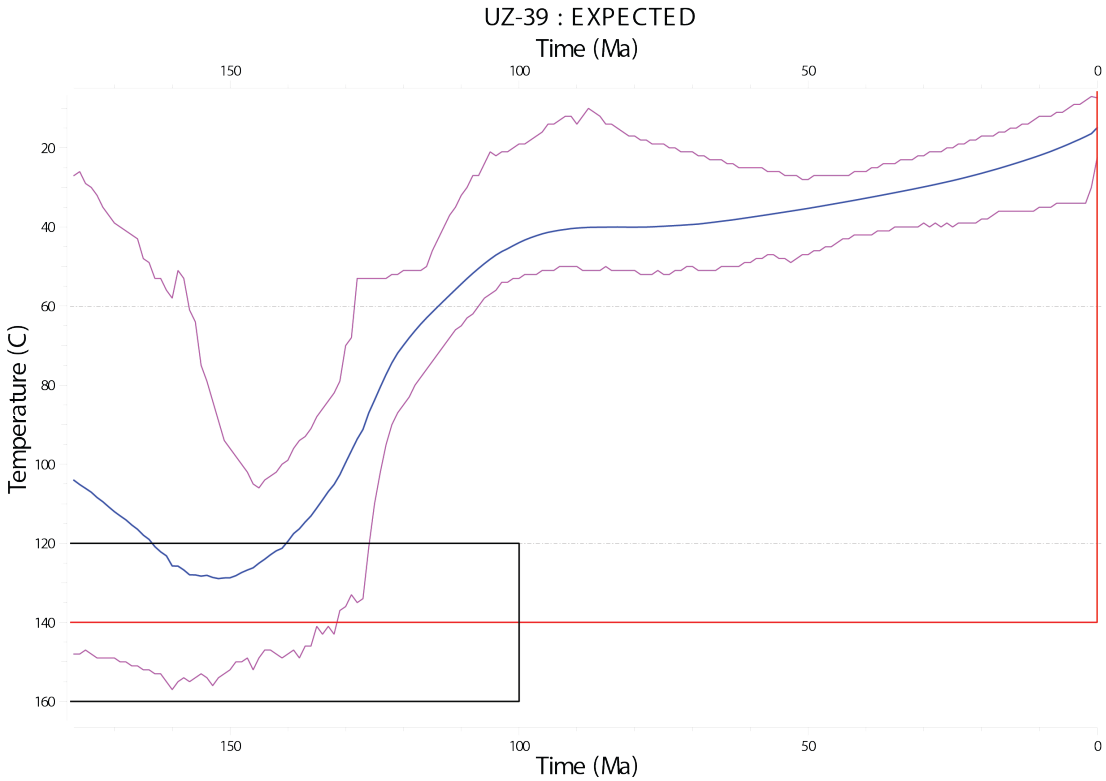

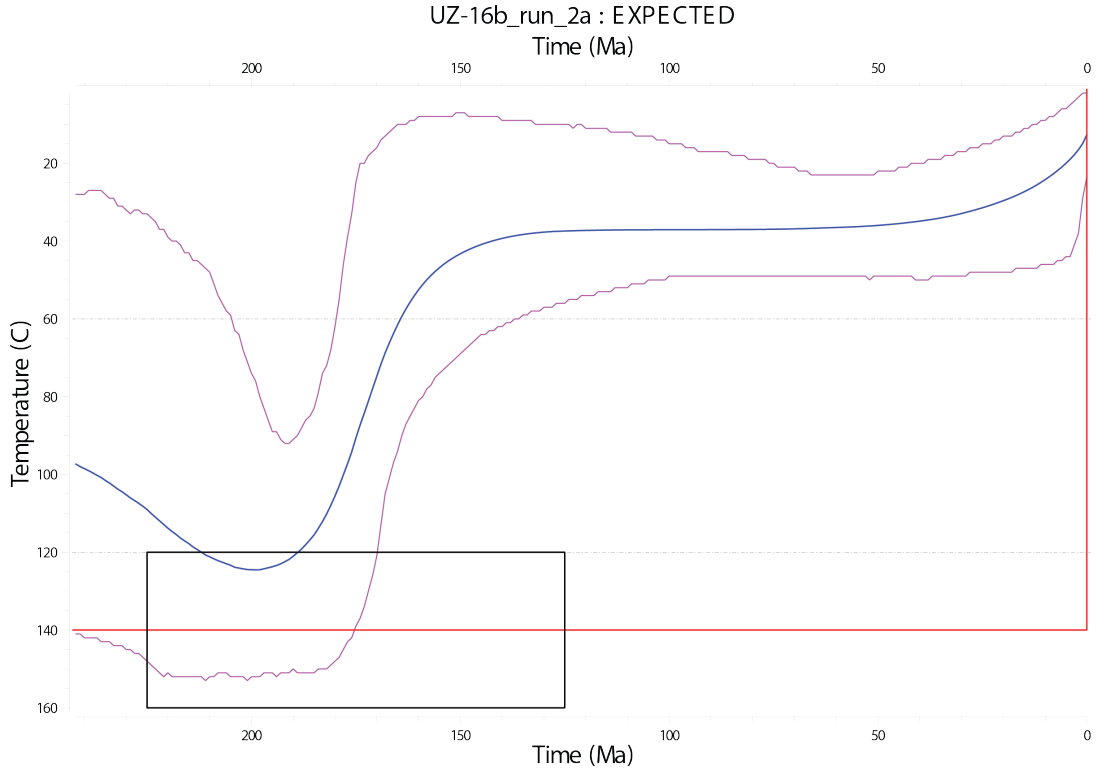

Nurata Range Thermal Models_7

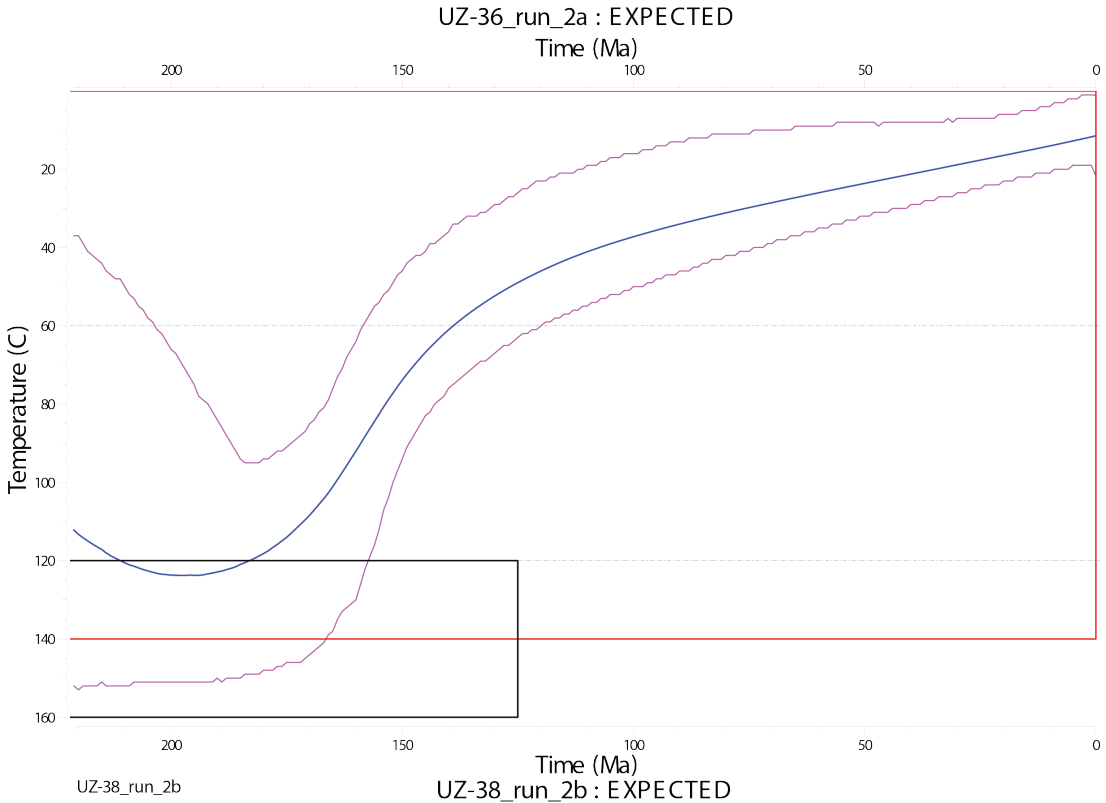

UZ-38_run_2b

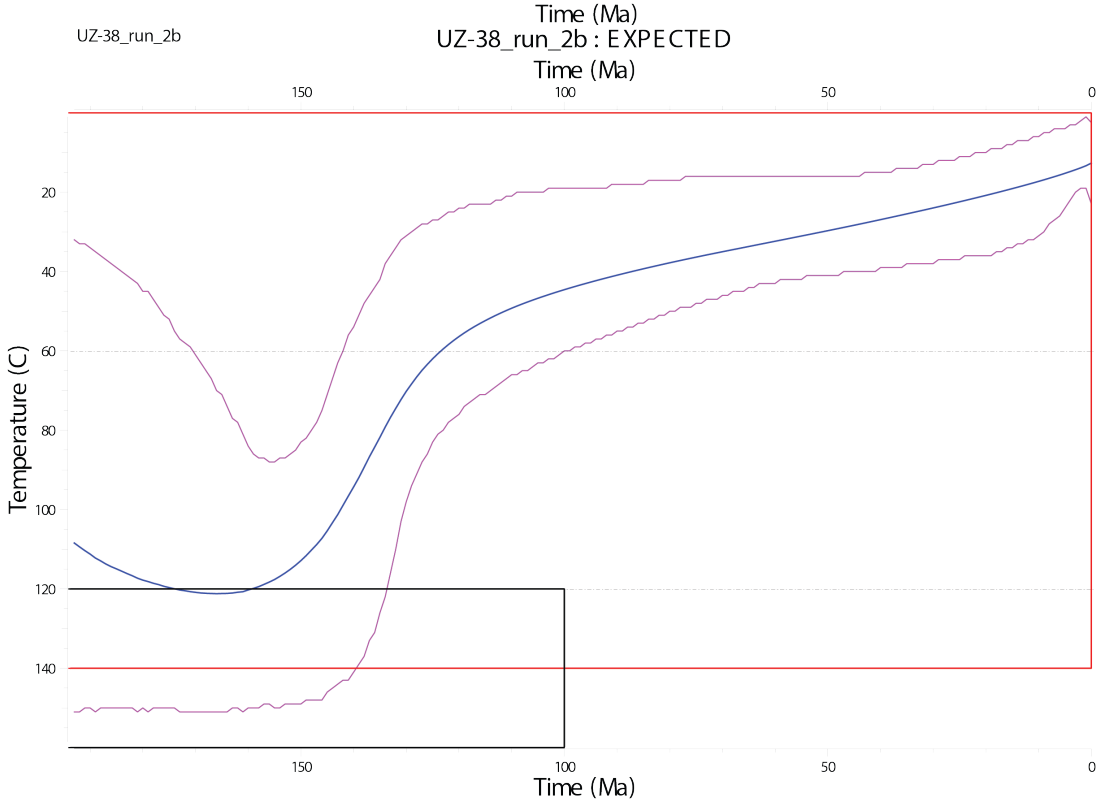

Nurata Range Thermal Models_8

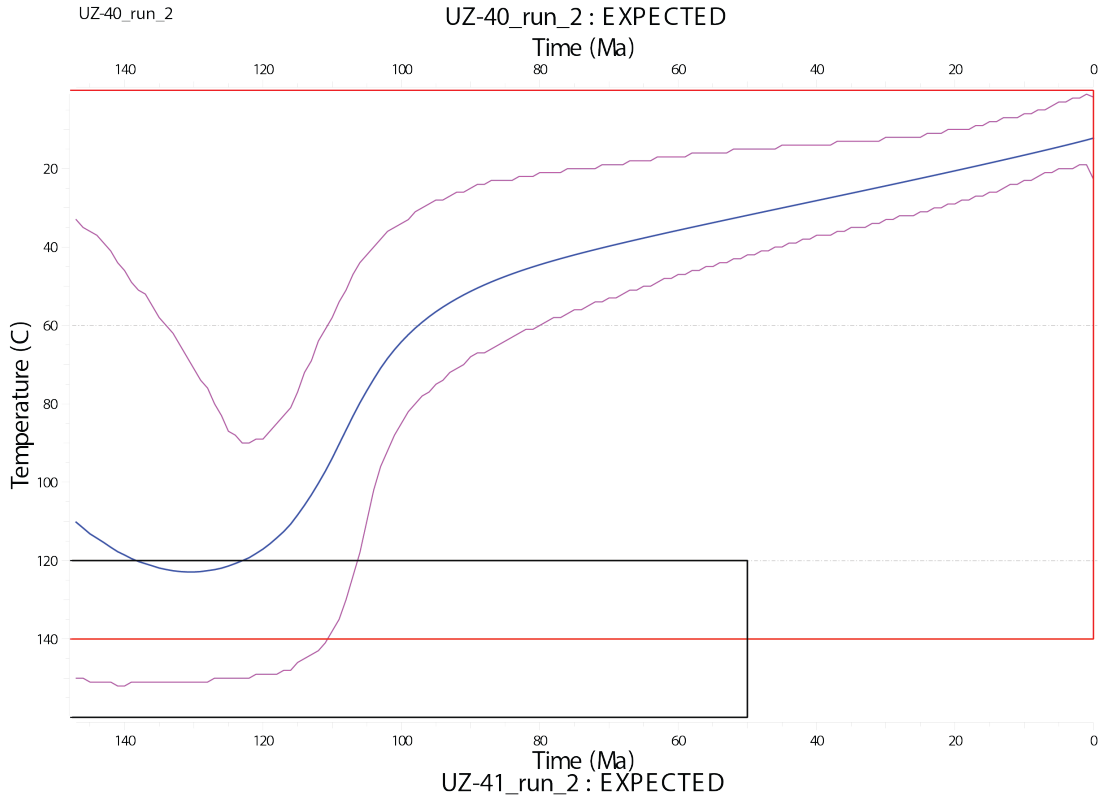

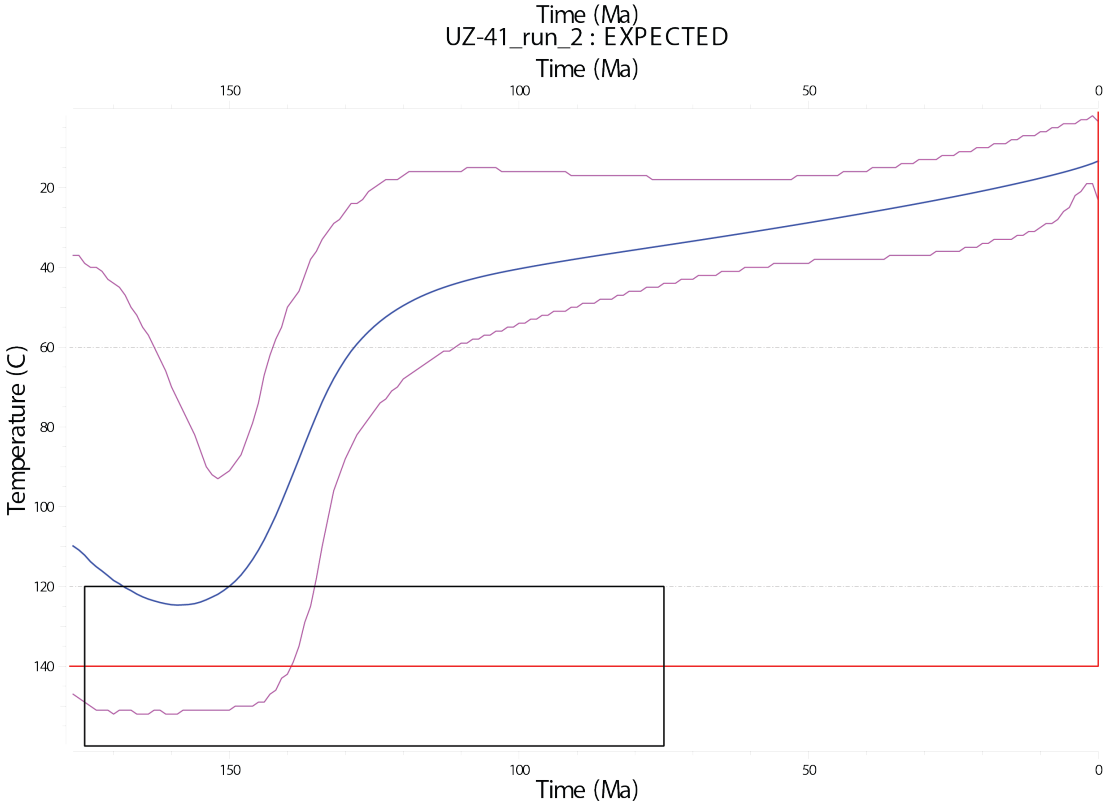

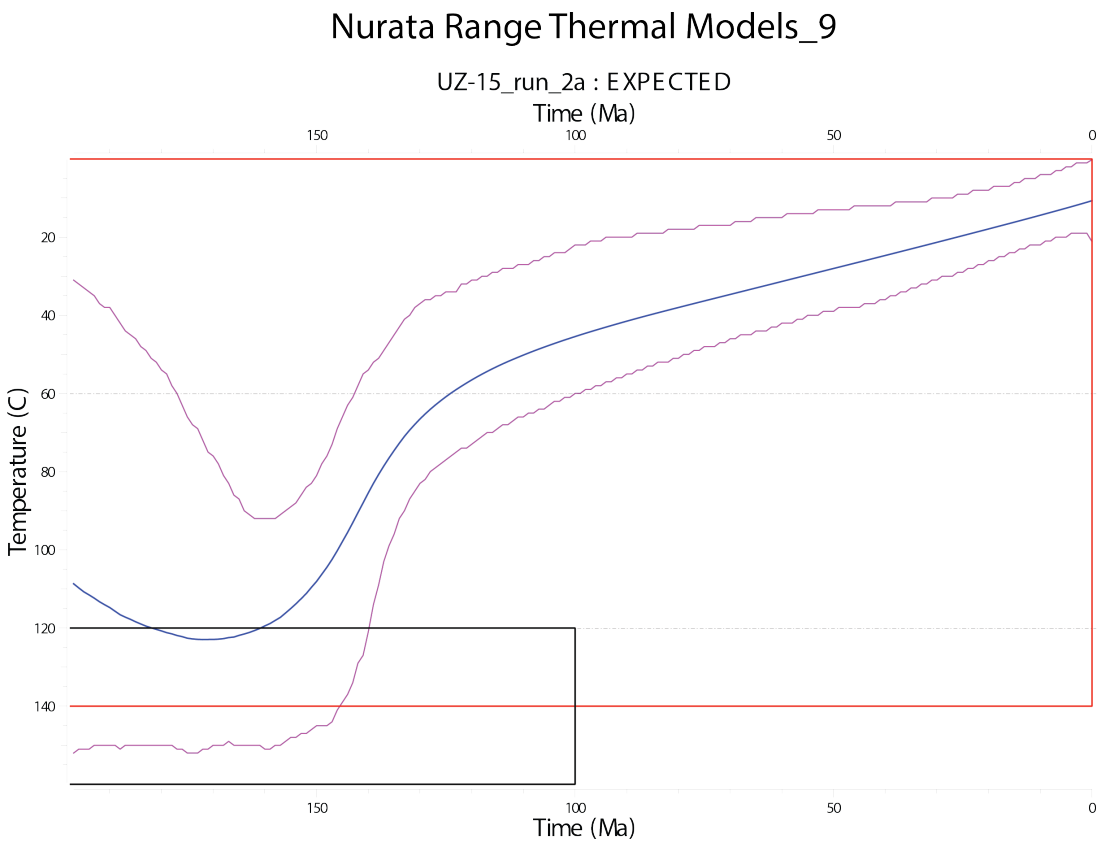
Nurata Range Thermal Models_9
UZ-15_run_2a : EXPECTED
Time (Ma)
150
100
50
0
20
40
60
80
100
120
140
Temperature (C)
150
100
50
0
Time (Ma)

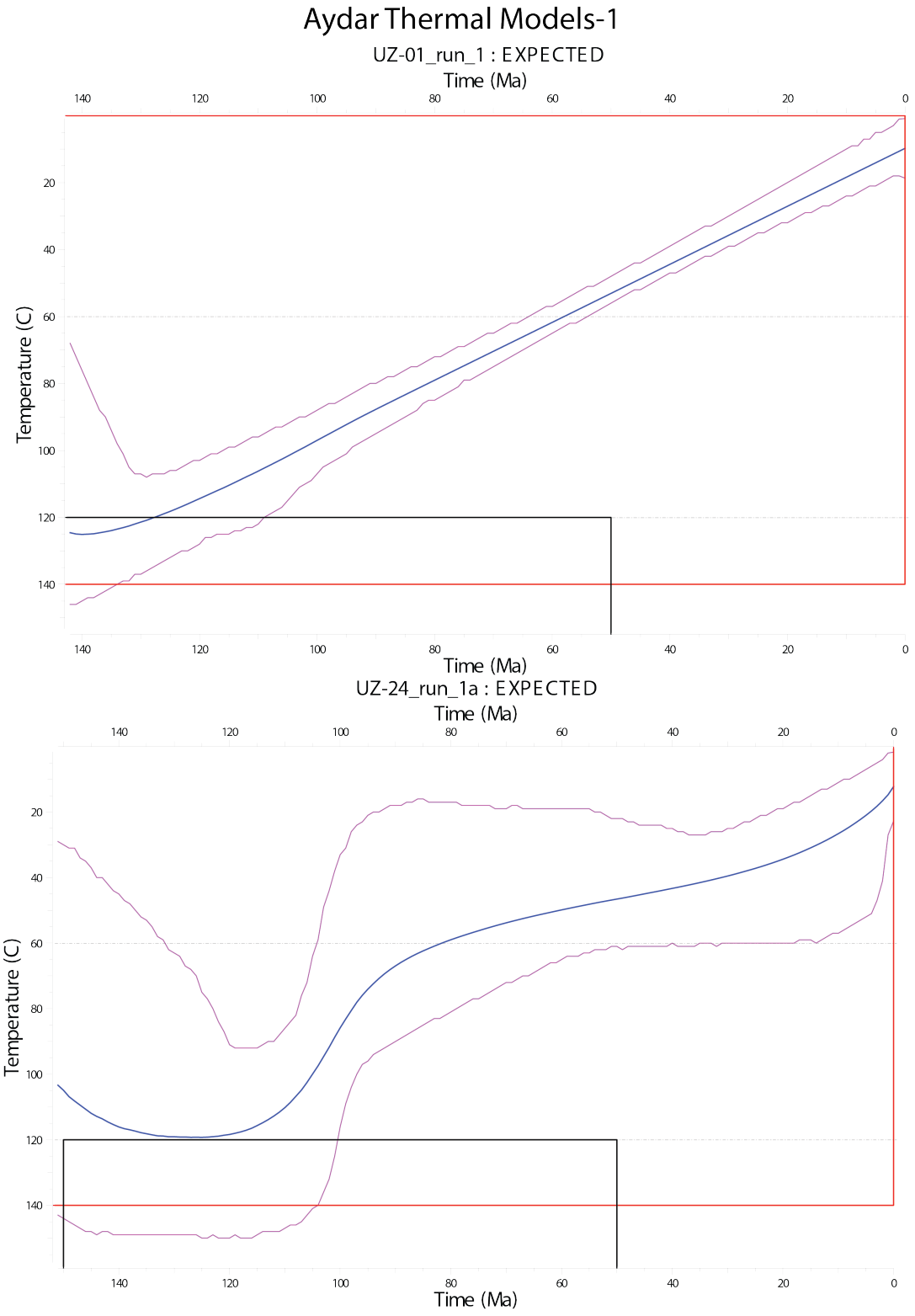
Aydar Thermal Models-1
UZ-01_run_1 : EXPECTED
Time (Ma)
Temperature (C)
UZ-24_run_1a : EXPECTED
Time (Ma)
Temperature (C)
Time (Ma)

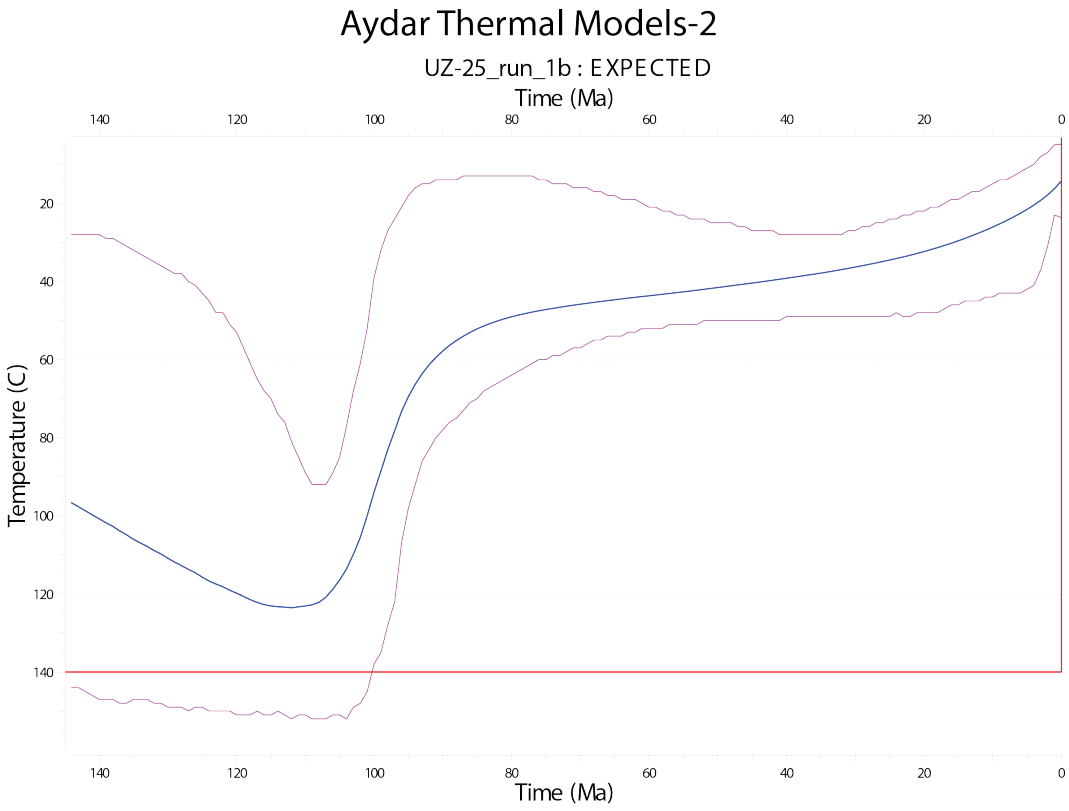
Aydar Thermal Models-2
UZ-25_run_1b : EXPECTED
Time (Ma)
140
120
100
80
60
40
20
0
Temperature (C)
20
40
60
80
100
120
140
Time (Ma)

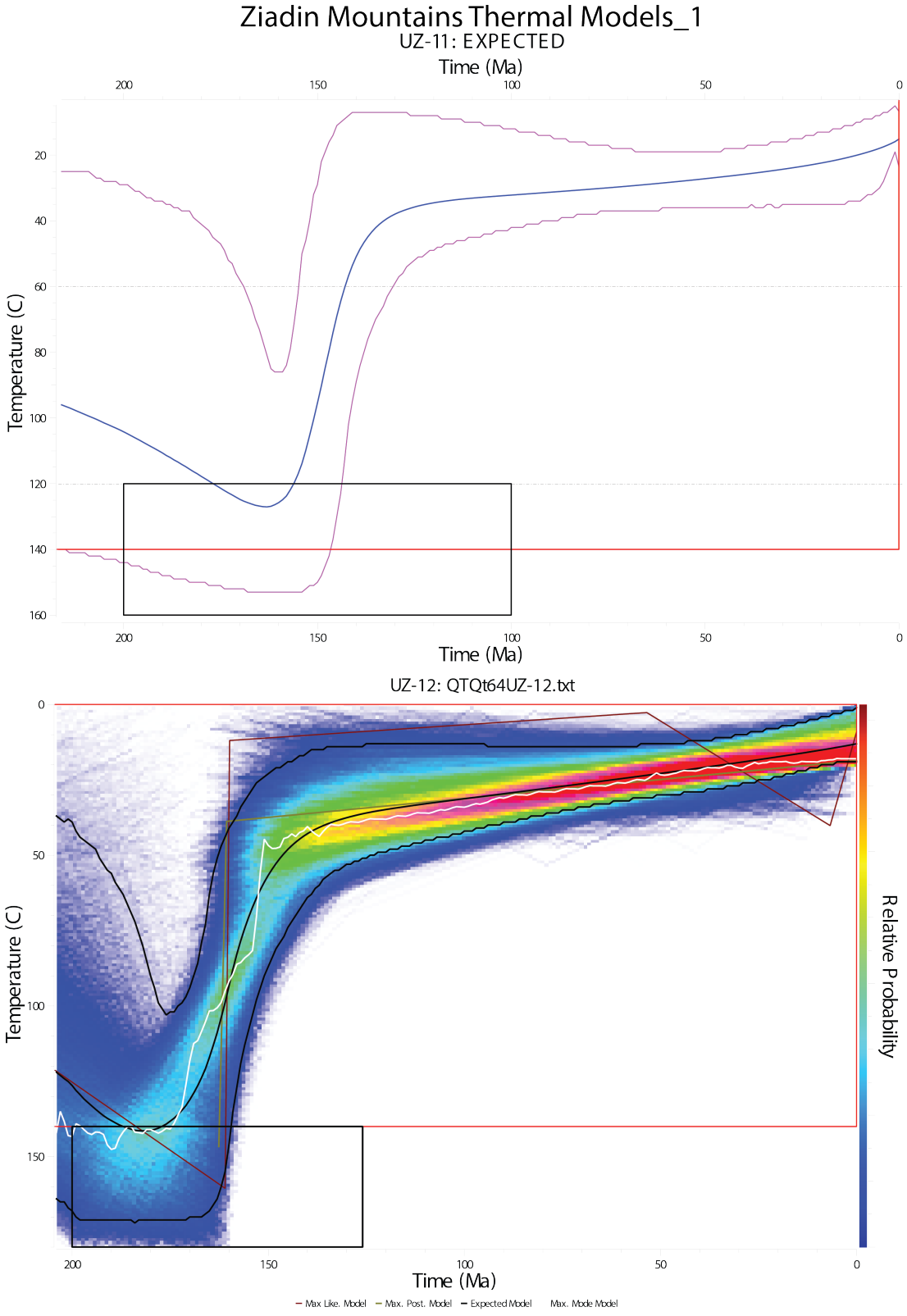
Ziadin Mountains Thermal Models_1
UZ-11: EXPECTED
Time (Ma)
200
150
100
50
0
Temperature (C)
20
40
60
80
100
120
140
160
UZ-12: QTQt64UZ-12.txt
Relative Probability
Max Like. Model
Max. Post. Model
Expected Model
Max. Mode Model

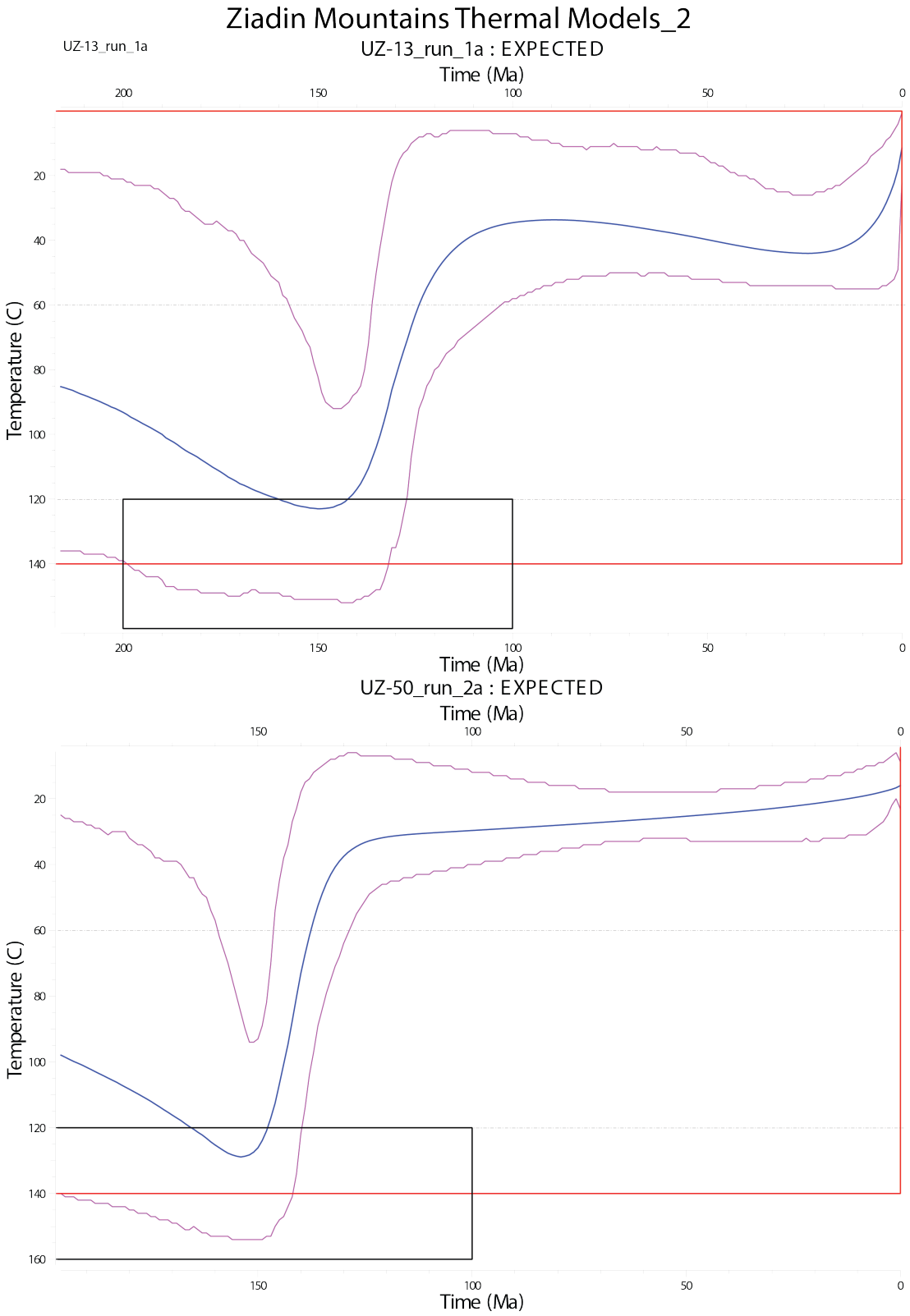
Ziadin Mountains Thermal Models_2
UZ-13_run_1a
UZ-13_run_1a : EXPECTED
Time (Ma)
200
150
100
50
0
20
40
60
80
100
120
140
Temperature (C)
Time (Ma)
UZ-50_run_2a : EXPECTED
Time (Ma)
150
100
50
0
20
40
60
80
100
120
140
160
Temperature (C)
Time (Ma)

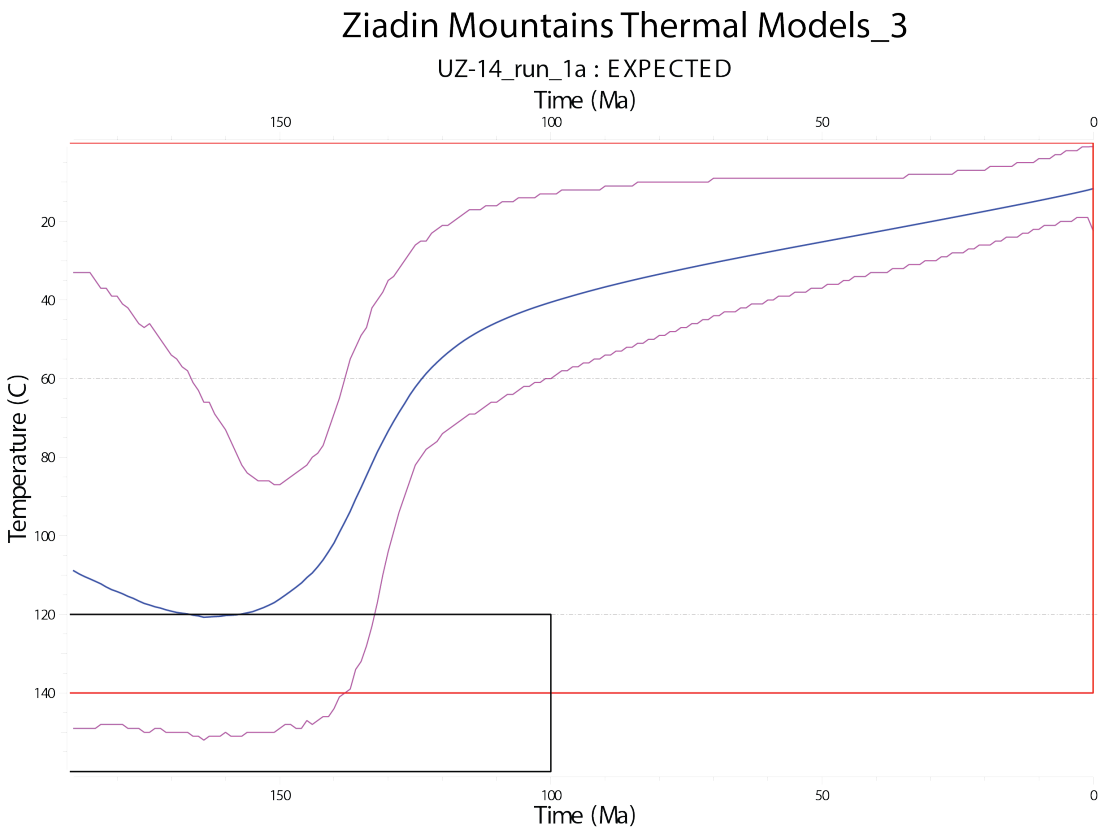
Ziadin Mountains Thermal Models_3
UZ-14_run_1a : EXPECTED
Time (Ma)
150
100
50
0
20
40
60
80
100
120
140
Temperature (C)
150
100
50
0
Time (Ma)

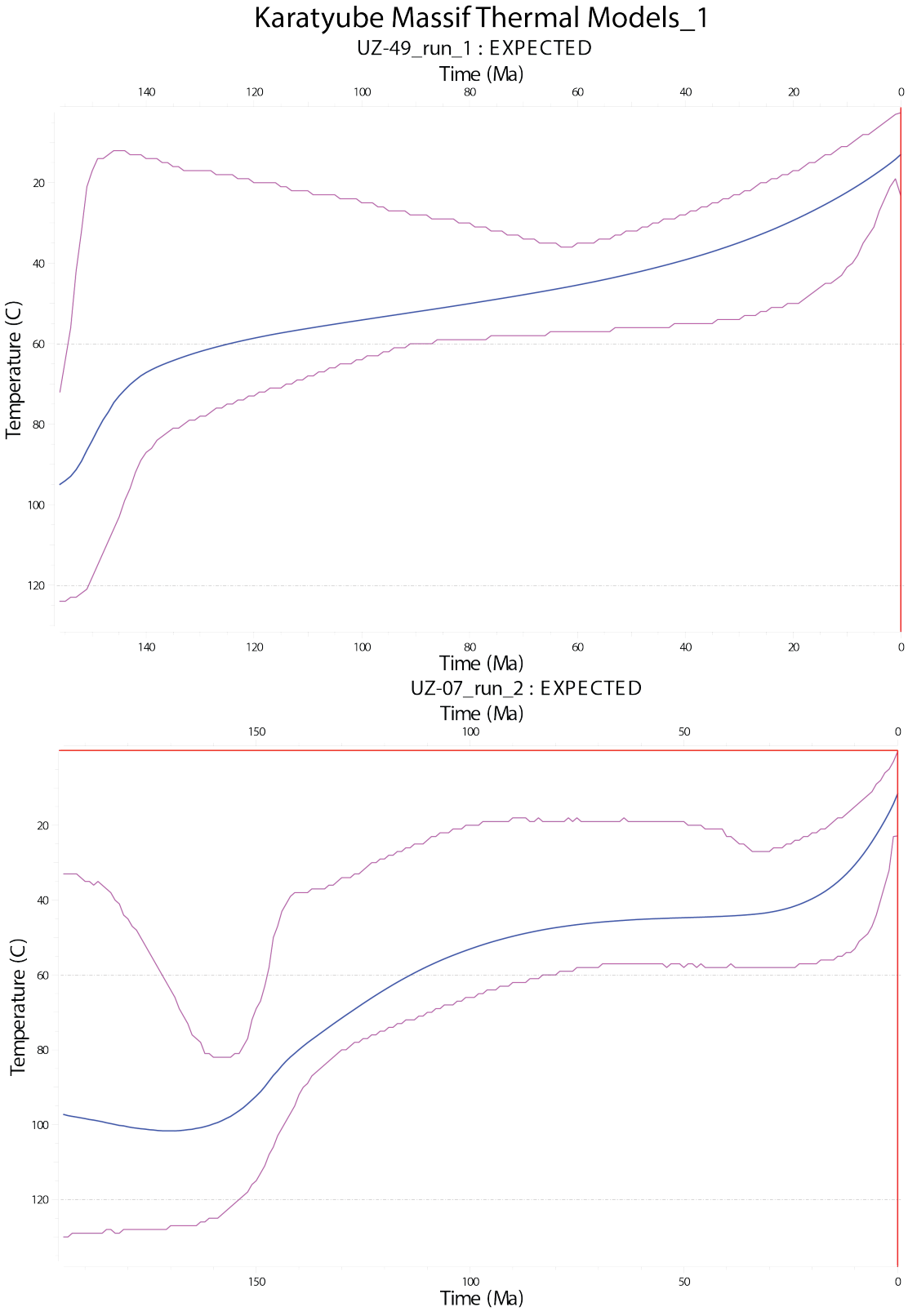
Karatyube Massif Thermal Models_1
UZ-49_run_1 : EXPECTED
Time (Ma)
140
120
100
80
60
40
20
0
Temperature (C)
20
40
60
80
100
120
Time (Ma)
UZ-07_run_2 : EXPECTED
Time (Ma)
150
100
50
0
Temperature (C)
20
40
60
80
100
120
Time (Ma)

Karatyube Massif Thermal Models_2

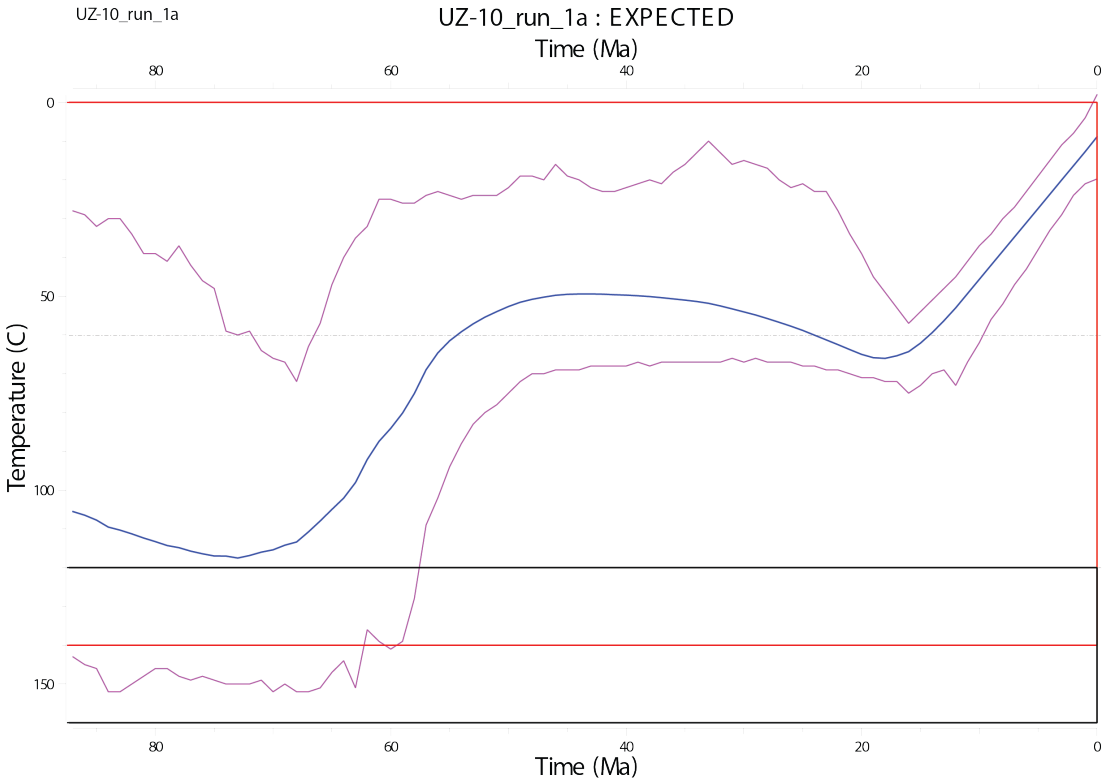

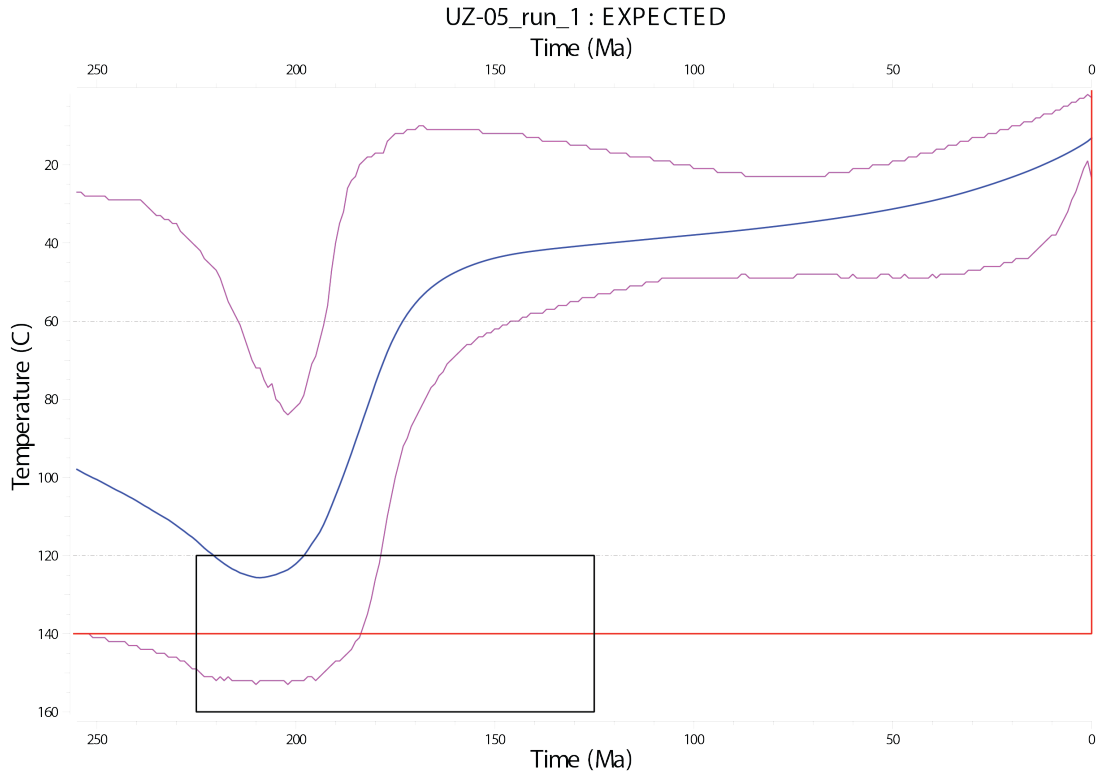

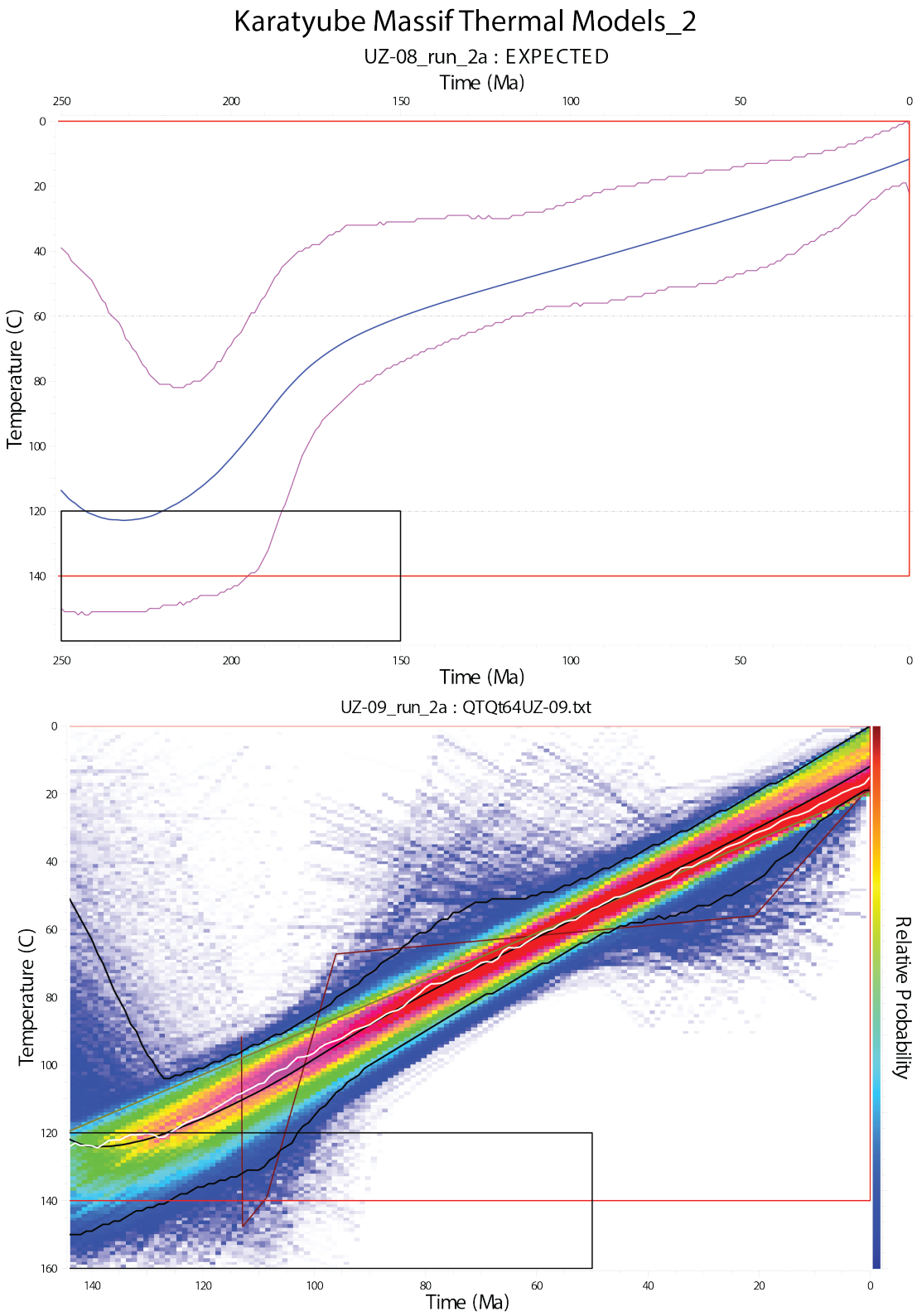

6.4 Supplementary File 4

Thermal history modelling parameters following Flowers et al. (2015).

Supplementary File 5: Thermal history model input table for simulations of the Kyzylkum-Nurata Segment, Uzbekistan and Tajikistan, based on framework established by Flowers et al. (2015)

1. Thermochronologic Data

Samples and data used in simulations

Simulation inputs			Data Source	All data
Sample Region	AHe	AFT		
Bukantau				
UZ-19		×	Supplementary File 1 and 4	yes
UZ-20		x	Supplementary File 1 and 4	yes
UZ-21	×	×	Table 2 and Supplementary File 1 and 4	yes
UZ-22		×	Supplementary File 1 and 4	yes
UZ-23		×	Supplementary File 1 and 4	yes
Kuldjuktau				
UZ-28		×	Supplementary File 1 and 4	yes
UZ-29a		×	Supplementary File 1 and 4	yes
UZ-29b		×	Supplementary File 1 and 4	yes
UZ-30		×	Supplementary File 1 and 4	yes
UZ-31		×	Supplementary File 1 and 4	yes
UZ-32		×	Supplementary File 1 and 4	yes
Nurata Range				
UZ-02		×	Supplementary File 1 and 4	yes
UZ-04		×	Supplementary File 1 and 4	yes
UZ-15		×	Supplementary File 1 and 4	yes
UZ-42		×	Supplementary File 1 and 4	yes
UZ-43		×	Supplementary File 1 and 4	yes
UZ-44		×	Supplementary File 1 and 4	yes
UZ-16a		×	Supplementary File 1 and 4	yes
UZ-16b		×	Supplementary File 1 and 4	yes
UZ-35		×	Supplementary File 1 and 4	yes
UZ-36		×	Supplementary File 1 and 4	yes
UZ-37		×	Supplementary File 1 and 4	yes
UZ-38		×	Supplementary File 1 and 4	yes
UZ-39	×	×	Table 2 and Supplementary File 1 and 4	yes
UZ-40		×	Supplementary File 1 and 4	yes
UZ-41		×	Supplementary File 1 and 4	yes
UZ-48		×	Supplementary File 1 and 4	yes
Tymski				
UZ-11		×	Supplementary File 1 and 4	yes
UZ-12		×	Supplementary File 1 and 4	yes
UZ-13		×	Supplementary File 1 and 4	yes
UZ-14		×	Supplementary File 1 and 4	yes
UZ-50		×	Supplementary file 1 and 4	yes
Syr Darya				
UZ-01	×	×	Table 2 and Supplementary File 1 and 4	yes
UZ-24		×	Supplementary File 1 and 4	

UZ-25	×	×	Table 2 and Supplementary File 1 and 4	yes
Gissar				
UZ-05		×	Supplementary File 1 and 4	yes
UZ-07		×	Supplementary File 1 and 4	yes
UZ-08		×	Supplementary File 1 and 4	yes
UZ-10	×	×	Table 2 and Supplementary File 1 and 4	yes
UZ-49		×	Supplementary File 1 and 4	yes

Data treatment, uncertainties, and other relevant constraints

AHe Data

He dates (Ma): Single grain AHe ages were from Supplementary File 2 modelled individually

Error (Ma) applied in modeling: error of 1σ was used from Supplementary file 1

r (µm): Equivalent spherical radius of each grain

AFT data

Cl wt%: From Supplementary file 1

Lengths: Length data for all samples is available in Supplementary File 4

Initial mean track length: 16.3 µm

Track length reduction standard: 0.893

2. Additional geological information

Assumption	Explaination and data source
As all the samples were granitoid and there was no evidence for re-heating. Samples we assumed to have come from >120°C through the APAZ	

3. System- and model-specific parameters

He radiation damage model : Flowers et al. 2009

FT annealing model : Ketcham et al. 2007

FT c-axis projection : Not used

Modeling code : QTQt 5.6.0 PC

Statistical fitting criteria : Default QTQt values

MCMC Parameters : Burn-in = 200,000, Post-burn-in = 200,000